EXPERIMENTAL INVESTIGATIONS OF ANHYDROUS AND WET ETHANOL COMBUSTION IN A SPARK IGNITION ENGINE

A thesis submitted for the degree of
Doctor of Philosophy

by

Thompson Diórdinis Metzka Lanzanova

Department of Mechanical, Aerospace and Civil Engineering
College of Engineering, Design and Physical Sciences
Brunel University London

May 2017

Abstract

Experimental investigations of anhydrous and wet ethanol combustion in a spark ignition engine.

The demand for higher spark ignition engine efficiency has been pushed by stricter CO_2 legislation worldwide. Greenhouse gases mitigation and reduction on the use of fossil fuels is a global concern. For these reasons, the use of renewable and low carbon liquid fuels, such as ethanol, have considerably grown in the last decades. Due to the azeotropic ethanol-water mixture nature, the ethanol energy production cost considerably increases to achieve purity levels above 95%. Thus, the use of higher water-in-ethanol contents (so called wet ethanol) may improve the ethanol life cycle energy balance and result in a cheaper fuel. At the same time, new engine technologies, such as direct injection and variable valve actuation, have propitiated the spark ignition engine to reach higher efficiency levels than in the past. Even then, the low part load spark ignition engine efficiency is still a problem.

This research investigates the application of ethanol, wet ethanol and gasoline in a naturally aspirated single cylinder research engine equipped with an electro-hydraulic fully variable valve actuation system. Experimental thermodynamic engine tests were carried out in the four-stroke spark ignition operation mode at several engine loads and stoichiometric combustion. The effects of direct fuel injection and port fuel injection on engine operation were investigated. Initial studies with anhydrous ethanol were carried out to find the most promising valve strategies to be used when applying wet ethanol. The conventional throttled spark ignition valve strategy was investigated. The effect of the positive valve overlap period on the engine operation parameters and emissions were described. Unthrottled spark ignition operation with either early and late intake valve closure (EIVC and LIVC, respectively) load control methods were compared to understand the potentials of each strategy to increase SI engine efficiency. A comprehensive study on the effects of the intake valve lift for the EIVC load control method was carried out. Residual gas trapping methods as exhaust rebreathing and negative valve overlap were tested using the early intake valve closure load control method. Spark assisted compression ignition was achieved at some operating conditions.

Another study comparing the use of anhydrous ethanol, wet ethanol and gasoline was developed for three different valve strategies: conventional throttle SI valve strategy, variable positive valve overlap through intake profile phasing, and negative valve overlap with EIVC load control. In each presented study the gas exchange process, combustion, engine-out emissions and engine performance were discussed. The best valve events strategy for wet ethanol spark ignition operation is presented and the use of PFI and DI injection methods commented. It was possible to achieve similar engine indicated efficiency when using wet ethanol with 15% of water volumetric content to that achieved with commercial gasoline when using advanced valve events strategies. Comparing the wet ethanol baseline case to its best valve events and injection strategies scenario, 11.6% (from 2.0 to 4.5 bar IMEP loads) and 3.9% (from 6.0 to 9.0 bar IMEP loads) average relative efficiency gains could be achieved.

Keywords: Spark ignition engine; fully variable valve actuation; unthrottled SI operation; residual gas trapping; direct and port fuel injection; anhydrous ethanol; wet ethanol.

Acknowledgements

This has been a long journey and many people supported me to achieve this goal.

Firstly, I am sincerely grateful to my supervisor Prof. Hua Zhao for the most valuable technical lessons and guidance during this journey. His support and confidence on my work were imperative to overcome all barriers along the way.

I would like to thank my previous supervisors: Prof. Mario Martins (UFSM) for the encouragement and all support to come to Brunel. Prof. Paulo Romeu (UFSM), and Prof. Horácio Vielmo (UFRGS), for the incentives to pursue the PhD abroad.

I would like to thank my research colleagues from Brazil Rafael Sari, Gabriel Tatsch, Joelson Bilhão, Carlos Falcão, and Dr. Jonas Tibola for the incredible support and friendship.

I wouldn't be at this point without the huge technical and motivational support of all my colleagues from the Centre for Advanced Powertrain and Fuels Research: Dr. Ian Zhan, Dr. Jun Ma, Dr. Quan Liu, Dr. Nehemaia Alozie, Dr. Apostolos Karvountzis, Mohsen, Hassan, Emad, Akira, Mahmoud, Wei, Reza, Khalifa, Ray and Meghna Danji. Each one of them has in some way contributed to the conclusion of this work.

At the same time, there is a huge thanks to the brilliant technicians Chris Allan, Willian, Eamon and Andy Selway. Your professionalism, patience and friendship were of major importance to achieve high standard results on time.

Dr. Macklini Dalla Nora, Vinicius Pedrozo, Jessika Bridi, and Thiago Santos, you were not only PhD colleagues sharing the same scholarship program, you've been part of my family in UK. Thank you my friends!

I would like to thank my mother Nilva, and my father Jorge, for teaching me how to rise after falling, and for all the love and support. Thanks to all my family, for the motivation and support to come to UK.

Finally, I would like to thank my beloved wife Thais who was at my side in good and bad times. Who had the patience and love to understand the problems along this path. Who motivated me to live more than the PhD life. Thank you for being at my side during this journey!

Table of Contents

List of Figures

List of Tables

Nomenclature

AC	Alternate current
AKI	Anti-knock index
BDC	Bottom dead centre
CA50%	Angle of 50% mass fraction burned
CAD	crank angle degree
CAD	Crank angle degree
CAI	Controlled auto-ignition
CAPF	Centre for Advanced Powertrain and Fuels Research
COV_{imep}	Covariance of IMEP
CPS	Cam profile switch
CR	Compression ratio taking in account TDC and BDC cylinder volumes
CRP	Compression ratio given by
CR_P	Effective compression ratio taking in account a polytropic compression
CRV	Compression ratio given by the IVC
CR_v	Effective compression ratio at IVC
CVVL	Continuously variable valve lift
DAQ	Data acquisition card
DDGS	Distiller's Dried Grain and Solubles
DI	Direct injection
DVRT	Differential variable reluctance transducer
e	Ethanol-in-gasoline v/v
E95W05	Hydrous ethanol (5% water-in-ethanol v/v)
ECU	Engine control unit
EGR	Exhaust gas recirculation
EIVC	Early intake valve closure
EIVO	Early intake valve opening
ER	Exhaust rebreathing
EU	European union
EVC	Exhaust valve closure
EVO	Exhaust valve opening
Exx	Ethanol-gasoline mixture (xx% of ethanol-in-gasoline v/v)
ExxWyy	Wet ethanol (yy% of water-in-ethanol v/v)
FDA	Flame development angle
FDA	Flame development angle
FF	Fully flexible

FID	Flame ionization detector
FTIR	Fourier transform infrared spectroscopy
FVVA	Fully variable valve actuation
GDP	Gross domestic product
GHG	Greenhouse gases
GRON95	Unleaded 95 RON UK gasoline
H_a	Air humidity
HCCI	Homogeneous charge compression ignition
H_t	Total humidity (from air and wet ethanol water)
IMEP	Indicated mean effective pressure (net)
ISCO	Indicated specific CO
ISNOx	Indicated specific NOx
ISTHC	Indicated specific THC
IVC	Intake valve closure
IVO	Intake valve opening
k_{FID}	FID correction factor to unburned oxygenated compounds
k_w	Dry-to-wet correction factor
L	Connecting rod length
LEVC	Late exhaust valve closure
LHV	Lower heating value
LIVC	Late intake valve closure
LPSI	Low speed pre-ignition
MFB	Mass fraction burned
$m_{fuel,c}$	Fuel mass per cycle
$\dot{m}_i$	Mass flow rate of component "*i*"
MON	Motor octane number
NDIR	Non dispersive infrared
NEDC	New European driving cycle
NVO	Negative valve overlap
PCU	Port fuel injector control unit
PFI	Port fuel injection
P_i	Indicated power
p_i	Instantaneous in-cylinder pressure
PMEP	Pumping mean effective pressure
PRF	Primary reference fuel
PRR	Pressure rise rate
PVO	Positive valve overlap
RGF	Residual gas fraction
RH	Relative humidity
RIEG	Relative indicated efficiency gains

RON	Research octane number
S	Stroke
SACI	Spark assisted compression ignition
SI	Spark ignition
SP	Saturation pressure
SPI	Stochastic pre-ignition
T_a	Ambient temperature
TDC	Top dead centre
THC	Total unburned organic species (corrected UHC)
UHC	Unburned hydrocarbons
UHC	Unburned hydrocarbons
u_i	Molar mass fraction of i gas
v/v	Volume-to-volume ratio
VCR	Variable compression ratio
VCU	Valve control unit
V_d	Engine displacement volume
VVA	Variable valve actuation
W_{ALF}	Hydrogen fuel content
$W_{c,i}$	Indicated work per cycle
W_{EPS}	Oxygen fuel content
WLTP	Worldwide light duty test procedure
WOT	Wide open throttle
WTT	Well-to-tank
WTW	Well-to-wheel

η_C	Combustion efficiency
η_{GE}	Gas exchange efficiency
η_I	Indicated efficiency
η_{Otto}	Thermodynamic efficiency of the Otto cycle
η_T	Thermodynamic efficiency
[i]	i gas concentration in ppm
α	FID response factor correction for oxygenated contents
γ	Ratio of specific heats

Chapter 1. Introduction

1.1. Preface

The transport sector accounts for almost one quarter of total used energy in developed countries and most of this energy comes from fossil fuels. In the last decades, the growing energy supply demand and environmental concerns led the research for new renewable and environmentally friendly energy sources and cleaner ways of using the old ones. Thus, stricter emission legislation has pushed internal combustion engines to reduce the local impact of its pollutant emissions on human health (e.g., lung and coronary diseases) and on the local environment (e.g., acid rain, smog). Even then, CO_2 generation is inevitable when burning fuels.

Low carbon fuels (which results in less CO_2 generation when accounting their whole life cycle) have been implemented worldwide in order to reduce CO_2 emissions. Bioethanol is an old known automotive fuel used by Otto in the first spark ignition engine. Due to its most common origin (a product of starch fermentation), ethanol can be produced from high yield agricultural crops, which also makes it a renewable fuel. In the ethanol life cycle, greenhouse gas (GHG) emissions are counterbalanced by crop photosynthesis during feedstock formation, and thus results in lower, or even negative, when compared to fossil fuels. Also, for many of the ethanol production methods, which also depend on the crop origin, the wheel-to-well energy balance is positive: more energy is released during the use of ethanol and its co-products than used in the production phase. Ethanol has been mainly employed as a gasoline enhancer and substitute in spark ignition engines.

The energy demand to achieve higher ethanol-in-water purity than 95% significantly increases fuel cost due to ethanol-water azeotropic mixture nature. Thus, this is another point to be explored in order to reduce ethanol production energy demand and fuel cost. On the other hand, the use of the so called wet ethanol generates combustion degradation which reduces engine efficiency. So, special strategies to use wet ethanol in SI engines are necessary.

Even though several studies about controlled auto-ignition (CAI) combustion concepts showed that higher engine efficiency could be achieved, these concepts still not fully applicable for real world applications. Thus, stoichiometric spark ignition (SI) operation is stills the best option for ethanol application. In this route, engine downsizing has been explored as a way to increase SI engine efficiency. It consists in reducing engine

displacement and number of engine cylinders while increasing specific torque density through charging. At low loads, the smaller engine has to operate with higher trapped charge density in order to promote the same power as the original size engine one. To attain that, increased throttle opening is necessary. Thus, lower pumping work occurs. In this way, engine downsizing is also an approach for reducing pumping work at part load.

Naturally aspirated engine dethrottling by variable valve actuation and increased internal residuals is also a way to improve SI engine efficiency. For this reason, many different variable valve actuation mechanisms have been employed by the industry. In the same context, direct fuel injection also enabled higher engine efficiency due to knock mitigation and lower enrichment requirements.

Lately, introduction of personal electrical passenger vehicles has occurred. Although is reality, the complete change from internal combustion engines to electrical motors in the automotive sector still presents an energy supply problem from both the point of view of batteries and electrical energy generation. If the electrical energy source is not clean, the total CO_2 emissions of an electric vehicle can be similar to that of an internal combustion engine vehicle. In addition, the power density of a battery is several times smaller than that of liquid fuels and this still a challenge.

For all these reasons, this work is focused on the application of anhydrous and wet ethanol to internal combustion SI engine operating at stoichiometric conditions. Advanced valve events strategies are explored in order to reduce spark ignition wasted energy and increase engine efficiency.

1.2. Research objectives

The primary goal of this research is to improve the naturally aspirated four-stroke spark ignition engine efficiency at different loads using ethanol, wet ethanol and gasoline via thermodynamic engine experimental testing exploring a fully variable valve actuation system. The specific objectives of this research comprise:

- To assess the compromise between wet ethanol energy production cost (from literature data) and engine energy output which provide an optimized water-in-ethanol content that improves wet ethanol life cycle energy balance;

- To investigate different load control methods (throttling, early intake valve closure and late intake valve closure) in order to improve SI engine part load efficiency;
- To explore different residual gas trapping strategies using the fully variable valve actuation system in order to improve wet ethanol operation efficiency;
- To investigate the combustion characteristics and emissions of the different valve strategies with the different fuels.

Some of these objectives are in line with the proposed works of previous theses developed in the same engine operating in four-strokes mode [1], [2].

1.3. Thesis outline

The first chapter provides the thesis scope and its objectives, providing the information about each chapter. A literature review is presented in Chapter Two with coherent essential topics to provide arguments and theoretical knowledge to support the methodological choices and result discussions. The main topics are: transportation energy demand scenario; gasoline engine basic principles; advanced combustion concepts and non-conventional valve strategies; use of ethanol in internal combustion engines; overview on the ethanol production process; use of wet ethanol in internal combustion engines.

The following chapter presents the experimental setup details, with description of the engine and equipment used. The calculation methodology used to analyse the acquired data in order to assess gas exchange and combustion process, engine-out emissions and engine performance is also provided in this chapter.

The results are presented from Chapter 4 to Chapter 7, and Figure 1.1 presents the main idea of each result chapter and their interconnection. The literature review in Chapter 2 provides an initial assessment on the wet ethanol life cycle energy balance taking in account the production process and the final use in the SI engines. Thus, it provides an answer to the best water-in-ethanol content which increases wet ethanol life cycle energy balance.

Chapter four explores the influence of the positive valve overlap period in the conventional SI profile valve strategy with throttle load control. Two studies were carried with anhydrous ethanol. The first aimed in understanding the influence of the positive valve overlap with fixed valve profiles while second study investigated the

possible benefits of the use of the intake phase concept in order to increase engine efficiency. This chapter provided baseline cases for the Chapters 5, 6 and 7.

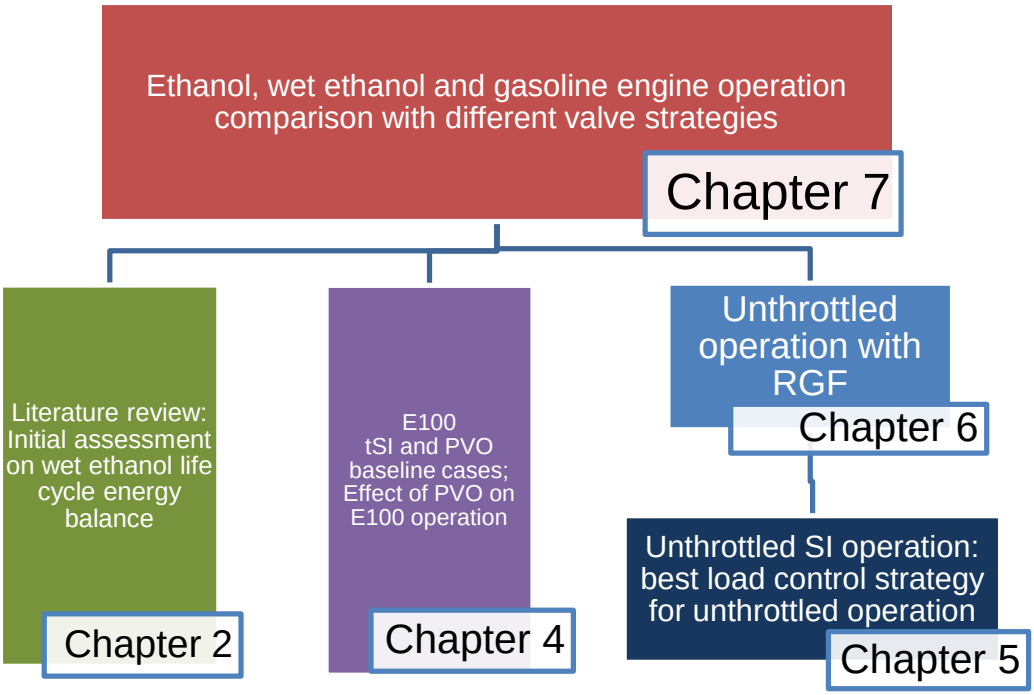

Figure 1.1. Demonstration between chapters connection

Chapter five investigates the SI unthrottled operational with load control through IVC. Early and late intake valve closure concepts were compared to a conventional throttle SI valve profile concept to define the load control method with the higher chance to improve engine efficiency. Another study was carried on to understand the effects of the maximum valve lift on the engine operation. Both PFI and DI operation were investigated.

Chapter Six investigates the use of NVO and exhaust rebreathing (ER) strategies to promote anhydrous ethanol operation with increased residual gas fraction. EIVC load control was used with NVO and ER. Different loads were investigated from low load to WOT with port and direct fuel injection strategies.

Chapter Seven integrates all results from the previous chapters. The best load control and residual gas trapping methods from previous chapters were tested for wet ethanol, anhydrous ethanol and gasoline. Engine performance, emissions and combustion were discussed and the best valve strategy and fuel injection method for wet ethanol operation was proposed.

Chapter Eight presents the research main findings regarding the impact of different valve strategies and wet ethanol in the naturally aspirated SI engine. Future work recommendations are proposed to explore the gaps not covered by this study.

Chapter 2.

Literature review

2.1. Introduction

Climate change is an unneglectable reality. Although this is a cyclic phenomenon, the recent climate change scenario cannot be explained by historical data alone and there is clear evidence that these changes are driven by human generated greenhouse gas (GHG) emissions such as carbon dioxide, methane and nitrous oxide [3]. A huge share of these emissions results from fossil fuel exploration and burn to support population and economic growth. For these reasons, nations have agreed to reduce global greenhouse gases emissions in order to hold the global average temperature below 2°C above pre-industrial levels through the adoption of the Paris Protocol agreement [4].

The transportation sector accounts for about 25% of total carbon dioxide emissions in the European Union and about 30% in USA [5], [6]. Looking at the current global transportation sector fuel consumption future estimative (Figure 2.1), gasoline engines and diesel engines are responsible for around 75% of consumed energy. An increase of 50% in energy consumption is expected compared to 2012 scenario in the next two decades. Advances in internal combustion engines are expected to

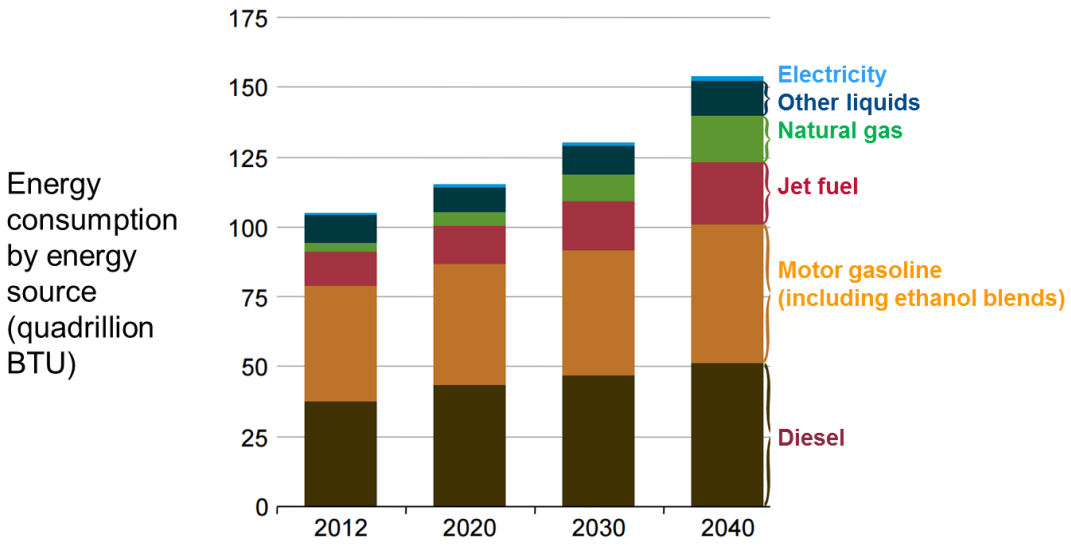

Figure 2.1. Transportation sector energy consumption estimative (adapted from [7])

decrease gasoline and diesel energy consumption share to around 2/3 of total energy consumption. Even then, the number of passenger vehicles is expected to grow supported by growth in per-capita levels, especially in emerging economies. The freight vehicles fleet is also expected to grow at a related rate to Gross Domestic Product (GDP) of countries [8]. At the same time, there will be a considerable increase in jet fuel and natural gas use especially, which are essentially fossil fuels as well. Thus, this scenario shows increasing GHG emission trends based especially in fossil fuels.

The main reason for the lower share of road vehicles energy demand is more stringent legislation limits which are directed to reduce fuel consumption and CO_2 emissions (g CO_2/km). Investigating passenger cars only, EU 2015 legislation set average manufactures' fleet target limits on fuel consumption of 5.6 l/100 km for gasoline cars and 4.9 l/100 km for diesel. These limits will be reduced to 4.1 l/100 km of gasoline or 3.6 l/100 km of diesel in 2021. As different size vehicles need to be fit in these limits, a g CO_2/km to vehicle weight curve has been proposed taking in account the new European driving cycle (NEDC). Thus, heavier vehicles could emit more g CO_2/km than lighter vehicles. At the same time, extremely low emission vehicles (below 50 g CO_2/km) have a higher weight in the average fleet count. Thus, manufacturers have been pushed to produce hybrid and fully electrified vehicles to support dirtier vehicles and reduce rate of technology application in conventional vehicles. Other countries have similar rules, as shown in Figure 2.2.

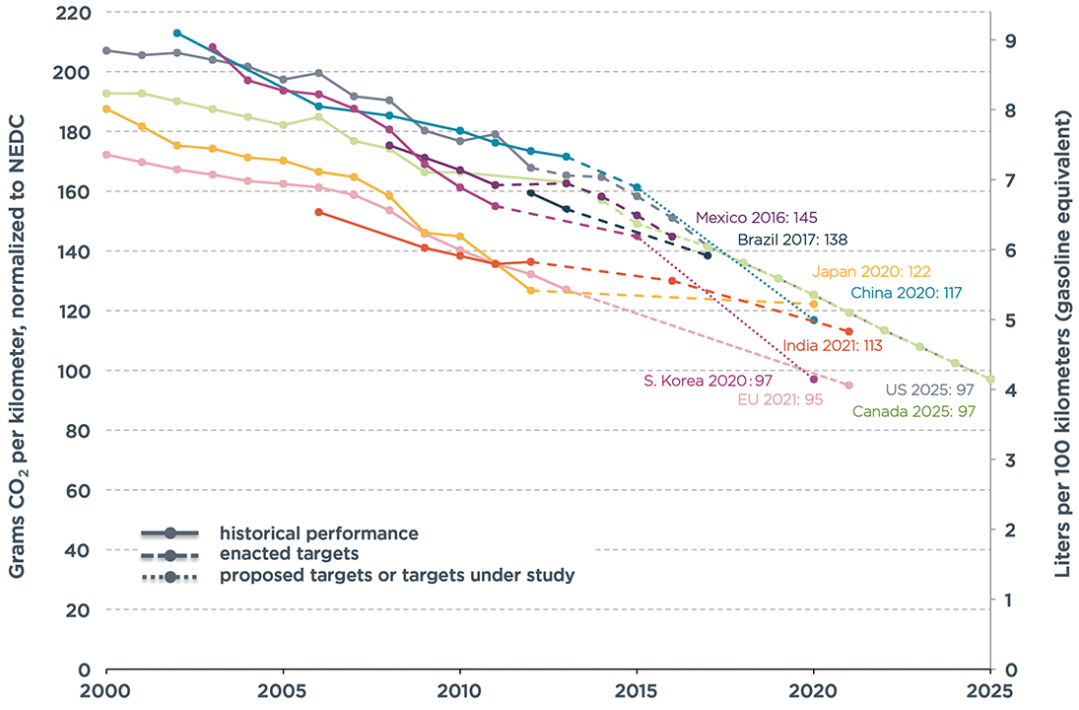

Figure 2.2. Historical fleet CO2 emissions performance and current or proposed light commercial vehicle/light truck standard (adapted from [9]);

A recent problem raised is that driving cycles can't effectively express real driving conditions. For this reason, there is a discrepancy between the disclosed manufacturer fuel economy and the one felt by the costumers. In reality, higher g CO_2/km still being emitted and the customer is expending more fuel than expected. For this reason, a worldwide light duty test procedure (WLTP) have been discussed in order to achieve a closer to reality picture and reduce such discrepancies.

Also in this context, diesel engines have been historically more efficient than gasoline engines. For this reason, EU diesel market share have increased to more than 50% of total fleet since the 90s, with some countries presenting diesel car market shares higher than 70%. On the other hand, diesel is known to have a much more complex NOx after-treatment system and emit more particulate emissions than gasoline engines. Such emissions are known to have deeper impact in local air pollution and be more harmful for human health. The recent "Dieselgate" scandal has turned attention of policy makers against both light duty and heavy duty passenger vehicles. Thus, many cities around the globe have manifested the intent to promote diesel engines ban in urbanized centres. This will lead to heavier vehicle electrification and more gasoline vehicles. Even then, it is highly important to understand that depending on how the electricity is generated, there will be only local emissions improvements with possibility of increase in total CO_2 emissions, especially if coal is used.

Due to such events, gasoline engines have received renewed attention. The increased demand for more efficient and cleaner engines has promoted engine downsizing as a major trend. It consists in reducing the engine displacement and number of cylinders while using super/turbo-charging to increase power density. Thus, the engine is pushed to operate in heavier load regimes, which are more efficient especially due to lower throttling losses. At the same time, the turbine recovers some of the energy lost from the exhaust gases.

Engine downsizing has been especially supported by gasoline direct injection (DI) technology which enabled the extension of knock free operation by promoting charge cooling with elevated combustion efficiency. Turbocharging technology has also been improved to recover more wasted power from the exhaust gases (less back pressure). Concepts with coupled electric motors/generators have been investigated in order to overcome low speed turbo-lag problem and store energy surplus.

Other technologies have been proposed to meet near future legislation limits. Engine electrification strategies such as start/stop systems, electric oil and water pumps, and better thermal management are being used to decrease fuel waste. Variable valve train

technologies have been implemented to decrease fuel consumption and reduce emissions in part load operation. Lubricant advances and low friction coatings/components have been designed to improve engine performance. Particulate filters have been implemented in DI engines and soon will be also required in PFI (port fuel injection) engines to meet particulate emissions standards. In addition, the several degrees of hybridization have been applied. The heavier the vehicle gets, the heavier degree of hybridization will be required in order to meet the emission legislation limits. Even then, stoichiometric combustion stills a near future tendency to keep the cost-effectiveness of the spark ignition (SI) engine hardware, once the three-way catalyst still the best option to tackle gasoline engine emissions.

In such scenario, a larger introduction of carbon neutral energy sources is required to further reduce greenhouse gas emissions. Even if full electrification is applied, only with the use of renewable and clean energy sources the CO_2 emissions problem will be tackled. For these and several other reasons which will be further explained, this research focusses on the application of ethanol to spark ignition engines.

2.2. Gasoline engines

2.2.1. Four-stroke spark ignition engine operation fundamentals

The four-stroke engine operating principle can be described by four phases (induction, compression, expansion, exhaust) of 180 crank angle degrees (CAD) each, taking two crank revolutions to complete a thermodynamic cycle. Considering instantaneous valve events, the intake valve opens (IVO) in the top dead centre (TDC) and charge mixture is induced to the cylinder while the piston moves downwards. The intake valve closes (IVC) in the bottom dead centre (BDC) and the charge is submitted to a near isentropic compression while piston travels towards top dead centre. Combustion occurs instantaneously and adiabatically at top dead centre. The increase in pressure occurs due to the exothermic reaction which increases charge temperature and forms new molecules. The hot burned gases are isentropically expanded during the expansion stroke while the piston travels from TDC to BDC. The exhaust valve opens in the BDC and the burned gases are expelled from the cylinder while the piston moves upward towards TDC. At TDC the exhaust valves close and intake valves open, initiating a new cycle. The theoretical efficiency, η_{Otto}, of the so called Otto cycle is given by:

$$\eta_{Otto} = 1 - \frac{1}{CR^{\gamma-1}} \quad (1)$$

where CR is the compression ratio given by the relationship between in-cylinder volume at BDC and TDC, and γ is the ratio of specific heats. Thus, a higher compression ratio would be desirable to increase the engine efficiency with the highest possible fluid properties γ.

In the reality, the valve events do not occur instantaneously and start at the TDC or BDC. The combustion occurs during a finite period, starting several degrees before TDC, and finishing after TDC, with combustion duration and phasing directly affecting the engine's capability to produce work. Different fuels provide different combustion available energy by promoting different levels of enthalpy destruction due to high combustion temperature. Especially during combustion and expansion, fluid to combustion chamber wall heat transfer reduces the gases available energy to be converted into work. The specific heat ratio varies according to charge composition (smaller than 1.4 maximum value of air). Thus, thermodynamic engine modelling has been used in order to assess the effects of these phenomena in SI engine efficiency [10]–[13].

The combustion process in the spark ignition engine can be divided in four main phases [14]:

1st – Spark and flame initiation stage: the voltage rise between the spark plug electrodes promotes an electrical breakdown, which creates an electrical arc that can be affected by the flow field in the vicinity of the spark plug. Later, during this initial stage, the self-sustained flame propagation is established being affected by chemical kinetics, mixture composition, flow field, spark energy released and geometry-related parameters.

2nd – Initial flame development stage: the duration of this stage is around 30% of the total combustion duration, reason why is one of the most important regarding cyclic variability. Initially, an almost spherical surface flame kernel is formed after the spark breakdown. After an initial growth period, dominated by mixture composition and thermodynamic conditions, the interaction between the flame front and the turbulent eddies starts. Due to the reduced size of the kernel, the largest eddies in the flow can convect it from the electrodes [15]. Normally, due to uncertainties in the in-cylinder pressure measurement, the FDA (flame development angle) can be accessed for the CAD duration between spark and 5% MFB [16] or 10% MFB.

3rd – Turbulent flame propagation stage: this stage corresponds to the period between 10% and 90% of mass fraction burn. It is affected by the flame front area, which is

affected by spark plug location, mixture composition (which affects the laminar flame speed) and turbulence intensity (which increases the flame front area by flame wrinkling). The flame front grows in size from the initial kernel with a preserved shape until it is quenched near the wall [16]. However, the mean velocity field and local air/fuel mixture play a minor role during this stage as a large number of local events are averaged for the final effect. So, for a specific engine operating condition, this stage shows less duration variability than the two previous stages

4th – Flame termination stage: at this point the flame front area reaches the cylinder wall and the flame is quenched. Some remaining entrained unburned pockets may still burn. Post flame unburned hydrocarbons and carbon dioxide oxidation still occurs if enough temperature is available to support the chemical mechanisms.

According to several works [16], [17], between the four main stages of combustion, the flame initiation and flame-kernel development stages are most important in terms of cyclic variability of IMEP. As the turbulent flame propagation stage is roughly constant, the cyclic variability in the first and second combustion stages are responsible for the variability in the combustion phasing that lead to peak cylinder pressure variability. Thus, the acceleration of the early flame kernel development tends to reduce cyclic variability and increase the maximum charge dilution limit. Also, as the cycle-by-cycle air variability of the intake process changes both bulk and local composition of the in-cylinder charge and flow structures, it directly affects the initial combustion stages and so the variability of the IMEP.

Considering the two large in-cylinder flow structures swirl and tumble, studies have shown that these large flow motion scales break up in small scales during the late stage of the compression increasing the turbulence during combustion [18]. The tumble motion is the large scale fluid motion generated during the intake stoke around an axis perpendicular to the cylinder centre line. While the piston is moving towards TDC, during compression, initially the tumble increases due to angular momentum conservation. Later, in the compression stroke, the large flow structure is distorted due to wall shear stress and decays in smaller turbulence structures [19], [20]. Swirl is the rotational fluid motion around the cylinder axis. On the contrary of the tumble, due to the an almost solid-body nature of such large scale flow motion, its decay to smaller turbulence scales is less affected by wall friction and the angular momentum can be well sustained until the end of the compression stroke [21]. So, the increase of the tumble in-cylinder motion is expected to generate higher turbulence levels prior to combustion than the increase in the swirl [22], [23]. Even then, swirl motion can help to accelerate flame growth rate and convect the early flame kernel from the spark plug

[15] helping in reducing the early flame contact to the spark electrodes, thus increasing flame kernel growth due to lower heat transfer rates [24].

Conventionally, swirl has been used in two valve SI engines and diesel engines, while tumble has been preferential for four valve engines due to valve cylinder head symmetry aspects which difficult swirl generation. The use of such in-cylinder flow motion is of major importance for lean burn engines, where the laminar flame speed is lowered and the flow field has more time to distort the flame until the end of combustion [25]. Also, the flow field directly affects the in-cylinder heat transfer, and as swirl is maintained during the combustion process, extreme fluid motion may decrease engine overall efficiency by increasing heat losses [21], [26].

A problem that directly limits engine efficiency is knock phenomena. Knock is the uncontrolled auto-ignition of the end gas ahead of the flame front [27], [28]. Knock can be caused by several mechanisms. Between then, end gas auto-ignition due to pressure temperature in-cylinder evolution, hot surface fuel auto-ignition (exhaust valves, piston crown, and others), lubricant contaminants in the combustion chamber [29] (specially calcium [30]). It is characterized by an audible metallic “pinging” sound caused by a sharp rise in the heat release rate which sets up pressure waves in the cylinder.

Due to knock’s connection to temperature and pressure, when advancing spark timing, the point when knock starts is known as knock-limited spark timing. In modern engines, knock can be detected by microphone like sensors. When specific frequencies occur which are linked to knock occurrence, the engine management system retards the spark timing. Thus, this directly reduces engine efficiency by retarding the combustion phasing. A second measure that can be taken, especially at high engine speed and high exhaust gas temperature, is to promote over fuelling [31]. This reduces knock intensity by reducing charge temperature while exhaust temperature is also reduced protecting exhaust after treatment and turbine components. Thus, the compression ratio of the SI engines is directly limited by knock occurrence.

High load engine efficiency is limited by compression ratio which is directly influenced by fuel anti-knock characteristics. High knock resistance fuels are less prone to knock leading to higher engine efficiency. Fuel knock resistance is measured by research octance number (RON) and motor octane number (MON) tests (each test is taken at different intake air temperatures and engine speeds). These tests compare the knock limit operation with that of iso-ocatane and n-heptane mixtures, referred as primary reference fuels (PRFs). The volume percentage of iso-octante on the mixture gives the

octane number according to the test. As MON test is performed at higher intake air temperature (159 °C to 52 °C of RON), auto-ignition process occurs for lower octane amount than in RON. The difference between RON and MON is known as sensitivity [32]. A parameter called anti-knock index (AKI) is also used to describe the anti-knock characteristic of fuels, being the average between RON and MON.

A more intense and very destructive form of knock with very high in-cylinder peak pressure and intense knock amplitudes is mega/super knock. It occurs only in downsized engines due to high specific load operation. This phenomena is also termed low speed pre-ignition (LPSI) or stochastic pre-ignition (SPI) [33]. Even though knock and pre-ignition events are related, those two events are not the same thing, and SPI events are not always followed by knock [34], [35], as shown in Figure 2.3. Although several explanations for these phenomena exist, SPI occurrence and prediction is still not well explained, thus there is still no effective control method over such phenomena. Although this is a very important phenomena, it does not happen in naturally aspirated engines and will not be further commented.

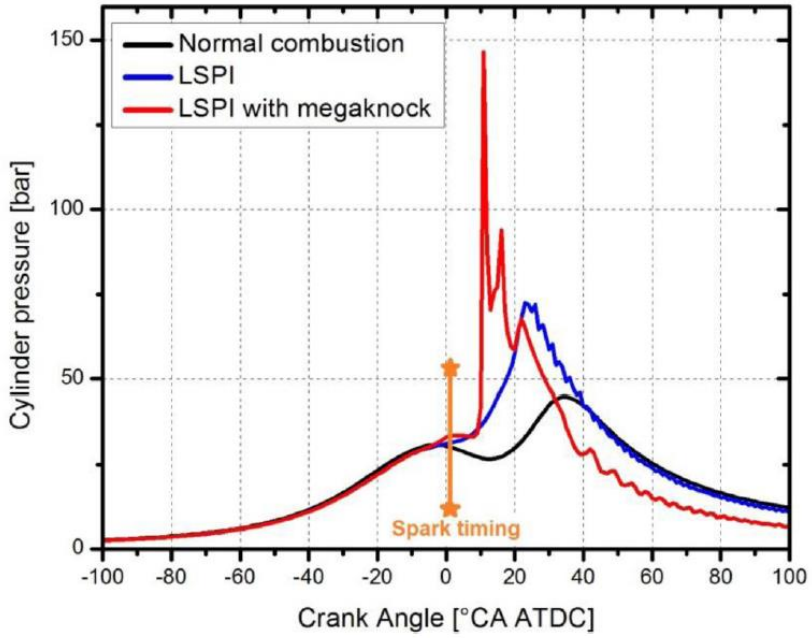

Figure 2.3. In-cylinder pressure LPSI and mega knock at 2000 rpm, adapted from [35].

While knock limited operation reduces high load SI engine efficiency, part load efficiency is impaired by the load control method based on reducing intake pressure. As SI engines are required to operate at stoichiometric levels through most part of the engine map due to the three-way catalyst limited operation range, there is a restriction

regarding the fuelling dosing. Thus, different fuel flow rates are required for different loads while the air-to-fuel ratio needs to be kept constant. This results in low air quantity requirement for low loads and high air requirement for higher loads (comparing the same speed). The air flow rate is normally controlled using a butterfly valve, so called throttle, before the intake air plenum. This valve restricts the flow rate creating a low pressure environment in the flow elements between the throttle and the intake valves.

Figure 2.4 shows the valve timing profile of a near conventional SI throttled engine to illustrate the effect of throttle load control method. The intake valve opening (IVO) was set to open near TDC. It can be noticed that as the IVC occurs during the end of the exhaust stroke, the in-cylinder pressure drops near to the intake port pressure. At this point, cylinder charge residuals can flow back to the intake manifold, returning to the cylinder during the intake stroke. Due to the throttled operation, in-cylinder pressure is reduced below the inlet manifold pressure while the piston motion goes from the TDC to the BDC. The relative pressure gradient between the exhaust stroke and intake stroke is the responsible factor for the work consumption during the low load four-stroke throttled operation gas exchange phase. Adversely, with turbo-charged engines, when intake pressure is lower than exhaust pressure, work is obtained from the pumping loop. Due to the small intake to exhaust valves overlap, low load internal residuals are limited to the combustion chamber volume and the amount of charge that is flown back to the intake manifold during the overlap.

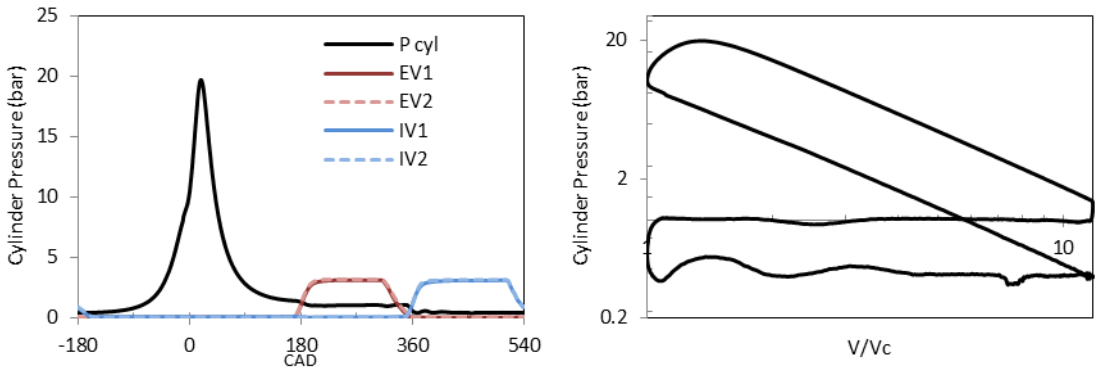

Figure 2.4. Near conventional intake and exhaust valves profiles – Pressure x CAD diagram and logP x logV diagram. 1500 rpm 2 bar IMEP ethanol DI operation.

In addition, all valve events affects the SI engine performance. In the presented case, the intake valve closure event was set to some degrees after the TDC to take

advantage of the gaseous inertial effects – so called ram effect. In higher loads, even with the piston changing its moving direction, the gaseous column inertia keeps filling the cylinder until a certain point. This effect also depends on the intake wave propagation phenomena (intake tuning) which change the according to engine speed. In low load and low speed, due to low intake gas inertial effects, some fresh charge can be sent back to the in-cylinder ports.

During the IVC event the compression starts. Thus, the IVC point is related to the effective compression ratio given by the valve closure (CR_v). There is a compression ratio compromise between efficiency and knock as the final charge state (in-cylinder pressure and temperature) dictates how the combustion process will take place and how much of the available energy will be converted into work. Moving the IVC away from the BDC may change the point where compression starts, as will be discussed later. Thus, SI engine efficiency is impaired by pumping losses at low loads while knock reduces engine efficiency at high loads.

The exhaust valve opening controls the maximum expansion work and the has influence in initial exhaust phase pumping work. Commonly, EVO is advanced to the expansion stroke to take advantage of the higher in-cylinder pressure to ease the exhaust process at higher speeds and high load (blow down). The early EVO decreases the exhaust phase pumping work while reducing the total work produced during the expansion work. The blow down process is also used to increase the amount of exergy available in the turbine of turbo-charged downsized engines. This way, the exhaust gases pass through an over expansion in the turbine which produces more work than would be produced during the late expansion phase. In the Figure 2.4 case, the EVO was set very close to the expansion BDC. This way, when the exhaust stroke effectively begins, the in-cylinder pressure is already stabilized near the exhaust pressure. There is virtually no blow down, and the maximum piston expansion work can be achieved, increasing the cycle efficiency.

The exhaust valve closure (EVC) event controls the amount of exhaust gas backflow from the exhaust ports to the cylinder during the initial phase of the intake stroke at low loads. At high loads, due to the inertial effect of the exhaust gases, the use of valve overlap may increase the burned gas scavenging process and increase volumetric efficiency. Thus, different mechanisms for variable valve actuation have been proposed as the optimum valve timings are dependent on engine speed and load.

2.2.2. **Variable valve actuation mechanisms**

The conventional throttled load control method used in four-stroke gasoline engines with conventional fixed camshafts result in high pumping losses at part load operation. Also, there is a considerable efficiency loss compromise to propitiate good combustion stability at the wide range of speed and loads without power compromises at wide open throttle (WOT). Thus, variable valve actuation (VVA) has been adopted by the automotive industry to increase not only part load engine efficiency but also full load performance.

Several different VVA mechanisms were developed in the last decades to enable different degree of valve actuation freedom. Although fully variable valve actuation (FVVA) mechanisms are already available for production engines, such systems are considerably more expensive then simpler ones. So, only some parcel of the market adopts it based on a cost benefit scenario to attend fuel consumption legislation. In general, the larger the vehicle, the higher the valve actuation freedom necessary to help to achieve CO_2 emissions legislation. Thus, variable valve actuation mechanisms can be divided into systems with camshafts and those without camshaft.

One of the most basic variable valve actuation mechanisms is based on cam profile switching (CPS), initially proposed by Honda with its VTEC system. It has two discrete intake cams with different profiles designed for low load/speed (small lift and shorter duration) and high load/speed (high lift and larger duration) [36]. These systems provide low load higher efficiency by partial dethrottling which reduces pumping work. In this work, the term dethrottle will be used to denote wider throttle opening while unthrottled will be used to denote WOT condition with load control through other means than throttling. Another basic mechanism is cam phasing, which may increase or decrease valve overlap, for example. This is achieved by phasing the timing chain to the camshaft [37]–[39]. Many manufacturers use both systems at the same time in order to have more benefits [40]–[42].

Other systems based on camshafts which provide a larger degree of valve actuation freedom are the so called continuously variable valve lift (CVVL) systems. These systems provide both cam phasing and valve lift freedom. Several mechanisms have been proposed, between them, the most famous are BMW Valvetronics [43], [44], Schaeffler UniAir [45], [46] (used by FIAT Chrysler), and Nissan Variable Valve Event and Lift (VVEL) system [47]–[49]. Three dimensional cam lobes have also been used by the industry (Ferrari and Alfa Romeo) [50]. Figure 2.5 shows some of the valve strategies enabled by a CVVL system.

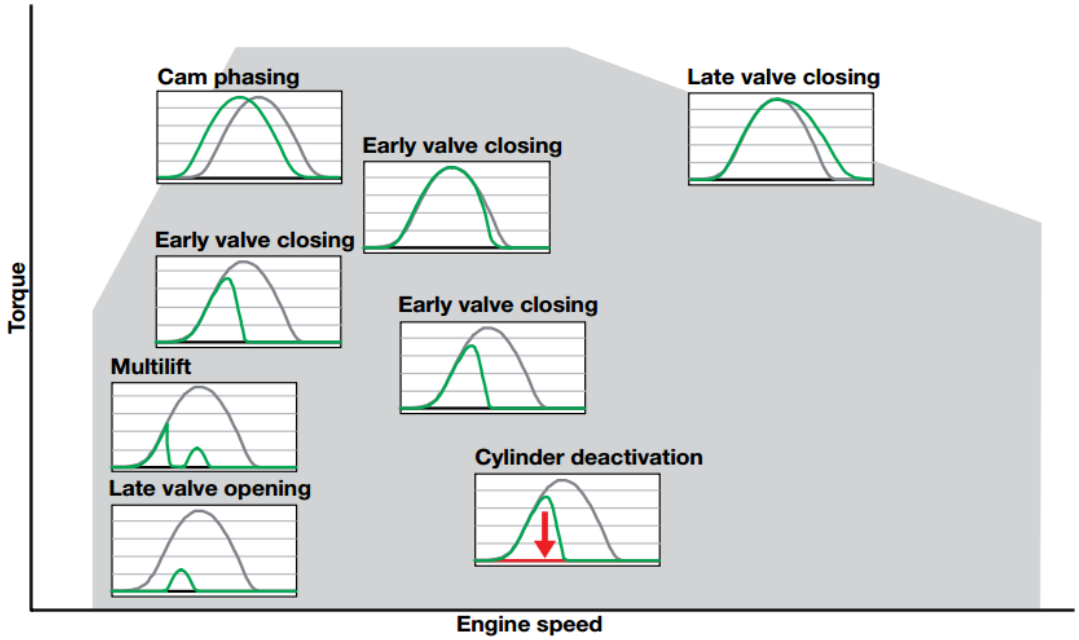

Figure 2.5. UniAir valve strategies according to engine load and speed [51].

Lastly, fully flexible variable valve actuation (FVVA) systems not based on camshafts (camless) have been proposed [52]–[59]. These systems can be electro-hydraulic [54]–[57], electro-pneumatic [52], [59] or electro-magnetic [58]. They provide fully independent valve actuation, with the possibility of two and four-stroke operation in the same engine [60]. Even though it is a promising technology for light duty vehicles, only the electro-pneumatic based system from Freevalve has been implemented in high end production engines [59]. The main gains of such systems are the possibility of any valve strategy actuation, which in turn may improve engine efficiency by reducing pumping losses (unthrottled operation) and enhancing combustion.

2.2.3. **Unthrottled SI operation with variable valve actuation**

The use of VVA systems enables the use of different valve events at different lifts, as showed in Figure 2.5. This directly affects the pumping loop. Basically, there are two ways of reducing the pumping losses. The first one which is applicable with conventional SI valve profiles is to dilute the fresh air to increase the charge density and reduce intake stroke to exhaust stroke pressure difference. This can be achieved using air or exhaust gases charge dilution. The problem regarding lean operation (air dilution) in SI engines is the necessity of an additional NOx after treatment system, which would considerably increase the gasoline hardware cost. Even though lean

operation (air dilution) would result in higher engine efficiency than EGR dilution due to better thermodynamic properties [61]. This strategy won't be further commented as this study focuses only on stoichiometric engine operation. On the other hand, the dilution by EGR can be used while maintaining the stoichiometric air fuel ratio, thus, enabling the use of the three-way catalyst. This can be achieved by external EGR (external line from the exhaust to the intake) or internal EGR, so called residual gas (RGF) trapping. Internal EGR can be achieved by burned gas backflow from the cylinder to the intake ports or from the exhaust ports to the cylinder, and RGF trapping by early EVC. In this work, as all methods of increasing burned gas content are promoted by valve actuation, RGF trapping and internal EGR denote burned gas dilution originated from previous cycles. The second way to reduce pumping losses is to change the intake valve closure point from near the BDC to either advanced or delayed positions.

2.2.3.1. Early intake valve closure (EIVC)

In this method, the intake valve is closed before the piston reaches the BDC, during the intake stroke. It would be preferred if the valve was closed at the exact moment that enough air was supplied for the required load which is only possible with CVVL system. This would result in WOT operation and very low pumping losses. Partial dethrottling is achieved with the low lift/duration cam profile in CPS mechanisms. A characteristic of the EIVC strategy is that after the IVC, the in-cylinder charge passes through an over-expansion phase, decreasing its temperature and density.

Mikulic et al [62] showed fuel economy improvements of about 12% when using both EIVC and port-deactivation for part load operation in a 4 valve per cylinder engine. Fuel condensation during the over expansion phase was found to be problem for charge homogeneity. The use of port-deactivation was found to improve burning rate. Kreuter et al [63] also found improvements on fuel consumption. It was stated that the gains regarding pumping losses reduction would not be fulfilled if measures to support mixture formation and combustion by means of valve deactivation of low valve lift were taken.

Urata et al. [64] used an CVVL system to study the effects of EIVC. Three main factors that deteriorated combustion stability when applying EIVC were denoted: lower gas temperature in the end of compression stroke, weaker in-cylinder gas motion, and low residual gas backflow to the intake ports. Twin spark plug design was used to overcome idle combustion stability problem. The same problems regarding combustion

deterioration were found by Nagumo et al [65]. Hot wire anemometry showed that there was an initial increase in turbulence and mean flow gas velocity during the intake stroke, which decreased to very low levels during the compression stroke. This effect was further investigated through CFD simulations [66], [67] and optical flow measurements [68]–[70]. Cleary and Silvas [71] investigated an engine equipped with a CVVL system and reported that minimum valve duration and maximum lift with advanced IVO position was required to minimize fuel consumption. Due to the lower effective compression ratio caused by the EIVC, Shiga et al [72] highlighted the possibility of increasing the compression to achieve even higher engine efficiency. Some of these works used partial throttling with valve overlap to retain residuals in part load operation.

Ojapah et al [73], [74] characterized the particulate emissions of E0, E15 and E85 fuels at 3.2 bar IMEP for EIVC and other valve strategies. For E0 and E15, particulate emissions were lower for the EIVC compared to conventional throttled SI operation while for E85 the opposite trend occurred. The given explanation was that for E85 there was higher charge inhomogeneity due to longer injection durations. This also resulted in higher CO emissions. Even then, E85 provided better engine efficiency compared to the other tested fuels.

More recently, EIVC have been applied in turbocharged downsized engines in order to improve engine efficiency by partial dethrottling [42]. In some works, low lift/duration (EIVC) shown better potentials for fuel improvement than the long lift/duration (LIVC) camshafts [75]–[77].

2.2.3.2. Late intake valve closure (LIVC)

This method consists on delaying the intake valve closure several degrees after the BDC. This results in charge backflow to the intake manifold. In order to enable WOT operation with LIVC, intake valve closure should occur when enough charge is trapped inside the cylinder for the desired load. Automotive industry already takes advantage of this concept in engines with only intake cam phasing technology. The conventional 220 CAD to 240 CAD intake profile duration is enough to partial dethrottle the engine if the IVO is set to near TDC. Thus, IVC will occur from 30 to 50 CAD ABDC, or even more delayed [78]. At higher loads, the advance of the camshaft towards the exhaust stroke, which increases the valve overlap, enables better scavenging and higher volumetric efficiency.

When using LIVC, valve flow losses may increase the pumping work at higher speeds during early compression phase [79] and partial throttling would be suited for operation at some loads (especially low loads). Part load efficiency gain could be overcome by low compression ratio with the increase in engine speed due to limited time for gas backflow, which would require delayed LIVC periods. As mentioned in [53], [70], near idle operation with LIVC would require a spark advance before the IVC in order to increase peak in-cylinder pressure and temperature for stable combustion due to very low effective compression ratio.

Sellnau and Rask [80] compared different unthrottling strategies by valve actuation. LIVC showed good potential in reducing pumping work and reducing NOx emissions while increasing volumetric efficiency at low RPM. Lower knock tendency and longer combustion duration were also reported due to lower combustion temperatures [81]. This has been used in turbocharged engines to reduce knock tendency at higher loads [82]. When using high knock resistance fuels as ethanol, higher than conventional compression ratios should be used in order to benefit from the knock tendency reduction from the LIVC strategy [83].

Experimental [68] and CFD works [67] shown that with LIVC there is still tumble maintenance during the compression stroke and the promotion of higher turbulence in the end of compression stroke. This helps in accelerating the flame development process when compared to EIVC. Another important point stated in this study is the lower charge heating from the cylinder walls process during the compression stroke due to lower flow field mean velocity, which affects combustion stability. [84] also stated that intermediate LIVC periods (60 CAD to 100 CAD) were found to decrease ignition delay due to increased turbulence levels.

Comparing EIVC and LIVC, the later would be more suitable for turbocharged engines instead of EIVC because it requires less intake pressure [85] to enable same load operation. In the other hand, EIVC has been found to be more suitable for naturally aspirated engines operating at part load and WOT [86]. Even then, all assessed works regarding LIVC have shown fuel consumption gains compared to conventional SI throttled operation cam profiles.

2.2.3.3. Positive valve overlap (PVO)

Another method to dethrottle the engine is positive valve overlap. PVO has been used extensively by the industry in engines with cam phasing technology. It enables charge

dilution by two methods: advancing the IVO (early IVO - EIVO) before the TDC or delaying the EVC (late EVC – LEVC) after the TDC. In both methods there is burned charge backflow. When using EIVO during the exhaust phase, higher in-cylinder to intake system pressure pushes burned gas to the intake ports, which are further admitted to the cylinder during the intake stroke. Conversely, when using LEVC, the higher exhaust to cylinder pressure pulls exhaust gases back to the cylinder during the intake stroke. In both cases, there is the need for intake partial throttling, otherwise the pressure difference between the cylinder and intake system or exhaust and cylinder will be too small and the inertial effects of the flow will make the method ineffective.

The use of PVO can be very effective in increasing RGF which may led to lower NOx emissions but directly influences engine stability and THC emissions [87]. Asymmetrical valve overlap has been shown to modify the amount of RGF and can be used to improve idle operation [88]. Because of the higher pressure difference between the exhaust and the cylinder, small overlaps with LEVC are more effective to retain more residuals[89]. In a 4 valve per cylinder engine, the use of different intake valve lifts could be used to increase burning rates and increase combustion stability with large overlaps while reducing NOx emissions [90]. Lately, PVO has been explored as a means to attain CAI and SACI combustion at higher loads because of the capability to achieve high RGF [91]–[94].

In naturally aspirated engine PVO helps to increase high end torque due to better scavenging promoted by inertial effects [95]. In turbocharged engines to improve scavenging and increase the air mass flow rate through the turbine, moving the compressor operating point away from the surge limit to a more efficient point [96].

2.2.3.4. Negative valve overlap (NVO)

The use of hot residual gas trapping through negative valve overlap (NVO) has been extensively investigated in order to promote auto-ignition in the CAI/HCCI combustion and achieve high efficiency and low NOx emissions in four-stroke SI engines [97]–[100]. In this concept, the early exhaust valve closure, before TDC, and late IVO, after TDC are the responsible effects to trap hot residuals. The early EVC traps the combustion residuals inside the combustion chamber which are further recompressed while the piston moves upward until the TDC and further re-expanded until the late IVO. During this phase, the hot gases act as a spring, returning some of the work received during the recompression in the further expansion phase.

If considering a perfect adiabatic isentropic recompression phase, the recompression work balance should be zero and the best IVO would be exactly symmetrical to the EVC. So, the pumping work of such phase would be negligible when compared to the PVO operation. The high heat transfer of the very hot recompressed residuals contributes to reduce the charge temperature and pressure. When comparing the charge state during the recompression and expansion phase at the same cylinder volume, the in-cylinder pressure during the expansion is lower, resulting in a negative pumping loop.

For unthrottled operation, the amount of induced fresh air is limited due to the presence of hotter residuals. So, the higher the NVO period (assuming that stable operation can be achieved), the lower is the maximum achievable load. The use of throttle is an effective method for load control but increases the pumping work. With the FVVT unit, it would be possible to control load both by advancing the EVC and by throttling when keeping the IVC constant.

It has been shown elsewhere that the direct fuel injection during the NVO period can result in fuel reforming. The resulting products of such process are highly reactive radicals which increase the charge ignitability in CAI operation. It has also been shown that a split injection, with only one part of the fuel been injected during the NVO, would result in higher fuel reforming and better charge auto-ignition properties [101]–[103].

2.2.3.5. Exhaust rebreathing through exhaust valve reopening

The rebreathing method through exhaust valve reopening is a different approach to increase residual gas fraction. It consists in reopening the exhaust valves during the intake stroke to promote exhaust gas backflow to the cylinder. Alternatively, there is intake re-breathing which consists in opening and closing the intake valve during the exhaust stroke to promote burned gas backflow to the intake ports. The mass of residuals is controlled by length of the rebreathing event and the interaction with other valve events. Load control can be done either by throttle or using EIVC strategy.

As discussed elsewhere [104], when the reopening occurs simultaneously to the intake event, there is more time for in-cylinder heat transfer to reduce the final charge temperature. In the other hand, when reopening the exhaust valve during the late intake stroke, the final charge temperature prior to compression is higher and higher effective compression ratio is expected, which can result in more stable combustion in

low load operation with high RGF dilution. Exhaust rebreathing results in-cylinder thermal stratification [105] and has been used to promote CAI combustion [106]–[108].

2.2.4. **Variable compression ratio (VCR)**

Another way to increase SI engine efficiency, as previously discussed, is to increase compression ratio. Unfortunately, gasoline anti-knock quality is not enough to support higher compression ratio at high load operation and spark retard is required at some parts of the map. Thus, variable compression ratio has been proposed in order to get the benefits from high compression ratio at lower loads, and lower compression ratio at higher loads. This way, the engine can operate at MBT in almost all operating points and the efficiency is increased.

Infinity (a luxury brand from Nissan) has released the first variable compression ratio engine in the market. This system is based on multi-link mechanism that changes the relative distance of the piston (at TDC) to the crankshaft centre and it can provide continuously variable compression ratio between a certain range [48]. Discrete two step VCR based on an eccentric small end connecting rod bearing [109] and based on connecting rod length variation through hydraulic pistons [110] are the most promising technologies to be implemented in the near future. Although there are benefits from the use of VCR, real life fuel economy gains of two step VCR may depend on the driving style and can be considerably lower than those found on the test bench. The gains of continuously VCR are higher than those of two step VCR, but they still linked to driving style [111].

2.2.5. **Advanced gasoline combustion modes**

Advanced gasoline combustion modes based on auto-ignition and low temperature combustion have been proposed as an alternative to increase gasoline engine efficiency. CAI (controlled auto-ignition) combustion is based on the auto-ignition of the charge due to pressure and temperature (usually in the order of 1000 K to 1100 K [104] for gasoline) similar to what happens in compression ignition engines. Homogeneous charge compression ignition (HCCI) term is normally used when the charge is homogenous (as in PFI applications) while CAI term is more general and includes inhomogeneous charge compression ignition (as in DI applications). The main advantages of the CAI combustion are the fast heat release at low temperatures which

decreases heat losses, increases fuel conversion efficiency and highly reduces NOx emissions compared to a conventional flame propagation combustion process. As CAI combustion concept is not limited by flammability limits, extreme lean and diluted charges can be used to achieve higher thermodynamic efficiency. This also leads to the possibility of reducing pumping losses due to unthrottled operation. The adverse effects of the low temperature combustion are low combustion efficiency due to increased CO and THC emissions (caused by the temperature effect in the oxidation mechanism) and high influence of boundary conditions (which result in difficult combustion controllability and transient behaviour). Due to the fast heat release rates, noise and durability are also a constraint.

Due to the conventional low compression ratio of gasoline engines to promote enough charge thermal energy for auto-ignition, three common methods have been proposed:

- Increased compression ratio: the increased compression (16.5:1 [112] and higher) leads to high temperatures in the end of the compression stroke which results in the auto-ignition of the charge. This approach is very similar to that of CI engines, and high heat release rates increase the rate of pressure rise and peak pressure, thus, CI engine hardware is required.

- Intake air heating: the increase in the intake air temperature has been proposed to reach fuel auto-ignition temperature near the TDC. Electrical heating [113] and exhaust heat recovery [114] have been proposed as strategies. One of the problems regarding intake air heating is the high-energy consumption to achieve the required start of compression temperature, which in lower loads can be of the same order of the engine produced power. Another problem is still combustion controllability, as combustion phasing is mainly controlled by boundary conditions. Thus, indirect combustion methods, as late fuel injection, and fast thermal management have been proposed to control combustion phasing.

- Hot residuals: several methods to increase hot residuals and charge thermal state have been proposed. Between them, hot external EGR introduction in the intake manifold can be implemented in conventional gasoline engines. Valve timing based methods as PVO [92], NVO [60], [98] and ER [112] have been extensively studied. For both external and internal hot residual methods, the

transient response of the engine and complex combustion control is still a challenge.

Up to now, the automotive industry has not been capable to provide a single four stroke gasoline CAI engine due to the necessary technological advances in control and after treatment systems which makes such engines not cost effective. Mazda has promised to launch a CAI/HCCI engine on the market in 2018, which may be a game changer for gasoline engines efficiency [115].

An intermediate step between CAI combustion and SI combustion is the so called spark assisted compression ignition (SACI) [98], [116]. In this combustion mode combustion control is achieved using a spark. Like what happens in knock phenomena, the compression of the end gas increases its temperature until it reaches the auto-ignition state. Thus, flame deflagration combustion is accelerated and there are gains in thermodynamic efficiency.

In SACI combustion, the heat release rate during the end gas auto ignition is kept at acceptable levels using residual gas charge dilution. Similar approaches to those of hot residual gases to achieve CAI/HCCI have been used [94], [116]–[118]. Due to the spark control, charge composition is constrained by flame propagation limits, but considerable efficiency gains can be achieved even at stoichiometric operation due to a faster combustion at lower temperatures. This combustion mode has also been proposed as mode switch strategy between SI and HCCI and to extend the pure HCCI operation range.

2.3. Bioethanol

2.3.1. Social, economic and environmental aspects

First generation bioethanol is produced from fermented sugars from different agricultural food crops: wheat, maize (corn), triticale, rye, barley, sweet sorghum, sugarcane, sugar beet, cassava, and others. The main production steps for ethanol production from cereals are milling, saccharification, fermentation, distillation and dehydration. If the ethanol is produced from sugar syrups (molasses), a by-product from sugar refining process, only fermentation, distillation and dehydration processes are further needed.

There are many distinct coproducts during ethanol production depending on the crop used. For certain grains, as wheat and corn, there is still around 5% of starchy material bonded to other molecular structures that still cannot be converted to shaccarose. This starchy material and other solubles that have not been converted during the ethanol production process are further sold as DDGS (Distiller's Dried Grain and Solubles), used for animal feeding [119]–[121]. In the so called dry-milling, only DDGS are sold as co-products while in the wet-milling process different parts of the grains are separated and more value is added in form of different products.

In sugar-cane ethanol production, the residual cane bagasse can be burnt in furnaces to generate steam. This can be used to suppress all ethanol plant power requirements when applied in steam turbines and even generate some electrical power surplus to be sold in the main grid [122], [123]. In addition, the resulting liquid residues from sugarcane ethanol production (vinasse) sugarcane can be used in biodigesters to produce biogas for heating and electricity generation [124]. The same happens in some cassava plants where biogas is produced during the fermentation process or when production residues are used in biodigesters [125][126]. Even the CO_2 emission released in some production phases can be bottled and sold as a coproduct for industrial use.

Summed to this, nowadays energy expense in ethanol production has been cut in half compared to 1980 [125]. Distinct aspects are related to the efficiency increase with the process integration of the ethanol production phases playing a major role. The production energy reduction itself is a great benefit but the implied reduction of fossil fuels (gas and coal mainly) usage increases even more the bioethanol sustainability.

Moreover, the agricultural activity designated to supply the ethanol chain production poses as great opportunity for social development due to job vacancies generation. The variety of crops that can be used for ethanol production enables the use of lands with topographical limitations for high quality food crops. While a big share of the production would go to food chain production, the production surplus can be employed in ethanol production. This method can be employed in developing countries to decrease external oil dependence, incentive the agriculture, industrial and commercial local activities, and even attract investment from abroad [127]–[130]. Lately, with the higher concern of local bioethanol production new studies have been conducted regarding economic viability of small-scale local ethanol production [129], [131], [132]. Not only the energy security of the countries can be increased using distinct bioethanol production models but also social and economic regional aspects can be enhanced.

Thus, several aspects motivate the transport sector to the promotion of energy matrix change from fossil fuels to renewable biofuels such as ethanol. In Brazil, the Pro-Álcool program promoted internal energy security and incentives to agricultural and industrial sectors connected to the sugarcane market in the 1970s as an answer to the first oil crisis and international sugar prices fluctuations [133], [134]. As a legacy of this programme, Brazil had E100 dedicated fuels during many years until the early 1990s. Nowadays, flexible fuel (FF) SI engines are present in the great majority of Brazilian cars and the customer can chose between hydrous ethanol (E95W05) or gasohol (E27) [135]. Even though the great majority of the FF SI engines accept any mixture of gasoline and ethanol, some can also run on natural gas (gasoline/ethanol mixtures or natural gas) [136].

USA also implemented tax credits to ethanol production in the late 1970s for the following reasons: to overcome international oil dependency [137]; to support the corn agricultural sector; due to growing environmental concerns regarding gasoline anti-knock additives (leaded gasoline). After 2005, USA government policies promoted huge ethanol production growth [138]. These actions promoted USA as the larger global ethanol producer in the following years, as shown in Figure 2.6. Nowadays, policy mandates require a minimum of 10% of ethanol in US gasoline (E10) but E15 is available in 28 states and E85 is expected to be available in 21 states by the end of 2017 [139].

As shown in the Figure 2.6, global ethanol production has doubled in the last decade, and more countries are promoting ethanol sector business in order to reduce GHG emissions and replace fossil fuels. Most of EU countries have committed to adopt E10 by 2020 [140], [141]. Actually, E5 is the most popular ethanol gasoline fuel blend in EU, with E10 available only in Belgium, Finland, France and Germany. Important markets as China and India intend to promote E10 mandates for 2020, with local intermediate mandates taking place. Most Latin America countries have mandates between E5 and E10, with the important market of Mexico with an E2 mandate taking place and an E25 mandate in Paraguay [142].

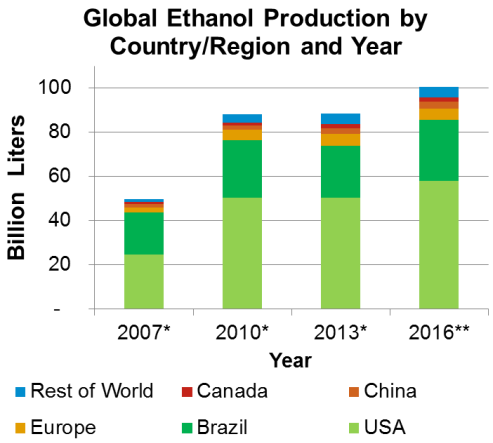

Figure 2.6. Global ethanol production by country/region and year, adapted from *[143] and **[144].

Even then, some caution must be taken in the land usage change for ethanol production. It is not desirable that land used for food production is turned to land for ethanol crop production. Also, natural resource areas including water and biodiversity must be highly considered when opening ground for plantation. When areas that has net sequestration of carbon are converted to plantation for bioethanol production, greenhouse gas emissions from this crop source would be even greater than the gasoline's [121], [129], [145]. Moreover, the recuperation of degraded lands (lands which must be restored due to contamination or soil degradation and cannot be currently used for agricultural production) and lands not being productive for long periods to be used in biofuels feedstock production is being encouraged by governments worldwide in distinct sustainable methodologies applied to each region, with distinct incentives and regulatory policies [141], [146], [147].

First generation ethanol GHG emission reduction compared to fossil fuels occurs mainly because during the agricultural crop plantation phase CO_2 is absorbed from the atmosphere due to photosynthesis. This contributes to reduce ethanol life cycle greenhouse gas emissions and increase the air quality. In the other hand, during fossil fuel life cycle, new CO_2 which was trapped in oil form, is released in atmosphere both in the drilling, refining and combustion process [121].

Many studies have been published comparing the CO_2 emission from ethanol and fossil fuels on its life cycle. For biofuel GHG emission life cycle analysis, other higher impact gaseous emissions such as nitric oxides and methane were considered, not only from the fuel burning phases but also from the fertilizers used during crop harvesting. Even then, studies claims that ethanol life cycle pollutant gaseous emissions from distinct

feedstock are reduced compared to fossil fuels, as shown in global reports presented in [147]–[149]. Table 2.1 presents well to tank (WTT), tank to wheel (TTW) and well to wheel (WTW) CO_2 equivalent emissions for ethanol and gasoline blends and diesel. It is important to note that WTT emissions are representative of the fuel production process. In the case of ethanol blends, the variations represent the production pathways. The negative values represent CO_2 emission absorption. Thus, depending on the ethanol production pathway it is possible to achieve near zero GHG balance when accounting the whole biofuel life cycle (WTW). It is important to emphasize that the emissions difference in the fuel utilization (TTW) when comparing E100 and E0 is similar and the main benefits are resultant from fuel production pathways. Even when comparing WTW worst ethanol production pathway to WTW conventional gasoline emissions, the fossil fuel results in higher GHG emissions. Nevertheless, ethanol usage is still linked to its production price, which is directly related to the energy consumption during the whole biofuel production cycle.

Table 2.1. WTT, WTW and TTW GHG emissions (CO_2 equivalents) for a selection different biofuels for 2010, adapted from [149]

Fuel	WTT g CO_2 /km	TTW g CO_2/km	WTW g CO_2 /km
E100	-127 to 30	146	19 to 176
E85	-82 to 29	143	61 to 171
E20	6 to 28	148	154 to 176
E10	17 to 28	150	166 to 178
Gasoline (E0)	29	156	185
Diesel	25	120	145

Other production pathways using nonfood crops would be able to provide more benefits regarding GHG emissions, no food competition, land usage change, between others. Second generation ethanol which is based in lignocellulosic nonfood crops and residues (such as wood industry waste, and corn and rice straw) conversion into sugar is a promising pathway in order to reduce ethanol competition to food and manage some industrial waste. The main problem is still the enzyme-based lignocellulose-to-ethanol process which is considerably more expensive when compared to the actual first generation ethanol production cost [138]. Third generation biofuels based on algae would also have the advantage of using non-arable lands, reducing land use competition [150]. More recent technologies which sequestrate CO_2 from the environment air and transform it into ethanol are the base of fourth generation ethanol.

Recently, scientists developed a catalyst made of carbon, copper and nitrogen and applied voltage to trigger a complicated chemical reaction that essentially reversed the combustion process [151]. Thus, CO_2 present in air was directly transformed into ethanol. While first generation ethanol industry is well established, second generation is still facing economic problems, although very promising. Third generation ethanol faces the same economic problem, with young technology and feedstock competition with the pharmaceutical industry which is much more profitable.

2.3.2. **Impacts of using ethanol in SI engines**

When applying ethanol to SI engines there are several aspects to be considered that contribute to improved engine efficiency. Ethanol has higher RON and MON than conventional gasoline which reduces knock tendency at higher loads and improves combustion phasing. This also provides chance to increase the compression ratio of dedicated ethanol engines compared to gasoline ones.

Additionally, ethanol has 2.6 times higher latent heat of vaporization (HOV) than gasoline per unit of mass and 4.2 times higher latent heat of vaporization for a stoichiometric mixture [152]. This reduces the charge temperature and may increase volumetric efficiency at WOT. In ethanol DI (EDI) engines, this helps in reducing knock tendency and extending MBT operation range. For this reason, GPFI and EDI SI concepts have been proposed. On the other hand, ethanol also presents higher Reid vapour pressure and its evaporation occurs at 78°C, while the different gasoline contents provide a distillation curve starting at around 30°C and finishing at near 200 °C. These properties decrease ethanol cold start capability and can result in higher oil dilution.

Ethanol combustion is faster than gasoline due to higher laminar flame speed, and occurs at lower temperature due to formation of more water molecules [152]. This increases the burned gas heat capacity and reduces combustion temperature. There is lower exergy destruction in ethanol combustion than in gasoline combustion due to lower temperature combustion and simpler molecular form. Thus, fuel energy is more efficiently converted to work [11]. For stoichiometric combustion and similar charge energy content, ethanol combustion produces more burned gas molecules and due to the oxygen presence in the molecule, ethanol presents higher EGR dilution tolerance (easier to oxidize).

Conversely, ethanol's lower heating (26.9 MJ/kg) is lower than that of gasoline (42 to 44 MJ/kg). This results in higher volumetric fuel consumption when using ethanol only. On the other hand, the neat heating value per unit of air (stoichiometric mixture) is almost the same for ethanol and gasoline. Thus, there would be the same amount of input energy when using the different fuels for the same amount of air. The higher volumetric fuel consumption of ethanol is partially compensated by higher engine thermal efficiency operation due to ethanol better combustion phasing at high loads. Higher HOV reduces combustion temperatures, thus less fuel enrichment is required to protect after treatment system. In this way, downsized engines with increased compression ratio using intermediate ethanol gasoline blends (E30) can have similar volumetric fuel consumptions due to the ethanol thermodynamic advantages [153].

A problem to be considered when using ethanol is its corrosive nature. This may cause premature failure of fuelling system and special coating and different materials are required compared to commercial gasoline [154]. The conventional water content present in hydrous ethanol fuel (around 5%) also aggravates metallic corrosion problem [155].

Regarding ethanol engine-out gaseous emissions, the increase in ethanol-in-gasoline port fuel injected content resulted in reduction of non-methane hydrocarbons (NMHC) and CO, while aldehyde emissions and unburned ethanol increased considerably [156]. In direct injection engines, THC emissions can be higher for higher ethanol-in-gasoline contents. This is explained by the longer injection duration to supply higher volume of fuel which may result in fuel impingement, and lower combustion temperature due to higher HOV. Even then, ethanol does not produce benzene and butadiene emissions (considered as highly toxicity emissions) as in gasoline, thus, it considered as a cleaner fuel [152]. In general, NOx emissions are reduced when using ethanol compared to gasoline [157]. This occurs due to the NOx formation mechanism which is highly dominated by temperature. In the case of knock limited gasoline combustion, ethanol anti-knock behaviour led to higher in-cylinder pressure and temperatures due to better combustion phasing. This may result in higher NOx formation at a certain point [158].

2.4. **Wet ethanol**

According to [159], fuel ethanol production can be described as a five-stage process: raw material pre-treatment, hydrolysis, fermentation, separation and dehydration, and wastewater treatment. After fermentation phase, ethanol-in-water content

conventionally varies from 6% to 12% [160]. As ethanol and water form a completely miscible azeotropic mixture, distillation can be used to separate ethanol from water until 96% (v/v) ethanol purity. This mixture is called hydrous ethanol, and used as automotive fuel in Brazil. Thus, while for some works presented in literature this is treated as E100 fuel, in the current work it will be treated as hydrous ethanol (E95W5) to differentiate from the anhydrous ethanol (E100 with higher than 99.1% of ethanol v/v) used in the context of the tests.

To obtain higher ethanol-in-water contents, further dehydration is still required. Conventionally, extractive distillation using ternary azeotropic mixtures are used by the addition of benzene, heptane, cycloexhane, or other hydrocarbons to the ethanol/water mixture. The new azeotrope boils at lower temperature than the ethanol/water azeotrope separating the hydrocarbon and water from ethanol at high energy cost [161]. A more modern method consists in the use of molecular sieves with zeolite material [162]. This technique is based on hydrophilic zeolite material which contains big enough pores to absorb water molecules (2.8 Å) but smaller than ethanol molecules (4.46 Å) which are separated. Comparatively, the molecular sieve energy expense is lower than that of the extractive method but the initial costs are higher. Thus, ethanol-water separation processes (distillation and dehydration) are the most energy intensive process in the ethanol production steps.

One of the characteristics regarding the distillation process is the exponential increase in the energy expense during distillation after 80% ethanol-in-water content after [160], [163]–[167]. This trend is demonstrated in Figure 2.7, which was adapted from several sources. Many researchers proposed the use of wet ethanol with higher water content rather than that of hydrous ethanol to reduce fuel production cost. As shown in Figure 2.8, for USA corn ethanol scenario, a considerable WTT energy gain could be expected if possible to use wet ethanol instead of anhydrous ethanol. Even though the data shown in Figure 2.7 gives a good indication of the distillation process and Figure 2.8 shows the possible benefits of using wet ethanol, increases in process optimization and new technologies may change this trend. Thus, distillation data from [163] would result in more benefit for higher water content wet ethanol while for the [165]*** scenario, it would not be economically viable to stop distillation before 90% of water-in-ethanol.

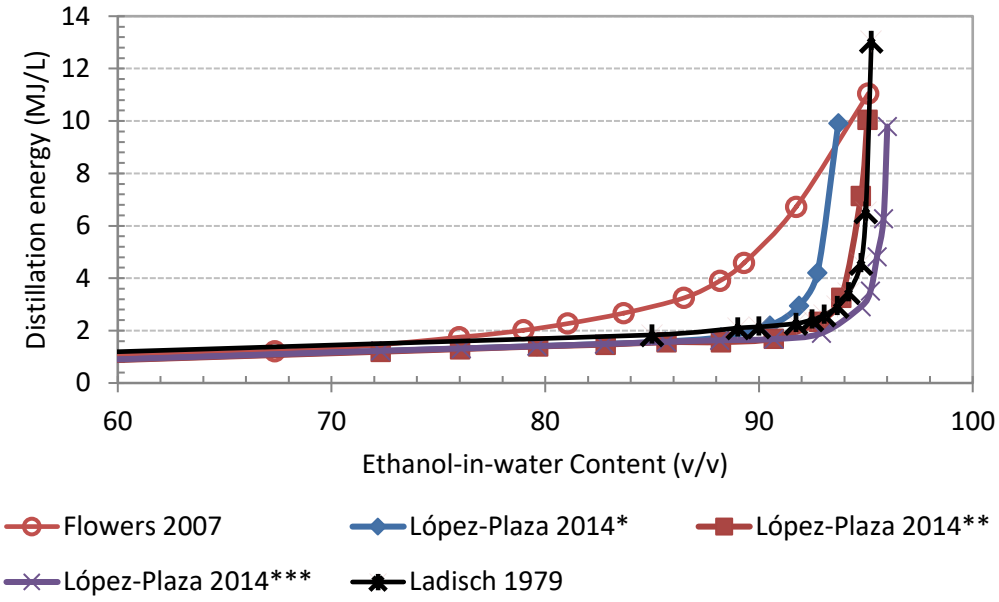

Figure 2.7. Ethanol distillation energy per litre. Number of Distillation Stages: * 8 stages; ** 12 stages; *** 19 stages. Adapted from [160], [163], [165].

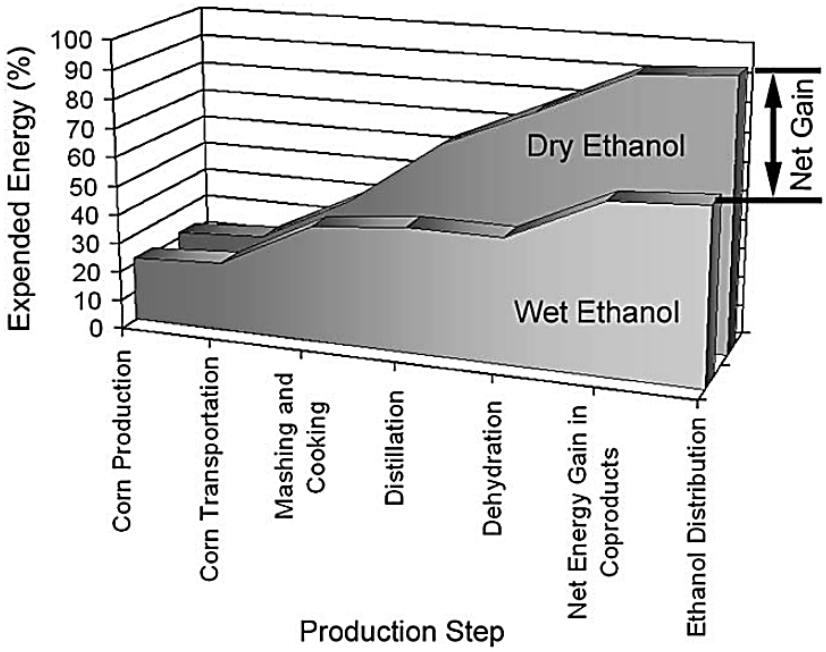

Figure 2.8. Comparison of net energy balance for anhydrous and wet ethanol (E65W35) taking in account all ethanol production steps [164].

Other ethanol production data worldwide were taken into account in order to find the possible WTT advantages in other scenarios worldwide. For the Brazilian scenario, ethanol production based on three different crops on corn [168], sugarcane [169] and

cassava [170] was found in the literature. For Asian scenario, a cassava based ethanol production was found [125], and for USA scenario, three corn based scenarios were taken into account [163], [171]. All data used are presented in Appendix 1. For exemplification purposes, data from [169] is presented in Table 2.2. As most data presented crop production energy expense in MJ/L of ethanol produced, and crop to ethanol conversion energy expense (industrial conversion energy expense), tables were separated accordingly. If only distillation energy was available (without separation between distillation and dehydration), as in the case of [169], it was considered that 62.2% of that energy was spent during distillation and 37.8% of that energy was spent in dehydration as presented by [171]. The energy expense to water-in-ethanol content ratio data was taken from [160]. The main objective of this evaluation was not to find the exact energy gain value possible to achieve when using wet ethanol, but to build a map showing in which scenarios and how much of water-in-ethanol would be suitable for an optimized energy cost to fuel energy ratio.

Table 2.2. Energy expense for sugarcane ethanol production in Brazil [169].

Salla 2009 [169]		
Sugarcane Ethanol		
Sugarcane Plantation		
Sugar Cane Crop Production Phase	**Energy Expense (MJ L^-1)**	**% Energy expense**
Area preparation	0.1	0.47%
Plantation	0.1	0.47%
Agricultural inputs	0.9	4.21%
Crop maintenance	0.3	1.40%
Harvesting	0.3	1.40%
Transport to industry	0.2	0.93%
Energy depreciation	0.1	0.47%
Sub Total	**2**	**9.35%**
Ethanol Production phase		
Milling	0.7	3.27%
Hydrolisis / sacharification / broth treatment	13.8	64.49%
Fermentation	0.1	0.47%
Distillation	**4.7**	**21.96%**
Machine Maintenance	0.1	0.47%
Sub Total	**19.4**	**90.65%**
Total	**21.4**	**100.00%**
ETHANOL ENERGY / PRODUCTION ENERGY	**0.99**	

Applying the distillation and dehydration energy expense as function of the ethanol-in-water concentration to the energy expense in production it was possible to estimate the energy savings of each proposed scenario (shown in Appendix 1). Dividing fuel LHV by total energy expense in fuel production (TEEFP), it was possible to build trend lines showing the relative energy gain for each wet ethanol composition, as shown in Figure 2.9. All scenarios showed energy gains for ethanol-in-water contents over 85%. The net energy gain is not higher in many cases because co-products were not accounted. Even then, from this figure it can be implied that wet ethanol containing between 10% to 15% of water content would result in the near maximum energy gain for most scenarios.

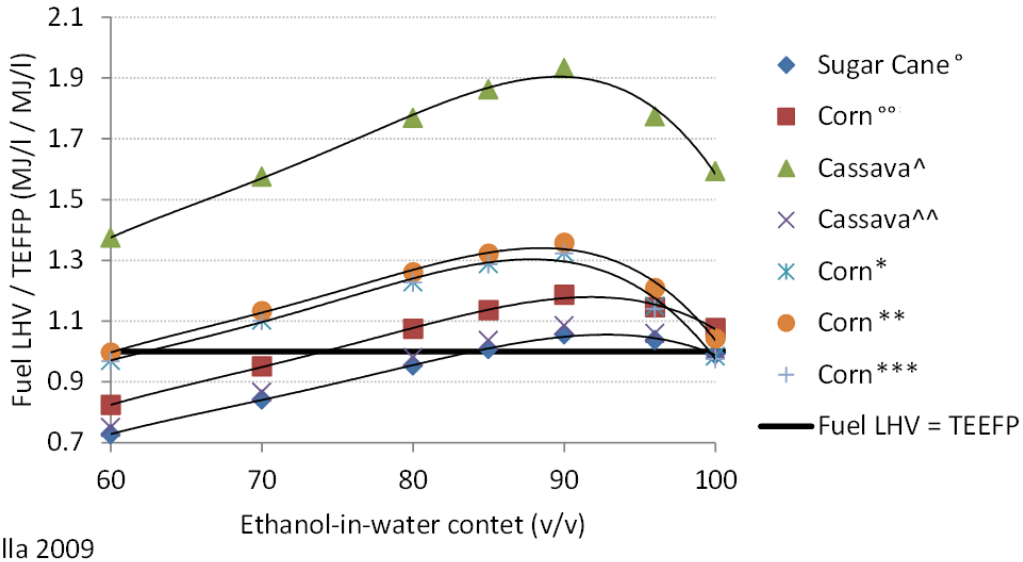

° Salla 2009
°° Salla 2010
^ Salla 2008
^^ Dai 2005: Considering the distillation energy fraction equal to Salla 2008.
* Flowers 2007
, * Shappouri 2002, dry and wet milling respectively
Total energy expended in fuel production (TEEFP)

Figure 2.9. Fuel LHV to total energy expense in fuel production (TEEFP) ratio for distinct ethanol-in-water content and different crops production scenarios.

The data presented by the trend Shappouri** [171] was used by the author to evaluate the potential energy reduction in the wet ethanol utilization when also accounting the engine usage inefficiencies caused by the higher water content [172]. Different ethanol-in-water concentrations and different air/fuel ratios were tested. Figure 2.10 presents the final results regarding the normalized operating costs which are the application of a

normalized production cost to the engine fuel consumption for tested scenario. From these results, the energy operational cost is minimized when operating the engine with wet ethanol with water content between 10% and 20%.

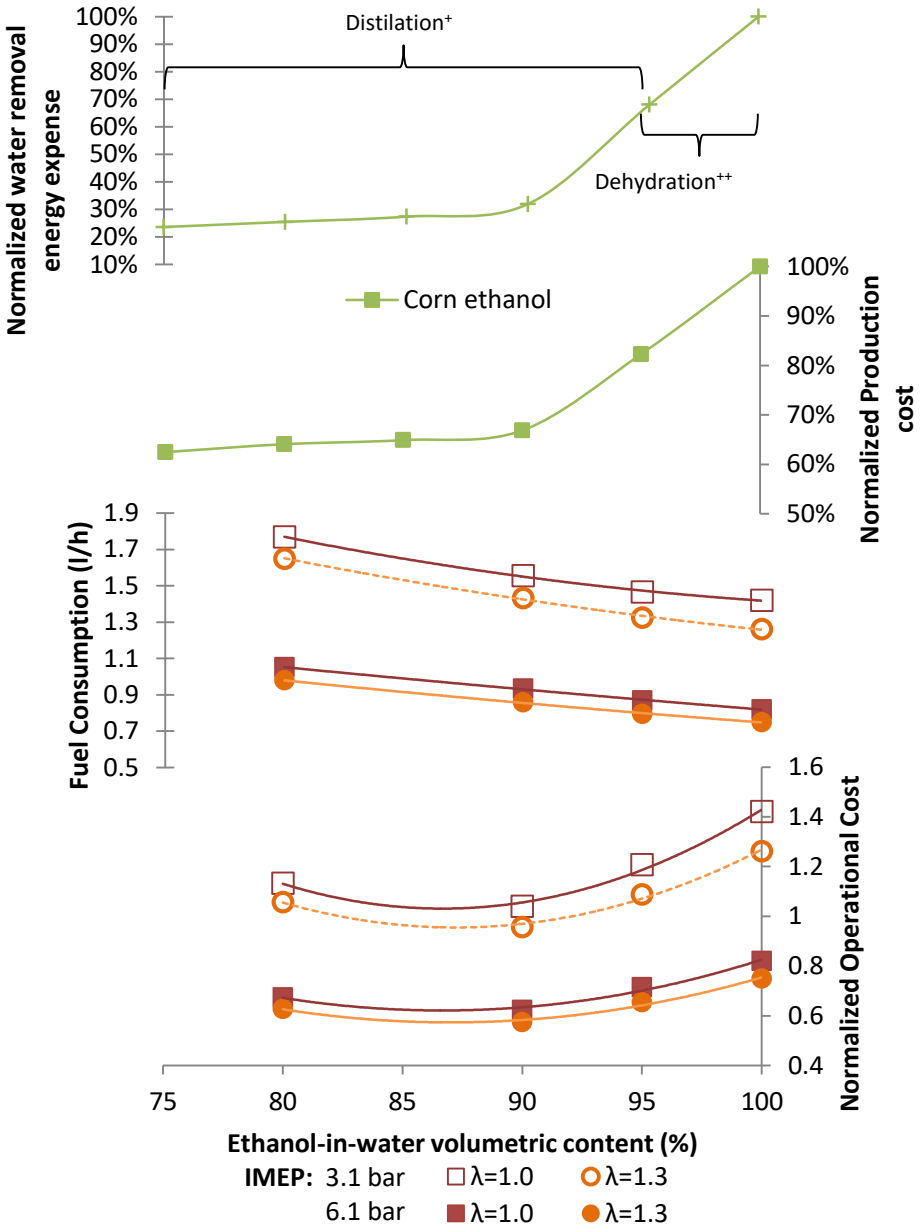

Figure 2.10. Wet ethanol production and usage cost as function of the ethanol-in-water volumetric content. +[160]; ++[163], adapted from [172].

A more detailed study [173] considering industrial process optimization approaches for wet ethanol production showed that at 86 wt% of ethanol (around 90% v/v) the energy consumption would be optimized leading to around 10% energy savings. The monetary saving could be around 8% as well as the ethanol refinery CO_2 emission reduction.

2.4.1. **Wet ethanol application in SI engines**

Previous works related to wet ethanol are presented in this section. Hydrous ethanol works (E95W5) are not presented due to the low water content and high amount of literature for such topic.

The application of wet ethanol in internal combustion engines have been reported since before the Second World War as described by Wiebe and Porter's report of 1949 in the US scenario [174]. During the second world war, due to the low octane gasoline used, wet ethanol was injected in the intake system of aircraft engines to decrease charge temperature and reduce knock tendency. This allowed momentarily power boost used during take offs and dogfights. Automotive application of wet ethanol for knock mitigation during acceleration and full throttle operation was investigated in this report. The increase in gasoline octane rating was highlighted one of the most important factors to increase engine efficiency. In such a scenario, power output was limited due to the low octane gasoline used (reported to be from 77 and 86 RON). The use of alcohol-water mixture injection in the intake system was shown to enable the use of higher engine compression ratios. The result was better fuel economy and higher power output. Another important point highlighted was the possibility to operate the engine with higher spark advance, which also increased the fuel economy and power output. Such studies were motivated by the fast increase in oil demand which could be reduced with the use of more efficient vehicles.

Reports from the 1980s in the US [175], [176] present results from an unpublished report of Deardorff (1979) with engine thermal efficiency of a six-cylinder in line engine gasoline engine running on different wet ethanol mixtures. Carburettor jet nozzles were modified the enable operation with ethanol as well as spark timing adjustments. A charge heater was also used. Water-in-ethanol content of 10% provided the best engine thermal efficiency but the generated power per unit of fuel volume decreased considerably due to lower heating value of ethanol-water mixtures.

A catalytic igniter technology was used in order to promote the combustion of wet ethanol with 30% of water content [177]–[179]. Different engines were tested during the project. Initially a small engine was modified to operate with wet ethanol and later the system was tested in a demonstrator vehicle. The catalytic igniter was installed inside a pre-chamber which propagated a torch ignition like combustion through the combustion chamber. This system was used due to reported difficulties in cold start and requirement of high energy spark systems which were not able to promote stable combustion. Considerable NOx emission reduction (around 90% at some tested points)

and higher engine thermal efficiency were reported for the vehicle tests comparing gasoline and wet ethanol at stoichiometric operation. CO emissions were reported to decrease with wet ethanol due to CO water-gas shift mechanism. On the other hand, hydrocarbon emissions increased substantially.

Brewster [180] investigated the application of wet ethanol containing up to 20% of water on a mass basis. This was investigated on a four-cylinder air-assisted direct injection (DI) turbo-charged engine at high loads (from 10 to 20 bar BMEP). It was demonstrated that wet ethanol requires more advanced spark timing. For delayed spark timing, wet ethanol produced higher exhaust gas temperature due to longer combustion duration. At MBT, wet ethanol exhaust temperature was reduced due to higher charge heat capacity. The increase in water-in-ethanol content resulted in longer flame development angle and combustion duration. Thus, there was BMEP reduction with the increase in water-in-ethanol content for different intake air pressure. Brake thermal efficiency presented a complex behaviour, but in general intermediate water content (7% water content in mass) presented better efficiency. The reduction of the in-cylinder temperature and pressure gradients showed the potentiality of water in knock mitigation. NOx was reduced and THC emissions increased with water in-ethanol content increase due to temperature related effects.

Dal Bem[181] studied the use of E75W25 (wet ethanol) and E99W1 (anhydrous ethanol) in a modified four cylinder in-line 1.0 litre flex fuel PFI engine with two compression ratios of 13.6:1 and 16.2:1 at full throttle. For the 13.6:1 compression ratio and increased water content, there was considerable reduction of power and torque with significant specific fuel consumption increase. Spark timing advance was required and exhaust temperatures were reduced. Engine thermal efficiency was slightly lower. CO and NOx emissions were considerably reduced while THC emissions doubled. Higher peak torque and power were found when comparing wet ethanol with 16:1 compression ratio and anhydrous ethanol with 13.6:1. CO and THC highly increased while NOx was reduced. Anhydrous was not run at 16.1:1 compression ratio. In-cylinder pressure sensors were not used and there were no comments regarding knock.

Several studies targeted the use of wet ethanol with HCCI combustion. Megaritis et al [182], [183] studied the effect of forced induction on ethanol HCCI combustion promoted by NVO residual gas trapping method in a four cylinder PFI engine. Wet ethanol was investigated in order to reduce pressure rise rates at higher engine loads. It was found that water reduced in-cylinder temperatures, thus, lower lambdas were required as water content increased to promote stable HCCI operation. For this reason,

pressure rise rates were not attenuated and higher in-cylinder pressure occurred resulting in higher NOx emissions. Thus, the increase in water-in-ethanol content was not effective to increase HCCI operation range.

Intake air heating has been investigated by group with participants from University of California at Berkeley and Lawrence Livermore National Laboratories. Initial simulation studies were proposed in order to use 35% ethanol-in-water as fuel in order to increase ethanol life-cycle energy gains[163]. Later experimental studies in a TDi VW four cylinder modified engine shown the possibility to operate with up to 40% ethanol-in-water mixtures when using intake air pre-heating [164]. Incomplete combustion and excessive intake temperatures limited the operating range at higher water concentration. Comparing E60W40 (40% water-in-ethanol) and E100, CO emissions increased up to 250%, while hydrocarbon emissions increased more than 10 times at some tested cases. Peak pressure was found to reduce with the increase in water-in-ethanol content while heat release remained relatively constant. Later, intake boosting was tested with the same engine and the intake heating was provided by an exhaust heat recovery system [184]. Only one cylinder was used at this time. It was concluded that the separation of the last 20% water-in-ethanol content during distillation was the more energy intensive part of the ethanol production process. For this reason, water-in-ethanol content varied between 0% and 20% (v/v) was investigated. The best operating conditions were found for higher boost pressure and high equivalence ratios. And, in a later study, optimal operating conditions were found for the same setup for ethanol-in-water content up to 70%. It was found to be a trade-off between emissions and CA50 (controlled by the intake temperature). A delayed CA50 (between 7.5 and 12.5 CAD_{firing}) resulted in very low NOx levels but increased CO and THC emissions. Even then, it was important to use such combustion phasing in order to reduce pressure rise rates and ringing intensity.

A study focused on a small SI power generators running on wet ethanol [185], [186] showed that such engine could comply with 2011 emissions regulations when using a three-way catalytic converter. At an engine load of 3.8 bar BMEP, the brake efficiency using E95W05 (wet ethanol containing 5% of water) was near 20% [186]. In addition, it had been shown that the increase in water content reduced the overall engine efficiency and increased unburned hydrocarbon and aldehyde emissions. Oxides of nitrogen (NOx) emissions were reduced by nearly 80% when the water content was increased from 20% to 40%. The catalytic converter allowed reasonable emission reduction under stoichiometric operation. Severe engine parts wearing and oil lubricant contamination were reported. No combustion analysis was presented.

Wet ethanol (E75W25) reforming with exhaust gas heating was tested in a six cylinder 5.2 litre gasoline engine [187]. The reformer was a shell-in-tube heat exchanger and reformed products were delivered directly in the plenum. The reforming reaction is highly endothermic and produced a rich H_2 and CH_4 mixture (between other components), with a higher LHV than the wet ethanol. This increased engine thermal efficiency in 6%, while reducing NOx, CO and THC emissions in 70%, 50% and 80%, respectively, when compared to gasoline fuelling. Some drawbacks were that the reforming system had to be heated with the engine running on gasoline and the system was almost of the same size of the engine itself.

Several works focussing in a pre-chamber spark ignition engine concept have been reported by the Department of Mechanical Engineering from Federal University of Santa Maria [188]–[190]. The engine used was an air-cooled naturally aspirated single cylinder 0.668 litre diesel engine with a swirl chamber. The diesel injector was replaced with a spark plug and an ethanol PFI system was installed. It enabled stable operation with water-in-ethanol contents up to 40% because the combustion initiated inside the swirl chamber and propagated to the main combustion in a torch ignition like combustion concept. These studies showed that combustion duration was increased due to the reduction in combustion temperature with the increase in water-in-ethanol content. This led to lower NOx emissions and increase in CO emissions.

A more recent study reported that wet ethanol with 10% of water resulted in a faster flame propagation combustion with a constant intake air pressure [191]. The study was performed in a single cylinder optical SI engine equipped with both PFI (port fuel injection) and DI at very low load (nearly 1.5 bar IMEP). Combustion duration increased when using water-in-ethanol fractions above 10% and shortened under PFI operation. DI operation resulted in higher level of droplet diffusion burn in the flame development images when compared to PFI operation. The optical results showed that the increase in water content decreased the flame distortion and corrugation.

In a previous work published by the author [172] on the same engine of the current work, part load (3.1 and 6.1 bar IMEP at 1500 rpm) SI lean throttled operation with wet ethanol (up to 20% water-in-ethanol content) was investigated. Direct fuel injection was tested with a spray orientation designed for in-cylinder stratification (modified for the studies presented in this thesis). Thus, high levels of CO emissions were found for stoichiometric operation. At stoichiometric condition, there was a trade-off between CO and THC emissions as water-in-ethanol content increased. For anhydrous ethanol, there was lower THC emission with higher CO emissions. As water-in-ethanol content increased CO was reduced while THC increased. This occurred due to fuel oxidation

temperature dependence. The increased water content was effective in reducing combustion temperature, thus, there was reduction in NOx emissions with the increase in water content. Adversely, the increase in water content led to higher FDA and combustion durations which deteriorated thermodynamic efficiency. Even then, it was possible to achieve stable operation at lambda 1.30 for E80W20. Indicated engine efficiency was found to decrease with the increase in water-in-ethanol content and increase for leaner mixtures due to lower pumping losses and better thermodynamic characteristics. A conclusion from this previous work was that the direct injection system strategy would need to be improved to increase combustion efficiency to reach higher wet ethanol operation efficiency.

Investigating the wet ethanol works it could be expected that the water addition to the fuel will reduce the combustion temperature due to both dilution and kinetic mechanisms. This would lead to longer combustion with a higher fraction of unburned hydrocarbons and intermediate species but lower NOx formation. The increased latent heat of vaporization of the water compared to the fuel, makes it very attractive to reduce charge temperature when using direct injection method. Care should be taken to avoid fuel film deposition when using the PFI method. On the other hand, the presence of water on ethanol increases its corrosion characteristics and may become a problem to the fuelling system.

2.5. Summary

This chapter presented a literature review of the basic four-stroke SI engine combustion process, knock phenomena, and discussed some characteristics of CAI and SACI combustion. Advanced valve timing strategies were presented and their applicability according to hardware requirements were investigated. The discussion was focused on ways to increase SI stoichiometric engine efficiency.

Bioethanol production process and its socio-economic impacts were described. The theoretical energy savings of using wet ethanol, as proposed by several researchers, in order to reduce ethanol usage production cost and footprint were presented and discussed. The impacts of using ethanol in an SI engine were presented and the use of wet ethanol in engines with similar combustion concepts to that explored in gasoline engines. A water-in-ethanol composition between 10% and 15% (v/v) was found to result in the best energy expense to fuel production energy input ratio.

Chapter 3.

Experimental setup and Methodology

3.1. Introduction

This chapter presents the test facilities used during the engine testing and the data analysis methodology. The experiments were carried out in a camless single cylinder research engine at the Centre for Advanced Powertrain and Fuels Research (CAPF) at Brunel University London, United Kingdom. This engine is capable of operating in two stroke and four stroke cycles [60]. In the studies presented here, four-stroke operation was explored. This section will present the experimental methodology, which consists of engine and test cell facilities, data acquisition system and engine parameters analysis.

3.2. Experimental setup

Figure 3.1 presents a schematic of the experimental facilities and Figure 3.2 presents the camless engine test cell (with emphasis in the single cylinder engine and the hydraulic reservoir with pump system in green). In Figure 3.1 the engine parts are presented in black; intake air parts in orange; data acquisition and control in red; the emission analyser in navy blue; engine dynamometer in yellow; fuel supply system in light blue; engine lubrication conditioning system in green; coolant conditioning system in purple. The engine was mounted on a seismic bed connected to the ground by vibration dampers. The dynamometer was composed of an alternate current (AC) dynamometer which enabled both motored and fired operation.

The air used by the engine was at room pressure and temperature. Room temperature was kept between 28 °C to 33 °C using the laboratory building ventilation system and an electrical heater (for cold days). Air humidity was measured with a hygrometer and ambient pressure was measured using a mercury column barometer. The circles with letters P and T represent pressures and temperatures, respectively, monitored and acquired during the tests. K-type thermocouples were used for the temperature measurements, while different pressure sensors (average or transient) were used according to the measured parameters, further details will be provided in the sections to follow.

3.2.1. **Engine specifications**

Table 3.1 presents the engine specifications. The engine was comprised of a Ricardo single cylinder research engine crankcase and a special pent roof 4-valve cylinder head. The valve actuation was enabled by fully variable electro-hydraulic actuators installed over each one of the valves. This enabled independent valve control over all engine operation range.

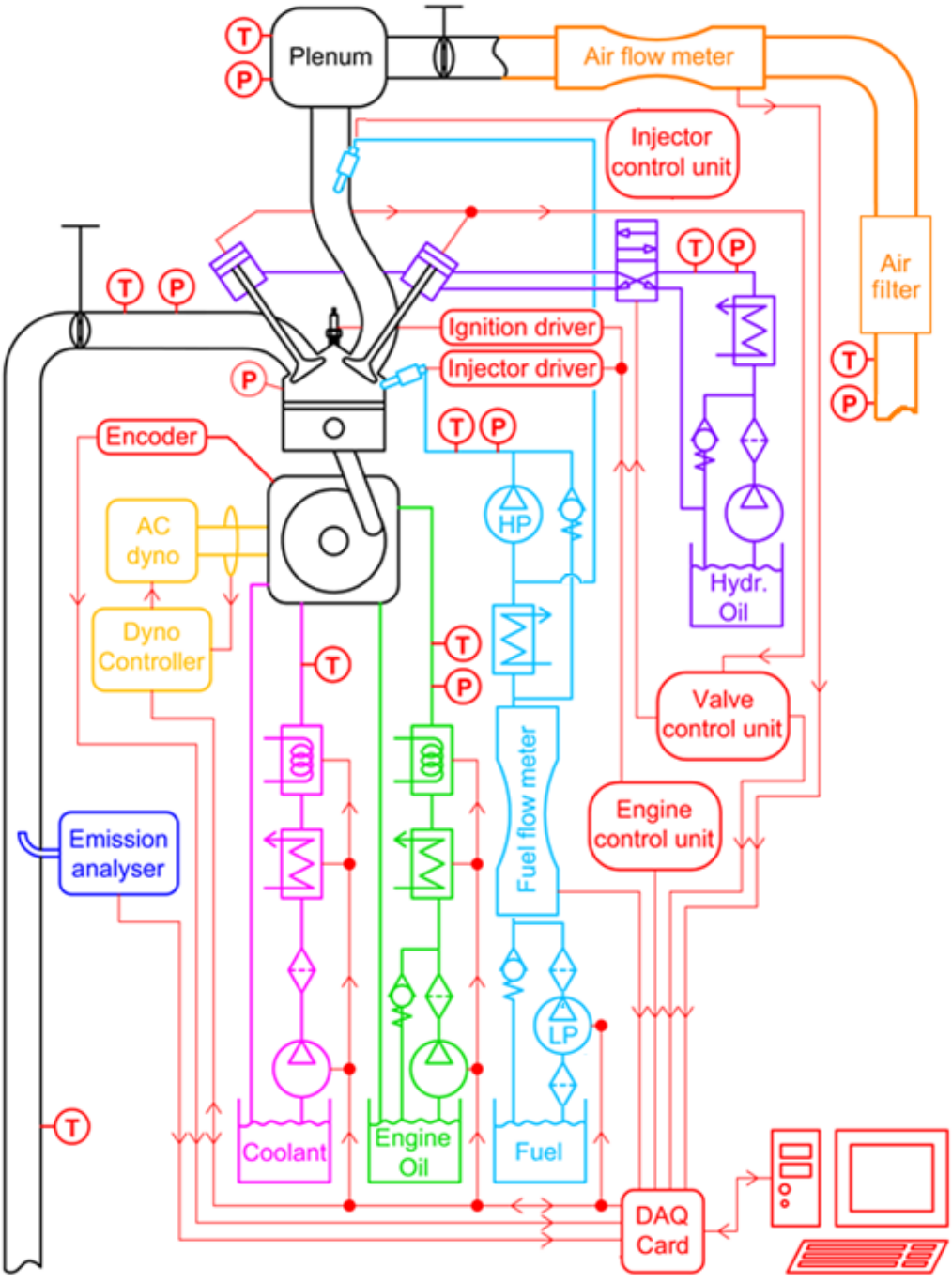

Figure 3.1. Schematic representation of the research engine and test cell facilities.

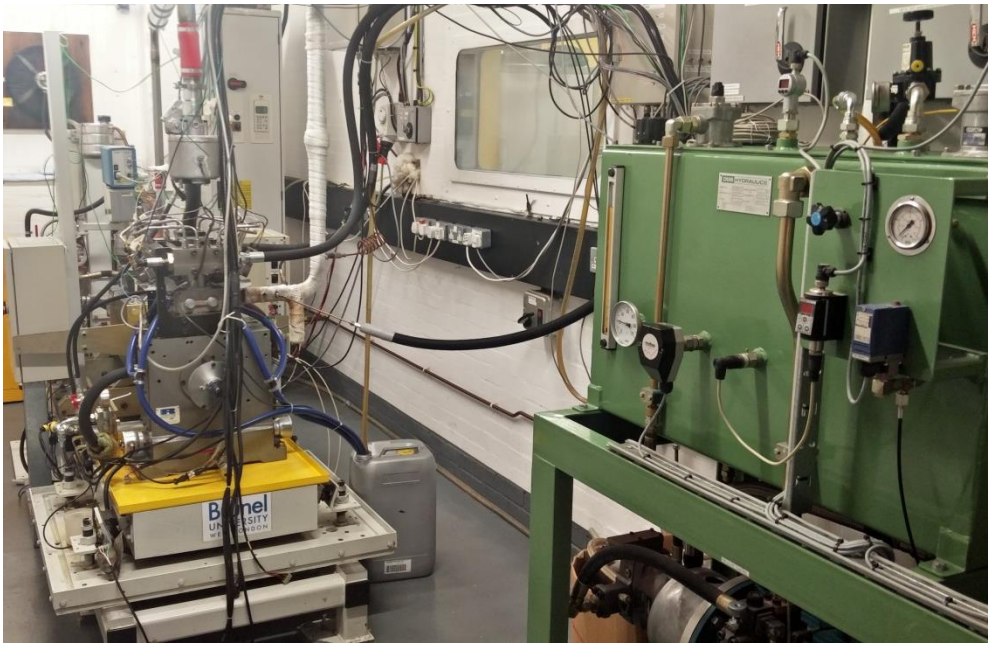

Figure 3.2. Engine test bed and hydraulic system.

Table 3.1. Engine specifications

Bore x Stroke; B/S ratio	81.6 mm x 66.9 mm; 1.22
Displacement volume	0.350 dm^3
Compression ratio	11.8 : 1
Combustion chamber	Pent roof
Connecting rod length	144.5 mm
Number of valves	4
Intake valves diameter	28 mm
Exhaust valves diameter	30 mm
Intake ports design	Reverse tumble
Max speed (four-strokes)	6500 rpm
Max peak pressure	110 bar
Average peak pressure	90 bar
Fuel supply	DI and PFI

The engine bore to stroke ratio was 1.22, which was not suitable for heat transfer. This design was chosen in order to improve two-stroke burned gas scavenging process and reduce fresh air short circuiting. The scavenging process was supported by a high intensity reverse tumble flow promoted by upward intake tumble ports design. Even though the design targeted two-stroke poppet valve operation, the high tumble was

effective in promoting turbulence generation near the combustion top dead centre in the four-stroke operation mode which accelerated combustion. The exhaust valves diameter was bigger than the intake valves diameter. The reason is that the scavenging process in two-stroke engines with poppet valves is more dependent on the exhaust system restriction than in the intake restriction (which is necessarily boosted). In addition, intake valves masks were used to reduce intake to exhaust fresh charge short circuiting in two-stroke boosted operation. This tended to increase in-cylinder heat transfer compared to unmasked valves (due to higher surface) and decreased valve flow discharge coefficient.

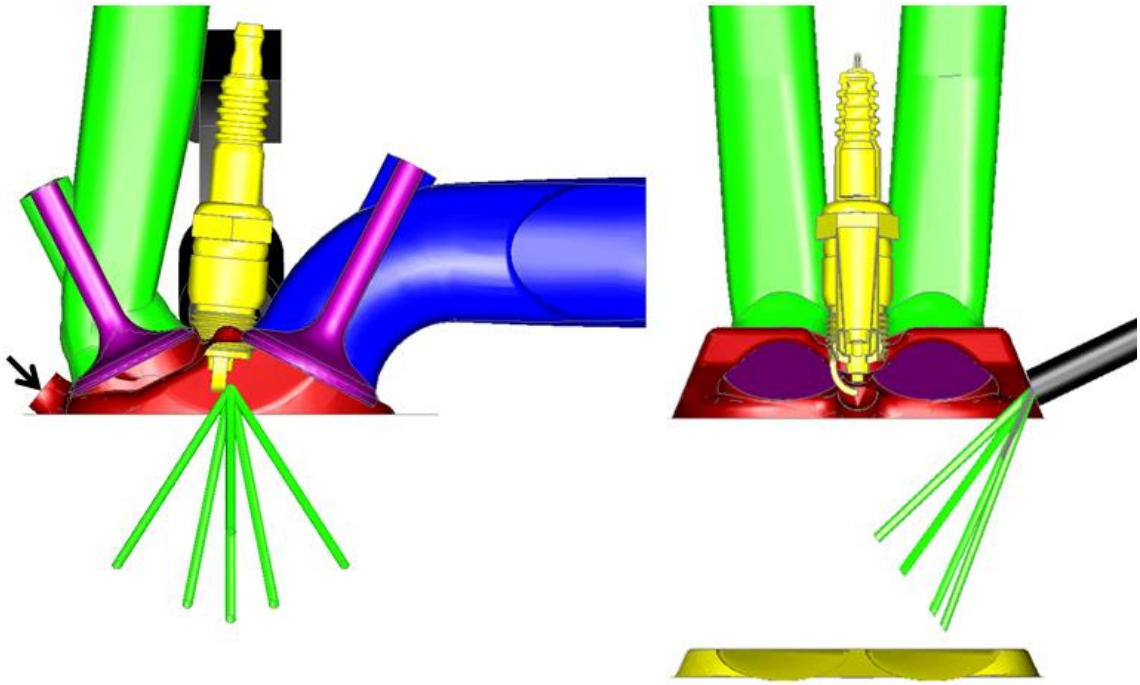

Figure 3.3. Combustion chamber, and intake and exhaust ports, and direct injection spray details.

The combustion chamber was a pent roof design with a 126° angle between intake and exhaust valves. The cylinder head presented a dome design with small pockets for the valves. Figure 3.3 presents the intake (in green) and exhaust (in blue) ports, and the combustion chamber (in red). The spark plug (Denso Iridium IXU 24) was centrally mounted with a coil-on-plug integrated ignition driver (Bosch 0 221 604 006). The six-holes direct injector (Magneti Marelli IHP 072) was side mounted, between the intake and exhaust valves. The spray pattern pointed downwards to the cylinder head.

Originally, a single slit direct injector was installed between the intake ports (pointed by the arrow), which is now replaced by an in-cylinder pressure transducer.

3.2.2. **Fuelling system**

Modifications have been made in the fuelling system with the installation of a port fuel injector. Thus, the engine could operate with both DI and PFI systems at the same time, as shown in Figure 3.1. The fuel system was comprised of the low pressure and high pressure sides. The fuel reservoir was a 15 litre aluminium tank designed for racing purposes to endure ethanol and methanol. The fuel was pumped from the reservoir by the low pressure fuel pump (LPFP) BOSCH 0580 254 044 through a 100 µm filter (with stainless steel cleanable element and magnetic debris collector) and pressurized to 3.5 bar pressure. This pump and filter were supposed to stand alcohol's corrosive effects as both were designed for racing. The first filter was installed before the fuel pump in order to protect it from any particles from the reservoir. Even then, during approximately 24 months of tests, two filter and pump sets failed due to particles formed in the fuel tank. The ethanol corrosive effect was enhanced by the increased water-in-ethanol content which attacked different parts of the fuelling system. After the LPFP, another thinner 30 µm filter was used to protect the high pressure line side from any debris from LPFP damage. The low pressure line was controlled by a spring loaded diaphragm pressure regulator. The return line was connected to the fuel reservoir.

After the LPFP, the 3.5 bar pressurized fuel passed through an Endress+Hauser Promass 83A Coriolis flow meter type, with a maximum error of ±0.2% in the flow studied range. This flow meter is based on tube induced oscillations caused by fluid flow velocity. Constant induced oscillations pulses are emitted towards the tube. Phase shifting (twisting) is measured in the inlet and outlet side as consequence of fluid inertia. A higher flow velocity would induce greater oscillating tube deflection, which was also corrected by fluid density, thus, temperature and pressure. Due to the high response rate of such equipment, it is suitable for transient flow measurements, even though the fuel flow rate was averaged to a certain number of cycles. The flow meter installation in low pressure line side avoided fuel cavitation, which reduced measurement uncertainties and flow oscillations.

The fuel flow meter was installed in a way that no fuel backflow was possible and the whole high pressure line side loop was placed after the flow meter. After the flow meter

the fuel was pressurized to up to 150 bar by a high pressure fuel pump (HPFP) Bosch 0 261 520 016 three piston @ 120° reciprocating type. The HPFP was run by an AC motor with speed control in order to keep the fuel flow rate through the pump at acceptable levels. A SUN hydraulics 0BZ9K1 pressure regulator was used to maintain the pressure at the desired levels. A Druck PTX 500 (0.3% full scale error) was installed near the DI injector to monitor the fuel injection pressure. The return line from the high pressure side was positioned before the HPFL inlet. A water cooled heat exchanger was installed between the return line outlet and the HPFP inlet to keep the fuel temperature at near ambient temperature.

A low pressure line branch positioned after the heat exchanger fed the port fuel injector (twin spray Bosh EV 14) installed between the intake plenum and intake ports. The PFI injector mounting was designed in a way that each spray cone would target one of the runners leading to each intake port, as show in Figure 3.4. The actual positioning in the engine is rotated 90° clockwise compared to the figure, thus, the sprays are downwards positioned. The PFI injector timing and pulse width were controlled by a dedicated MOTEC M600 ECU.

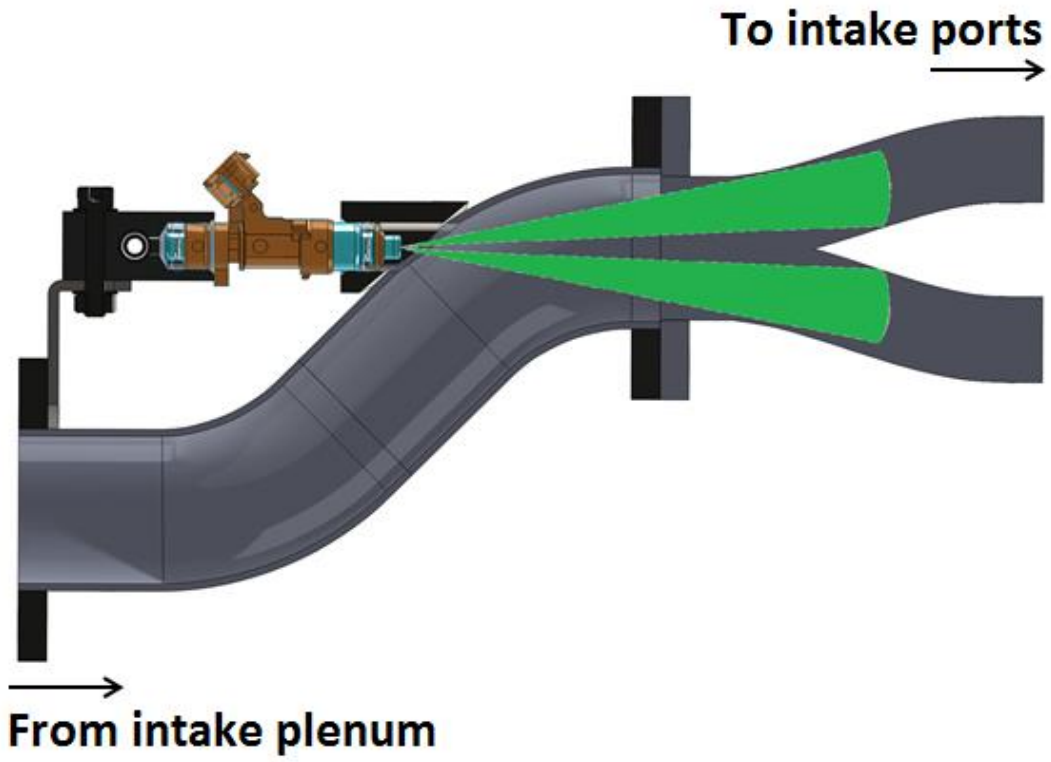

Figure 3.4. Port fuel injector schematics.

As previously discussed, the original single slit type DI injector was replaced by a multi-hole injector. This was installed between the intake and exhaust ports in the place of the old in-cylinder pressure sensor. The DI injector modifications were done during the early period of this research, with Dr. Macklini Dalla Nora [192]. Due to these modifications, two adaptors were installed to accommodate the DI injector and AVL GH15D piezoelectric transducer, which will be better described. The pressure transducer adapter was flux mounted to the combustion chamber and the pressure sensor tip distance from the combustion chamber was set accordingly to the recommended guidelines. Figure 3.5 presents the DI injector mounting. A Life Racing direct injector driver was used to control DI injector opening duration.

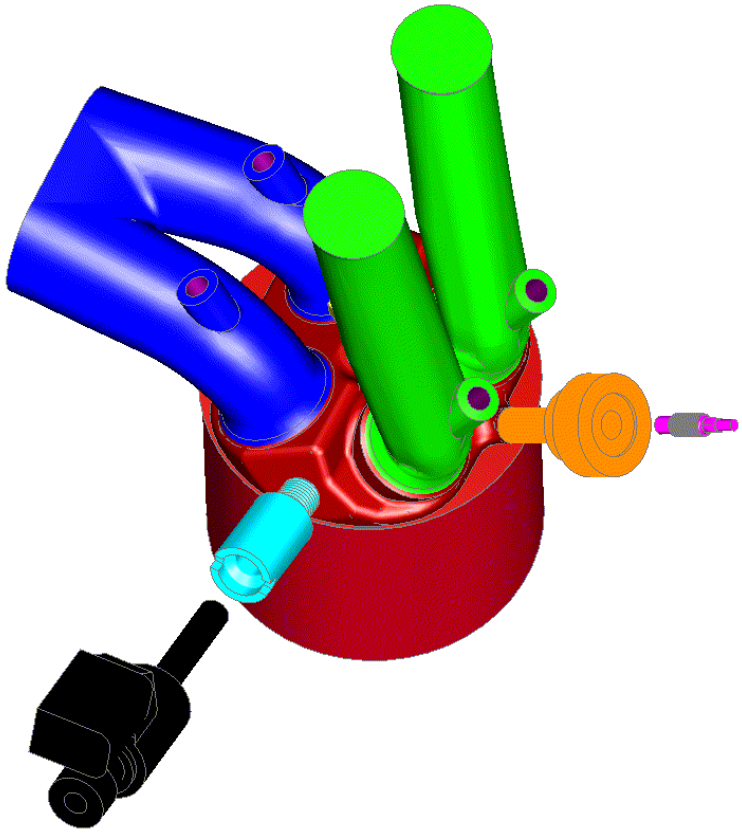

Figure 3.5. Cylinder head assembly with the Magneti Marelli multi-hole fuel injector (black) and the AVL pressure transducer (pink), besides the demanded adaptors (light blue and orange, respectively). Adapted from [192].

3.2.2.1. Fuel preparation

Cereal non-denatured anhydrous ethanol (E100) from Haymankimia (at least 99.1% ethanol-in-water v/v) was used for the splash blend wet ethanol mixtures. All tests were done with the same batch ethanol. The blends were done by mixing de-ionized water

with anhydrous ethanol, mixing the desired water-to-ethanol volume content in an ethanol appropriate container. The sum of water and ethanol initial volumes was 10 litres and the volume measurement was done using a one litre (±10 ml at 20 °C) measuring cylinder. The final mixture volume was smaller than that of the individual species due to water and ethanol molecular interaction. Also, due to measuring cylinder uncertainty and mixtures variabilities, there was some deviation from the expected water-in-ethanol mixture content, which was measured using a bulb alcoholmeter (± 1% uncertainty at 20 °C). Thus, small volumes of ethanol or water were added in order to reach the desired water-in-ethanol volumetric composition (validated by the bulb alcohol meter measurements). After this step, a volumetric flask of 250 ml (± 1 ml at 20 °C) was used to weigh the final mixture density in a 0.1 g resolution scale. The ethanol-in-water volumetric content conversion from density to volume was taken from [193] which was based on EU Directive 76/766/EEC of 27/9/1976. After the final mixture adjustments, the wet ethanol fuel was stored in appropriate containers. The fuel density was monitored online during the tests using the fuel flow meter density measurement capability. Due to the hygroscopic nature of ethanol, there was a maximum water-in-ethanol variation in order of 0.5% from the initial test value. Despite of some uncertainties involved in the fuel mixture preparation process, the expected ethanol-in-water mass content was not expected to vary more than ±2.0%. Thus, Table 3.2 show the considered values for fuels used in this work.

Table 3.2. Fuel properties

Fuel properties	Gasoline	Ethanol (E100)	Wet ethanol (E85W15)
Normalised chemical formula	$CH_{1.93}O_{0.027}$	$CH_3O_{0.5}$	-
Density at 293 K (g/cm^3)	0.72-0.75	0.79	0.85
Research octane number (RON)	95	109	-
Heat of vaporisation (kJ/kg)	350	840	-
Oxygen content (m/m)	0.027	0.348	-
Lower heating value (MJ/kg)	42.1	26.9	21.5
Vapour pressure at 293 K (kPa)	45.0-100.0	5.7	-

For all further calculations, the water-ethanol fuels were considered as a two elements mixture. Thus, the fuel LHV was estimated taking in account the estimated mass of ethanol in one kilogram of fuel mixture. The water content was not considered as a

fuel, and the final fuel chemical formula for the oxidative part of the mixture was considered as ethanol chemical formula only. Thus, as will be explained later, the water content of the mixture was accounted for separately in all exhaust emission calculations.

Gasoline (GRON95) was conventional unleaded 95 RON UK gasoline from a gasoline station. It was considered as a mixture 8% of ethanol and 92% of gasoline ($CH_{1.87}$ [95]). The 8% of ethanol was considered in order to obtain near 2.7% of oxygen content in mass when adding ethanol, one of the preferential gasoline's oxygenated additives.

3.2.3. **Emission Analyser**

A Horiba 7170DEGR gas analyser system was used to measure the exhaust gas emissions during the tests. Carbon monoxide (CO), carbon dioxide (CO_2), unburned hydrocarbons (UHC), oxygen (O_2) and nitrogen oxides (NO_x) were measured. Before every engine test, the gas analyser was heated up and calibrated with span gases in order to assure measurement linearity. The whole procedure used to take between 30 minutes to 1 hour, depending on the ambient temperature. The exhaust gases were supplied to a first unit using a heated line (190 °C) in order to avoid water condensation.

A flame ionization detector (FID) unit FIA-725A was responsible for the wet basis UHC measurements within a range of 0-50000 ppm v/v. The working principle is based on a hydrogen-helium diffusion flame established with high purity air where hydrocarbon species are introduced, broken in smaller radicals, oxidized and produce ions. The ions produced are collected by two electrodes and the charge is directly proportional to the number of carbons present in the hydrocarbon molecule [194]. While the relative response of the FID to distinct hydrocarbons is very linear according to the number of carbon atoms in the molecule, carbonyl carbons (R-C=O) produce negligible ionization. Thus, the resulting response from the FID is lower when oxygenated organic compounds such as alcohols and aldehydes are present in the exhaust emissions than that of only hydrocarbons. Carbonyl containing species with only one carbon such as formaldehyde and carbon monoxide also produce negligible response. For this reason, UHC needed to be corrected when using ethanol fuels.

After this step, the sample was dried in a chiller unit, and all other emission measurements were evaluated in dry basis. CO and CO_2 emissions were measured with an AIA-72X module using non dispersive infrared (NDIR) method. This method

consists of the emission of infrared light of the same wavelength which is absorbed by a specific molecule. Thus, the difference between the emitted light and received light after passing through the sampled mean is proportional to the molecular concentration.

A heated chemiluminescence detector model CLA-720MA measured NOx emissions. The exhaust sample passed through a catalyst which converted all NO_2 emissions in NO. Then, this sample was injected in an ozone rich (O_3) reactor where the light emission from the NO to NO_2 reaction was measured and converted to volume. At alternate times, exhaust samples containing NO_2 (without passing through the catalyst) were also injected in the reactor. Thus, total NOx and only NO measurements were possible. The range was 0-50000 ppm v/v.

A MPA-720 unit based on paramagnetic principle was used to measure O_2 concentration of 0-25000 ppm. The measurement is based on the paramagnetic property of the O_2 molecule. The sample is injected between two poles of an electromagnetic induced field. The pressure around the magnetic poles changes according to the concentration of oxygen, and this pressure is measured by a microphone and converted to O_2 concentration.

As the exhaust gas sample took some time to travel from the exhaust system to the Horiba gas analyser, the emission data was always time averaged. The emissions analyser directly communicated to the data acquisition system through CAN based protocol using Ethernet connection.

3.2.4. **Data acquisition and control**

The data acquisition and control systems shown in red in Figure 3.1 are basically comprised of an engine control unit (ECU), valve control unit (VCU), PFI control unit (PCU), data acquisition (DAQ) card and three PCs. Thus, Figure 3.1 shows a simplified version of the real data acquisition and control system. The main difference is that there are three computers: PCU unit computer, the engine coolant and oil systems are controlled by the dynamometer PC controller, and the data acquisition system and main ECU is controlled in another computer.

The ECU is based on a Dual core Ricardo rCube, and it was responsible for controlling spark timing and direct injector parameters. It was connected to the host computer through CAN protocol. Engine parameters were modified using ETAS Inca V5.4 user interface. The VCU unit which received signals from the valves differential variable

reluctance transducers (DVRT – used to measure the instantaneous valve linear displacement) and acted on the valve actuators was connected to the main ECU. Thus, intake and exhaust valve events were directly controlled through the same ETAS Inca V5.4 interface.

The data acquisition system was based on an in-house transient combustion analysis program developed by Dr Yan Zhang (a similar screen to that used to monitor and save the engine data is presented in Figure 3.6). This software received data from a National Instruments 6353 USB X card with 32 analogic inputs and 1.0 mega samples per second multichannel capability. The software logged all shown data in batches of 100 cycles. Crank angle related data was saved individually for each crank angle and cycle, while averaged data was saved for each cycle.

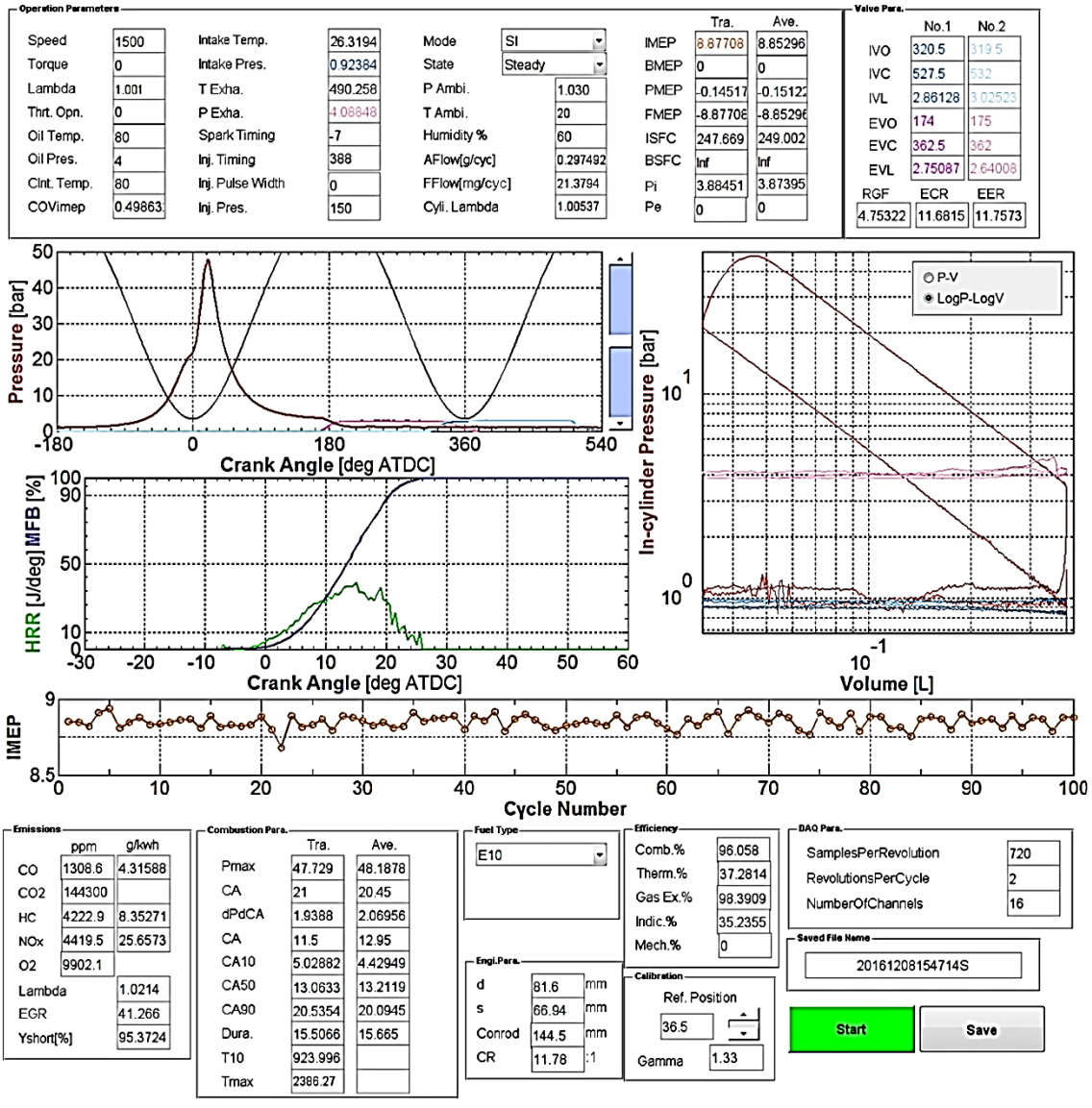

Figure 3.6. Transient data acquisition and combustion analyser.

A 720 pulse per revolution (ppr) LeineLinde encoder was installed on the crankshaft. The trigger signal was used to position the TDC while the 720 ppr signal was used as signal clock to acquire crank angle based data from in-cylinder pressure transducer, intake and exhaust pressure transducers, and each one of the valves DVRTs. This software version showed valve related events considering near 0.5 mm valve lift. Later, valve lift data was re-processed in order to provide events at 0.15 mm with higher accuracy. Injection timing and spark timing were measured with current meter pick-ups attached to the injectors' cables and the cable from the ECU to the ignition driver. As previously cited, the data acquisition software also received all emissions data from the Horiba analyser through CAN protocol. In addition, air/fuel equivalence ratio (λ) data was measured using a wide band lambda sensor in the exhaust pipe. This data was acquired by CAN protocol enabled by the use of a MOTEC lambda meter interface.

The port fuel injector control unit (PCU) was a MOTEC m880 ECU which received crank angle signal from the encoder. The PCU was able to control either the DI or PFI injectors using simple two-way electrical switches. Thus, while the main ECU controlled the DI injector (without remaining channels to control the PFI system), the PCU controlled the PFI injector.

The in-cylinder pressure was measured using an AVL GH15D piezoelectric transducer. This sensor was capable of measuring continuous pressure variations of up to 250 bar and presented a linearity of ±0.3%. The sensor sensitivity was 0.19 pC/kPa. The working principle is based on the creation of electric charges when a force is applied to the quartz crystal element inside the sensor (a property of such material). Thus, a Kistler 5011B10 charge amplifier was used to measure the generated charge and convert to voltage (which could be read by the DAQ system). The charge amplifier main configurations used were long time constant (high pass filter) of more than 1000 seconds and no low pass filter. The expected resulting error of such systems is lower than 1%.

Instantaneous intake absolute pressure was monitored using a Kistler 4007BA20F piezoresistive pressure transducer installed in the intake plenum. This sensor was connected to a Kistler 4618 amplifier which sent a 0-10V signal to the DAQ card. Instantaneous exhaust pressure was initially monitored using a Kistler 4007BA5F piezoresistive water cooled pressure transducer connected to a similar amplifier. This sensor was used to validate the pegging methods. Later on, it was changed for a Gems 3100 series absolute pressure transducer to monitor exhaust mean pressure.

Thus, engine control parameters such as spark timing, valve timings and DI fuel injection were controlled using the INCA interface. Port fuel injection parameters were controlled using MOTEC interface. Throttle opening was controlled using a mechanical lever connected while the intake pressure was monitored at the data acquisition software interface. All tests were done at fixed load of 1500 rpm, enabled by the active dynamometer control.

Load was controlled manually by changing three main parameters: fuel injection pulse width, intake air amount (either by throttle actuation or modified intake valve closure), and spark timing. Thus, to achieve a desired load at stoichiometric condition all these parameters were controlled simultaneously.

3.2.5. **Dynamometer and hydraulic system**

A 48 kW AC current four quadrant dynamometer from CP Engineering enabled both motored and firing operation at engine speed up to 6000 rpm. An ABB ACS800 power driver was used to control the electrical motor. The user interface was enabled by a PC based Cadet V12 software. This system allowed constant speed and constant torque tests, at steady state or transient conditions, although only constant speed tests were evaluated in this research (1500 rpm ±5rpm). The dynamometer and its components are shown in yellow in Figure 3.1. The load cell, responsible for torque measurements, was a SSM S-type Interface load cell with 0.5% full scale linearity to up to 330 Nm. In addition, the dynamometer control system was also responsible of supplying engine oil (green in Figure 3.1) and coolant (pink in Figure 3.1). Engine oil was supplied at 4.0 bar and 90 °C, while engine coolant (50% water to 50% ethylene-glycol mixture) was supplied at 90°C. The temperatures were closed loop controlled using electrical heaters and liquid-to-liquid heat exchangers.

The valve train unit (presented in purple in Figure 3.1) was fed with hydraulic oil (at 120 bar and 50 °C) from a DGB Hydraulics unit with 225 litres oil capacity (the green metal equipment shown in Figure 3.2). The independent valve actuation was enabled by four Moog UK electrohydraulic valves which acted at each one of the four hydraulic actuators. The opening and closure events were controlled by the VCU which received the signal from the Lord DVRTs (resolution of 6 µm and measurement uncertainty of ±1%) sensor amplifier. The valves event control strategy (regarding opening and closure speeds) was pre-defined and it was only necessary to choose the opening timing, closure timing and maximum valve lift on INCA software. Maximum intake valve

lift was 8.0 mm and maximum exhaust valve lift was 9.0 mm. Even then, there wasn't a safety system that avoided piston to valve contact and prevented engine failure in the case of wrong input data. Thus, for safety reasons, most of the tests were evaluated at 3.0 mm valve lift as after 3.5 mm valve lift there would be piston to valve contact in the TDC.

3.3. Data post-processing and analysis

Each operating point was saved at least three times. Thus, 300 cycles were acquired, with 100 consecutive cycle batches. The saved data was imported to an Excel spreadsheet where it was automatically averaged using a user developed visual basic code. In addition, all valve timing events, emissions and efficiency parameters were re-calculated. The main reasons were: the emissions conversion calculation (from ppm to g/kW h) used in the data acquisition software didn't take in account the added water-in-fuel content to transform dry basis measured emissions to wet basis; the in-cylinder pegging method of the software was not suitable for unthrottled operation through EIVC load control; the pumping work calculation took into account the in-cylinder pressure from $BDC_{exhaust}$ to BDC_{intake} not considering the valve events variation. Another point considered for the post-processing was that it would be necessary to recalculate the in-cylinder pressure prior to the effective compression ratio analysis.

3.3.1. In-cylinder pressure pegging methods

In-cylinder piezoelectric transducers show pressure variations but not an absolute pressure value. For this reason, the measured in-cylinder pressure data needed to be offset according to an absolute pressure reference. This procedure is called pegging. In conventional spark ignition engines with conventional valve timing, the most common pegging method is based on offsetting the in-cylinder pressure to make the instantaneous in-cylinder pressure at BDC_{intake} equal to the intake pressure. Another method is to equalize the end of the exhaust stroke in-cylinder pressure to the exhaust system back pressure [195]. The problem is that with unconventional valve timings, when the valves are closed during the pressure comparison window, both methods do not work. Some of the unconventional valve timing methods that show problems are early intake valve closure and negative valve overlap with EIVC load control, for

example. Several other methods using absolute pressure transducers installed directly in the liner near the bottom dead centre have also been reported in the literature.

For this work a thermodynamic pegging method based on forced polytropic compression with fixed ratio of specific heats index was used. This method has been extensively used by industry data acquisition systems and has already been proven as an effective pegging method [196]. The pressure correction was applied as:

$$p_{actual} = p_{measured} + p_{correction} \tag{2}$$

$$p_{correction} = \frac{p_2 - p_1}{\left(\frac{V_1}{V_2}\right)^{\gamma} - 1} - p_1 \tag{3}$$

where P_i and V_i are the instantaneous in-cylinder pressure and volume at the crank angles 1 and 2 situated during the compression stroke, after the IVC event but before the spark event. The polytropic index used was 1.33.

Figure 3.7 shows a comparison of the three described pegging methods. In the left side the difference between forced polytropic compression pegging and intake pegging is null, while the difference to the exhaust pegging is around 0.02 bar. In the right part, the intake pegging was moved to the intake valve closure moment. It can be seen that the intake pegging method cannot be used even when considering the IVC event. On the other hand, exhaust pegging and forced polytropic compression pegging were very similar, less than 0.02 bar difference. Thus, forced polytropic pegging was used for all tested valve timing strategies.

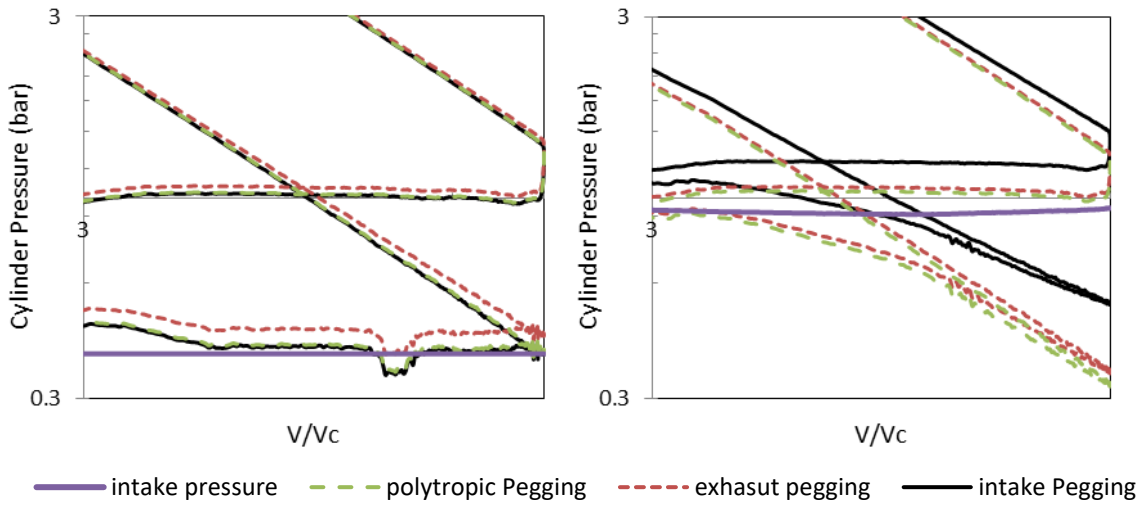

Figure 3.7. Comparison between pegging methods.

3.3.2. **Heat release analysis**

The heat release analysis was based on first law of thermodynamics for a closed system. Thus, the energy balance of the system considered the variations of: combustion generated heat dQ_{ch}, system boundary work dW, fluid internal energy change dU_s and fluid to wall heat transfer dQ_{ht}. Thus, this could be considered as a single zone combustion analysis as there was no separation between the burned and unburned gas zones.

$$dQ_{ch} = dW + dU_s + dQ_{ht} \tag{4}$$

The variation of the fuel heat release and fluid to wall heat transfer were grouped in only one term, apparent heat release dQ_{net}, which means the variation of the fluid internal energy and boundary system work (piston work). After some mathematical manipulation (which has been extensively discussed in several engines text books [95], [197]) the apparent heat release can be calculated as:

$$\frac{dQ_{net}}{dCAD} = \frac{\gamma}{\gamma - 1} p_i \frac{dV_i}{dCAD} + \frac{1}{\gamma - 1} V_i \frac{dp_i}{dCAD} \tag{5}$$

The ratio of specific heats was kept constant as 1.33 as suggested by [197]. The instantaneous cylinder volume was calculated through the equation

$$V = V_{TDC} 0.5(CR + 1)\left[\frac{2L}{S} + 1 - \cos\theta - \left(\left(\frac{2L}{S}\right)^2 - \sin^2\theta\right)^{\frac{1}{2}}\right] \tag{6}$$

where L is the connecting rod length and S the stroke.

The end of combustion was set as the point where the expansion trace followed that of a polytropic expansion and the beginning of combustion was set as the spark timing moment. The mass fraction burned curve was calculated initially by the integration of the heat release rate during the whole combustion and later normalized to the maximum heat release rate value (100% MFB). Flame development angle (FDA, 0-10% MFB), main phase combustion duration (10-90% MFB), and centre of combustion (CA50%) were calculated taking in account the moments from the MFB curve.

Pressure rise rate (PRR) was calculated correlating the pressure variation to the crank angle variation. The maximum pressure rise rate during combustion of 5.0 bar/CAD was chosen as a knock indicative parameter based on [94]. Spark timing advanced

was limited in order to limit PRR, even though audible ringing was also taken in account to limit spark timing advance before 5.0 bar/CAD max PRR levels.

3.3.3. **Overall engine parameters**

The calculation methodology for the efficiency related parameters was based on net indicated mean effective pressure:

$$IMEP = \frac{\int_{-180}^{540} p_i dV}{V_d} = \frac{W_{c,i}}{V_d} \quad (7)$$

where $W_{c,i}$ is the indicated work per cycle and V_d is the engine displacement volume. The crank angle "zero" was defined as the TDC_{firing}. The IMEP was used through the whole work to compare engine operating load.

The net indicated efficiency which represents the efficiency that fuel energy was transformed in work by the engine was calculated as:

$$\eta_I = \frac{IMEP.V_d}{m_{fuel,c}.LHV_{fuel}} \quad (8)$$

where $m_{fuel,c}$ is the fuel mass flow per cycle and LHV_{fuel} is the lower heating value of the fuel.

As part of the engine work was expended during the gas exchange process, the pumping mean effective pressure was calculated to represent the engine load lost during such processes:

$$PMEP = \frac{\int_{EVO}^{IVC} p_i dV}{V_d} \quad (9)$$

and the gas exchange efficiency η_{GE} was calculated as the relationship between the total available work per cycle to the work produced during the period when the valves were closed:

$$\eta_{GE} = \frac{IMEP}{IMEP - PMEP} \quad (10)$$

The combustion efficiency which related the wasted fuel energy due to incomplete combustion was calculated as:

$$\eta_C = 1 - \frac{\sum \dot{m}_i . LHV_i}{\dot{m_{fuel}} . LHV_{fuel}} \quad (11)$$

where $\dot{m}_i$ was the mass flow rate of the considered "i" exhaust gas as CO, THC and H_2, and LHV_i was their respective lower heating value, while $\dot{m}_f$ was the fuel flow rate.

Thermodynamic efficiency (gross) parameter was used as indicative of how well the combustion process took place and it was calculated as:

$$\eta_T = \frac{\eta_I}{\eta_{GE} . \eta_C} \quad (12)$$

The engine's operation stability was monitored by the covariance of IMEP over 100 cycles. This parameter expressed the variation in the indicated work per cycle due to combustion and flow variability. A general maximum value of 5.0% was accepted to consider engine stable operation, but at certain points the maximum accepted value was decreased to 3.0%:

$$COV_{IMEP} = \frac{IMEP_{std}}{IMEP_{average}} * 100 \quad (13)$$

Finally, the indicated power was calculated as from the indicated cycle work and engine frequency.

$$P_i = W_{c,i} f \quad (14)$$

3.3.4. **Engine-out emissions**

The engine-out emissions measured by the Horiba gas analyser were post-processed to be converted from ppm to g/kWh following the UN Regulation number 49 [198]. All gases measured in dry basis were transformed to wet basis taking in account the air humidity and water-in-fuel content. No NOx humidity and temperature corrections were applied.

The main exhaust gases to be converted from ppm to g/kWh were CO, NOx and UHC following the equations:

$$ISCO = \frac{u_{CO}[CO]k_w\dot{m}_{exh}}{P_i} \quad (15)$$

$$ISNOx = \frac{u_{NOx}[NOx]k_w\dot{m}_{exh}}{P_i} \quad (16)$$

$$ISTHC = \frac{u_{HC}[UHC]k_{FID}\dot{m}_{exh}}{P_i} \quad (17)$$

where u_i is the molar mass fraction of the each gas, $[\,i\,]$ is the gas concentration in ppm, k_w is the dry-to-wet correction factor, $\dot{m}_{exh}$ is the exhaust mass flow rate, P_i is the indicated power and k_{FID} is the FID correction factor which will be explained later. It is important to note that the unburned hydrocarbon nomenclature UHC has been changed to THC (total unburned organic species) in order to differentiate the corrected carbon count emissions from the original one. These parameters were calculated as:

$$\dot{m}_{exh} = \dot{m}_{air} + \dot{m}_{fuel} \quad (18)$$

$$\dot{m}_{air} = \dot{m}_{dry\,air} + \dot{m}_{humidity} \quad (19)$$

$$\dot{m}_{fuel} = \dot{m}_{actual\,fuel} + \dot{m}_{water} \quad (20)$$

The exhaust mass flow rate was calculated as the sum of wet air mass flow rate $\dot{m}_{air}$ and fuel mass flow rate $\dot{m}_{fuel}$, while the dry air and water (present in air) were calculated taking in account the water saturation pressure polynomial estimation suggested by [199]:

$$\begin{aligned} SP = {} & 604.8346 + 45.9058(T_a - 273.15) + 1.2444(T_a - 273.15)^2 \\ & + 0.03522481(T_a - 273.15)^3 + 0.00009322061(T_a - 273.15)^4 \\ & + 0.000004181281(T_a - 273.15)^5 \end{aligned} \quad (21)$$

were T_a is the ambient temperature. With RH as the relative humidity, and p_a the ambient pressure, air humidity H_a (in grams of water per kilogram of dry air) was calculated as

$$H_a = \frac{6.211\ RH\ SP}{p_a - \frac{(RH\ SP)}{100}} \tag{22}$$

$$\dot{m}_{dry\ air} = \frac{\dot{m}_{air}}{1 + H_a} \tag{23}$$

$$\dot{m}_{humidity} = \dot{m}_{dry\ air} H_a \tag{24}$$

The molar mass fraction of each gas was calculated according to specified values from the [198]. As the considered gasoline was composed of pure gasoline and ethanol, the weighted average of the u_i was used, taking into account each fuel fraction in the mixture.

Table 3.3. Raw gas molar mass fraction of the exhaust gases for gasoline and ethanol [198].

Exhaust gas	$\boldsymbol{u_i}$	
	Gasoline	Ethanol
CO	0.000966	0.000980
NOx	0.001587	0.001609
UHC	0.000499	0.000780

The dry-to-wet correction factor k_w applied to CO and NOx emissions was dependent not only on the ambient conditions, but also on the added water content from the fuel:

$$k_w = 1.008\left(1 - \frac{1.2442H_t + 111.19W_{ALF}\left(\frac{\dot{m}_{fuel}}{\dot{m}_{dry\ air}}\right)}{773.4 + 1.2442H_t + 1000\left(\frac{\dot{m}_{fuel}}{\dot{m}_{dry\ air}}\right)k_f}\right) \tag{25}$$

$$k_f = 0.055594W_{ALF} + 0.0070046W_{EPS} \tag{26}$$

where W_{ALF} and W_{EPS} were the hydrogen and oxygen contents in the fuel, respectively. The original air humidity factor was replaced by the total humidity factor H_t to take in account the water-in-fuel added additional content.

$$H_t = H_a + H_f \tag{27}$$

$$H_f = \dot{m}_{water}/\dot{m}_{dry\ air} \tag{28}$$

The parameter k_{FID} was multiplied by the UHC (ppm) in order to take in account the low response of the FID system to oxygenated compounds. Specific studies regarding SI ethanol fuelled engines with exhaust gas speciation using FTIR spectroscopy or gas chromatography showed that the exhaust organic emissions have a considerable share of unburned ethanol, acetaldehyde and unburned hydrocarbons [199]–[201]. Thus, when FID is used to measure the THC emission of ethanol fuelled engines, a correction response factor *α* should be used.

The relative concentration of ethanol to aldehydes and hydrocarbons in ethanol-gasoline blended fuelled engines is affected primarily by ethanol concentration in the fuel and by the engine operating conditions, as shown in [199]–[201]. Even then, some attempts to find a general formulation to correct the FID measurements to take in account the low response from oxygenated emissions have been proposed [200], [202]. The difference in the ppmC1 emissions after using the FID correction was less than 10% [200] when compared to speciation methods (GC) to count the organic unburned molecules in the exhaust emissions. Distinct literature sources present similar *α* FID response factors for acetaldehyde and ethanol. Thus, a value of *α*=0.7 was used in this study as this is an average value between the response factor of ethanol (0.74) and acetaldehyde (0.67) (the major oxygenated organic emissions). Thus, the corrected FID response could be calculated according to the ethanol volumetric concentration "e" in the fuel and the response factor "*α*".

$$k_{FID} = \frac{1}{1 - (1 - \alpha)\sum z_i} \tag{29}$$

$$\sum z_i = 0.608e^2 + 0.092e \tag{30}$$

3.3.1. **Considerations about measurements uncertainties**

The covariance of indicated efficiency and different gaseous emissions (measured ppm) were calculated similarly to the covariance (COV) of IMEP as: standard deviation of the measured/calculated parameter divided by the mean value of the same parameter for the selected number of cycles. COV was chosen instead of the standard deviation to give an easier estimate of the variation range of each parameter.

Table 3.4. Covariance of calculated indicated efficiency and measured exhaust gas emission concentration (ppm) data. The discussed data is presented in Figures 4.2 and 4.3.

tSI - Injection sweep - Regarding Figures 4.2 and 4.3 data

IMEP (bar)	Injection timing (ATDCintake)	Indicated Efficiency (%)	COV Ind Eff (%)	ISCO (g/kWh)	COV CO (%)	ISTHC (g/kWh)	COV THC (%)	ISNOx (g/kWh)	COV NOx (%)
2	28	25.7%	2.4%	8.1	3.2%	7.9	2.3%	6.7	9.9%
	90	25.3%	3.0%	22.2	6.1%	7.6	2.2%	3.6	2.4%
3.1	28	29.1%	1.6%	6.7	0.7%	6.6	1.1%	9.7	2.3%
	59	29.0%	1.9%	22.6	3.3%	7.1	1.5%	7.3	1.2%
	90	29.2%	1.9%	21.2	3.5%	7.3	3.5%	8.1	8.8%
	120	28.9%	1.9%	22.3	3.7%	7.3	1.6%	7.0	2.2%
	150	28.6%	2.2%	32.4	6.1%	9.3	2.2%	7.5	2.6%
	180	28.2%	2.5%	42.0	5.3%	11.1	2.3%	6.0	1.8%
4.5	28	32.3%	1.1%	8.3	3.4%	6.1	1.6%	11.3	5.4%
	91	32.0%	1.4%	26.0	3.5%	6.2	1.9%	8.5	2.6%
6.1	28	34.3%	1.2%	9.5	4.5%	5.1	1.9%	13.3	1.5%
	60	34.1%	1.3%	21.4	3.0%	5.2	1.0%	12.6	2.8%
	90	33.9%	1.1%	25.8	4.4%	6.2	3.4%	11.9	2.5%
	120	33.7%	1.1%	22.8	3.4%	7.7	3.1%	11.5	6.7%
	150	33.3%	1.4%	26.3	4.0%	10.5	3.3%	11.0	4.0%
	180	32.8%	1.3%	28.6	6.1%	17.1	2.1%	10.9	2.2%
7.5	28	35.7%	0.8%	9.6	2.8%	4.7	2.5%	15.5	3.8%
	90	35.2%	1.1%	21.7	2.7%	6.4	3.3%	15.4	1.3%
9	28	36.4%	0.7%	12.9	3.8%	4.6	3.8%	15.7	0.5%
	90	36.0%	1.1%	19.6	4.3%	6.4	4.4%	16.4	1.4%
WOT	28	36.8%	0.6%	13.2	2.8%	4.3	3.9%	17.0	0.7%
	90	36.1%	0.9%	22.4	4.2%	7.3	4.2%	17.2	0.9%
	150	35.0%	1.3%	17.2	3.3%	16.6	2.2%	18.7	1.3%
	180	34.0%	1.4%	19.5	4.7%	24.9	1.5%	15.9	3.5%

The great majority of indicated efficiency values showed COV below 5.0%, which would be around expected uncertainty level of such calculated parameters. On the other hand, exhaust gas emissions COV was higher, also due to the cyclic variability of the combustion process itself. Thus, exhaust emission parameters uncertainty would be expected to be below 10%, as shown in [199]. Taking this in consideration, the present work discussion will be based on the mean values of the selected number of cycles and the trend behaviour.

3.4. Summary

The engine test cell facilities and engine controls were presented alongside with the employed sensors details. The data acquisition system and post-processing methodology were discussed and the mathematical correlations used to calculate several properties and engine parameters were presented. The valve train strategy used in each test will be described in the results chapters.

Chapter 4.

Throttled PFI and DI spark ignition ethanol operation with positive valve overlap

Even though different combustion concepts (as CAI [99], [106], TJI [203]–[205] and GDCI [206], [207]) not necessarily based on spark for gasoline engines have been proposed, the major drawbacks are hardware cost, especially for the after treatment system. So, in order to improve the fuel economy of the conventional stoichiometric throttled SI operation, positive valve overlap operation has been widely used in the 4-stroke gasoline engine. It is achieved by advancing the IVO before the intake TDC and retarding the EVC after the TDC, resulting in a positive overlap of the intake and exhaust processes during which some of in-cylinder burned gas flows to the intake ports and some of exhaust gas flows back from the exhaust ports into the cylinder. At high speed and high loads, due to tuning and ram effects, the PVO concept can be used to increase scavenging and promote higher fresh air mass flow, which may increase power. Variable IVO and EVC timings can be achieved with simple cam phasing mechanisms. The drawbacks are that the IVC and EVO are also moved when the intake and exhaust durations are fixed by the cam lobe design. Thus, effective compression ratio and effective expansion ratio are changed.

Some studies have investigated the use of aggressive PVO in order to achieve higher residual gas fraction to achieve gasoline SACI. For fixed duration camshafts it was found that PVO would result in better efficiency than a lower duration camshaft for NVO [92]. PVO durations as large as 100 CAD were used in that work. Later, PVO with EIVO, LEVC and both strategies at the same time were studied for fixed duration camshafts [93], [94]. The backflow of burnt gases to the intake ports was less effective in increasing the in-cylinder thermal state than the exhaust rebreathing caused by the LEVC. While the EIVO resulted in EIVC and lower compression ratio, LEVC caused LEVO which highly increased exhaust pumping losses. The best compromise was found for PVO with both EIVO and LEVC at the same time.

A previous study was carried out on the Camless engine in order to analyse the comparative benefits of PVO to other valve timing strategies. When fuelled with gasoline, spark ignition combustion with PVO achieved the same indicated efficiency as the CAI combustion through NVO valve strategy at a load of 3.6 bar IMEP [60]. In another study conducted on the same engine with a more aggressive EIVO at 3.2 bar IMEP load using gasoline and ethanol [74], the PVO operation was found to be

characterised with a lower combustion efficiency when compared to CAI combustion with NVO, SI combustion with EIVC and conventional throttled operations.

The above studies on PVO were conducted for the fixed valve timing at a given load. In order to investigate and identify the full potential of the PVO operation with ethanol, it is necessary to study and understand the influence of the PVO valve timings and their effects on engine performance and emissions over a range of engine operations.

This chapter presents the systematic study of the use of the variable valve actuation system to understand the impacts of positive valve overlap on the spark ignition ethanol operation with throttling load control method. Two studies are presented in this chapter: the effect of PVO duration with fixed valve timing and the effect of intake valve profile phasing. Due to the FVVA system limitations, a reduced valve lift of 3.0 mm was adopted for both intake and exhaust valves to simulate the low lift operation of a switchable camshaft operated system in production and to enable PVO operation without valve to piston contact.

4.1. Spark ignition combustion of E100 with fixed positive valve overlap

4.1.1. Test methodology

Experiments were carried out on the single cylinder camless engine at 1500 rpm at IMEP of 2.1 bar, 3.1 bar, 4.5 bar, 6.1 bar, 7.5 bar and 9.0 bar. The engine was operated either with port fuel injection or direct fuel injections. Spark timing was varied with 2 CAD increment at each operating point in order to find the minimum spark advance for the best torque (MBT).

For each valve strategy the overlap between intake and exhaust valves was maintained constant by keeping the EVO, EVC, IVO and IVC constant. Three different PVO durations were tested: 6 CAD, 24 CAD and 41 CAD. They are respectively denominated as: throttled SI (tSI), PVO24 and PVO41. The valve opening and closure points were defined by the valve lift of 0.15 mm.

The actual intake valve lift profile used is presented in Figure 4.1. The target maximum valve lift was 3.0 mm. Although the tSI strategy would be possible at higher lifts, the other PVO strategies would result in piston-valve contact. So, this valve lift was chosen to ensure engine integrity. Exhaust valve opening was set to -10 CAD $ATDC_{intake}$ and

intake valve closure was set to 15 CAD ABDC. Thus, the gas exchange period was kept constant for all loads.

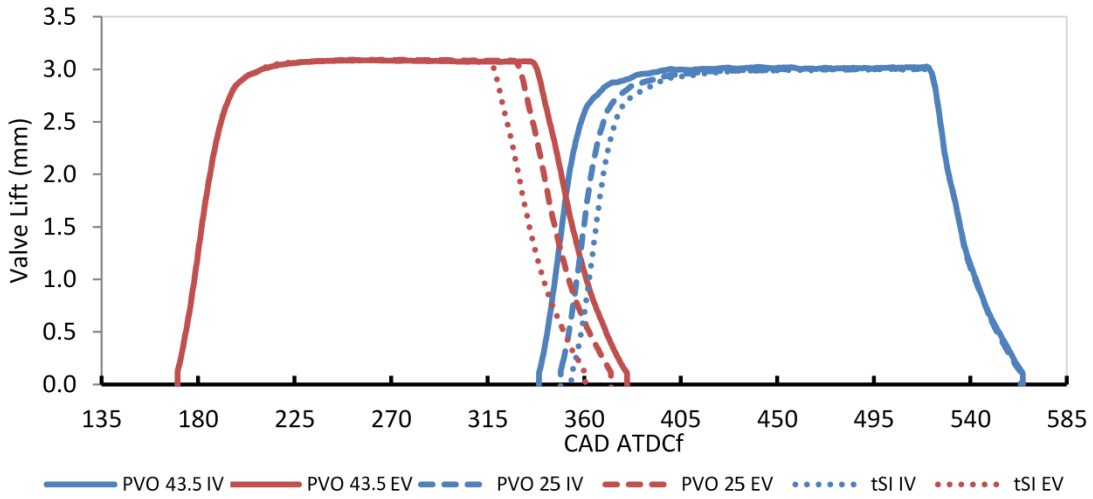

Figure 4.1. Intake and exhaust valve lift profiles used for the three different PVO strategies.

In order to provide different PVO durations, EVC and IVO were shifted from the TDC. Table 4.1 presents the IVO and EVC timings at 0.15 mm valve lift.

Table 4.1. IVO and EVC events of the different PVO strategies used for E100 tests.

Strategy	IVO ($ATDC_{intake}$)	EVC ($ATDC_{intake}$)	PVO duration
tSI	-6	1.5	7.5
PVO 25	-12	13	25
PVO 43.5	-22	21.5	43.5

Although the tSI strategy presented a small PVO of 7.5 CADs at 0.15 mm valve lift, it shown near zero overlap when for 0.3 mm valve lift. Considering the valve flow restrictions at such low lift, it could be considered that this PVO period would result in small iEGR in the absence of intake residual backflow or exhaust rebreathing.

4.1.2. **The effect of injection timing with E100 DI operation**

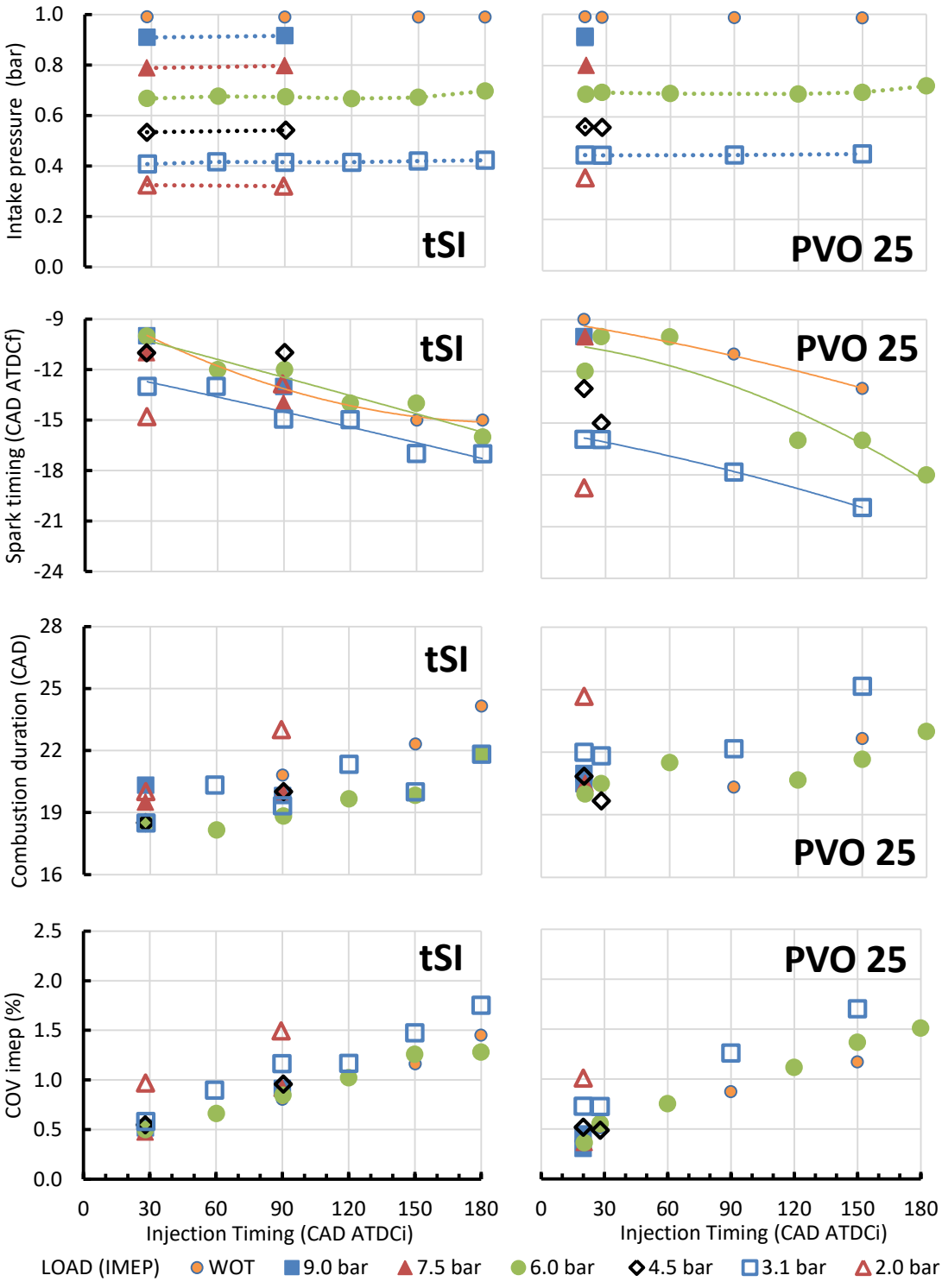

Figure 4.2.Effect of injection timing on intake pressure, spark timing, combustion duration, and COV_{imep} for tSI and PVO 25 valve timing strategies and different loads. E100 1500 rpm MBT operation.

The engine was supplied with a stoichiometric air/fuel ratio. When operated with port fuel injection (PFI), the PFI injection timing was set to TDC_{firing} in order to maximize time for ethanol vaporization and mixing with air. When operated with in-cylinder high pressure direct injection, the DI injection timing was varied in order to find a good compromise between emissions and efficiency. Figure 4.2 to Figure 4.4 presents engine operating performance, combustion and emissions for tSI and PVO 25 operations.

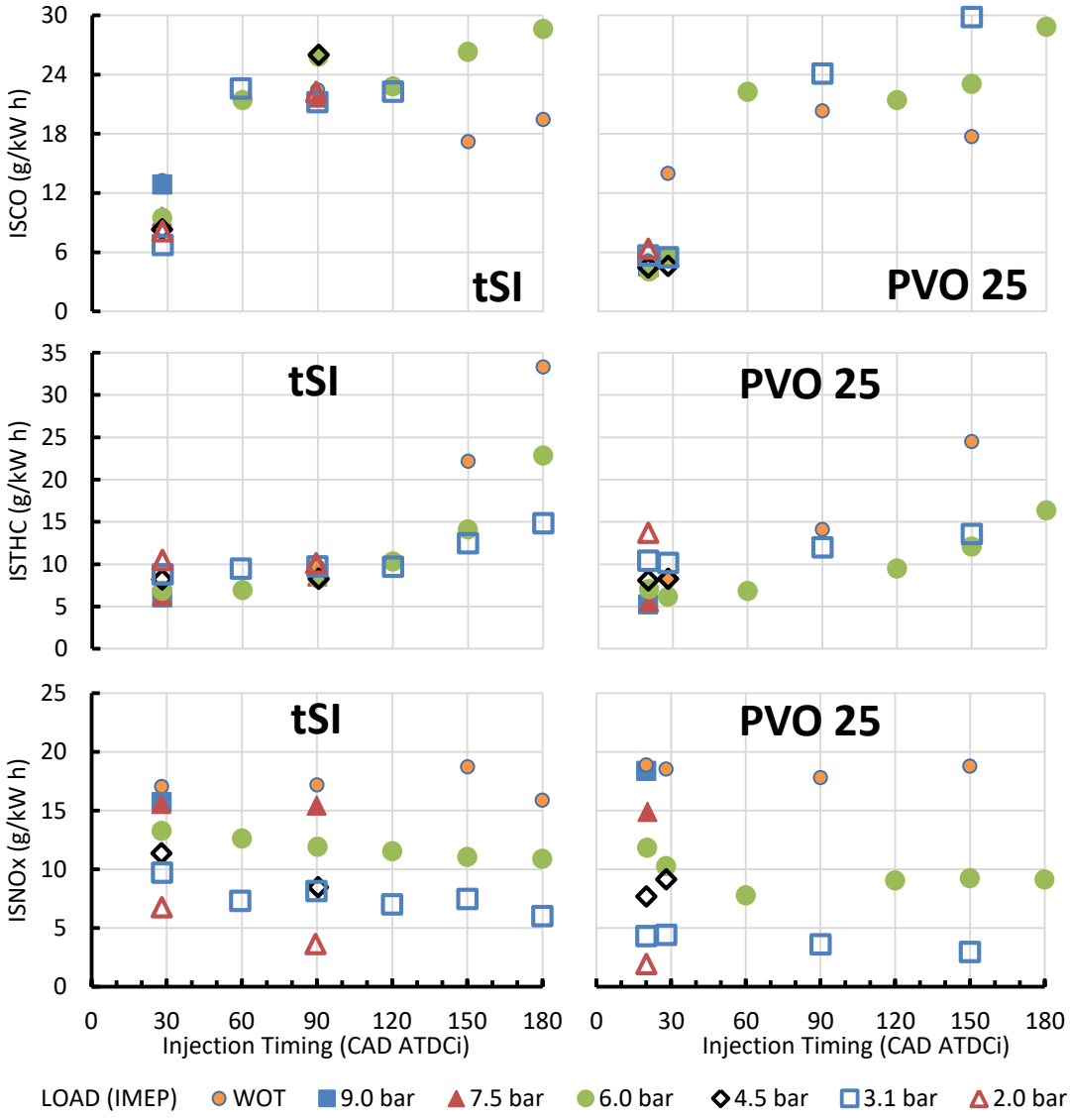

Figure 4.3. Effect of injection timing on indicated specific emissions for tSI and PVO 25 valve timing strategies and different loads. E100 1500 rpm MBT operation.

It could be concluded that the throttle opening had to be increased as the injection timing was retarded in order to keep the load (IMEP) constant. The charge cooling effect was more pronounced when the injection timing was delayed from the TDC. This

reduced the charge temperature and slowed the ignition and flame propagation process and led to more advanced MBT timings. In addition, the increased charge inhomogeneity with retarded injection led to significant increase in CO and uHC emissions. As result of the poor mixing process and longer combustion duration, cyclic variability (measured by the COV_{imep}) increased for later injection timings. In addition, it is assumed that fuel impingement could be a cause for increased THC when advancing the injection timing from 28 CAD ATDC to 20 CAD ATDC (PVO 25 data). Because of the expected lower combustion temperatures with delayed injection and higher charge inhomogeneity, the NOx emission was lower.

Because of the higher CO and uHC emissions, the combustion efficiency and hence the indicated efficiency decreased with the delay in the injection timing. Thus, to maintain the engine power output constant, more fuel had to be burned with additional air supplied at a higher intake pressure as the injection timing was retarded.

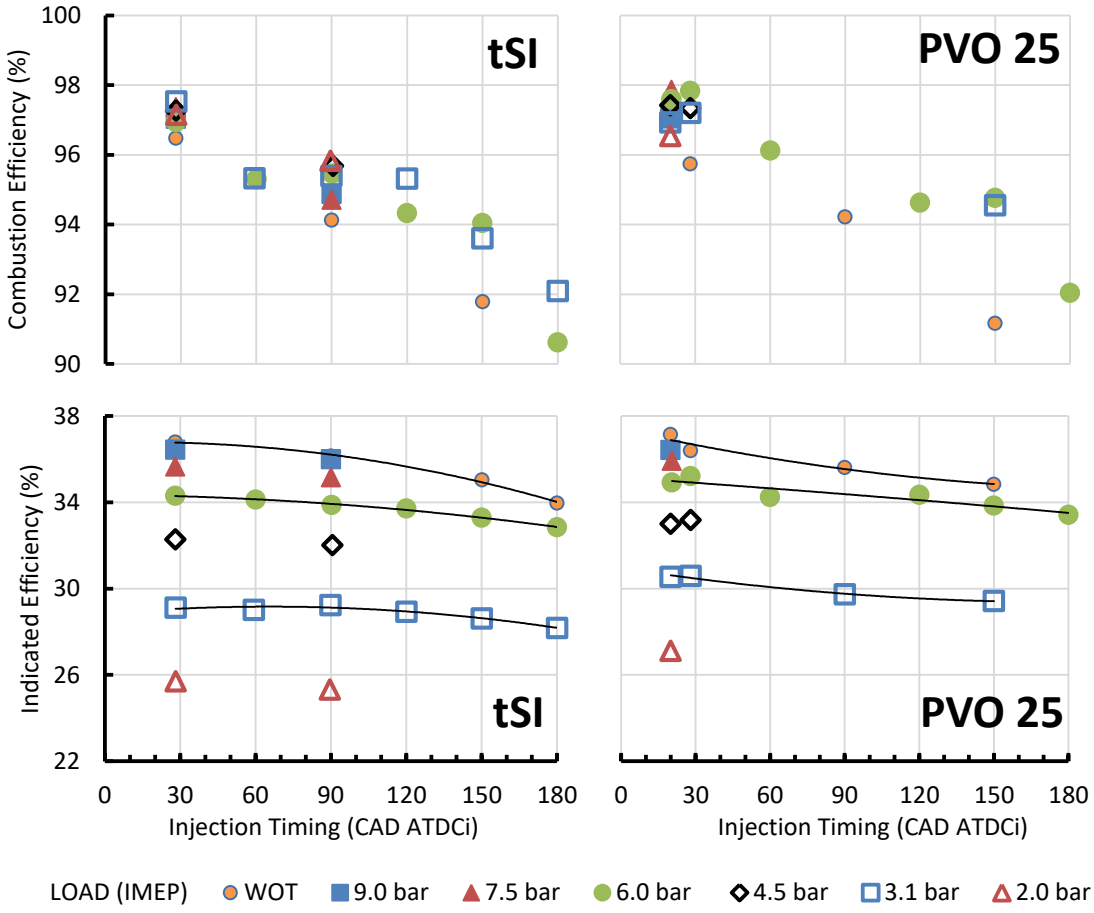

Figure 4.4. Effect of injection timing on combustion efficiency and indicated efficiency for tSI and PVO 20 valve timing strategies and different loads. E100 1500 rpm MBT operation.

The best compromise between the indicated efficiency and emissions could be reached when the injection timing was set 20 to 30 CAD $ATDC_{intake}$. Thus, the injection timing had been fixed at 28 CAD $ATDC_{intake}$ during the tSI operation and at 20 CAD $ATDC_{intake}$ for PVO 25 and PVO 43.5, as presented in the following studies.

Furthermore, the injection timing affected the WOT full load performance, as presented in Figure 4.5. The charge cooling effect caused by ethanol vaporization was most effective when injection took place in the middle of the intake stroke. The PVO operation was characterised with higher output because of the higher volumetric efficiency due to tuning and ram effects as previously mentioned.

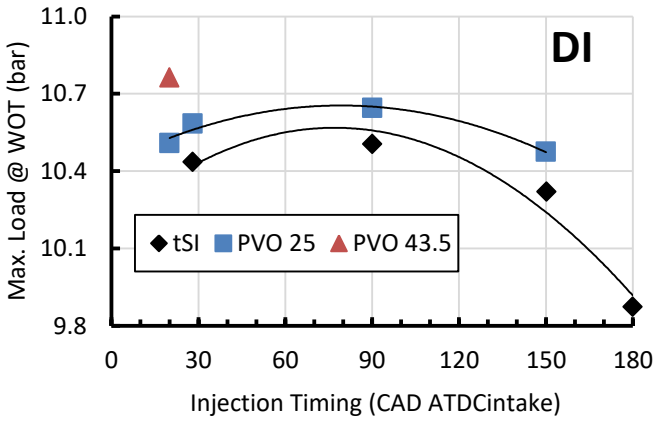

Figure 4.5. Effect of injection timing in WOT maximum load. E100 1500 rpm MBT operation.

4.1.3. **Comparative analysis between tSI, PVO 25 and PVO 43.5 valve timing strategies with DI and PFI strategies**

4.1.3.1. Gas exchange analysis

Figure 4.6 presents the effect of the PVO duration in the intake pressure, air flow rate, PMEP and gas exchange efficiency for different loads. The different PVO duration mainly affect the scavenging process. This resulted in the increase of required intake pressure with the increase in PVO. As the IVO was advanced relative to the TDC, more residual gas back flow occurred to the intake ports. Additionally, as the EVC was delayed relative to the TDC more exhaust gas back flown occurred from the exhaust ports to the cylinder. Thus, a higher residual gas fraction in the intake ports would require a higher intake plenum pressure in order to provide the same amount of fresh air. The increase in the intake pressure directly affected PMEP which was reduced. As a consequence, the gas exchange efficiency considerably increased with the increase

in the PMEP. Figure 4.7 presents the Log P x Log V diagrams of two loads with PFI for the different valve strategies. The increase in the pumping loop area with the increase in the PVO duration is graphically analogous to the increase in the PMEP.

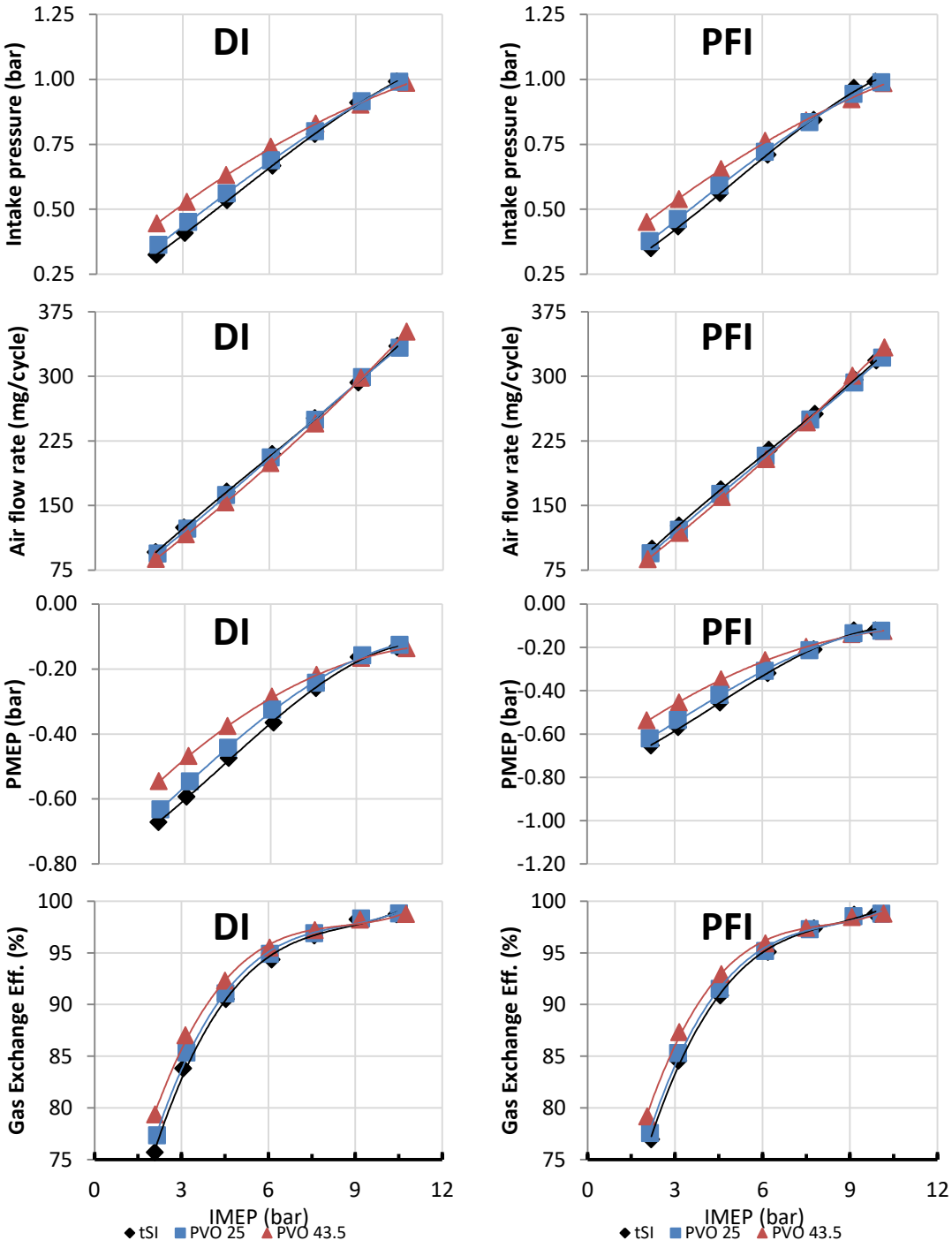

Figure 4.6. Effect of the PVO duration on the intake pressure, air flow rate, pumping mean effective pressure and gas exchange efficiency at different loads for DI and PFI injection strategies. E100 1500 rpm MBT operation.

As all operating conditions occurred at stoichiometric condition, less energy was required in order to attain the same load as the gas exchange efficiency increased. This directly affected the air flow rate which was initially reduced with the increase in the PVO as a result of relatively lower work loss during the pumping process. On the other hand, as load was increased and higher in-cylinder mass was trapped the inertial effect of the exhaust gases flowing through the exhaust valves tended to facilitate the scavenging process. For this reason, lower intake pressure was required as the PVO was increased at the higher loads.The PFI air displacement contributed to increase PFI cases intake pressure. Conversely, DI cooling effect contributed to reduce DI cases intake pressure. Considerably higher WOT maximum load occurred with DI due to lower charge density.

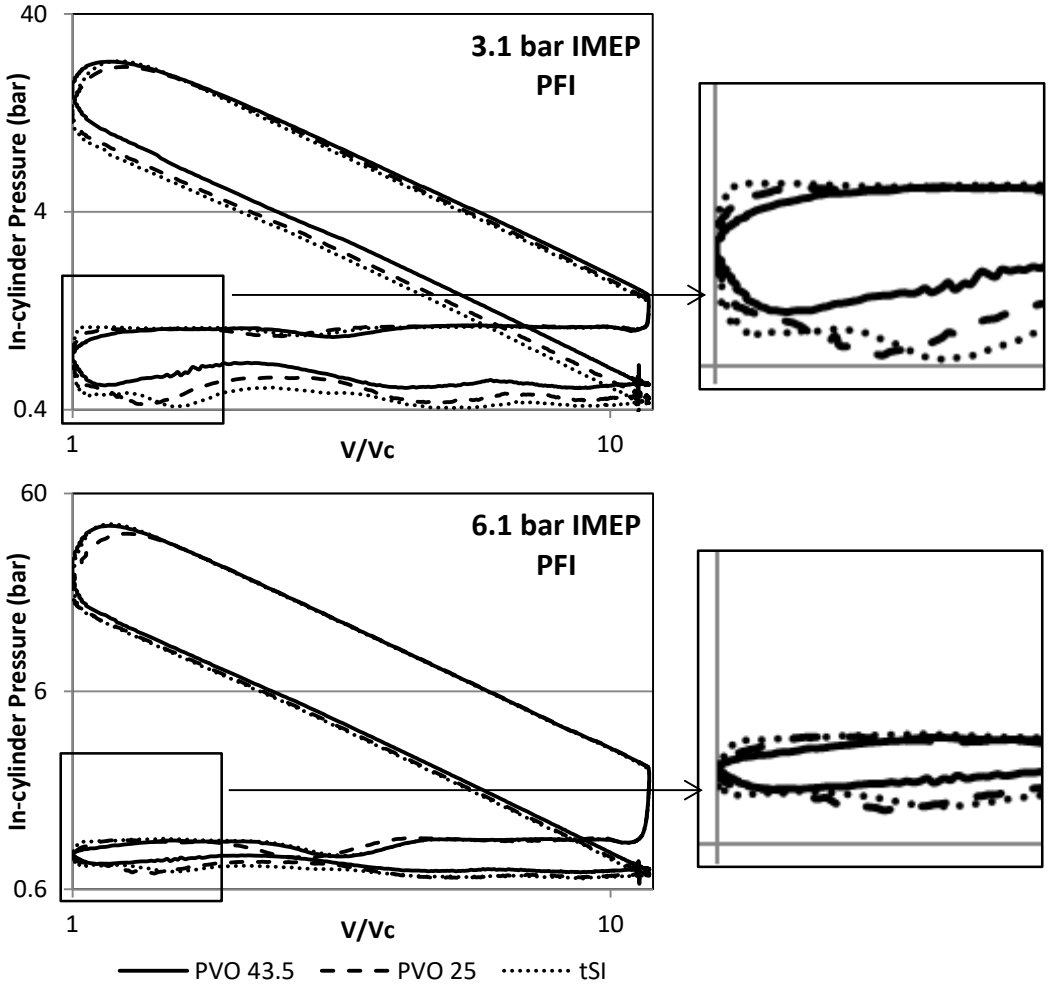

Figure 4.7. Effect of PVO duration in the Log P x Log V diagrams of PFI operation at loads of 3.1 bar and 6.1 bar IMEP – detail of the end of the exhaust stroke. E100 1500 rpm MBT operation.

Another point to be addressed regarding the gas exchange process is the residual gas backflow behaviour. This was a consequence of pressure difference between the cylinder and the intake ports after the IVO. In-cylinder pressure at IVO was always higher than atmospheric condition and presented a maximum variation smaller than 0.1 bar between the highest and the lowest load. However, the intake pressure varied more than 0.5 bar (between maximum and minimum tested loads). It is therefore expected that higher RGF quantity would be a result of the pressure difference and early IVO with enough time for the burned gas to backflow to the intake ports. This can be seen when investigating the late exhaust stroke phase of the Log P x Log V diagrams in Figure 4.7. The earlier IVC of the PVO 43.5 resulted in a bigger in-cylinder pressure drop before TDC as result of burned gas backflow to the intake ports. As PVO decreased and IVC was delayed towards TDC, the pressure drop was much smaller. The increase in the load resulted in lower pressure difference between the cylinder and intake ports, so, lower RGF were expected. At the highest loads it was expected that dynamic effects of the flow would improve scavenging process and reduce the RGF as the PVO increased.

In the work of Bucker et. al. [67], the influence of intake valve phasing on the in-cylinder flow structures of a four-valve cylinder head was investigated using PIV techniques. The major tumble flow structure shape was not shown to be altered in a symmetry plane between the intake valves. The mean turbulent kinetic energy absolute values and trends were very similar during the compression stroke even though there was some considerable difference in the mean kinetic energy and vorticity. For an offset plane from the symmetry plane, it was found a higher kinetic energy in the end of the compression stroke for later IVCs, and an increased deterioration of the tumble structures and turbulent kinetic energy for earlier IVCs. From the results shown in the paper, it could be implied that the in-cylinder flow motion in the early phase of the intake stroke is controlled by the IVO event. Even then, the evolution of the tumble flow structure during the compression stroke showed a higher dependence on the IVC event, especially in the extreme cases (the earlier or later IVC cases).

In another work from Johansson and Soderberg [68] using laser Dopler velocimetry, it was shown that for a valve overlap variation of 17 CAD (IVOs of 8 CAD BTDC and 9 ATDC, with EVC at 16 ATDC) using intake valve phasing, the evolution of the turbulence levels for each valve timing was very similar. On the other hand, there was a considerable variation between the different velocity components. Looking at the presented pressure traces of such work, it would not be expected residual gas

backflow to the intake manifold. Thus, the small intake phasing towards the compression stroke, didn't show any effect on the combustion process.

So, for the different valve overlap periods with constant IVC (cases presented in this sub-chapter) there is evidence that the tumble flow structure and turbulence kinetic energy may be affected at certain extent to influence the combustion process when considering that both IVO and EVC were changed. Even then, data could not be found in the literature for such cases, and for the sake of the discussion, the flow field variation effect in the combustion process due to different valve overlaps won't be considered for combustion parameters discussion.

4.1.3.2. Combustion characteristics

MBT spark timing and the crank angle of 50% MFB (CA50) for all the tested points are presented in Figure 4.8. MBT operation could be achieved in all tested conditions with

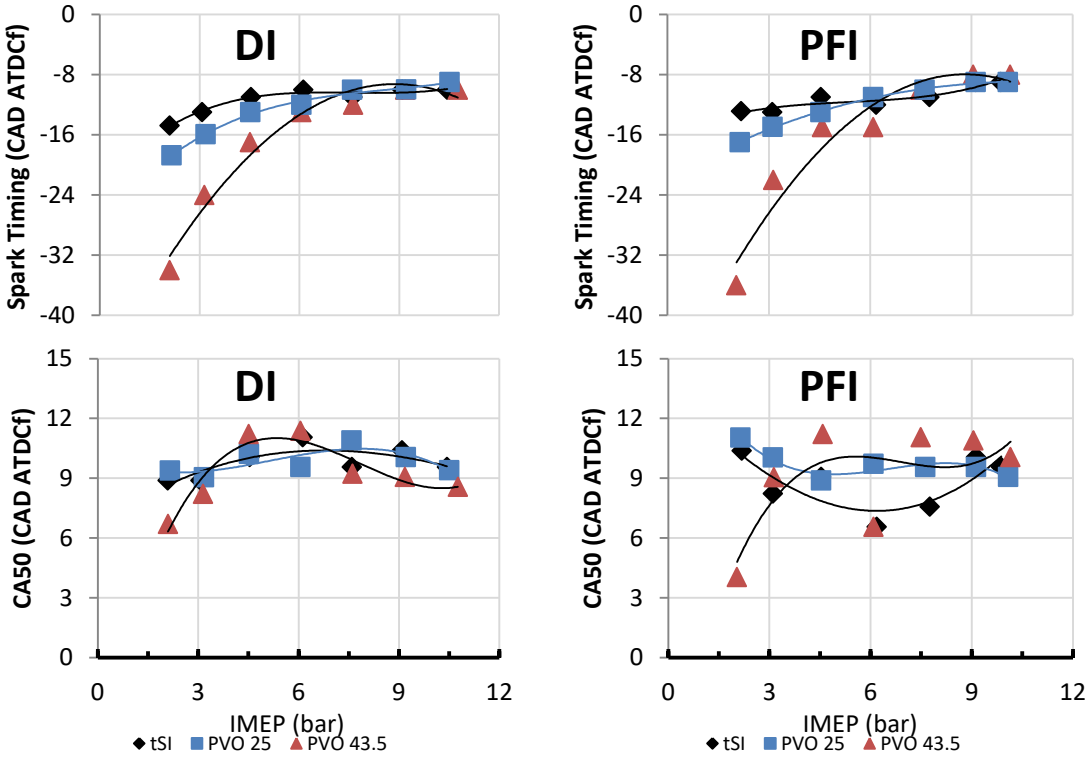

Figure 4.8. Effect of PVO duration on spark timing and CA50 at different loads for DI and PFI injection strategies. E100 1500 rpm MBT operation.

conventional spark ignition combustion. The increase in the residual gas fraction due to increased PVO required the advance of the spark timing in order to correctly phase the combustion. Most of the CA50 points thus occurred between 6 and 12 CAD ATDCf. The exception was the 2 bar IMEP PVO 43.5 point which required a more advanced combustion phasing due to high RGF in order to enable stable combustion and reduce the COV_{imep} (presented in Figure 4.9). In general, PFI spark timing was slightly less advanced than in the DI. This occurred due to the exacerbated DI cooling effect propitiated with ethanol.

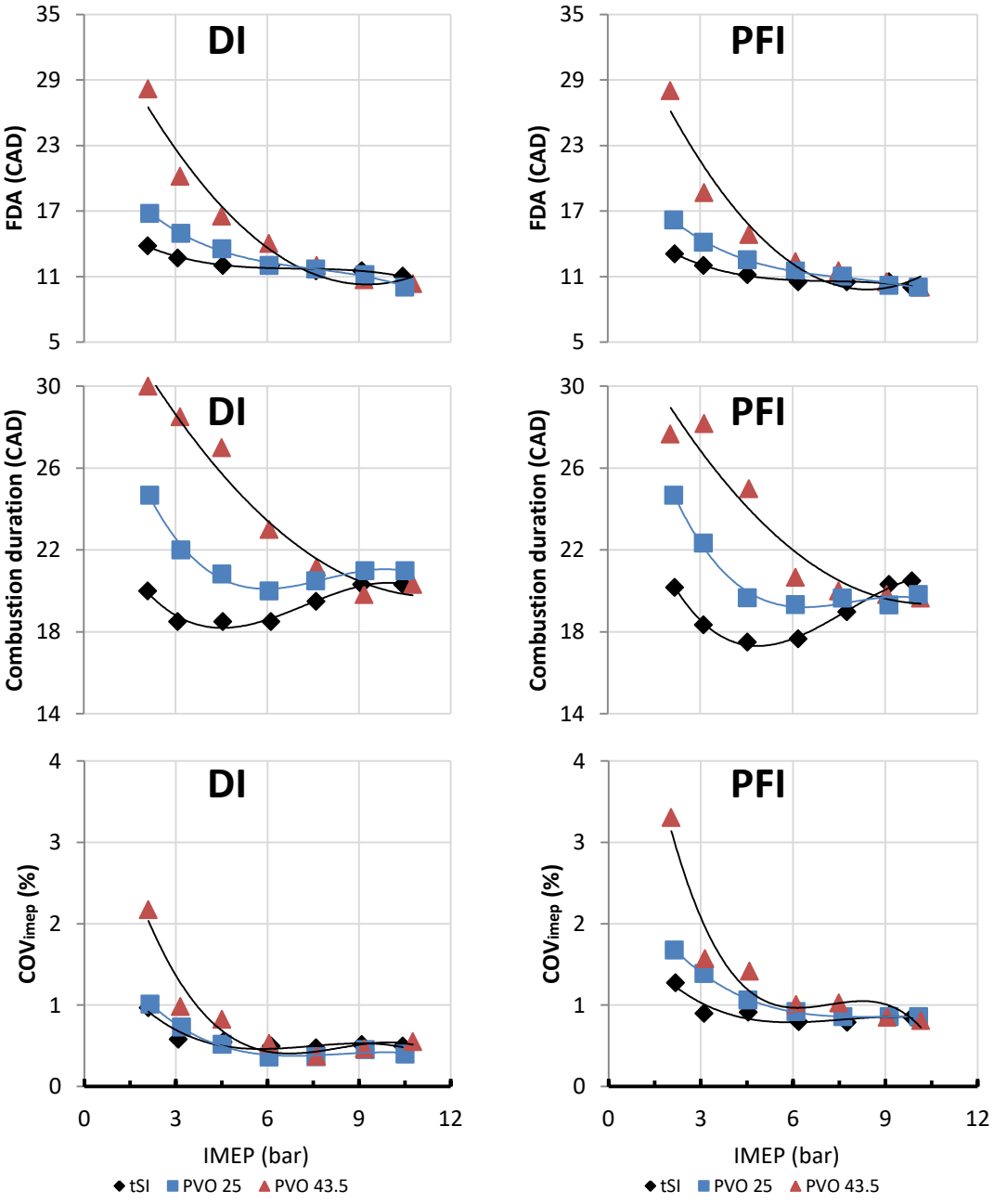

Figure 4.9. Effect of PVO duration on FDA, combustion duration and COV_{imep} at different loads with DI and PFI injection strategies. E100 1500 rpm MBT operation.

The increased RG content, which was the consequence of the higher PVO duration, increased both the combustion duration and flame development angle (0-10% MFB), as shown in Figure 4.9. The combustion durations and flame development angles of DI and PFI injection strategies have shown similar trends for each valve strategy, with very similar durations at each load. Thus, the increase on the COV_{imep} for all PFI cases occurred due to a more complex gas exchange process. In such cases the presence of fresh charge and burned gases in the intake ports was more prone to cyclic variability of the induction process, while in the DI strategy, the only the fresh air was partially mixed with the residual gases with delayed in-cylinder charge preparation.

Figure 4.10 presents the peak in-cylinder pressure, maximum rate of pressure rise and exhaust temperature data of the tested points. In general, in-cylinder peak pressure was independent of the PVO duration and injection strategy, while being a direct function of the load. The small differences could be attributed to slightly different combustion phasing. The maximum rate of pressure rise (MRRP) reduced for higher PVO up to a certain load, when it was expected that the enhanced scavenging process would reduce the RGF which increases the MRRP.

The cases with higher PVO were expected to result in lower temperature during combustion temperature. This is supported by the maximum pressure level which was very similar for different PVO duration at the same load and injection strategy. In such situations, the in-cylinder temperature would be lower as the air flow rate was almost the same and the in-cylinder mass was expected to be higher (due to higher RGF). Exhaust temperature (Figure 4.10) shows a complex trend related to both peak in-cylinder temperature, combustion duration and exhaust emissions. Generally, PFI provided lower exhaust gas temperature and pressure during the exhaust stroke. Figure 4.11 presents the effect of the injection strategy on the cycle pressure for the load of 6.1 bar IMEP for each valve timing strategy. The slightly higher compression pressure is also indicative of higher compression temperature which would lead to higher in-cylinder heat transfer.

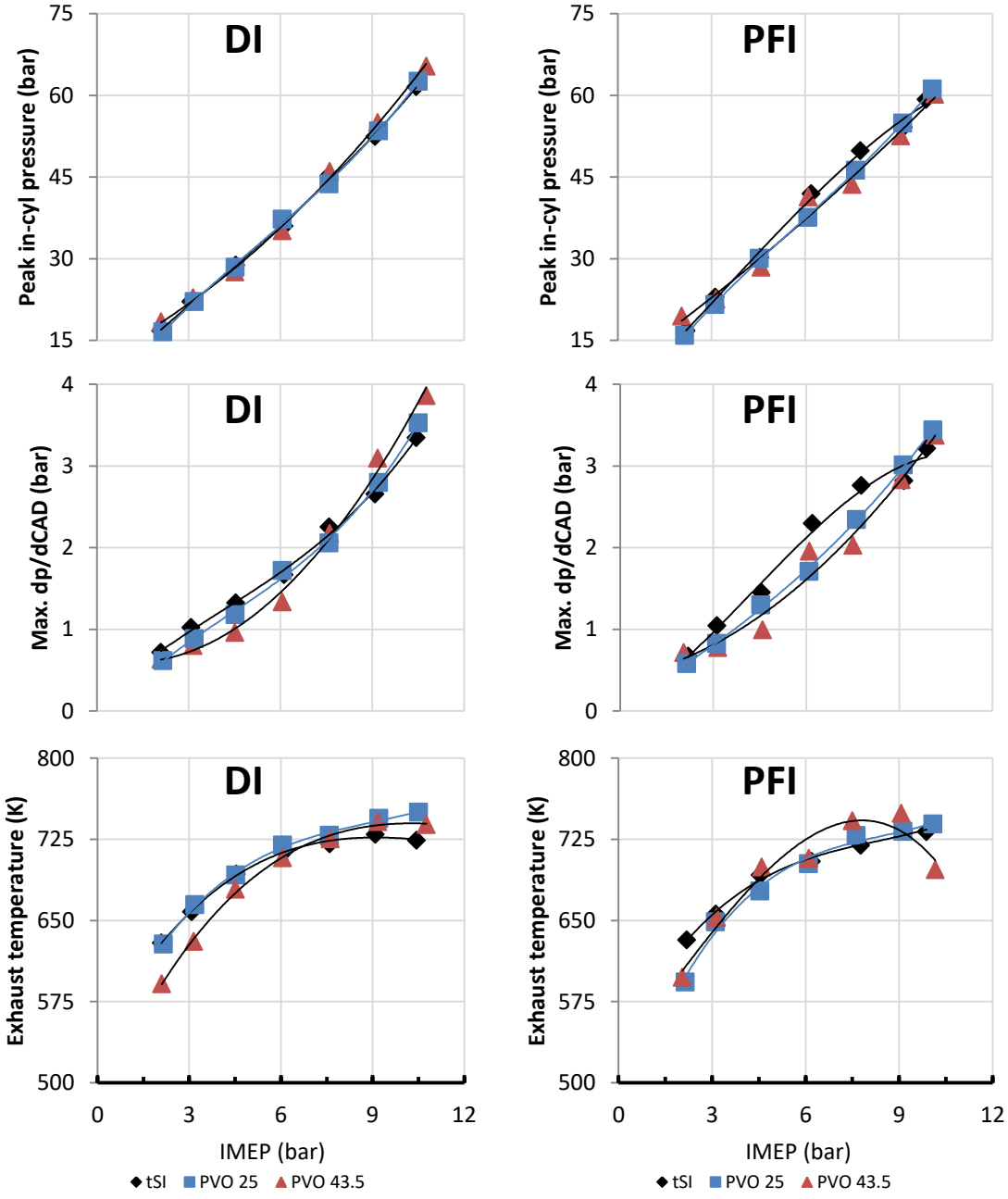

Figure 4.10. Effect of PVO duration on peak in-cylinder pressure, maximum pressure rise rate and exhaust temperature at different loads with DI and PFI injection strategies. E100 1500 rpm MBT operation.

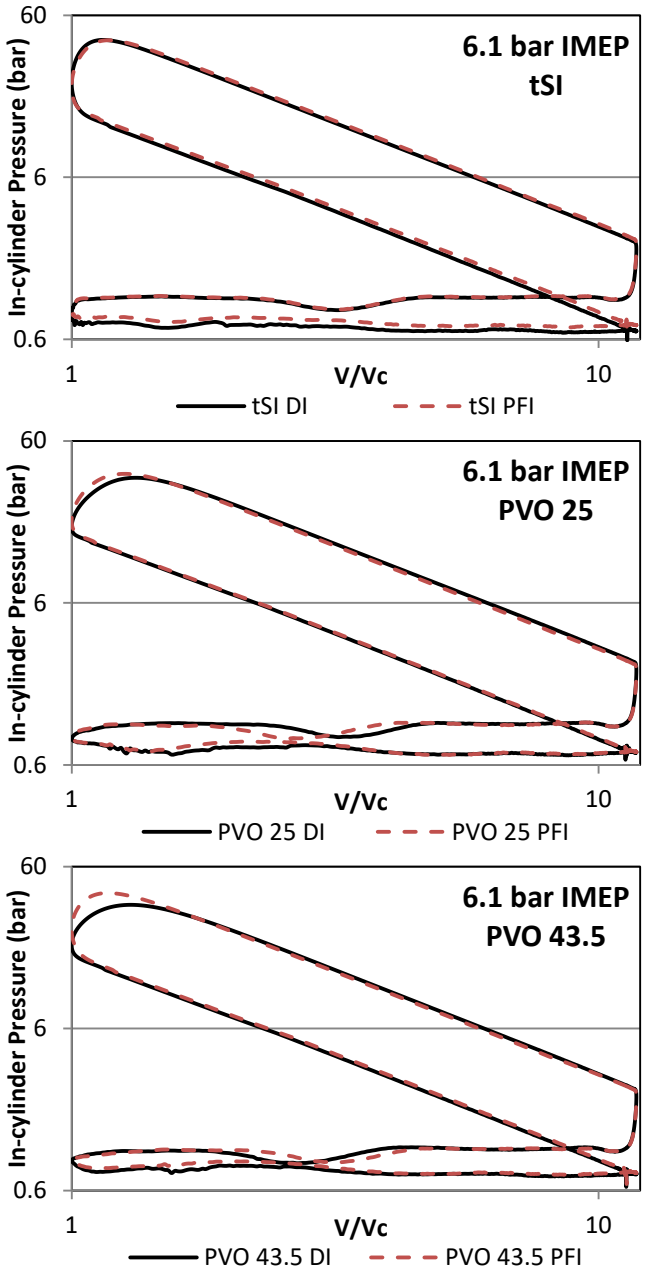

Figure 4.11. Effect of injection strategy on cycle pressure – Log P x Log V diagrams for different valve timing strategies. E100 1500 rpm MBT operation.

Charge temperature effects considerations:

The use of ideal gas law has been proposed to elucidate the effect of the different injection strategies and residual gas fraction on the in-cylinder temperature. The purpose here is not to provide an absolute temperature calculation (once the exact charge composition would need to be taken in account and accurate gas exchange process models would be required), but to

give an idea of how the temperature changes due to distinct overlap periods and injection method. For this purpose, the in-cylinder pressure and volume at 40 CAD $BTDC_{firing}$ were considered. Compression temperature was chosen due to the nature of the spark ignition combustion process.

Table 4.2 presents the measured in-cylinder pressure and estimated temperature at 40 CAD $BTDC_{firing}$ for the tSI (no valve overlap) cases. The calculated PFI temperatures were always higher than the DI temperatures for all loads. The average increase in temperature was around 3.1 %, for this three chosen load points. Considering that the heat transfer process depends on a temperature difference between the charge and the walls term, the increase in this term value would be even higher, directly impairing engine efficiency.

Table 4.2. Measured in-cylinder pressure and estimated temperature for the tSI case with three for three different loads and injection methods.

Load (bar)	Inj. method	Pressure (bar)	Temperature (K)
3.1	DI	3.01	561
	PFI	3.16	580
6.1	DI	4.92	570
	PFI	5.17	584
9.1	DI	6.70	563
	PFI	7.03	584

In order to elucidate the effects of residual gas fraction, the work of Alger and Wooldridge [208] was used to propose a guess of the residual gas fraction for the three different positive valve overlap tested strategies. In this work, different manifold pressures were tested for valve overlaps of 0 CAD, 30 CAD and 60 CAD at a speed of 1500 rpm. Such data was linearly interpolated in order to find estimates for the data of the 4.5 bar IMEP load and DI injection (which presents the same intake manifold range of the work). tSI was considered as zero overlap. Appendix 2 presents the estimated residual gas fraction due to the different positive valve overlap periods found when interpolation the literature values. Even though the bulk in-cylinder temperature during combustion is not representative for burned/unburned gas zone temperatures of the SI combustion, its magnitude represents the thermal state which the charge would

be submitted due to the combustion if it was a homogenous combustion. Thus, it considers the mass addition due to increased residual effects. So, temperature was evaluated for the angle of 16.5 CAD $ATDC_{firing}$, which is less around 0.5 CAD close from the angle of maximum pressure presented in all conditions. Table 4.3 presents the maximum temperature and parameters used for the calculation.

Table 4.3. Estimated maximum temperature for the different injection strategies and valve strategies; E100 fuelling at 1500 rpm.

Load	Inj. method	Valve strategy	Estimated RG (%)	Pressure (bar)	Temperature (K)
4.5 bar	DI	tSI	8.7%	28.8	2093
		PVO 25	13.2%	28.6	2019
		PVO 43.5	17.0%	27.4	1879
	PFI	tSI	8.4%	30.2	2139
		PVO 25	12.2%	30.0	2124
		PVO 43.5	16.1%	28.2	1970

4.1.3.3. Gaseous emissions

Figure 4.12 presents the CO, THC and NOx engine-out gaseous emissions. CO emissions in the DI cases present different trends according to the valve strategy. The injection timing difference between tSI and the other PVO cases was 8 CAD (28 CAD ATDC against 20 CAD ATDC, respectively). This could be a reason for the different homogeneity levels which increase the CO formation. When comparing the PVO 25 and PVO 43.5, there was a general trend of an initial decrease in CO formation with the increase in load and later CO formation increases. The higher CO at lower loads could be attributed to lower combustion temperatures. With the increase in the load, the higher in cylinder temperatures would enhance the ethanol molecules breaking and CO oxidation process. The later increase in the CO formation (after 7.5 bar IMEP load) occurred due to the increased ethanol mass injected at once. This results in increased charge inhomogeneity with local rich areas. On the other hand, PFI charge preparation would generate a more homogeneous charge independently of the load. Thus, the decreasing trend in the CO formation with the load was a consequence of higher in-cylinder temperatures which enhance the CO oxidation process.

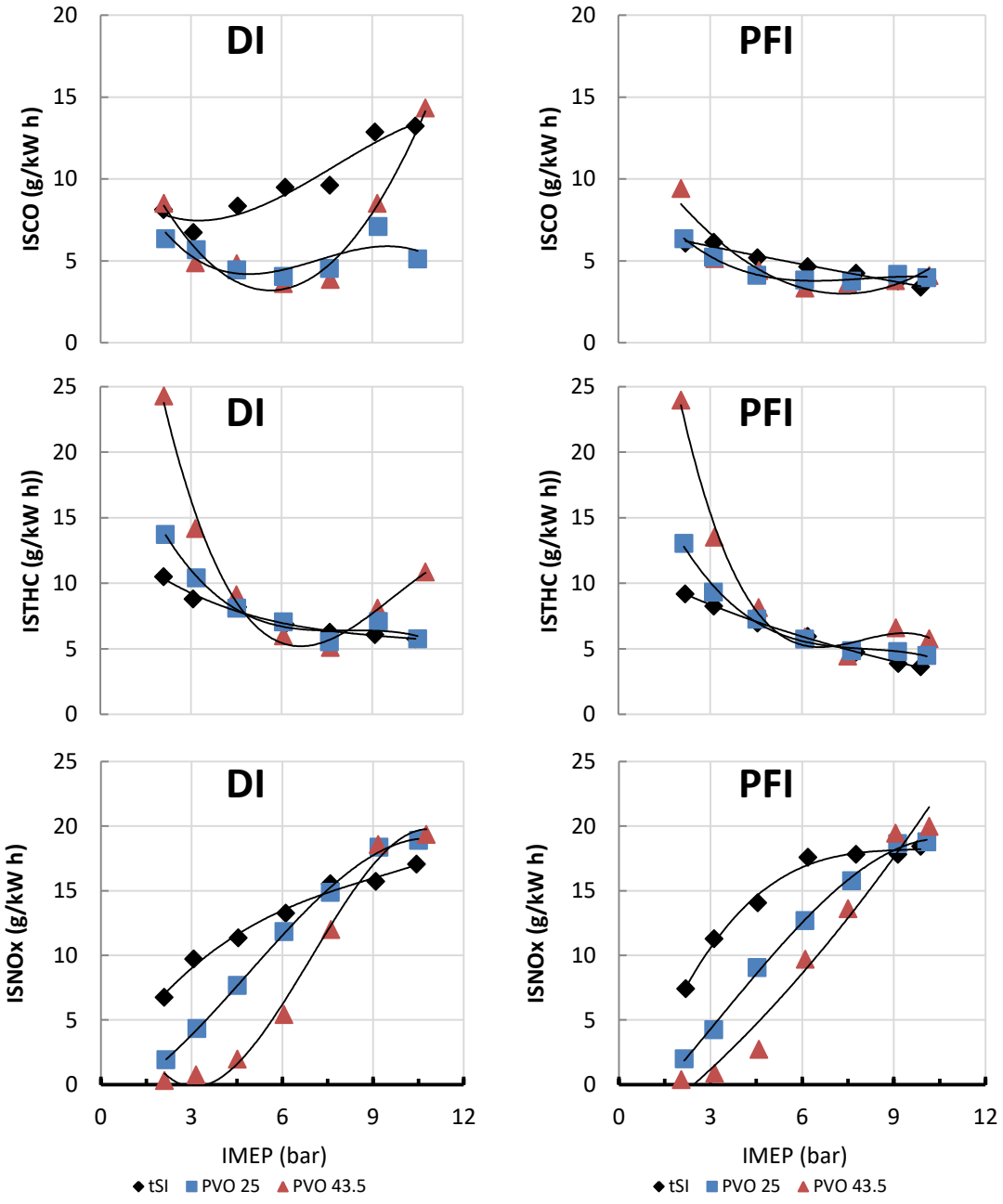

Figure 4.12. Effect of PVO duration on engine out emissions at different loads with DI and PFI injection strategies. E100 1500 rpm MBT operation.

The increased RGF content at low load for the PVO cases increased the THC emissions due to the lower temperature combustion. This reduced the ethanol break down and the broken radicals oxidation process. The later increase in the THC emissions for the PVO 43.5 case could be attributed to the enhanced scavenging process which promoted some fuel short circuiting. Until up to 6 bar IMEP load, THC emission of PFI and DI were almost the same. After this load, the increased fuel mass

direct injected in the cylinder at once probably resulted in some fuel impingement, thus resulting in slightly higher THC emissions.

NOx emissions were lower compared to the cases with higher PVO. This was a direct consequence of the lower combustion temperatures achieved with the higher RGF. At higher loads, when the scavenging process became better for the higher PVO cases, the combustion temperatures were higher and so were the NOx emissions. PFI operation resulted in higher NOx emissions due to expected higher combustion temperatures. When using DI method, the expected higher in-cylinder inhomogeneity would lead to a reduction in NOx emission.

4.1.3.4. Efficiency related parameters

Thermodynamic efficiency and combustion efficiency were also investigated in order to understand the indicated efficiency trend behaviour which is defined as the product of these efficiencies and gas exchange efficiency. Figure 4.13 present the efficiency related parameters. Gas exchange efficiency was previously presented in Figure 4.6.

Combustion efficiency trend was linked to CO and THC emissions. Therefore, PFI cases presented better combustion efficiency than DI cases as in general the THC and CO emissions of the PFI cases were lower. Even then, in most cases the combustion efficiency was between the range of 96.5 and 98.5%, showing a general trend of increase in combustion efficiency with the increase of the load due to reduction in THC emissions. The low combustion efficiency at 2 bar IMEP with PVO 43.5 occurred mainly due to high THC emissions (for both PFI and DI cases) as for the WOT PVO 43.5 DI case.

The thermodynamic efficiency trends show that the DI combustion process was more efficient. One of the reasons is the lower combustion temperatures which resulted in lower heat losses to the cooling system as a consequence of the DI cooling effect. Another reason would be the lower COV_{imep} which occurred as consequence of the more stable gas exchange and combustion processes. Regarding the different strategies, the longer PVO which provided lower combustion temperatures also provided lower heat loss, thus, the highest thermodynamic efficiencies.

The net indicated efficiency result was the correlation between all the previously discussed efficiencies. The main reason for the higher PVO 43.5 indicated efficiency at low and medium loads was the much higher gas indicated efficiency. The increase in

gas exchange efficiency with the load was also the main reason for the increase in the indicated efficiencies for all valve timing strategies. At higher loads, the low combustion efficiency (which increased combustion temperature due to lower RGF) was the main reason for the PVO 43.5 DI lower net indicated efficiency, while the decreased thermodynamic efficiency was the reason for the PVO 43.5 PFI case.

According to these results it can be concluded that longer PVO is desirable for improved engine efficiency. In turn, at high loads, this may increase maximum engine load at cost of engine efficiency.

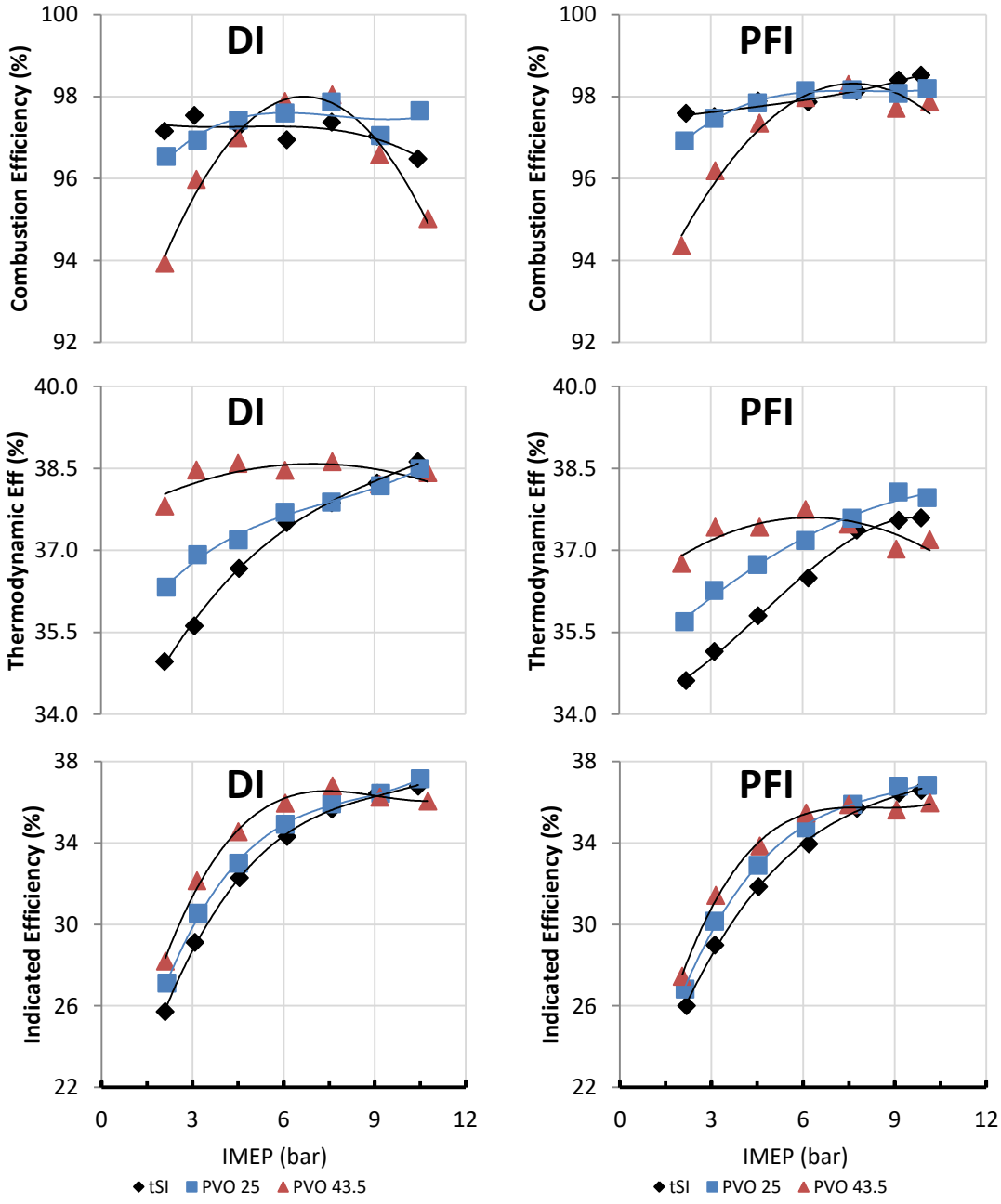

Figure 4.13. Effect of PVO duration on the efficiency related parameters at different loads with DI and PFI injection strategies. E100 1500 rpm MBT operation.

4.2. Spark ignition operation of E100 with positive valve overlap and intake valve phasing

The following two studies aimed to explore the intake phasing concept in order to further increase ethanol throttled SI operation efficiency. The first study aim to understand the effect of intake valve phasing at a constant load and speed. The second study aims to explore intake valve phasing in order to increase engine out efficiency for different loads compared to the fixed valve profile.

4.2.1. Effect of intake valve phasing on the E100 SI operation with DI injection.

4.2.1.1. Methodology

The intake valve profile of the PVO 43.5 was used as a baseline. Exhaust valve timing and duration were kept constant as in the previous tests. Intake valve opening and closure events were evenly moved in order to phase the intake period. Different PVO durations could be tested while keeping the intake profile duration constant. The tested valve timings are presented at Table 4.4. Intake duration was kept relatively constant while advancing the opening point before TDC and keeping exhaust valve timing fixed.

The load was fixed to 6.1 bar IMEP and was controlled using the throttle plate. Spark timing was varied in order to achieve MBT with stoichiometric air to fuel ratio. Injection timing was set to 28 CAD ATDCi for the non-baseline cases. The tested speed was 1500 rpm.

Table 4.4. Valve timing for intake phasing test at 6.1 bar IMEP, 1500 rpm, MBT operation, E100 DI timing 28 CAD ATDCi.

PVO dur (CAD)	IVO (CAD ATDCi)	IVC (CAD ATDCi)	IV dur. (CAD)	EVO (CAD ATDCi)	EVC (CAD ATDCi)	EV dur. (CAD)
43	-22	206	228	-190	21	211
52	-29	197	226	-190	23	213
63	-40	186	226	-190	23	213
72	-50	176	226	-190	23	213
83	-60	166	226	-190	23	213
92	-70	157	226	-190	23	213
104	-81	146	227	-190	23	213

4.2.1.2. Effect of intake profile phasing on gas exchange process

Figure 4.14 presents the gas exchange process's main parameters and intake valves related parameters. It should be noted that the baseline case is represented in the plots by the first result point from the right to the left. The initial advance of the IVO (phasing the whole intake period) increased the amount of burned gas backflow. In turn, it required a higher intake plenum pressure in order to supply the correct amount of air. This decreased the in-cylinder to exhaust port pressure difference during the early intake phase (before the piston reaches TDC) while increasing the period for the backflow process – opposite effects. A higher intake plenum pressure decreased pumping work while increasing gas exchange efficiency.

On the other hand, the consequent advance of the IVC, which was initially occurring after the BDC, increased the geometric compression ratio (CR_v) calculated in relation to in-cylinder volume at valve closing point. The further advanced of the IVC before the BDC resulted in reduction of the CR_v. The effective compression ratio, which is related to both in-cylinder pressure during compression and intake manifold pressure, was kept relatively constant until the intake valve closing period started to occur considerably earlier than the BDC. At this point, the flow restrictions started an over expansion phase as the intake valve was starting to close. This resulted in reduced effective compression ratio and consequent lower in-cylinder pressure at spark timing. Figure 4.15 present the log P x log V diagrams of three different PVO cases. The recompression period was more evident for the extreme case with PVO 104 CAD.

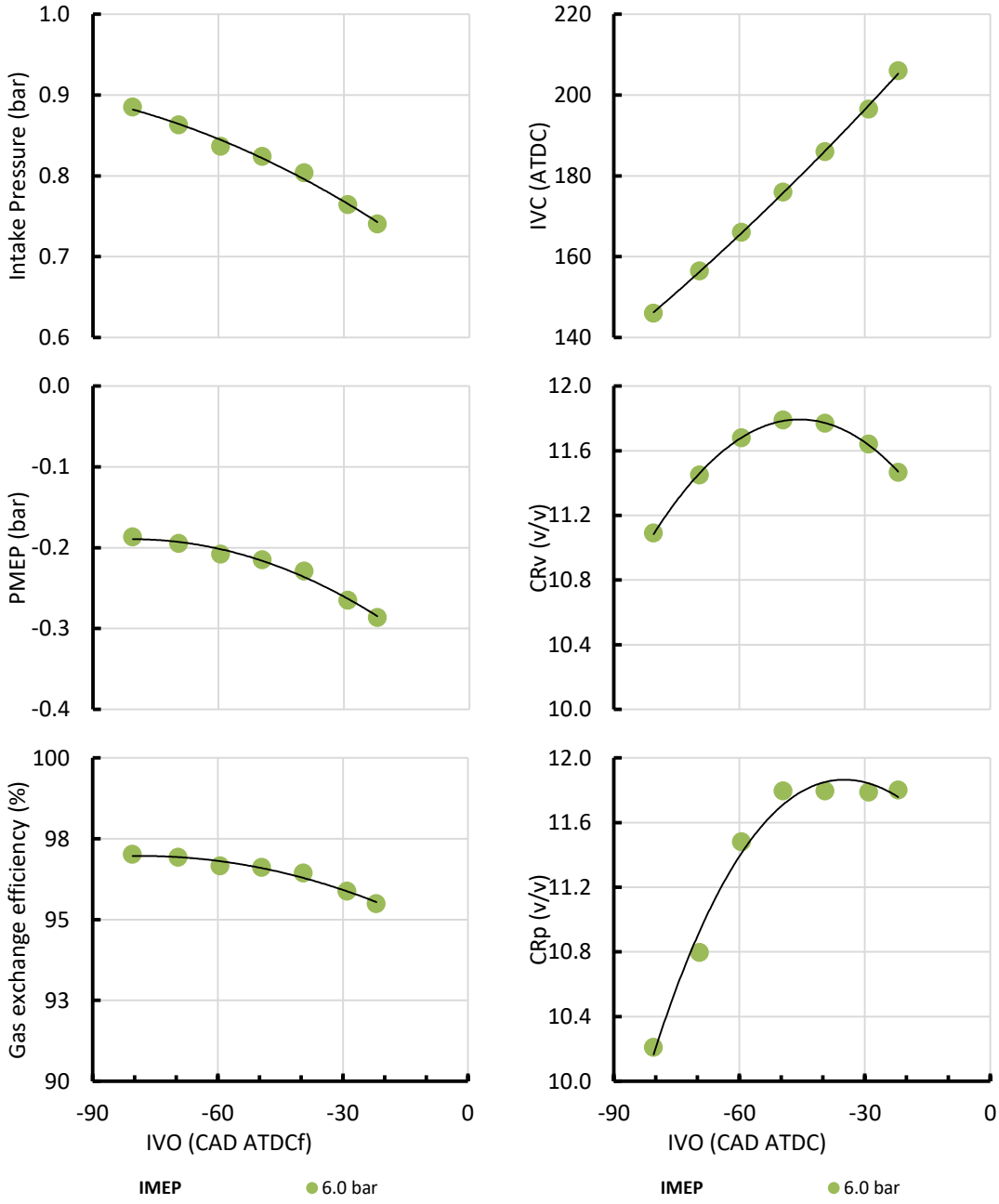

Figure 4.14. Effect of intake profile phasing in the gas exchange and valve related parameters. E100, 1500 rpm, 6.1 bar IMEP, MBT operation, DI timing 28 CAD ATDCi.

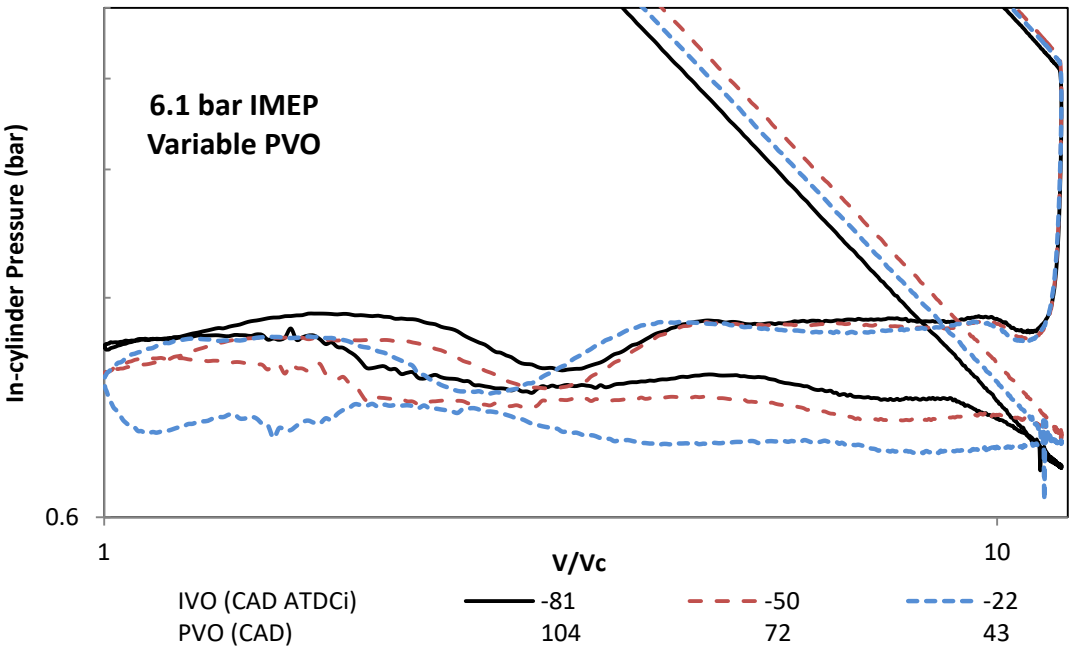

Figure 4.15. Effect of intake valve profile phasing in order to increase the PVO period – log P x log V/Vc diagram. E100, 1500 rpm, 6.1 bar IMEP, MBT operation, DI timing 28 CAD ATDCi.

4.2.1.3. Effect of intake profile phasing on engine combustion, emissions and efficiencies

Figure 4.16 presents the combustion, emissions and efficiency related parameters for different PVO as a consequence of intake profile phasing. Combustion process was considerably affected by the intake profile phasing. Spark timing had to be advanced in order to phase the combustion for MBT. Two main parameters had major influence on the combustion process: variation of the effective compression ratio and variation of the RGF. The RGF was expected to have a bigger initial impact when increasing the PVO duration from the baseline as the effective compression ratio was kept fairly constant (up to PVO 72 with IVO at -50 CAD ATDC). Around this point the RGF was expected to reduce as result of the reduction in the pressure difference. This influence of CR_p and RGF in the combustion process is shown in the combustion duration and FDA plot. While FDA showed a constant increasing trend, combustion duration showed an inversion trend. Even then, the combustion process was very stable as confirmed by the lower than 1.0% COV_{imep} at all cases. As shown in Figure 4.17, the increase in RGF content and reduction on RC_p decrease the peak heat release rate and increase combustion duration.

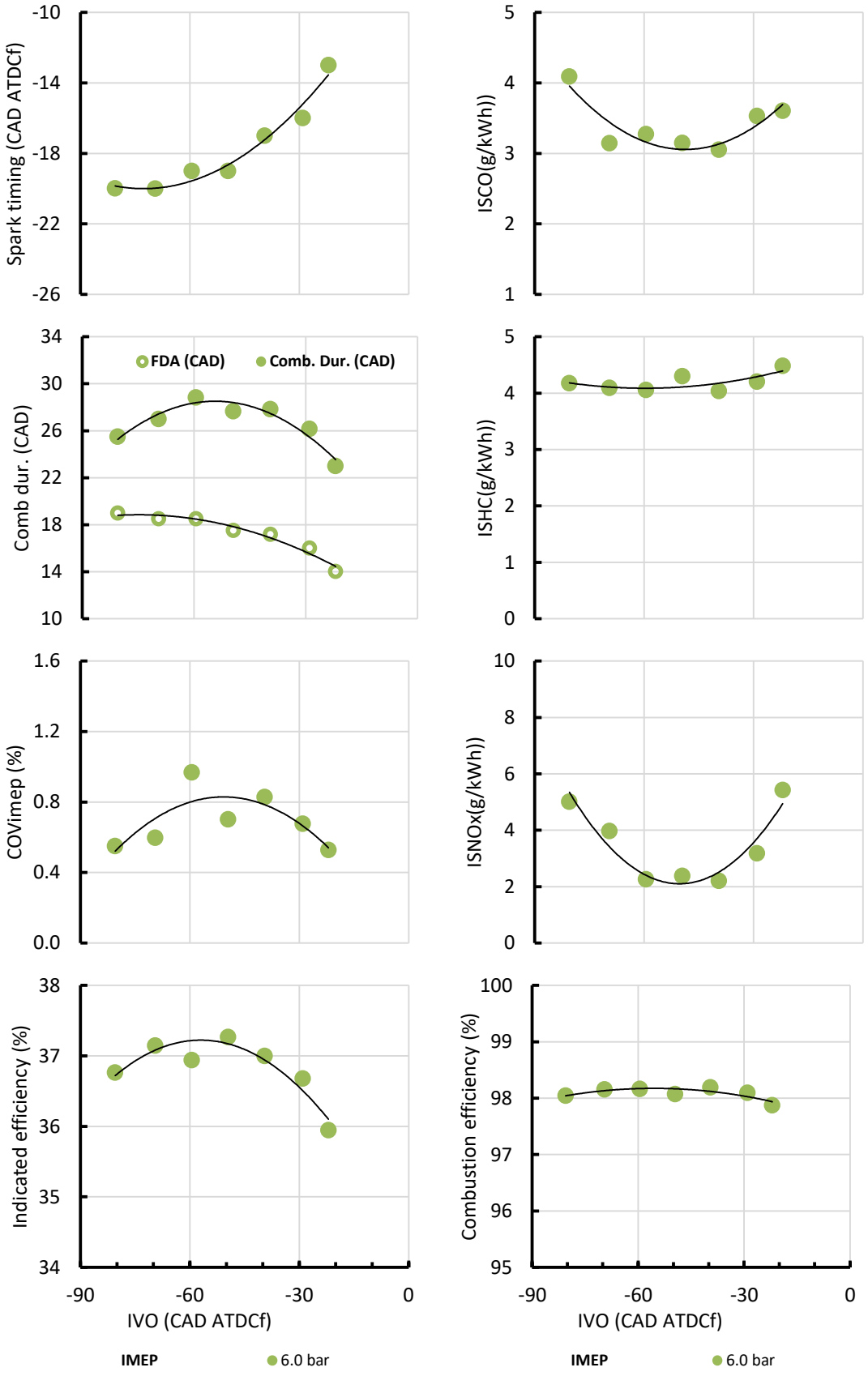

Figure 4.16. Effect of intake profile phasing in combustion, emissions and efficiency related parameters. E100, 1500 rpm, 6.1 bar IMEP, MBT operation, DI timing 28 CAD ATDCi.

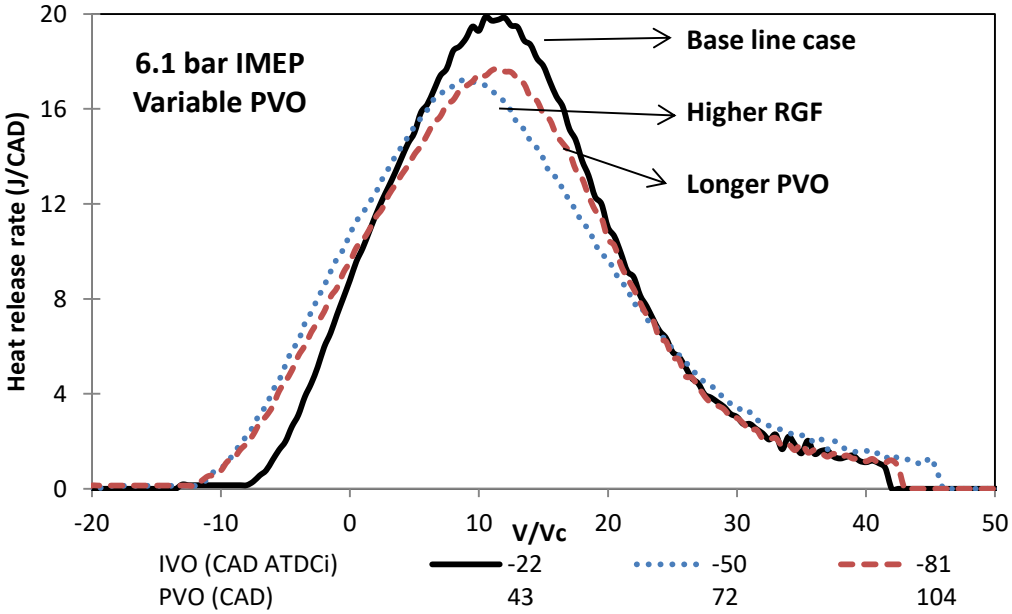

Figure 4.17. Effect of intake profile phasing on the heat release rate of three different PVO cases. E100, 1500 rpm, 6.1 bar IMEP, MBT operation, DI timing 28 CAD ATDCi.

Regarding CO specific emissions, the maximum variation (around 1 g/kW h) can be attributed to maximum lambda variations in the order of 0.01. It could be considered that there was no impact in the CO formation due to the increased PVO. The same occurred for THC emissions. Due to the nearly constant CO and THC emissions behaviour, combustion efficiency could be considered to not be affected by the PVO variation.

NOx emissions were considerably affected by the increase in the RGF. The maximum NOx reduction was more than 200% in comparison to the baseline case.

Gas exchange efficiency was thus the most important factor in order to increase the indicated efficiency relative to the baseline case. The second point was the RGF which was assumed to decrease combustion temperature (as shown in a previous discussion) and reduce heat transfer losses. For this reason, the cases expected to have the highest residual gas fraction were also the cases that provided the highest net indicated efficiency.

4.2.2. **Optimized intake profile phasing for high efficiency E100 SI throttled operation with DI and PFI strategies.**

4.2.2.1. Methodology

The loads of 2.0, 3.1, 4.5, 6.1, 7.5, 9.0 and WOT were also tested following the methodology previously presented. The tests were run at 1500 rpm and stoichiometric conditions with MBT spark timing. The main objectives were to evaluate efficiency gains and pollutant emission behaviour when using the intake phasing concept. DI timing was set to 28 CAD ATDCi, while PFI timing was set to TDCf. The results will be present for the optimized intake phasing points only.

4.2.2.2. Results

Table 4.5 presents the optimized valve timing for the increased efficiency trend. The fixed PVO (baseline) could not be run at 2.0 bar IMEP due to a 3 CAD longer PVO which resulted in high $COV_{imep.}$ Thus, the 2.0 bar IMEP variable PVO test was taken with a 5 CAD smaller PVO with 5 CAD delay on the IVO (comparing to the baseline).

Table 4.5. Valve timings used in the variable PVO experiment. E100, 1500 rpm, MBT operation.

	IMEP (bar)	PVO dur (CAD)	IVC (CAD ATDCi)	IVO (CAD ATDCi)	EVC (CAD ATDCi)	EVO (CAD ATDCi)
Fixed PVO	All loads	46	204	-25	22	-190
	IMEP	PVO	IVC	IVO	EVC	EVO
DI Variable PVO	2.1	41	209	-20	22	-190
	3.1	46	204	-25	22	-190
	4.7	68	184	-45	23	-190
	6.1	66	184	-45	21	-190
	7.6	67	184	-45	22	-190
	9.2	66	184	-45	22	-190
	11.0	66	184	-45	21	-190
	IMEP	PVO	IVC	IVO	EVC	EVO
PFI Variable PVO	2.0	36	216	-15	22	-190
	3.1	46	206	-25	22	-190
	4.5	67	186	-45	22	-190
	6.1	67	187	-45	22	-190
	7.3	77	183	-55	22	-190
	9.0	67	186	-45	22	-190
	10.3	46	206	-25	22	-190

At lower 3.1 bar load, due to the relatively higher intake ports to exhaust ports pressure difference, the PVO duration could not be increased further than 46 CAD (baseline). For higher loads the PVO duration was set to -66, around the maximum RGF point found at the previous study. For WOT PFI operation the PVO had to be decreased in order to prevent fuel short circuiting.

The increase in the PVO duration in relation to the baseline (fixed PVO) required higher intake air pressure due to higher RGF (Figure 4.18). This consequently decreased the pumping work. PFI air displacement required increased intake pressure. The increase in the RGF required spark timing advance. Even with more advanced spark timing, DI combustion duration and flame development angle tended to be longer for the variable

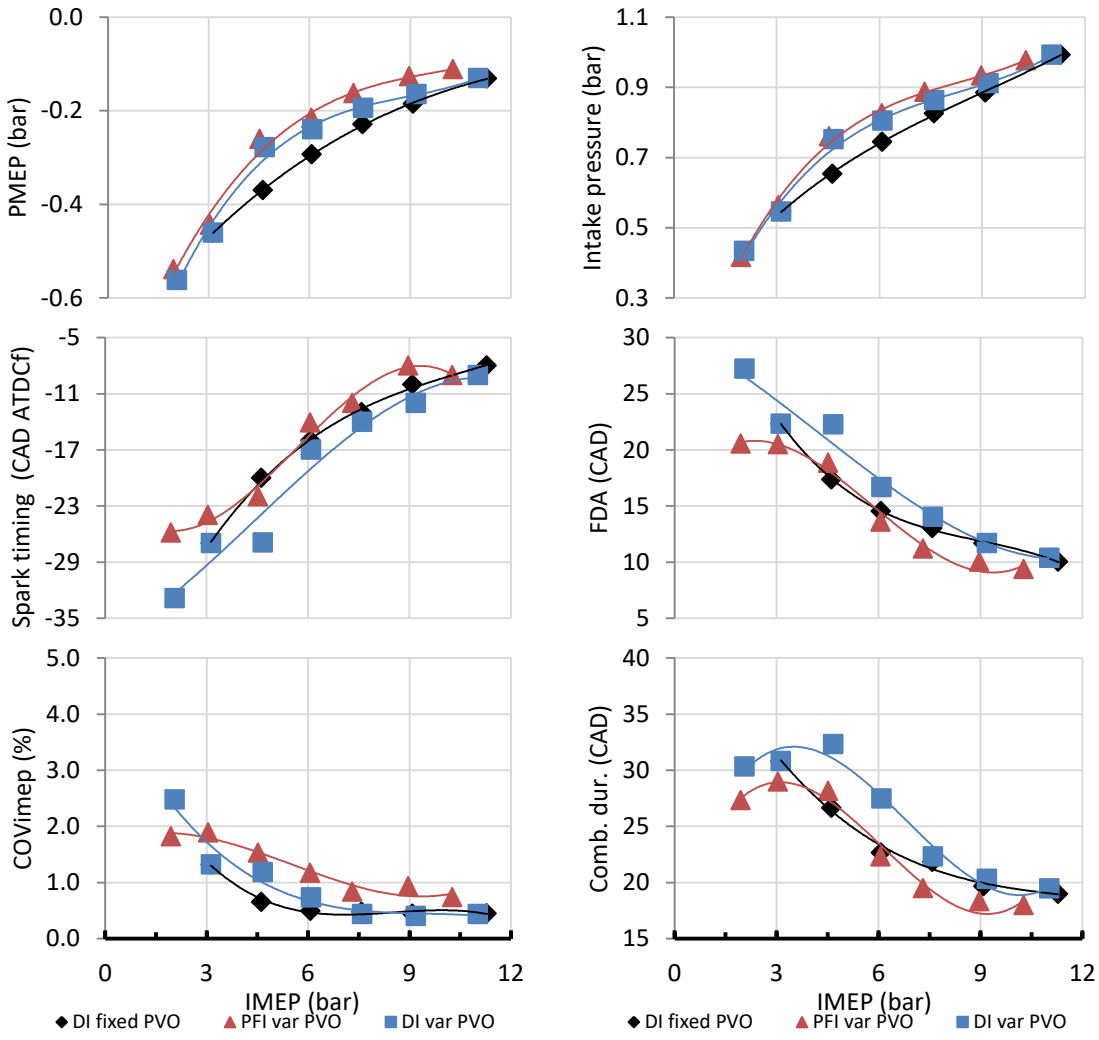

Figure 4.18. Effects of variable PVO on gas exchange and combustion parameters at different loads. E100, 1500 rpm, 6.1 bar IMEP, MBT operation, DI timing 28 CAD ATDCi. Optimized PVO valve timings.

intake phasing cases. Increased PFI combustion temperature at higher loads reduced combustion duration and FDA. PFI cyclic variability tended to be higher due to a more complex mixture preparation process.

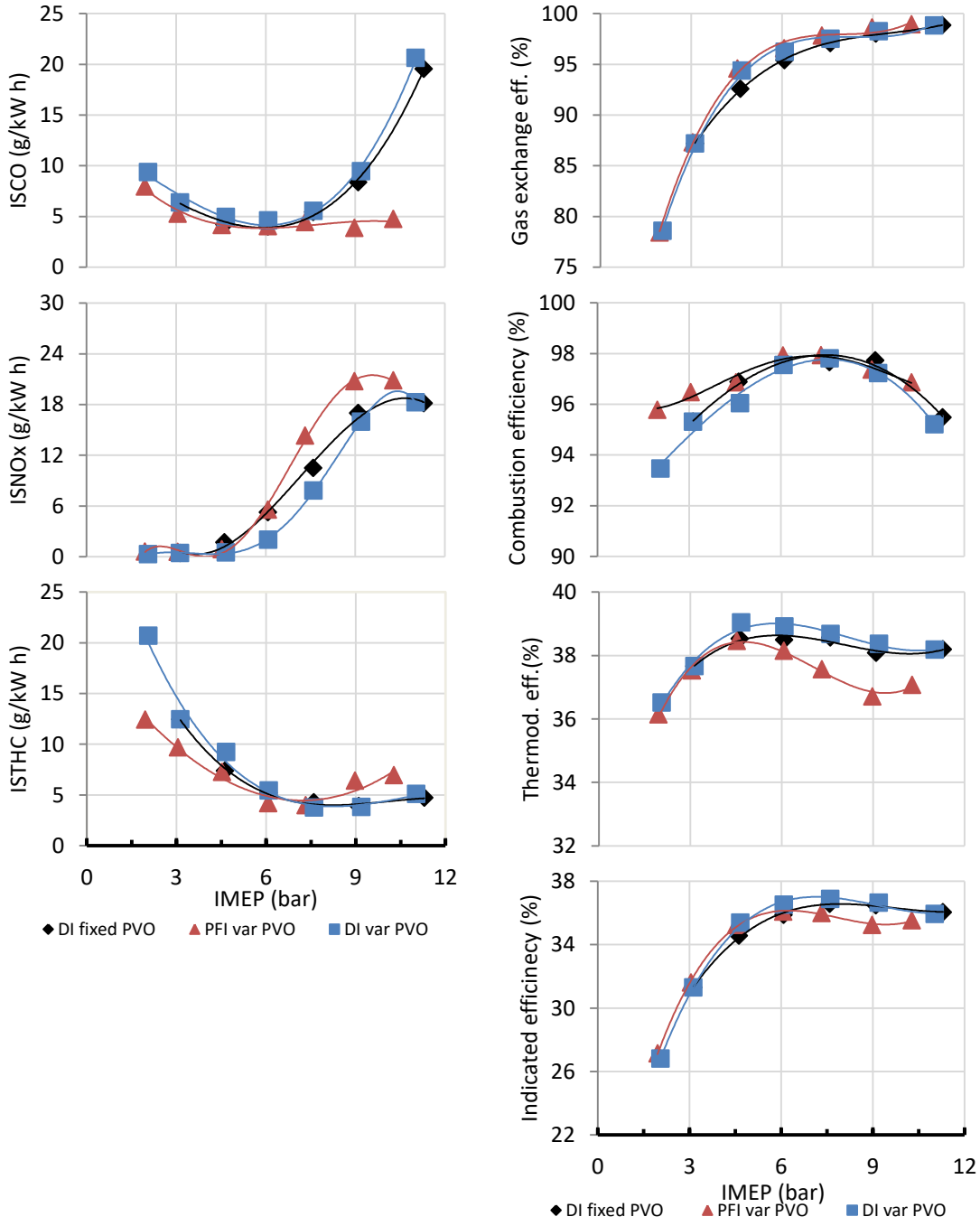

Figure 4.19. Effects of variable PVO on gas exchange and combustion parameters at different loads. E100, 1500 rpm, 6.1 bar IMEP, MBT operation, DI timing 28 CAD ATDCi. Optimized PVO valve timings.

NOx emissions provided a direct indicator of combustion temperatures. The increased RGF content of the variable PVO cases resulted in the lowest combustion

temperatures, thus, lower NOx emissions. DI cooling effect was responsible for further reduction in NOx emissions. It was possible to achieve ISNOx emissions lower than 0.35 g/kW.h for loads up to 4.5 bar IMEP with conventional spark ignition combustion.

Regarding CO emissions (emission data is presented in Figure 4.19), the slight increase in the CO emission for the variable PVO case with DI injection (compared to fixed PVO) was a consequence of lower combustion temperatures. As the CO offset was constant and the test points were taken individually for each load, this was not expected to be due to lambda variations. The PFI CO emissions were better at all loads due to better fuel preparation process. The single DI injection created a less homogeneous charge which increased CO emissions.

THC emissions followed the same trend for all strategies, regardless of the fuel injection method. At loads up to 4.5 bar IMEP, the small differences between cases followed the temperature trend. At higher loads, where higher combustion temperatures were achieved, both the DI cases provided similar results, with lower THC emissions from the PFI case due to the absence of any fuel impingement.

The longer PVO achieved at mid part load operation increased gas exchange efficiency considerably, following the opposite trend of the PMEP. DI variable PVO operation resulted in the lowest combustion efficiency due to higher CO and THC emissions. Lower CO emissions of the variable PVO with PFI resulted in the higher combustion efficiency at high load. Thermal efficiency was directly related to the combustion temperatures which increased heat loss. Thus, PFI provided the lowest thermodynamic efficiency, while the lower combustion achieved with variable PVO and DI resulted in the highest thermodynamic efficiency.

Indicated efficiency was a consequence of the relationship between the thermodynamic, gas exchange and combustion efficiencies. The main reason for the initial increase in net indicated efficiency with the increase of the load was the improved gas exchange efficiency which improved around 20% from 2.0 bar to 4.5 bar IMEP. At the same time, the increase in the combustion temperature improved the combustion process and the fuel conversion. The higher indicated efficiencies were achieved for the variable PVO strategy with DI. At lower 3.1 and 2.0 bar IMEP, the higher PFI combustion temperature increased the fuel conversion efficiency and resulted in the higher indicated efficiency. Further combustion temperature increase resulted in increased heat loss. Thus, DI provided better indicated efficiency at mid high loads.

The less homogeneous DI charge at high loads decreased the fuel conversion efficiency. The increase in THC for the 9 bar and WOT PFI operation could be attributed to fuel short circuiting. The relationship between these effects at loads higher than 6.1 bar IMEP resulted in the decrease of net indicated efficiency for both PFI and DI scenarios.

4.3. Summary

Different valve profiles based on conventional spark ignition engine valve profile were systematically studied in order to understand the its impacts in the throttled E100 spark ignition operation performance. Near idle to full load were tested at 1500 rpm to investigate the load range were the higher benefits could be attained when using different PVO configuration.

From the first study regarding the fixed valve profile it could be concluded that depending on the engine target – efficiency or performance – there are compromises between full load and part load engine performance. In the case of an engine designed to operate at rated power (generator or range extender), less PVO would result in best fuel consumption. On the other hand, for an engine running at different loads and speeds (as automotive engines) the longer PVO would increase the overall engine efficiency.

Regarding the intake phasing as residual gas trapping method, it was found that there is a limit for the maximum RGF when advancing the intake phasing. This limit was a trade-off between intake pressure and PVO duration. In this way, intermediate PVO duration (between the tested cases) resulted in the highest RGF and indicated efficiency. And as indicated by the literature, the main focus to increase SI engine efficiency at low load is the reduction in pumping losses.

Additionally, it was found that at low loads the use of hot residual gas backflow to the intake ports is a good strategy to propitiate stable combustion as the hot gases improve the charge thermal state up to a certain point. At higher loads it would be suitable to also introduce external cooled egr in order to operate at full throttle. This would help in reducing pumping losses, decrease combustion temperatures and heat losses, and therefore increased the indicated efficiency.

Regarding DI or PFI strategy, it was shown that the main reason for the lower PFI indicated efficiency is the decrease in thermodynamic efficiency at mid and high loads. This was attributed to increased heat losses as consequence of higher combustion

temperature in the absence of the in-cylinder DI cooling effect. Thus, external cooled EGR could be a solution to decrease PFI charge temperature and increase indicated efficiency.

Chapter 5.

Unthrottled E100 SI operation with early and late intake valve closure

5.1. Introduction

In order to improve on the low efficiency of the naturally aspirated SI engine at part load, different strategies can be used. Lean burn and exhaust gas recirculation (EGR) can be used to dethrottle the engine and reduce pumping losses. In addition, the use of Miller and Atkinson cycles, based on early or late intake valve closure, can also be applied to dethrottle the engine and reduce pumping losses.

As the intake valve closure point is shifted away from the bottom dead centre (either before or later, and not considering ram and tuning effects), less air is trapped in the cylinder leading to less energy released in a stoichiometric combustion. Therefore, variable valve closure strategy at wide open throttle can be used as a load control method. As is also demonstrated in the literature, this can reduce the part load pumping losses but adversely affects the in-cylinder flow and turbulence levels [53], [63], [66], [69]–[71], [112], [209].

Studies have shown that the large flow motions break up into small scale turbulent flows during the late stage of the compression increasing the turbulent burning velocity [18], [210]. The tumble motion is the large scale fluid motion generated during the intake stroke around an axis perpendicular to the cylinder centre line. While the cylinder is moving towards TDC, during compression, initially the tumble increases due to angular momentum conservation. Later in the compression stroke, the large flow structure is distorted due to wall shear stress and decays in smaller turbulence structures [19], [20], [211]. Swirl is the rotational fluid motion around the cylinder axis and its angular momentum can be well sustained until the end of the compression stroke [21]. In four-valve SI engines, with symmetric intake ports configuration, the increase in the tumble motion is expected to generate higher turbulence levels prior to combustion than the increase in the swirl [22], [23]. However, if not enough tumble motion is generated it can breakdown early in the compression stroke and generate lower turbulence levels [212].

The use of early intake valve closure (EIVC) strategy has been shown to promote an initial increase in tumble motion near BDC but also that the tumble structure may

breakdown in the middle of the compression stroke generating lower turbulence levels than the conventional throttled operation [69], [70]. On the other hand, the use of late intake valve closure (LIVC) is expected to maintain similar turbulence levels or even increase them compared to a conventional intake valve closure timing [67].

With the availability of more flexible variable valve actuation systems, either of EIVC and LIVC operations can be implemented. But there was little work reported on the direct comparison between the merits of the EIVC and LIVC in the same engine. Thus, the aim of this work was to identify which of the two would result in better fuel economy for unthrottled stoichiometric spark ignition operation with E100. The investigation was focused on the gas exchange process and its effects on combustion, engine out emissions and efficiency related parameters.

In addition, a comparative study between DI and PFI was performed to understand the possible gains when using each injection strategy. As the test engine had fully variable capability, the influence of the maximum intake valve lift was investigated to evaluate its effect on the engine operation for the best load control strategy.

5.2. Test methodology

Tests were carried at 1500 rpm at IMEP of 2.1 bar, 3.1 bar, 4.5 bar, 6.1 bar, 7.5 bar and 9.0 bar in order to compare the conventional throttled SI (tSI) operation to early and late intake valve closure load control methods. The intake valve opening, and exhaust valve closure and opening points were kept fixed during all tests. The overlap between intake and exhaust valves could be considered null, as the overlap was around 2 CAD with 0.15 mm valve lift. For this reason, the residual gas fraction could be maintained fairly constant for all load control strategies at each load. Thus, the impact of the IVC timing in the engine operation could be directly accessed.

An example of the actual intake valve lift profile used at 3.1 and 6.1 bar IMEP load with each load control strategy is presented in Figure 5.1.Table 5.1 presents the valve timings used for each load and load control method. For the tSI method the intake valve profile was kept constant and the load was controlled using a conventional throttle. For the EIVC/LIVC comparison study, the load was controlled by advancing or delaying the IVC with the wide open throttle. Intake and exhaust valve maximum lifts

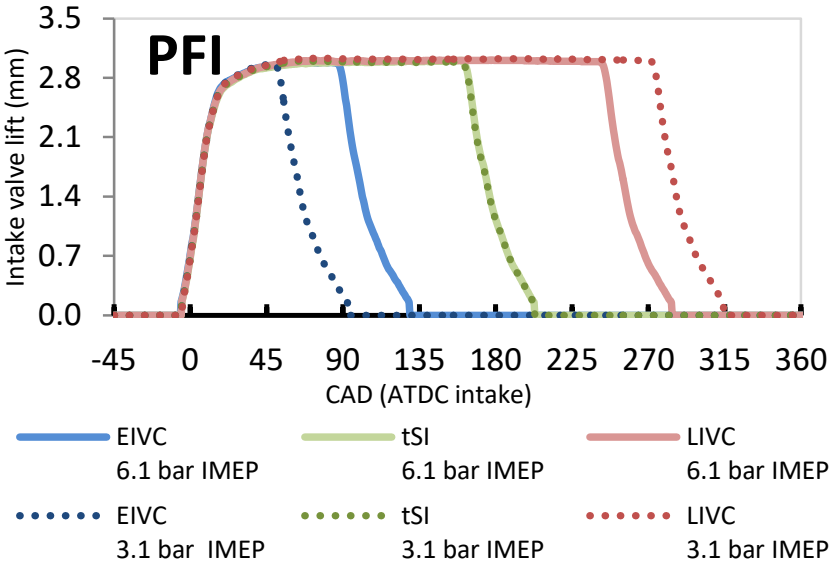

Figure 5.1. Intake valve lift profiles of 3.1 and 6.1 bar IMEP loads for different load control strategies and PFI injection strategy at 1500 rpm.

were kept constant at 3.0 mm target. This value was used to provide the same valve flow restriction while excluding the effect of the valve lift, and for safety reasons (at this lift the valves cannot hit the piston). The studies did not aim to show a valve timing optimization in the context of maximizing the engine efficiency. They were specifically designed to show the IVC impact in the engine operating parameters according to the chosen load control strategy.

PFI injection timing was set to the firing TDC, in order to provide the maximum time for ethanol vaporization and mixing with air. Spark sweeps with 2 CAD increment were run at each operating point in order to find the minimum spark advance for the best torque (MBT).

DI injection timing sweeps were run at 1500 rpm in order to find a good compromise between emissions and efficiency when using EIVC and LIVC. The injection timing results will be discussed in the next subsection. Based on the results presented in the previous section, the tSI DI injection timing was set at 28 CAD $ATDC_{intake}$.

Table 5.1. Valve timings used in the experiments with variable IVC as load control method.

Inj. strat.	Load control	IMEP (bar)	IVO (CAD ATDCi)	IVC (CAD ATDCi)	EVO (CAD ATDCi)	EVC (CAD ATDCi)
PFI	tSI	ALL LOADS	-6	206	-190	2
		IMEP	IVO	IVC	EVO	EVC
	EIVC	2.1	-7	82	-191	1
		3.2	-6	96	-191	2
		4.6	-7	114	-191	1
		6.1	-7	132	-191	1
		7.6	-7	152	-191	1
		9.2	-7	178	-191	1
		IMEP	IVO	IVC	EVO	EVC
	LIVC	2.1	-6	323	-191	3
		3.1	-6	317	-190	2
		4.6	-6	303	-190	2
		6.1	-6	287	-190	2
		7.6	-6	267	-190	3
		9.2	-6	234	-190	2
		IMEP	IVO	IVC	EVO	EVC
DI	tSI	ALL LOADS	-6	207	-190	1
		IMEP	IVO	IVC	EVO	EVC
	EIVC	2.2	-7	81	-191	2
		3.1	-6	92	-191	3
		4.6	-7	110	-191	2
		6.1	-6	128	-191	3
		7.7	-7	147	-191	3
		9.2	-7	169	-191	3
		IMEP	IVO	IVC	EVO	EVC
	LIVC	2.1	-6	324	-191	3
		3.1	-6	318	-190	2
		4.6	-6	305	-190	3
		6.1	-6	291	-190	2
		7.6	-7	273	-190	2
		9.1	-6	249	-190	2

5.3. Effects of Injection timing in the unthrottled E100 SI operation

5.3.1. Effect of injection timings on the performance and emissions during the EIVC operation with DI E100

Different injections timings were tested at various loads at 1500 rpm. The 3.1 bar and 6.1 bar IMEP loads were more extensively investigated. Effects of the injection timings on the MBT spark timing, combustion duration, and COV_{imep} are shown in Figure 5.2.

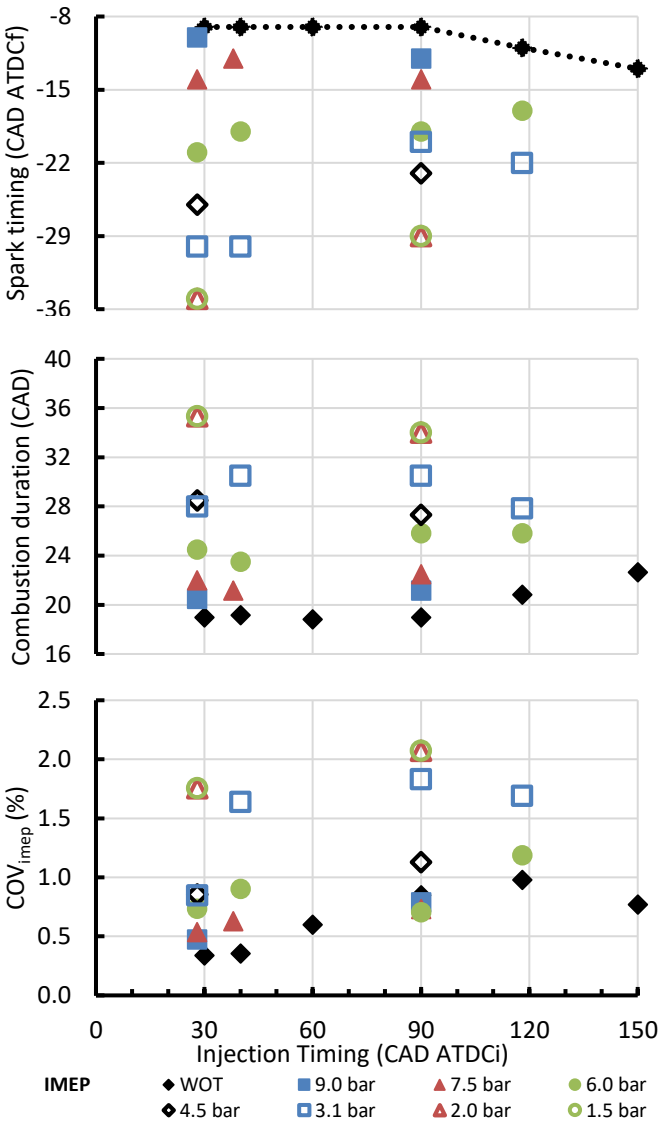

Figure 5.2. Effect of DI injection timing on the spark timing (MBT), combustion duration, and COV_{imep} for EIVC load control method and different loads. E100 1500 rpm MBT operation.

The variation of MBT with injection timings exhibited two distinct trends. At low loads, the later injection after 90 CAD $ATDC_{intake}$ led to retarded MBT and shorter combustion duration. Above 4.5 bar IMEP, the MBT timing and combustion duration was less affected by the injection timing. In general, later injections resulted in higher COV_{imep} as the cyclic variation in the mixture formation increased because of less homogeneous charge.

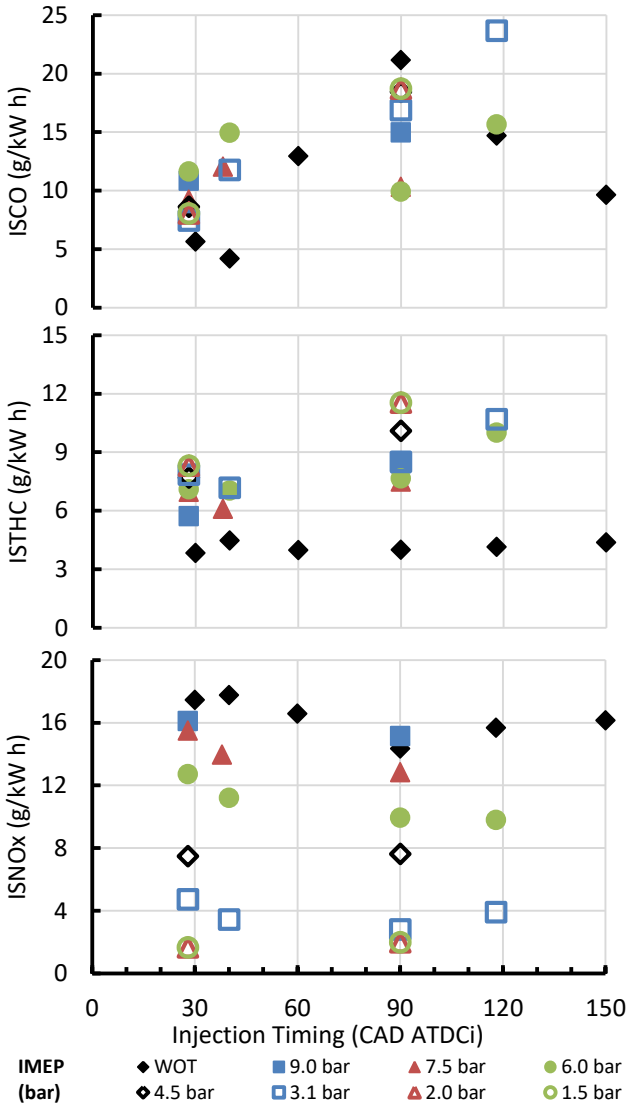

Figure 5.3. Effect of DI injection timing on indicated specific emissions for the EIVC load control method and different loads. E100 1500 rpm MBT operation.

Figure 5.3 presents the effect of the injection timing on the specific emissions. CO emission decreased at more advanced injection timings (nearer to the TDC), because of the more uniform mixture distribution. The THC emissions decrease that occurred

from 28 CAD to 40 CAD $ATDC_{intake}$ was an indicative that some impingement would be starting to occur. The later increase in THC emissions could be attributed to lower combustion temperatures and poorer fuel vaporization or even condensation due to the injection near the overexpansion phase.

NOx emissions tended to decrease for more delayed injection timings. This occurred due to lower combustion temperatures, as result of the more stratified charge and the influence of the cooling effect.

Figure 5.4 presents the combustion and indicated efficiency as result of different injection timings and different loads. The higher combustion efficiencies occurred for the more advanced injection timings. The increase in the combustion efficiency was directly correlated to the increase in the indicated efficiency, which also increased for the earlier injection timings. The same effect of injection timings on the combustion and emissions was also observed with the injection timing study of the PVO operation.

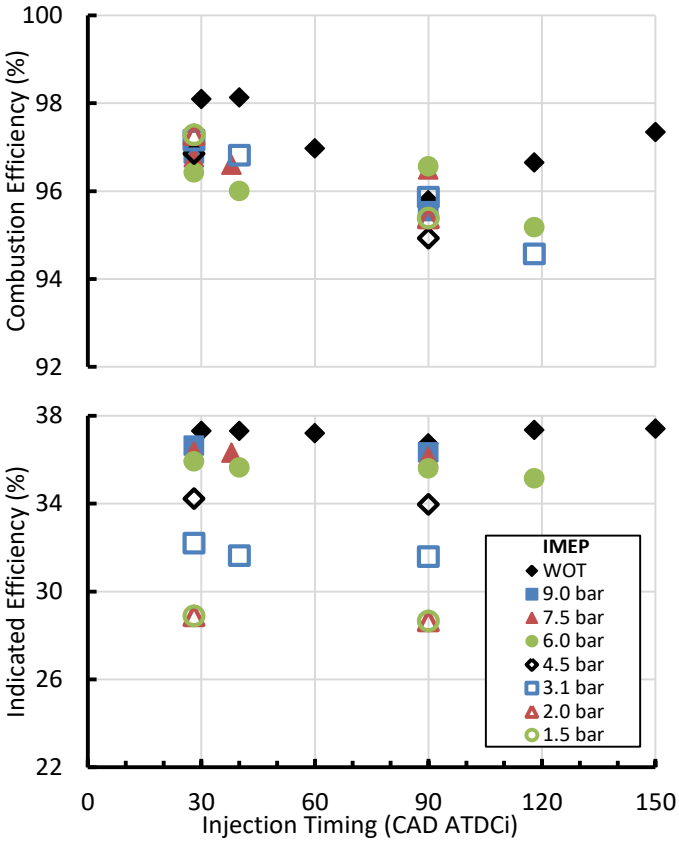

Figure 5.4. Effect of DI injection timing on combustion efficiency and indicated efficiency for EIVC load control method and different loads. E100 1500 rpm MBT operation.

5.3.2. **LIVC direct E100 injection timing optimization**

According to the PVO and EIVC experiments, the injection timings of 28 and 90 CAD $ATDC_{firing,}$ have been chosen for most of the LIVC experiments in order to reduce the number of points for all load points other than the 3.1 bar IMEP load. As shown in Figure 5.5, the MBT spark timing tended to be slightly advanced with later injection timings whilst the combustion duration remained constant. The COV_{imep} tended to increase at some of the loads.

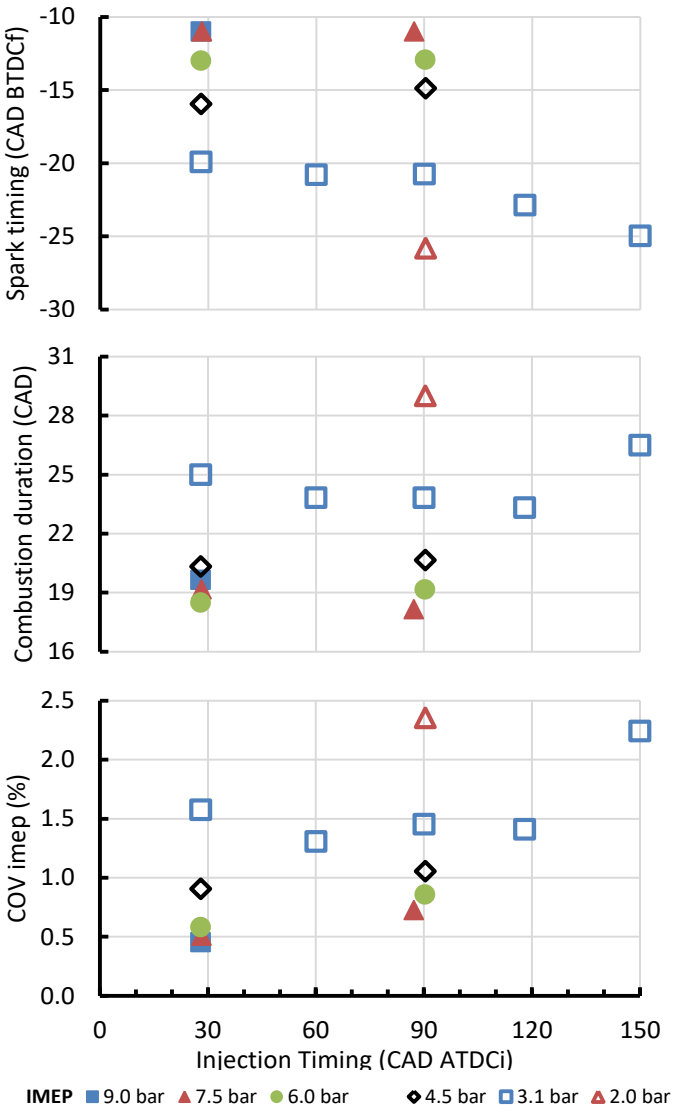

Figure 5.5. Effect of DI injection timing on indicated specific emissions for the LIVC load control method and different loads. E100 1500 rpm MBT operation.

As will be explained later, for the lower loads, 2.0 bar IMEP and below, it was not possible to use WOT, and for this reason, the 1.5 bar IMEP tests were not evaluated. Also, at 2.0 bar IMEP load the injection timing at 28 CAD $ATDC_{intake}$ resulted in unstable operation, and for this reason, it was tested only at 90 CAD $ATDC_{intake}$.

Figure 5.6 presents the effect of the injection timing in the specific emissions for the different loads. The CO and THC emissions tended to increase with delay in the

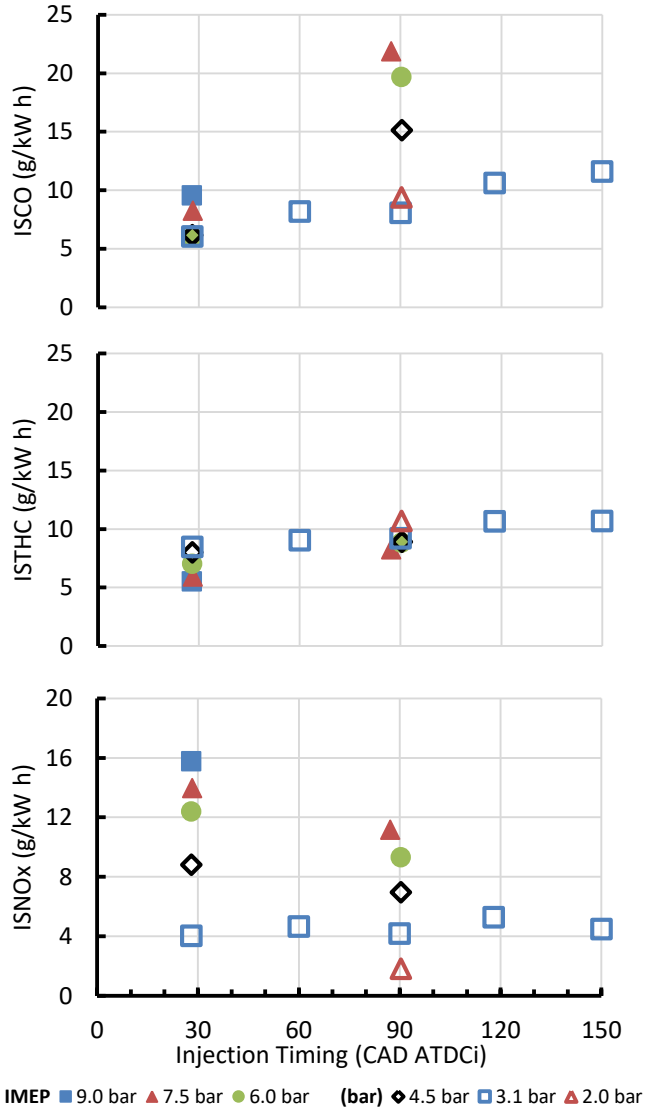

Figure 5.6. Effect of DI injection timing on indicated specific emissions for the LIVC load control method and different loads. E100 1500 rpm MBT operation. E100 1500 rpm MBT operation.

injection timing due to a shorter mixing period. The longer intake opening period of LIVC resulted in extended gas exchange period which promoted better mixture homogeneity than the EIVC strategy and resulted in similar trends to the tSI in the variation of combustion and emission with the injection timing. The later injection tended to decrease the NOx emission at higher loads due to cooling effect, probable less homogeneous charge and possible fuel droplets formed during the overexpansion phase. At 3.1 bar, the delayed injection timing required higher spark advance which increased the combustion temperature and resulted in the increase of NOx emissions with the delay in the injection timing.

The combustion efficiency dropped for later injection timings due to the increasing trend of THC and CO emissions. As the EIVC and PVO operations, the 28 CAD ATDC presented the best indicated and combustion efficiency. This value will be used in the following comparative study between EIVC, LIVC and tSI operations.

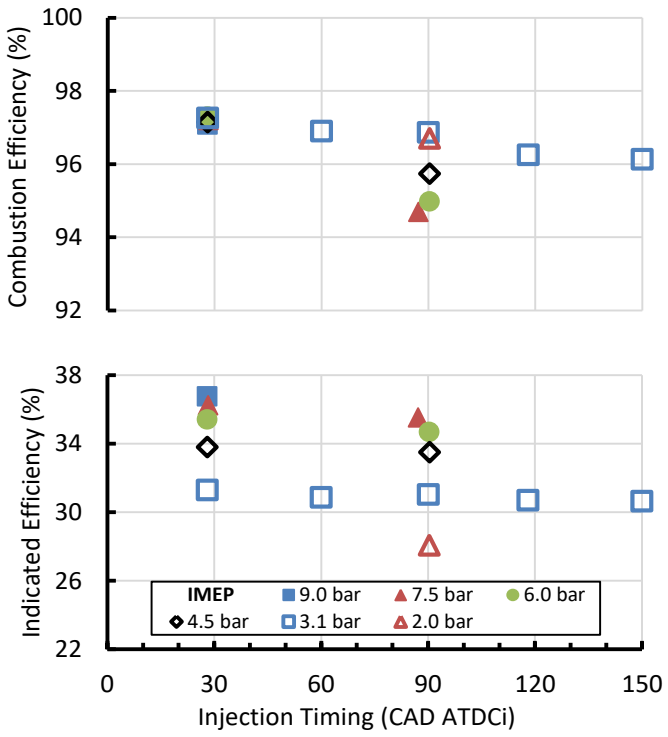

Figure 5.7. Effect of DI injection timing on the spark timing, combustion duration, and COV_{imep} for LIVC load control method and different loads. E100 1500 rpm MBT operation.

5.4. Comparative analysis between EIVC, LIVC and tSI using E100.

5.4.1. Gas exchange analysis

Figure 5.8 presents the IVC event necessary to achieve different loads for each strategy. In the case of conventional throttled operation, the restriction on the amount of air is provided by the reduced intake plenum pressure when closing the throttle. In the case of EIVC or LIVC operation, the amount of air trapped in the cylinder was a function of the instantaneous in-cylinder volume and the momentum of the flow at the IVC whilst the intake manifold pressure was near to atmospheric condition. For this reason, in order to reduce the load, the IVC event had to be advanced or delayed from BDC for the EIVC and LIVC strategies, respectively.

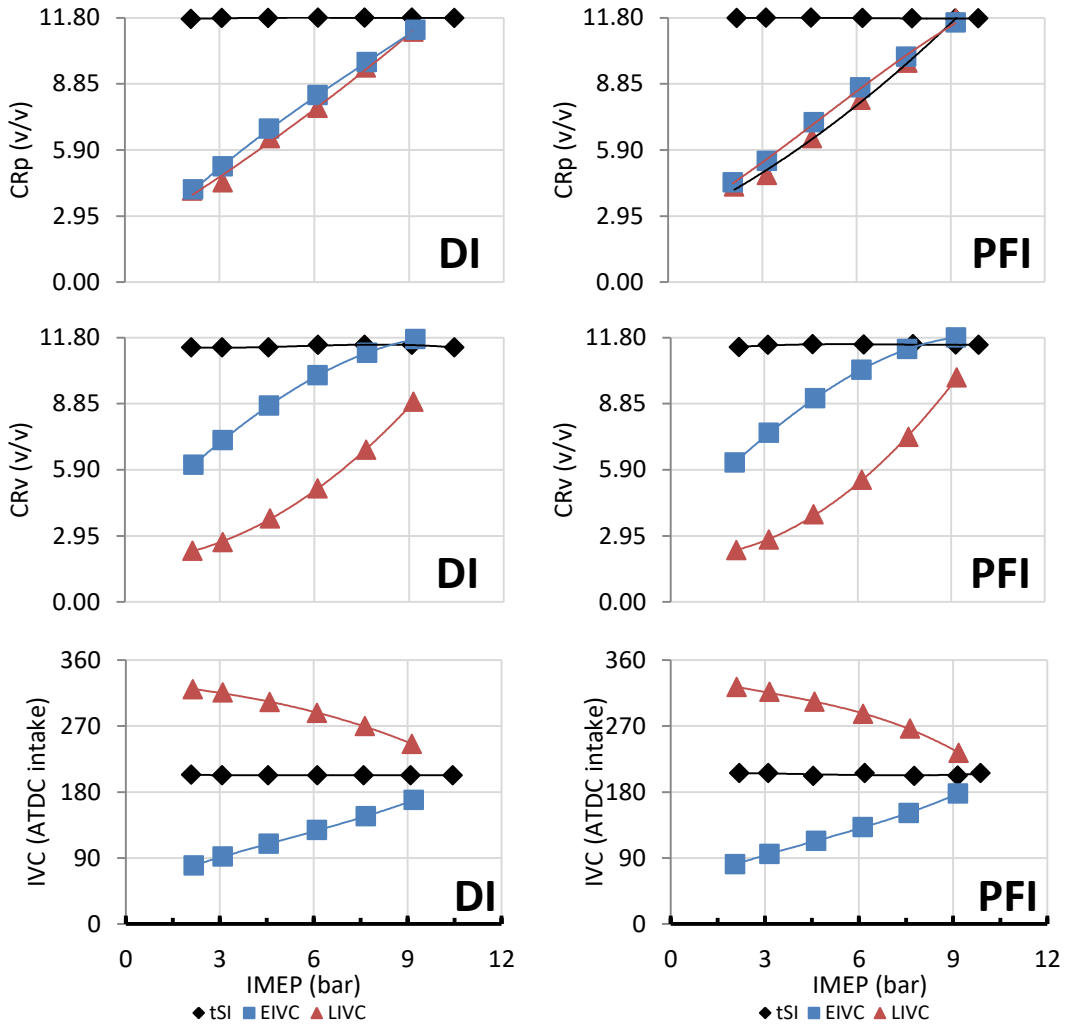

Figure 5.8. Effect of the load control method on the inlet valve closure timing, geometric compression ratio CR_v and effective compression ratio CR_p at different loads for DI and PFI injection strategies. E100 1500 rpm MBT operation.

As the IVC was varied, the geometric compression ratio, CR_v, deviated from the geometric compression ratio determined by the cylinder volumes at BDC and TDC. CR_v was calculated as the relationship between the TDC in-cylinder volume and volume at IVC. Very low CR_v values were achieved at the lowest loads when using the LIVC strategy. This occurred because the cylinder volume required to trap the amount of air was too small. Due to the valve restrictions and higher in-cylinder pressure required to dispose the excess air back to the intake manifold, an earlier compression phase occurred previously to the IVC event, as shown in Figure 5.9. Thus, for the LIVC strategy the CR_v was always smaller (for all loads) than the CR_p. The CR_p was calculated as the relationship between the instantaneous in-cylinder volume when a fitted polytropic compression process (fitted to the compression process while all valves were closed) reaches the intake pressure level and combustion chamber volume. Using this approach, the CR_p means the actual compression ratio to which the fluid is subjected starting at the intake pressure state. Figure 5.9 provides the graphical explanation of the calculation process of CR_p and CR_v.

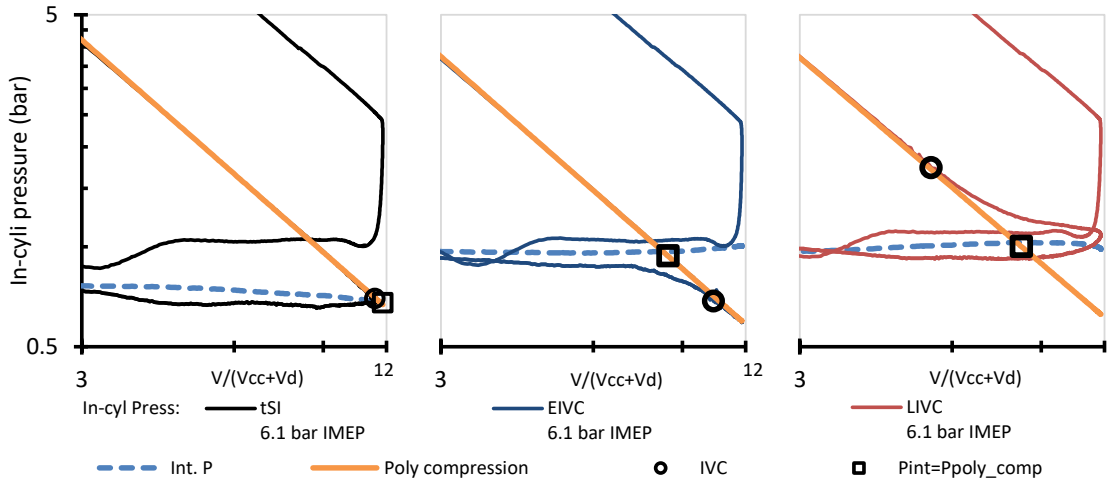

Figure 5.9. Effect of the load control method on the pumping loop of 6.1 bar IMEP load with PFI – Log P x Log V plots with in the intake valve closure and the effective compression ratio. E100 1500 rpm MBT operation.

Because of the reversed flow associated with the very late IVC during the compression stroke, at the 2 bar IMEP load, LIVC operation with WOT could not be achieved as the IVC had to be delayed to near to the TDC resulting in very low compression. As mentioned in [53], [70], this would require a spark advance before the IVC in order to

achieve stable combustion. For this reason, intake throttle was used to reduce intake manifold pressure to 0.9 bar when operating at 2bar IMEP and LIVC.

In the case of EIVC, the flow restrictions during the valve closure event started an over-expansion phase before the IVC event. Thus, the CR_p was lower than the CR_v. In turn, in the tSI cases the IVC event occurs slightly after the BDC. Even then, due to the valve restriction and irreversibility of the process, the polytropic compression started almost at the maximum possible compression ratio point.

When comparing the DI and PFI unthrottled operations, two main phenomena can cause the valve timing to be different at the same load; the displacement of the intake air by fuel vapour in PFI, and in-cylinder cooling effect by DI fuel. The DI cooling effect will increase the charge density and can be more prominent for the EIVC strategy when the direct injection takes place near the IVC. In the case of PFI operations, the intake air displacement would require IVC to be closer to BDC in order to admit the same amount of air. The PFI displacement effect would be more dominant in the case of LIVC strategy and at higher loads. This resulted in earlier IVC timings in the PFI operations than those of DI operations. In the tSI cases, the fuel displacement effect required higher partial load intake plenum pressure (Figure 5.10). Thus, the maximum load at WOT was reduced from 10.5 in DI operation to 9.9 bar IMEP in the PFI mode due to lower air flow rate.

Another point to be addressed to the LIVC characteristics is the pumping loss associated to the longer flow period while the intake valves were still opened, as shown in Figure 5.11. Ideally, for adiabatic and reversible flow processes, when the piston reached the BDC, the in-cylinder pressure would be equalized to the intake manifold pressure. During the initial compression phase, while the intake valves were still opened, the in-cylinder pressure would be just slightly higher than the intake pressure in order to promote the required in-cylinder charge backflow.

In reality, due to the valve flow restriction and to overcome the momentum of the fluid, the in-cylinder pressure increased to higher levels than ambient pressure. The flow losses would be increased in the LIVC case due to the longer period with the intake valves opened, as also stated by [63]. The increased flow losses occur due to the additional backflow process necessary to trap the right charge mass quantity for the desired load. Thus, for the LIVC strategy, valve flow restrictions needed to be surpassed twice in the fresh air trapping event (during the fresh air induction and in the subsequent backflow processes).The early compression phase reduced the total

available work from the power strokes and affected the PMEP. This work is represented by the purple delimited area in Figure 5.11.

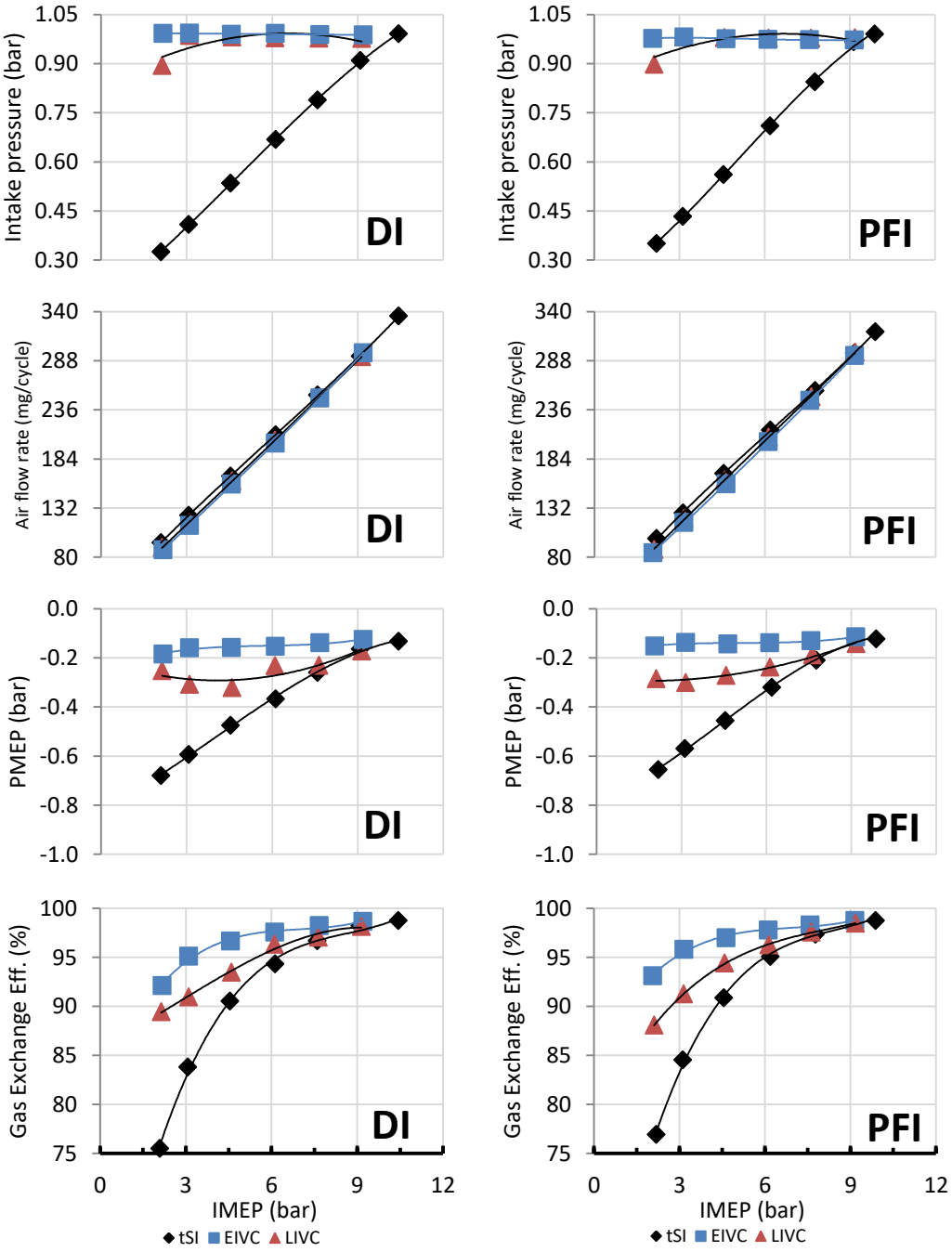

Figure 5.10. Effect of the load control method on the intake pressure, air flow rate, pumping mean effective pressure and gas exchange efficiency at different loads for DI and PFI injection strategies. E100 1500 rpm MBT operation.

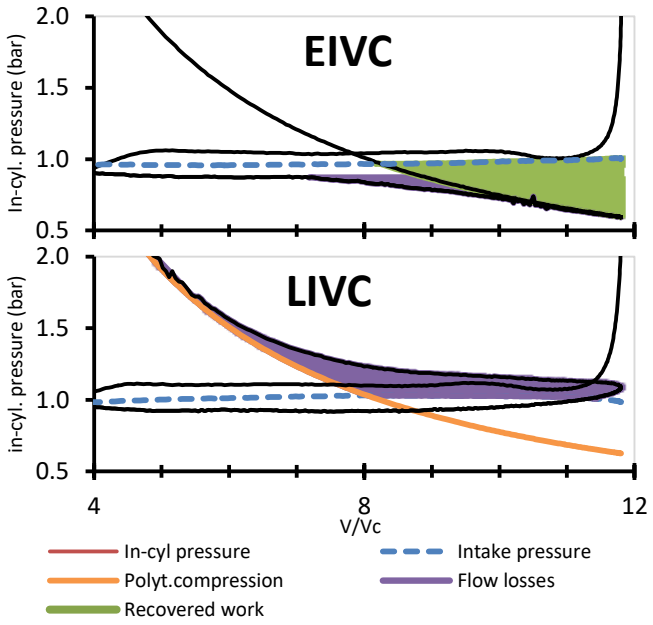

Figure 5.11. Log P x Log V plot with emphasis on the additional pumping work of the EIVC and LIVC load control strategies – 6.1 bar IMEP E100 1500 rpm MBT operation.

For the EIVC strategy the valve flow restriction needed to be surpassed only during a minimized period during the fresh air induction process while the intake valves were opened. Nevertheless, the valve flow restrictions increased the over-expansion pumping loop work at some extent during the intake valve closing phase (delimited by the purple perimeter in Figure 5.11). Ideally, the over-expansion period would only begin at the IVC following a polytropic compression behavior. Despite this, a major part of the over-expansion phase work (delimited by the green area) was recovered in the compression phase until the in-cylinder pressure was equalized to ambient pressure. For these reasons, EIVC PMEP work was smaller than LIVC PMEP.

In the tSI cases, the lower plenum pressure due to partially closed throttled created a considerable difference between in-cylinder pressure and ambient pressure during the intake phase. This resulted in the larger PMEP.

The variation in pumping work was directly translated to gas exchange efficiency, shown in Figure 5.10. Gas exchange efficiency calculation and physical meaning is explained in the methodology section. For the tSI strategy and at the lowest loads, almost 25% of the energy produced in the engine was used to overcome the pumping work. The increased flow losses during the backflow period of the LIVC strategy decreased its gas exchange efficiency as the load was reduced. When comparing PFI

and DI strategies, the higher intake pressure operation of the PFI cases is illustrated by its higher gas exchange efficiency.

If only the gas exchange work was to be considered, more energy would be consumed as pumping work (more negative PMEP) in the tSI. Thus, for stoichiometric combustion, more air was required in order to provide the same load. Thus, the low load EIVC and LIVC presented similar air flow rate while tSI presented the highest. As load increased and the difference between each strategy pumping losses decreased, the air flow rate tended to be equal.

5.4.2. **Combustion characteristics**

Conventional spark ignition combustion with flame propagation occurred in all tested cases. Combustion phasing was controlled through spark timing and MBT operation could be achieved without knock. Figure 5.12 presents the required spark timing for MBT and the point where 50% of the mass was burnt. The spark required in the different strategies was a function of load and initial compression temperature. In the EIVC strategy, the in-cylinder temperature prior to the spark was the lowest due to the over-expansion period which decreased initial compression temperature. This effect, added to the lower effective compression ratio, requested a more advanced spark timing in order to correctly phase the combustion. As the load increased, the over-expansion period was reduced and the CR_p increased, resulting in more retarded spark timing. In the case of the LIVC, the main reason for a more advanced spark requirement was the lower effective compression ratio. In the tSI case, the spark advance presented a smooth increasing trend as function of the load. The higher the load, the higher the in-cylinder temperature prior to the combustion and the more retarded the MBT spark timing. The combustion phasing behaviour of the PFI cases, when comparing the same load and different load control strategies, was in accordance to the literature: the longer the combustion, the more delayed was the CA50% from the TDC [13]. The advance of the CA50 in the longer combustion duration cases occurred in order to increase combustion temperature and achieve more stable combustion.

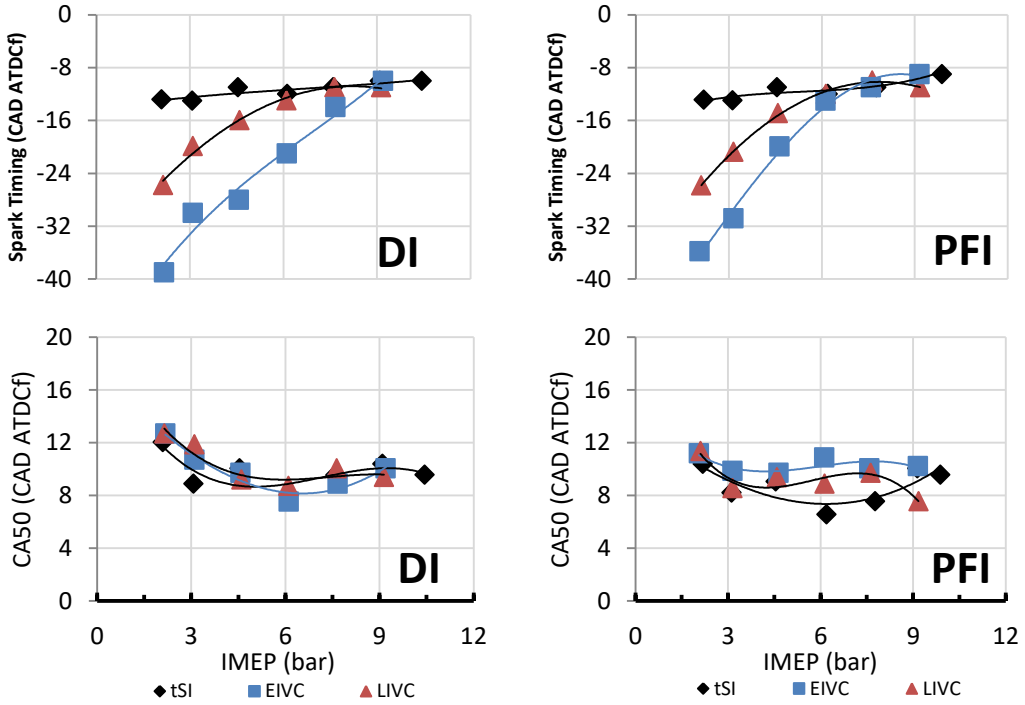

Figure 5.12. Effect of the load control method on spark timing and CA50% at different loads for DI and PFI injection strategies. E100 1500 rpm MBT operation.

The in-cylinder temperature prior to spark and at -35 CAD $ATDC_{firing}$ for the 3.1 bar and 6.1 bar IMEP PFI cases are plotted in Figure 5.13. The instantaneous averaged in-cylinder pressure and heat release rates of the same operating conditions are presented in Figure 5.14. The effects of the valve strategy in the flame development angle (FDA – period between spark and 10% of mass fraction burn), main phase combustion duration (10-90MFB – period between 10% and 90% of mass fraction burned) and cycle-to-cycle variability of the IMEP (COV_{imep}) are shown in Figure 5.15.

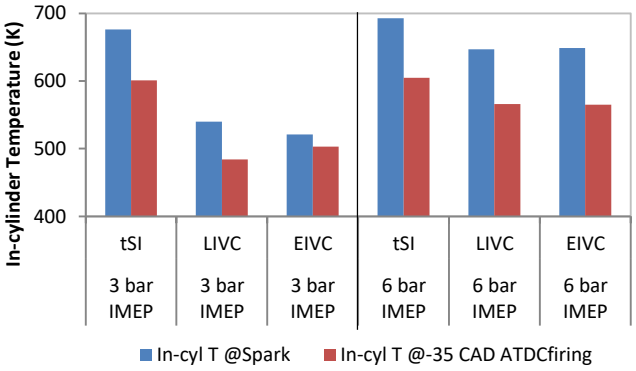

Figure 5.13. Effect of load control method on the in-cylinder temperature at -35 CAD $ATDC_{firing}$. E100 PFI 3.1 bar and 6.1 bar IMEP 1500 rpm MBT operation.

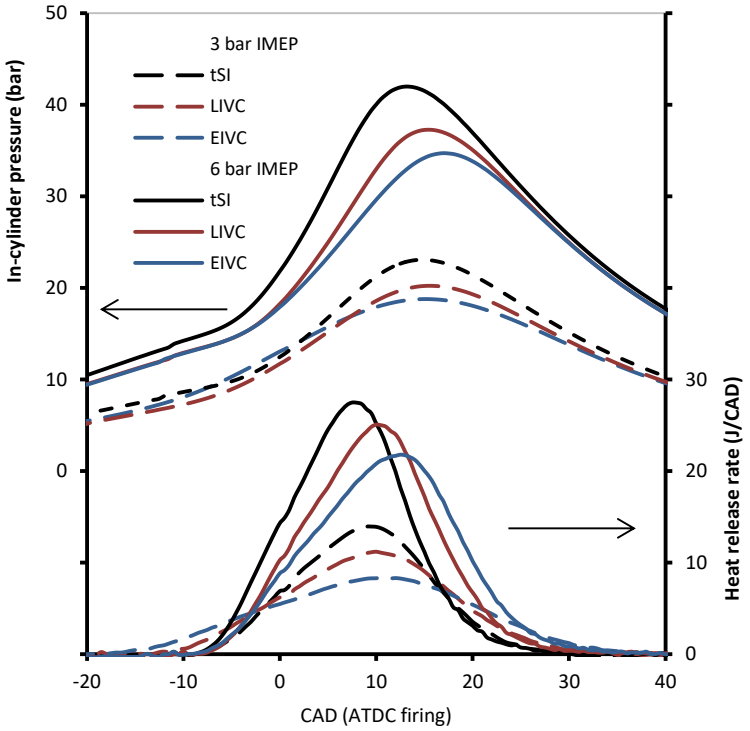

Figure 5.14. Averager in-cylinder pressure and heat release rates for different valve strategies and diferent loads. E100 PFI 3.1 bar and 6.1 bar IMEP 1500 rpm MBT operation.

The EIVC strategy presented both the longest FDA and combustion duration. This is explained by the expected lower in-cylinder temperature prior to ignition and expected low turbulence levels near the spark plug. As shown elsewhere [16], in the period right after spark, the initial flame development stage is governed by the thermodynamic state of the charge and mixture composition near the spark plug (which is expected to be fairly homogeneous due to the early DI and PFI). After an initial growth period, the interaction between the flame front and the turbulent eddies start. Flame front corrugation and wrinkling increase the flame front area. Due to the reduced size of the flame kernel, the largest eddies in the flow can convect it from the spark plug electrode. Later, during the turbulent flame propagation stage, the mean velocity field and local air/fuel ratio play a minor role in the main combustion duration, as a number of local events are averaged for the final effect. According to this, it could be expected that the earlier the IVC, not only the lower was the CR_p and in-cylinder temperature but also the turbulence levels. Additionally, the in-cylinder cooling effect also contributed to increase the FDA of the DI cases.

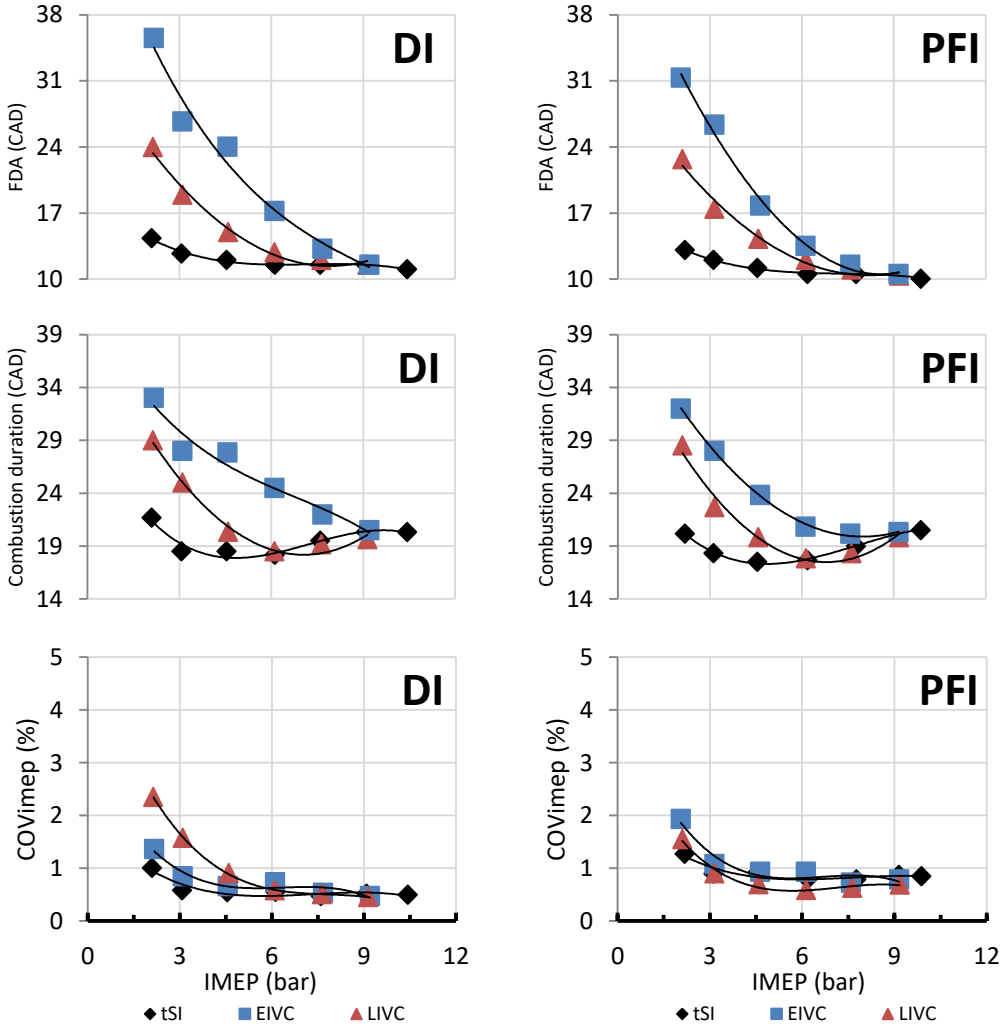

Figure 5.15. Effect of the load control method on flame development angle, combustion duration and COV_{imep} at different loads for DI and PFI injection strategies. E100 1500 rpm MBT operation.

As the load increased and the IVC became closer to the BDC, a more stable tumble structure was expected. This structure would last until the end of the compression stroke resulting in higher turbulence helping in the flame propagation process. So, as LIVC case presented even lower compression temperature than the EIVC case (comparing the in-cylinder temperatures of the 3.1 bar IMEP cases presented in Figure 5.13), it could be concluded that the considerable increase in the whole combustion process duration of the EIVC at low loads occurred mainly due to poor in-cylinder flow motion and low turbulence levels.

The lower LIVC CR_p decreased the pressure prior to spark to the same levels of the EIVC case. This resulted in lower temperature prior to combustion and longer FDA and combustion duration when comparing LIVC to tSI. Even then, the turbulence levels

were expected to be higher with the LIVC than the EIVC. Similar results comparing EIVC, LIVC and tSI at low load were reported elsewhere[112].

For the longer combustion durations cases, the peak heat release rate decreased and was delayed from the TDC. The same behaviour occurred to the peak in-cylinder pressure, as shown in Figure 5.14.

Even though the duration of the combustion was longer in the unthrottled cases, the COV_{impe} could be kept below 2% (excluding the DI operation at 2 bar IMEP). The higher cyclic variability of the DI LIVC low load cases would occur due to larger standard deviation of the mixture quality of later injections [53]. This would occur due to the very long period with the intake valve opened.

The resultant maximum in-cylinder peak pressure was fairly the same for both unthrottled strategies, with slightly higher results for the tSI strategy due to more advanced CA50. The exhaust temperature of the EIVC was the highest due to the considerably longer combustion duration (Figure 5.16.).

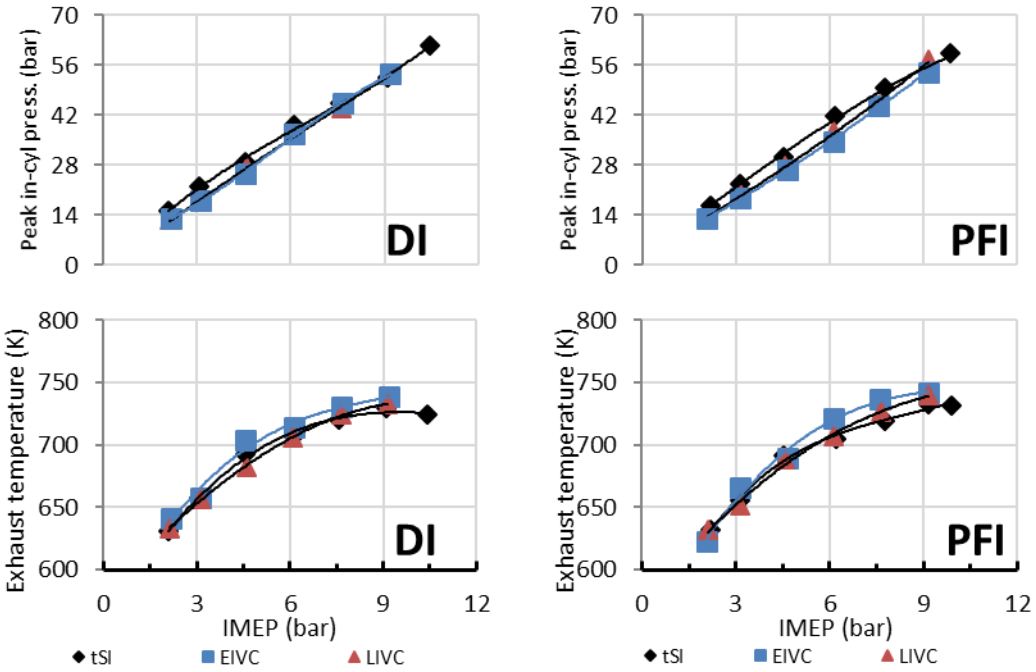

Figure 5.16. Effect of the load control method on maximum in-cylinder pressure, and exhaust temperature at different loads for DI and PFI injection strategies. E100 1500 rpm MBT operation.

5.4.3. **Gaseous emissions**

Figure 5.17 presents the gaseous emissions of the different load control strategies, DI and PFI injection, at different loads. In the case of DI operations, the start of injection was set at 28 CAD $ATDC_{intake}$. The start of the PFI injection was set to the compression TDC.

For the DI operation, the CO emission initially decreased with increasing load for both EIVC and tSI as more complete combustion took place with increasing combustion temperature. As the injected ethanol mass increased further, the CO emission rose as the mixture became less uniform. For the LIVC DI case, the CO emission was less affected by the load due to a longer gas exchange period with fuel backflow to the intake ports. For the PFI cases, the CO formation was not expected to be a result of locally fuel rich areas as the homogeneity level achieved with PFI was expected to be the same for all conditions. Even then, as CO formation is primarily dominated by air-fuel ratio and temperature, the small ISCO differences between cases could be attributed to different combustion temperatures and small deviations from the target stoichiometric lambda (as lambda control was manual).

In all cases, the total hydrocarbons emissions decreased with the increase in the load. Overall, the use of PFI injection resulted in better THC emissions because of the absence of any liquid fuel impingement. The cause for the lower THC emissions in the EIVC PFI case would be the longer combustion duration which increased the temperature during the expansion phase and increased the post combustion oxidation process.

As expected, NOx emission increased with the load because of higher combustion temperature. Te lower NOx specific emission of the EIVC and LIVC cases was a direct evidence of lower combustion temperatures. The pressure levels during combustion of the EIVC cases were lower than the LIVC ones and consequently the expected in-cylinder the combustion temperatures would be expected to be lower resulting in lower NOx emissions, which did not happen. This could explain by the increased period which the mixture was exposed to the high temperature of the flame due to considerably longer combustion durations, compensating the lower combustion temperatures. Comparatively, the DI operation resulted in lower NOx formation attributed to the lower combustion temperatures as result of the DI cooling effect and less homogeneous charge.

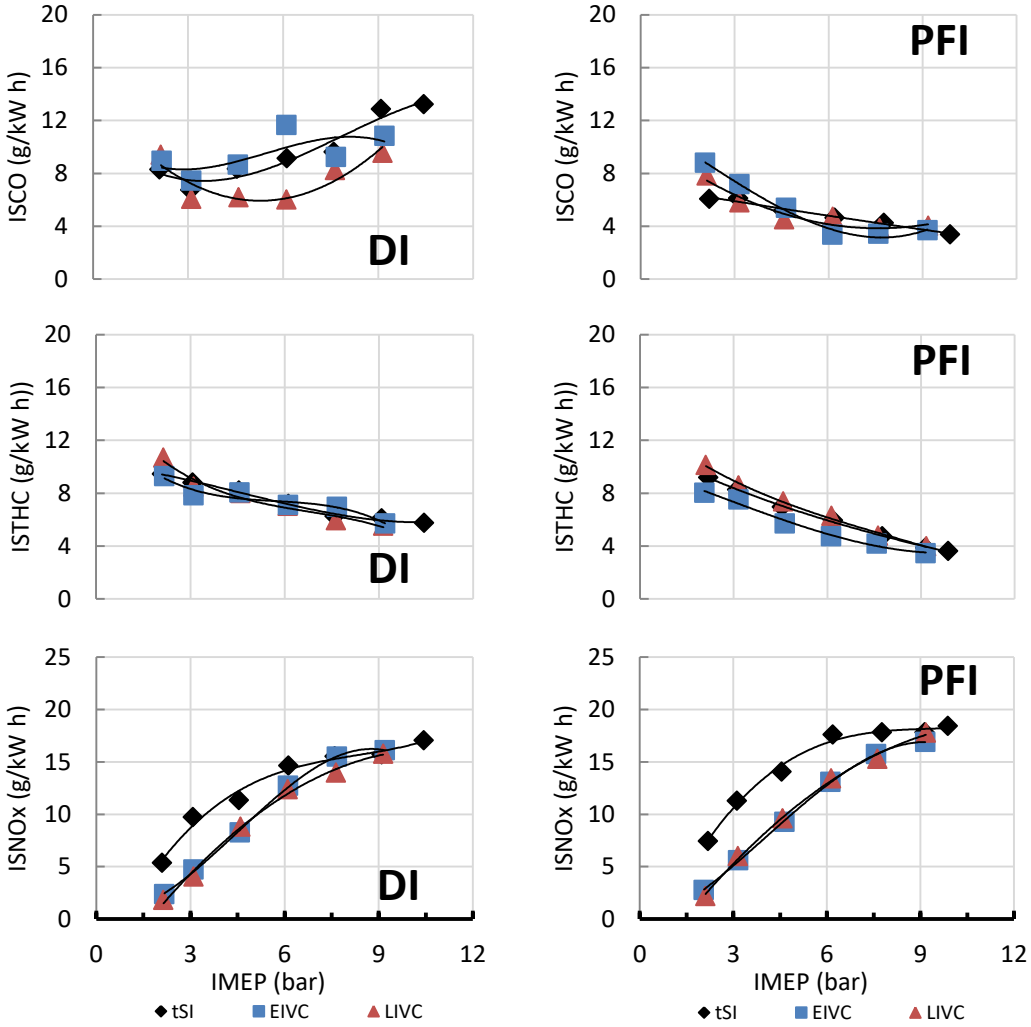

Figure 5.17. Effect of the load control method on the specific engine out emissions at different loads for DI and PFI injection strategies. E100 1500 rpm MBT operation.

5.4.4. **Efficiency related parameters**

As discussed and shown in Figure 5.10, EIVC provided the highest gas exchange efficiency, followed by the LIVC. The conventional throttled operation provided the lowest gas exchange efficiency. The combustion, thermodynamic and indicated efficiencies are shown in Figure 5.18.

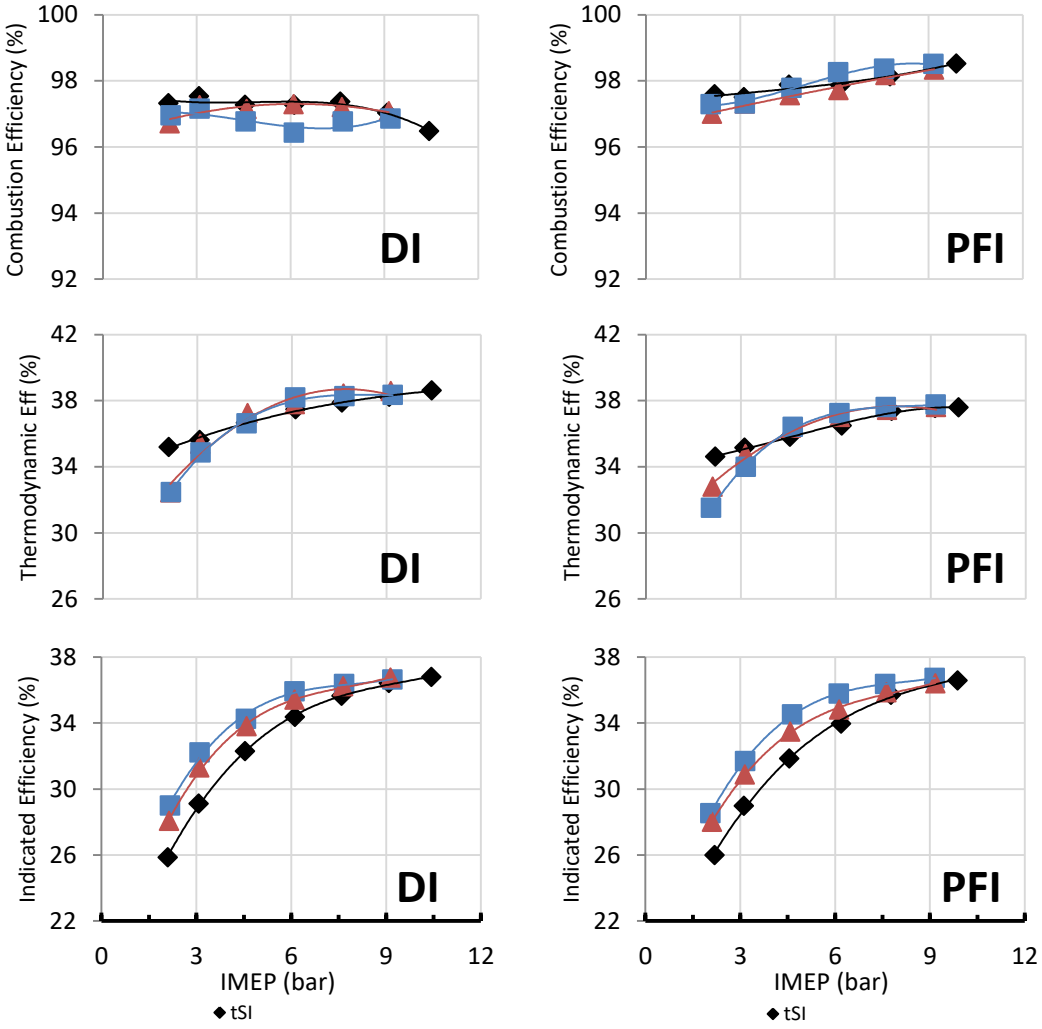

Figure 5.18. Effect of the load control method on efficiency related parameters at different loads for DI and PFI injection strategies. E100 1500 rpm MBT operation.

The combustion efficiency is closely related to CO and THC emissions. The better combustion efficiency improved at high load PFI operation for all the load control strategies and the combustion efficiency increased with the load because of the reducing trend in CO and THC emissions. Due to slightly lower THC emissions, EIVC PFI part load had the highest combustion efficiency. In the DI cases, the decreasing THC trend with an increasing CO trend with load resulted in a fairly constant combustion efficiency scenario around 97%. The highest PFI combustion efficiencies were greater than 98.5%.

The gross thermodynamic efficiency was calculated in order to assess the efficiency of the engine to convert the heat released during the combustion process into work. As all the operating points were run at MBT, the best combustion phasing which would increase the engine thermodynamic efficiency was achieved. At the lowest loads (2 and 3.1 bar IMEP) the long combustion process of the EIVC and LIVC strategies

degraded the thermodynamic efficiency. For loads higher than 4.5 bar IMEP, the lower combustion temperature reduced combustion heat transfer at a relatively faster rate. This results in increased thermodynamic efficiency to greater than tSI levels. Increased in-cylinder heat transfer could be one of the reasons for the slightly lower thermodynamic efficiency of LIVC strategy compared to the EIVC strategy. This would occur due to the backflow of the charge before the IVC which cooled the cylinder walls and increased the heat losses [112][112]. The lower thermodynamic efficiency of the PFI cases could be attributed to higher combustion temperatures.

The (net) indicated efficiency was calculated from the ratio of the in-cylinder gas work (from the pressure-volume diagram) and the total fuel energy delivered to the engine in one cycle. It is the product of the three previously discussed efficiencies. EIVC resulted in the higher indicated efficiency for all loads. For the lowest loads the comparatively smaller pumping work (compared to other strategies) and the good combustion efficiency counter balanced the lowest thermodynamic efficiency.

The good heat release process of the LIVC strategy was counter balanced by average gas exchange efficiency, the lowest combustion in the PFI case, and average combustion efficiency in the DI case. This resulted in intermediary net indicated efficiency compared to the other strategies, slightly lower than EIVC but considerably higher than the tSI net indicated efficiency.

The tSI case presented the lowest net indicated efficiency especially due to the impaired gas exchange efficiency. The slightly better fuel consumption of the DI cases compared to PFI was also reported elsewhere [70].

5.5. Effect of maximum valve lift in EIVC unthrottled operation with E100 PFI

EIVC tests were conducted only at 3.1 bar and 6.1 bar IMEP and 1500 rpm with different maximum valve lifts of 1.5 mm, 2.0 mm, 3.0 mm, 4.0 mm and 5.0 mm. Only PFI operation was evaluated. This way the effect of the maximum valve lift in the engine operating parameters could also be accessed.

5.5.1. **Gas exchange analysis**

As the EIVC strategy showed better potential in increasing SI engine efficiency than LIVC a second study was performed in order to understand the effects of the maximum valve lift in the engine operation. For this study, the investigations were carried at the loads of 3.1 bar and 6.1 bar IMEP at 1500 rpm. The target maximum valve lifts used were: 1.5 mm, 2.0 mm, 3.0 mm, 4.0 mm and 5.0 mm. Wide open throttle was used and the load was controlled by the IVC timing. Figure 5.19 presents the resultant intake valve lift profiles used in the tests.

In order to maintain the desired load, the EIVC had to be adjusted according to the set maximum valve lift. Figure 5.20 presents the required IVC and the calculated CR_v and CR_p. As the valve lift was increased, the IVC had to be advanced nearer to the TDC. This occurred because as the valve lift was increased the flow curtain area proportionally increased and the air flow was facilitated. In order to maintain almost the same amount of trapped air (to maintain the same load) a smaller inlet valve opening period was necessary. It should be pointed out that as the valve lift increases, the discharge coefficient (Cd) related to the curtain area decreases [95].So, at a higher lift, the relation between the isentropic flow rate and the actual flow rate is lower than that occurring at lower lifts. This effect occurs because of the flow dynamics and detachment of the boundary layer in the valve sit and the back of the valve. Thus, the

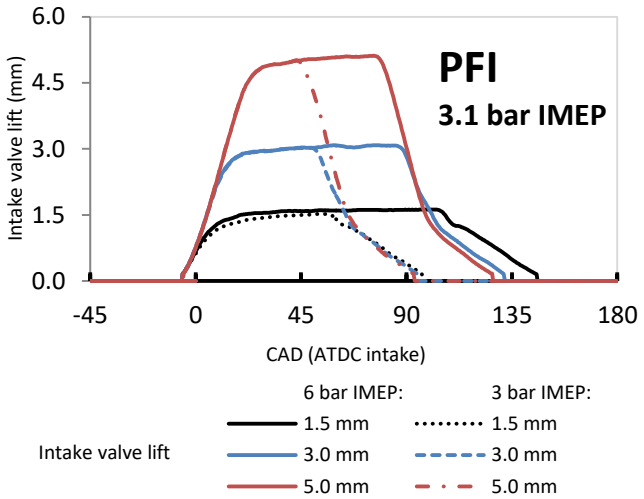

Figure 5.19. Intake valve lift profile for different maximum intake valve lifts and loads. EIVC valve strategy, PFI E100, 3.1 bar IMEP, 1500 rpm, MBT operation.

flow area at higher lifts resulted in a relatively higher flow restriction than that from the lower lifts. For this reason the IVC trend against valve lift was not linear as would the curtain area be. Also, as the load increased, the period which the flow was submitted to a higher valve lift (with higher Cd) increased. This resulted in a higher difference between the maximum and minimum lifts IVC for the 6 bar IMEP.

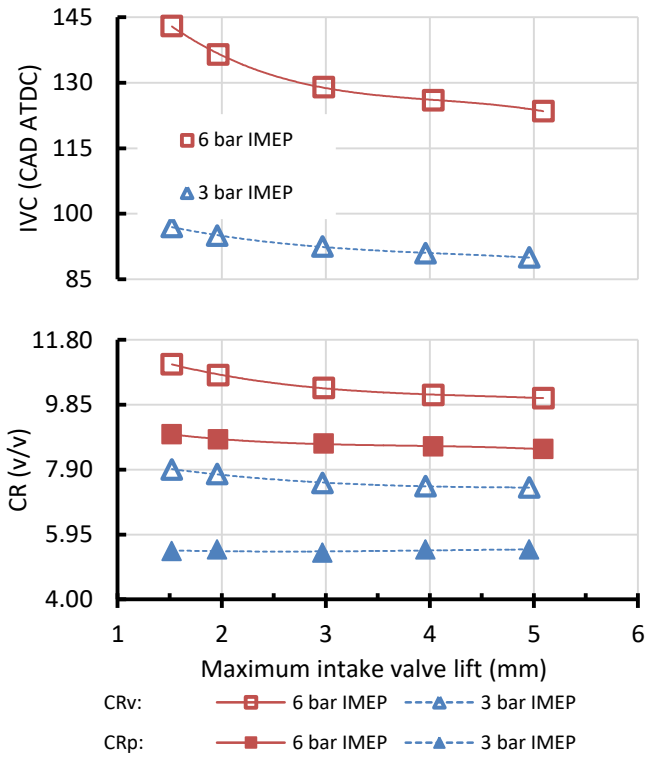

Figure 5.20. Effect of maximum intake valve lift on IVC and effective and geometric compression ratios. EIVC valve strategy, PFI E100, 3.1 bar and 6.1 bar IMEP, 1500 rpm, MBT operation.

The effect of the IVC in the CR_v was higher than in the CR_p. At lower lifts, even though the Cd was higher, the flow was more restricted by the reduced curtain area decreasing the in-cylinder pressure prior to the start of the valve closure period. Thus, even with a later intake valve closure, the minimum pressure of all lifts for the same load was almost the same and the compression pressure was almost the same for the same CAD. This resulted in an almost constant CR_p behavior.

Figure 5.21 presents the pumping loop of 3 different lifts of the 3.1 bar IMEP load and Figure 5.22 presents the pumping mean effective pressure and gas exchange efficiency for the different maximum valve lifts and loads. The increase in the PMEP

directly reflected in the gas exchange efficiency, which decreased as the valve lift was decreased. The absolute gain in the gas exchange process was 1.3% and 2.0%, for the 3.1 bar IMEP and 6.1 bar IMEP respectively.

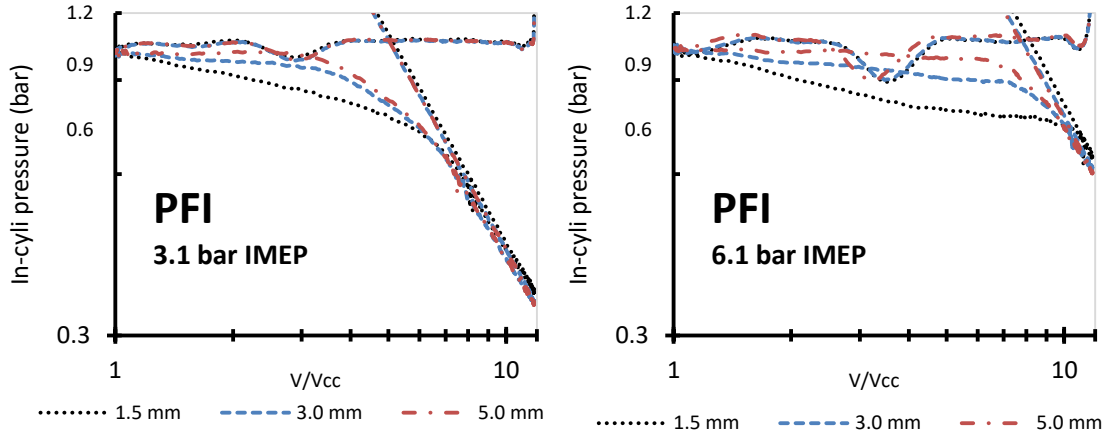

Figure 5.21. Effect of maximum valve lift on the pumping loop. EIVC valve strategy, PFI E100, 3.1 bar and 6.1 bar IMEP, 1500 rpm, MBT operation.

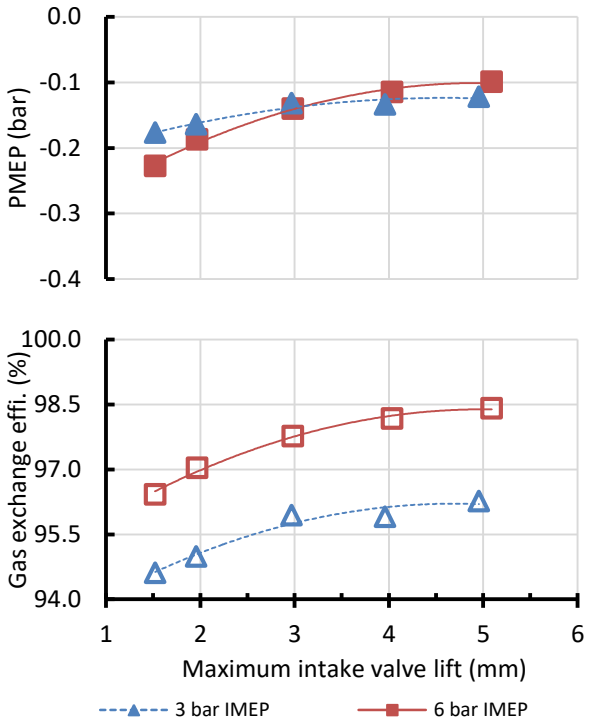

Figure 5.22. Effect of maximum valve lift on PMEP and gas exchange efficiency. EIVC valve strategy, PFI E100, 3.1 bar and 6.1 bar IMEP, 1500 rpm, MBT operation.

5.5.2. **Combustion characteristics**

Spark timing, flame development angle, combustion duration and COV_{imep} are presented in Figure 5.23. MBT could be achieved in all operation conditions and conventional spark ignition combustion occurred. The less advanced spark timing

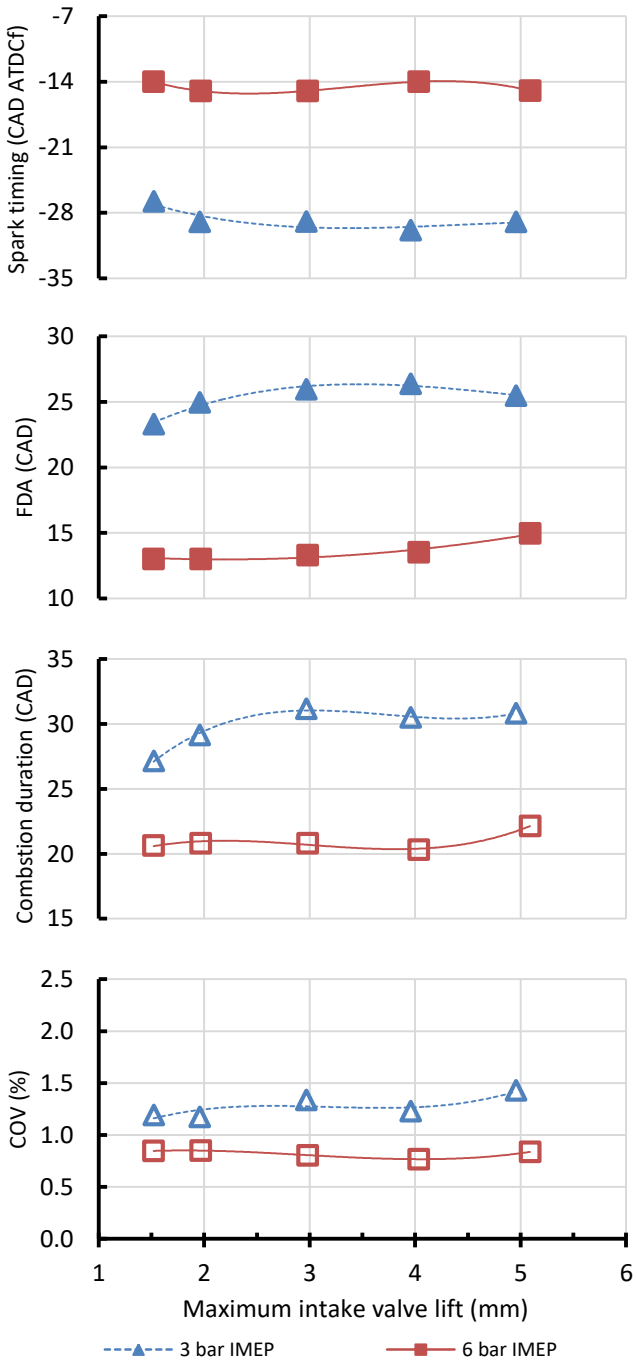

Figure 5.23. Effect of maximum valve lift on the spark timing, FDA, combustion duration and COV_{imep}. EIVC valve strategy, PFI E100, 3.1 bar and 6.1 bar IMEP, 1500 rpm, MBT operation.

occurred for the lowest lift but there was no recognizable trend between spark timing and maximum intake valve lift. Even with the delayed spark timing in the lowest lift case the FDA and combustion duration were the lowest. There was an increasing trend for the FDA and combustion duration as valve lift increased. One possible explanation for this would be that for lower valve lifts there was higher in-cylinder flow motion and turbulence generated by higher velocity of the air flow jets through the reduced valve curtain area. This trend was in agreement with [71], which stated that higher in-cylinder flow motion and turbulence could be achieved using low valve lift profiles at the cost of higher pumping losses.

Another parameter that helped to reduce the combustion process duration was the CR_p. Even though the variation of CR_p with the maximum valve lift was small, it could be seen from Figure 5.21 that the compression occurred at higher pressure. This would result in slightly higher temperature prior to spark which would enhance the combustion process in low loads.

The COV_{imep} was relatively low and, as expected, decreased with the load. As in the lower load, FDA and combustion duration increased with the valve lift, there was higher combustion variability which resulted in increase of the COV_{imep} with the valve lift. For the higher load, as higher temperatures were achieved, the combustion process was very stable and the COV_{imep} was almost constant with the increase in valve lift.

5.5.3. **Gaseous emissions**

Figure 5.24 presents the gaseous emission data of the 3.1 bar IMEP and 6.1 bar IMEP loads when operating at wide open throttle and using EIVC as load control strategy. There was no clear trend between CO emissions and loads. At the lower load, the CO emission was fairly constant until the lift of 4 mm, and then decreased. For the higher load, there was an increasing amount of CO with the valve lift probably caused by the increased inhomogeneity. As expected, due to the higher combustion temperature at higher load there was lower CO and THC. THC emissions remained fairly constant with the increase in the maximum valve lift.

As the maximum lift was increased and the effective compression ratio reduced, the lower temperature played a major role in reducing NOx emissions. The increase in load resulted in higher NOx emission as expected.

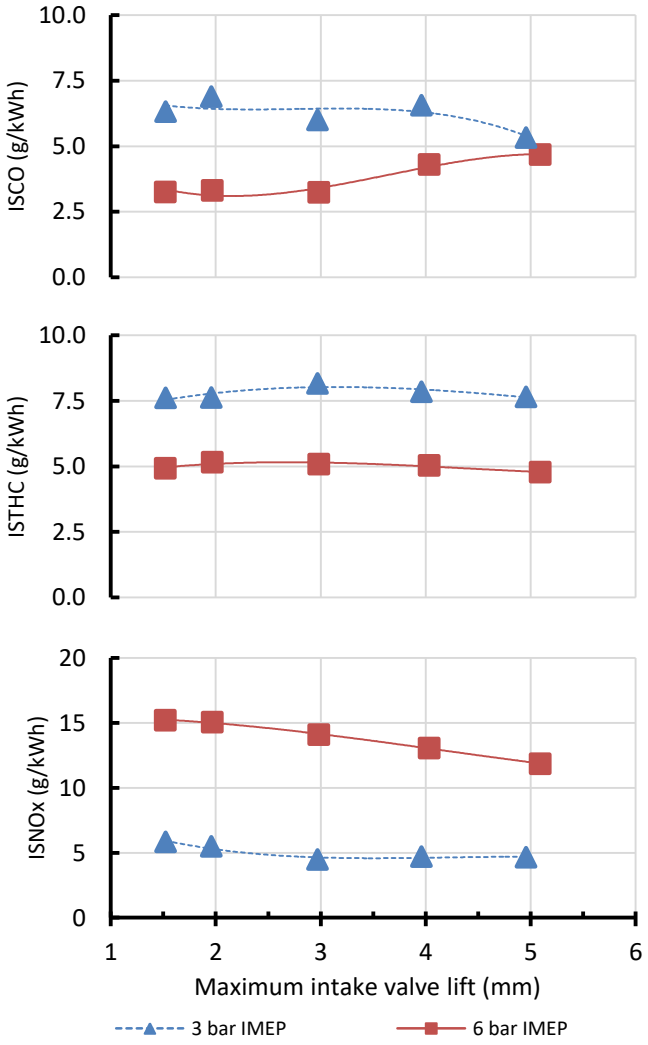

Figure 5.24. Effect of maximum valve lift on the indicated specific emissions. EIVC valve strategy, PFI E100, 3.1 bar and 6.1 bar IMEP, 1500 rpm, MBT operation.

5.5.4. **Efficiency parameters**

Figure 5.25 presents the effect of the valve lift on various efficiencies. The combustion efficiency was directly related to the THC and CO emissions. Despite of some changes in CO and THC emissions, the absolute difference between the maximum and the minimum efficiencies was around 0.25% for both loads. Considering all the uncertainties involved in the combustion efficiency calculation, such a small difference would be within the experiment uncertainty. Thus, it can be concluded that the valve lift had little effect on the combustion efficiency.

There was an increasing trend in thermodynamic efficiency with the increase in the maximum valve lift. A possible reason is that the combustion process at a lower temperature caused by the lower effective compression ratio in the higher lift cases could result in lower heat loss. The thermodynamic efficiency was reduced by 0.2% due to the lower effective compression ratio of the lower valve lift for both loads.

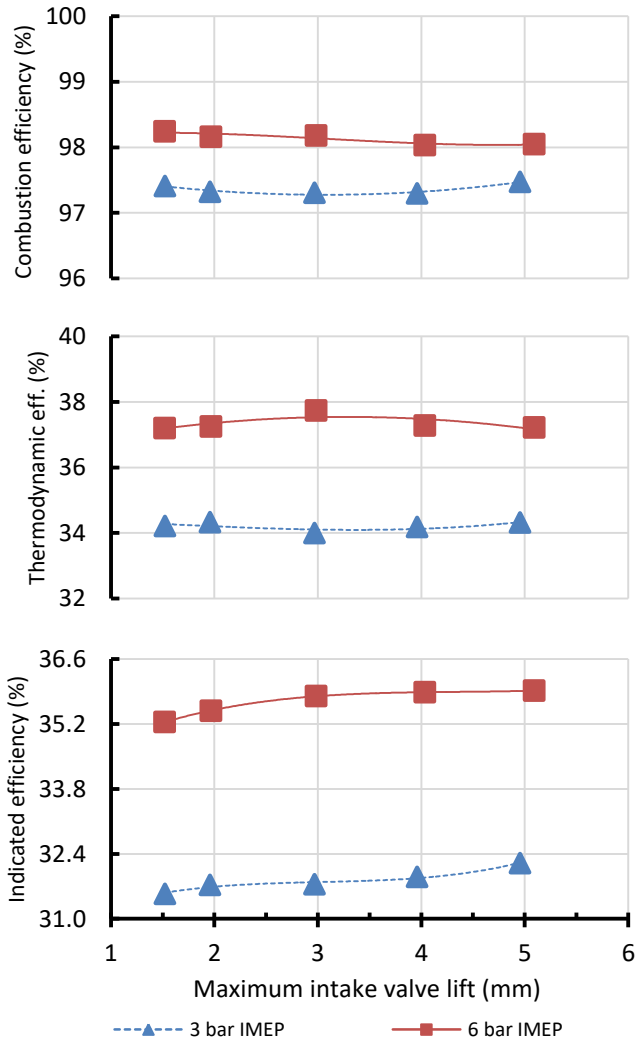

Figure 5.25. Effect of maximum valve lift on the efficiency related parameters. EIVC valve strategy, PFI E100, 3.1 bar and 6.1 bar IMEP, 1500 rpm, MBT operation.

Adversely, the lower compression ratio directly reduces the maximum theoretical efficiency of the engine. Even then, for the thermodynamic efficiency, the maximum absolute difference was around 0.20% for both loads. Such low values are not representative, once the experimental uncertainty is one order higher.

Amongst all efficiencies, the gas exchange efficiency was the main cause for the increased indicated efficiency with the valve lift, which varied 1.1% and 1.5% (absolute), for the 3.1 bar IMEP and 6.1 bar IMEP respectively. The absolute increase in the indicated efficiency was around 0.7% for both loads, which would represent a gain of 2.1% and 1.9% in the brake specific fuel consumption for the 3.1 bar IMEP and 6.1 bar IMEP loads, respectively.

5.6. Summary

The unthrottled naturally aspirated SI operation with ethanol through EIVC and LIVC load control strategies were studied in order to define which strategy has the better potential to increase the engine efficiency.

EIVC showed the best potential to increase the engine efficiency for all loads tested at the chosen speed. The main reason was the lower pumping losses resulting from the work recovered after the over-expansion phase. The major drawback of this strategy was the longer combustion duration at low loads attributed to poor in-cylinder charge motion due to the very early IVC. When ethanol was used, there was no knocking combustion for all three strategies.

The LIVC strategy showed slightly less improvement in the overall engine efficiency, because of the higher valve flow losses during the initial part of the compression stroke. However, the LIVC operation was characterised with faster combustion than the EIVC strategies.

The use of DI led to consistent gain in the overall engine efficiency over PFI, which could be attributed to lower heat losses caused by the charge cooling effect.

The increase in the maximum valve lift in the EIVC operation reduced the combustion efficiency but resulted in higher overall engine efficiency because of the greater gain in the gas exchange efficiency.

Overall, the results demonstrated that SI unthrottled operation with constant residual gas concentration was effective in increasing overall engine efficiency. Further studies will be presented in the following chapters regarding the use of IVC load control method with RGF trapping.

Chapter 6.

Unthrottled PFI and DI E100 operation with negative valve overlap and exhaust rebreathing

As shown in the previous chapters, the use of unthrottled operation with EIVC would increase engine efficiency by reducing pumping losses. Other ways to decrease the pumping loss is through the use of internal exhaust gas recirculation or residual gas trapping which can also lower the combustion temperature and hence NOx emissions and heat loss during combustion. One method is through the exhaust valve reopening, also known as exhaust rebreathing (ER), which achieves hot exhaust gas backflow from the exhaust ports to the cylinder during the intake stroke even with near atmospheric intake pressure. Alternatively, negative valve overlap (NVO) can be used. The simultaneous use of NVO with variable EIVC would be expected to further increase engine efficiency.

In this chapter, results will be presented for the anhydrous ethanol unthrottled operation with NVO and ER. A NVO period optimization study and ER optimization study are shown. The tSI operation was chosen as the baseline in order to provide a comparison to current technologies employed on production engines.

6.1. Exhaust rebreathing with DI and PFI E100 SI operation

6.1.1. Test methodology

Different exhaust valve reopening periods and timings were evaluated in order to find best trade-off between exhaust emissions and engine efficiency when using the exhaust rebreathing valve strategy. It should be noted that due to FVVA system limitations the opening and closing event of any valve could occur only once per cycle. For this reason, the exhaust process occurred with only one exhaust valve. The 2nd exhaust valve opening event occurred during the intake stroke to enable exhaust gas backflow to the cylinder. The target valve lift for both intake and exhaust valves were 3.0 mm in order to promote the same flow restrictions of the valves presented in the

previous chapters. The 2nd exhaust valve (2ndEV) event duration and position controlled the amount of residual gas backflow. Load was controlled by EIVC method. This way, the only valve timing parameters fixed were intake valve opening (-7 CAD $ATDC_{intake}$), and 1st exhaust valve opening (-189 CAD $ATDC_{intake}$) and closure (at TDC_{intake}).

The tests were taken at 1500 rpm with the stoichiometric air/fuel ratio for the loads of 2.0, 3.1, 4.5, 6.1, 7.5 and 9.0 bar IMEP (±5.0% IMEP). Spark timing was varied in order to achieve MBT operation and PFI timing was set to TDC_{firing}. The maximum spark advance was -45 ATDCf, before which misfires started to happen.

6.1.2. **Effect of 2nd EV event on 3.1 bar E100 PFI operation**

This experiment was designed to investigate the effect of the 2nd EV event on the low load engine operation. Initially, a late 2nd EV event (occurring during the BDC) with fixed duration was phased towards TDC_{intake} (cases 1 to 7), as shown in Figure 6.1. The initial duration was set in order to achieve COV_{imep} around 2.0% with the maximum spark advance of -45 ATDCf, which means that this is near the maximum RGF limit for stable combustion. Later, for the best indicated efficiency case, the duration of the 2nd EV event was increased (cases 6a, 6b and 6c).

Although the maximum lift target was 3.0 mm for both exhaust valves, the maximum valve lift was reduced (automatically by the FVVA control system) in order to maintain the 2nd EV event period constant due to the valve opening and closure velocities. There was no overlap between intake valves and 2ndEV from the first to the fourth case due to the late exhaust valve event. For the fifth case a small overlap occurred, but it wasn't enough to require a large IVC variation. For the sixth case the there was a larger intake and 2nd EV overlap and it required a larger intake period in order to induce the same amount of charge and keep the load constant. For the 7th case, intake valve event period was reduced due to the low piston speed which reduced RGF. Due to the increased 2nd EV event duration of the cases 6b and 6c, in-cylinder fresh charge was displaced by the back flown exhaust gases and required slightly longer intake duration. Table 6.1 presents intake valve parameter variation.

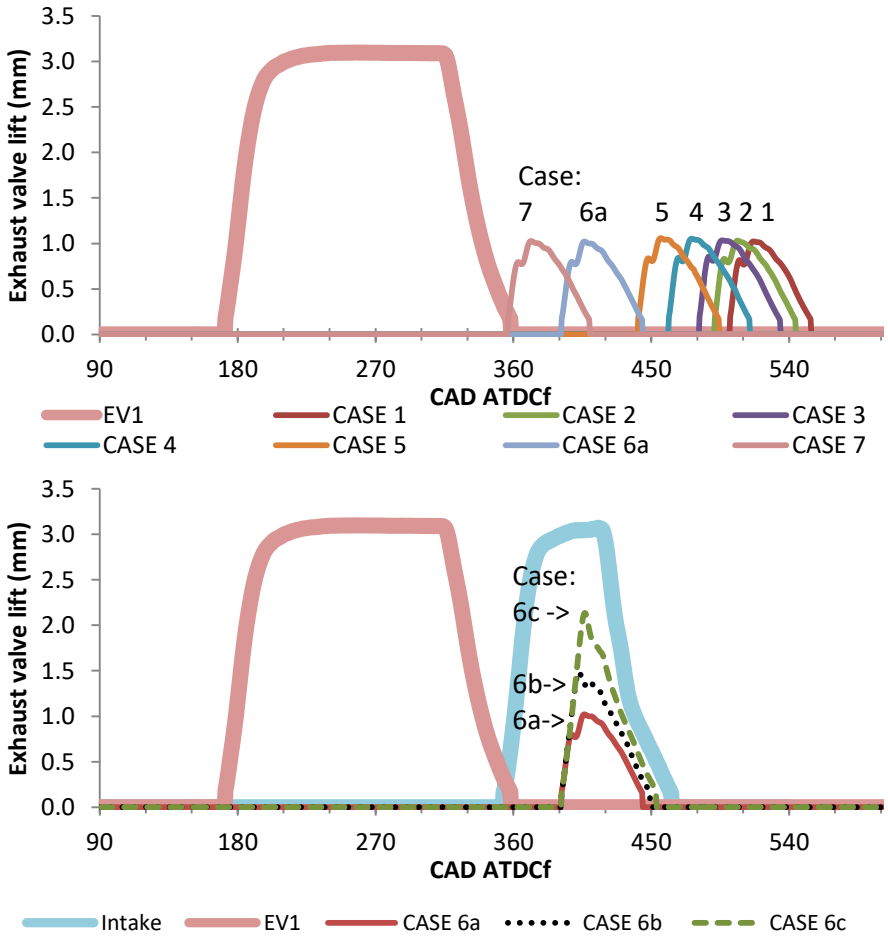

Figure 6.1. Exhaust valve lift profiles of the different tested cases 2nd EV event for the 3.1 bar IMEP load. PFI E100, 1500 rpm, MBT operation.

The variable 2nd EV event had direct impact on the pumping loop, as shown in Figure 6.2. Increased pumping loop occurred for the cases without rebreathing and intake overlap. This was consequence of the early over-expansion period caused by the EIVC followed by the 2ndEV event at low in-cylinder pressure. As the rebreathing period was advanced towards TDC_{intake}, the in-cylinder pressure during the rebreathing period was higher and the over expansion period pumping losses were smaller. Figure 6.3 presents the gas exchange efficiency and PMEP of all tested cases. The higher the work lost in the pumping cycle (more negative PMEP), the lower the gas exchange efficiency.

Table 6.1. Variation of the intake valve parameters according to the rebreathing case for 3.1 bar IMEP load. PFI E100, 1500 rpm, MBT operation.

CASE	IVC (CAD ATDCi)	Overlap between IV and 2ndEV (CAD)	Intake event duration (CAD)
1	458	-42.5	105
2	459	-32	106
3	459	-22	106
4	459	-2	106
5	459	18.5	107
6a	464	73	111
7	459	103.5	107
6a	464	73	111
6b	465	74	112
6c	466	75	113

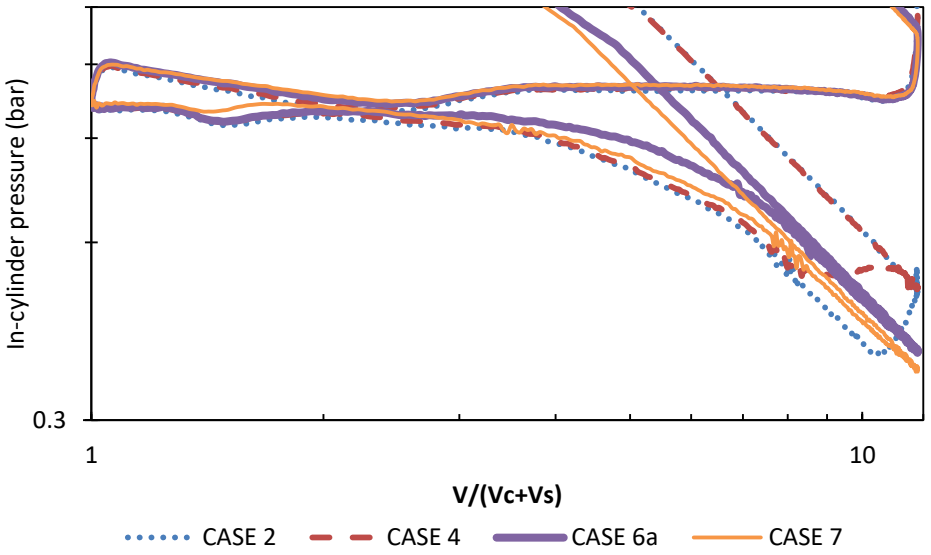

Figure 6.2. Log P x log V diagram with emphasis in the pumping loop for different 2ndEV even period. PFI E100, 1500 rpm, MBT operation.

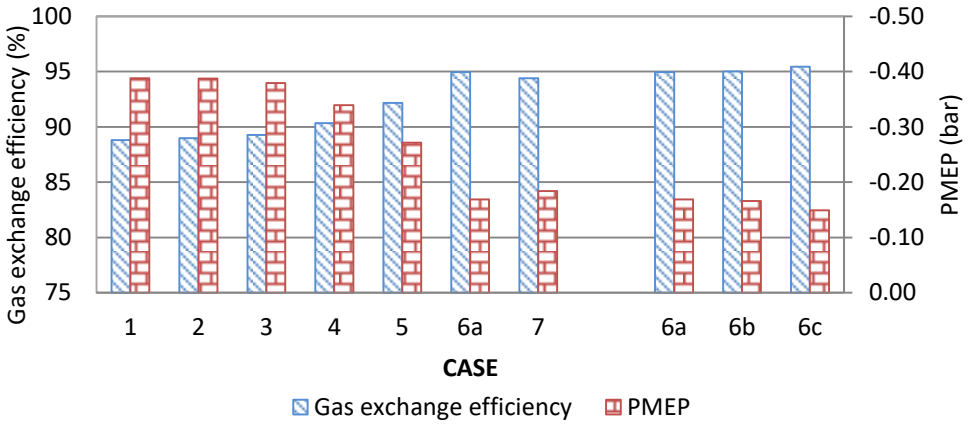

Figure 6.3. Gas exchange efficiency and PMEP for different rebreathing cases for 3.1 bar IMEP load. PFI E100, 1500 rpm, MBT operation.

Figure 6.4 shows the required spark timing for each case and the resultant COV_{imep} for MBT operation. The cases expected to operate with the highest RGF contents required the maximum spark advance of -45 CAD $ATDC_{firing}$. Conventional SI combustion occurred for all cases. Case 6a and 7 resulted in the lowest COV_{imep}, expected to be a consequence of both better gas exchange process and lower RGF.

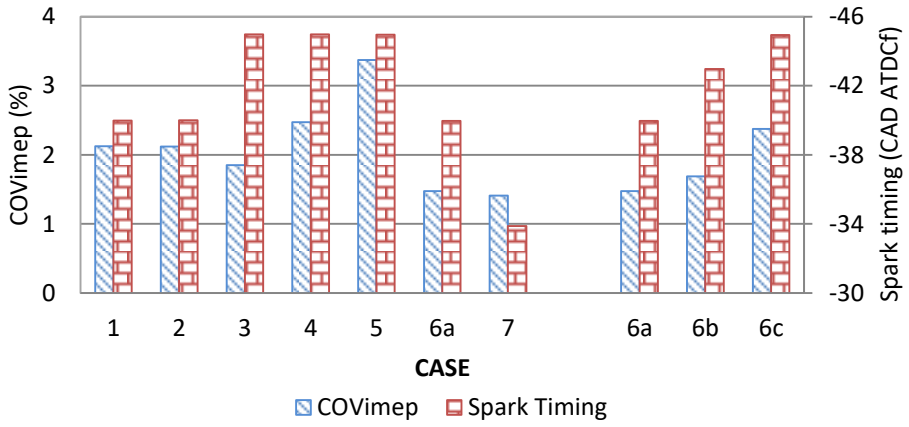

Figure 6.4. Spark timing and COV_{imep} for different rebreathing cases for 3.1 bar IMEP load. PFI E100, 1500 rpm, MBT operation.

Figure 6.5 presents the engine out emissions. CO emission could be considered constant for the cases 1 to 6, and the variation could be attributed to small lambda deviations. For the 7th case, the slight increase in CO could be related to the decrease in THC. For the cases 6a, 6b and 6c, the increase in CO and THC could be directly

related to expected increase in RGF content which would lower the combustion temperature and reduce CO and THC conversion. As a direct result of the THC and CO emissions, combustion efficiency was higher for the cases with the lowest emissions, as shown in Figure 6.6. NOx emissions were lower for the cases expected to have higher RGF.

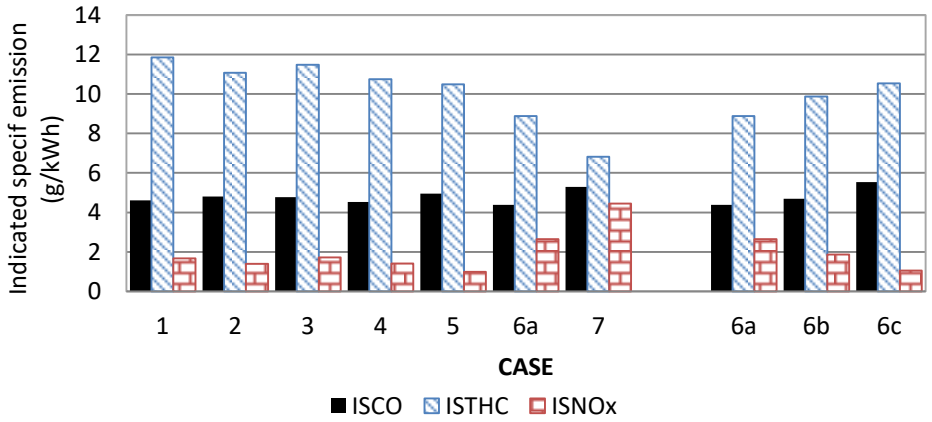

Figure 6.5. Indicated specific engine-out emissions for different rebreathing cases for 3.1 bar IMEP load, PFI E100, 1500 rpm, MBT operation.

The indicated overall engine efficiency is related to the gas exchange efficiency and combustion efficiency. Cases in group 6 which had the highest gas exchange efficiency and relatively good combustion efficiencies resulted in the highest indicated efficiencies. The lower indicated efficiency of case 7 was consequence of higher combustion temperatures due to comparatively low RGF which increased thermal losses. The reduction in the indicated efficiency for the 6c case could be attributed to the long combustion duration and slightly delayed combustion phasing due to the maximum spark advance limit.

From this study it could be concluded that for low load operation, the 2nd EV event results in higher indicated efficiency when occurring with some degree of overlap to the intake events. Both duration and phasing of the rebreathing event can be used to control the amount of residual gas.

Similar test methodology was then applied for all other tested loads and only the optimized cases for best indicated efficiency will be analysed.

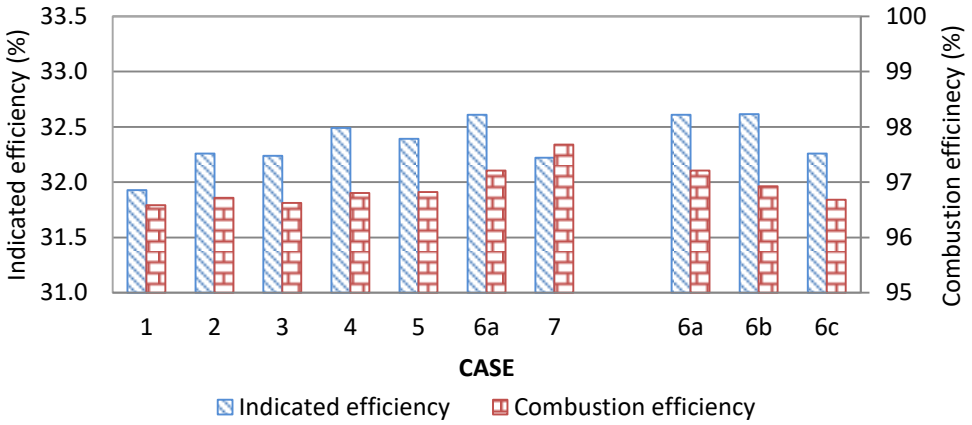

Figure 6.6. Indicated and combustion efficiencies for different rebreathing cases for 3.1 bar IMEP load, PFI E100, 1500 rpm, MBT operation.

6.1.3. **Exhaust rebreathing operation: overview on optimized valve timings**

Tests were carried following the methodology provided in the previous section in order to find the optimized valve timing for all proposed loads when using rebreathing strategy. The DI timing was 28 CAD $ATDC_{intake}$. Figure 6.7 presents the variation of the valve lift profile used at different load operations. Two different optimization approaches were used in order to simplify the tests:

- ➔ for low loads (2.0 and 3.1 bar IMEP), the rebreathing period was set (regarding it's positioning) while intake valves were opened during the later phase of the intake event;
- ➔ for 4.5 bar IMEP until 9.0 bar IMEP, the end of the rebreathing period was set to occur near the BDC in order to provide IVC near the BDC to increase combustion temperature and promote CAI combustion (if possible).

As shown in the last section, for the lowest loads, a good compromise between reduction of PMEP and COV_{imep} could be achieved when the 2^{nd} EV event was totally overlapping the intake events. As the EIVC load control was used, IVC was always delayed towards BDC in order to increase fresh air trapping in order to increase the load. For the 4.1 bar IMEP load the $2^{n\,d}$EV period was set to start at the IVC and end at BDC. This way, the in-cylinder pressure was maintained at higher levels during the whole intake period without the over-expansion period caused by the EIVC load control method. Thus, SACI combustion was achieved for PFI operation at MBT. The DI cooling effect resulted reduced the end gas temperature during combustion and

conventional spark ignition operation was dominant. The advance of spark timing after MBT would enable SACI operation for DI method at the cost of lower indicated efficiency due to bad combustion phasing and increased heat transfer with increase in NOx emissions.

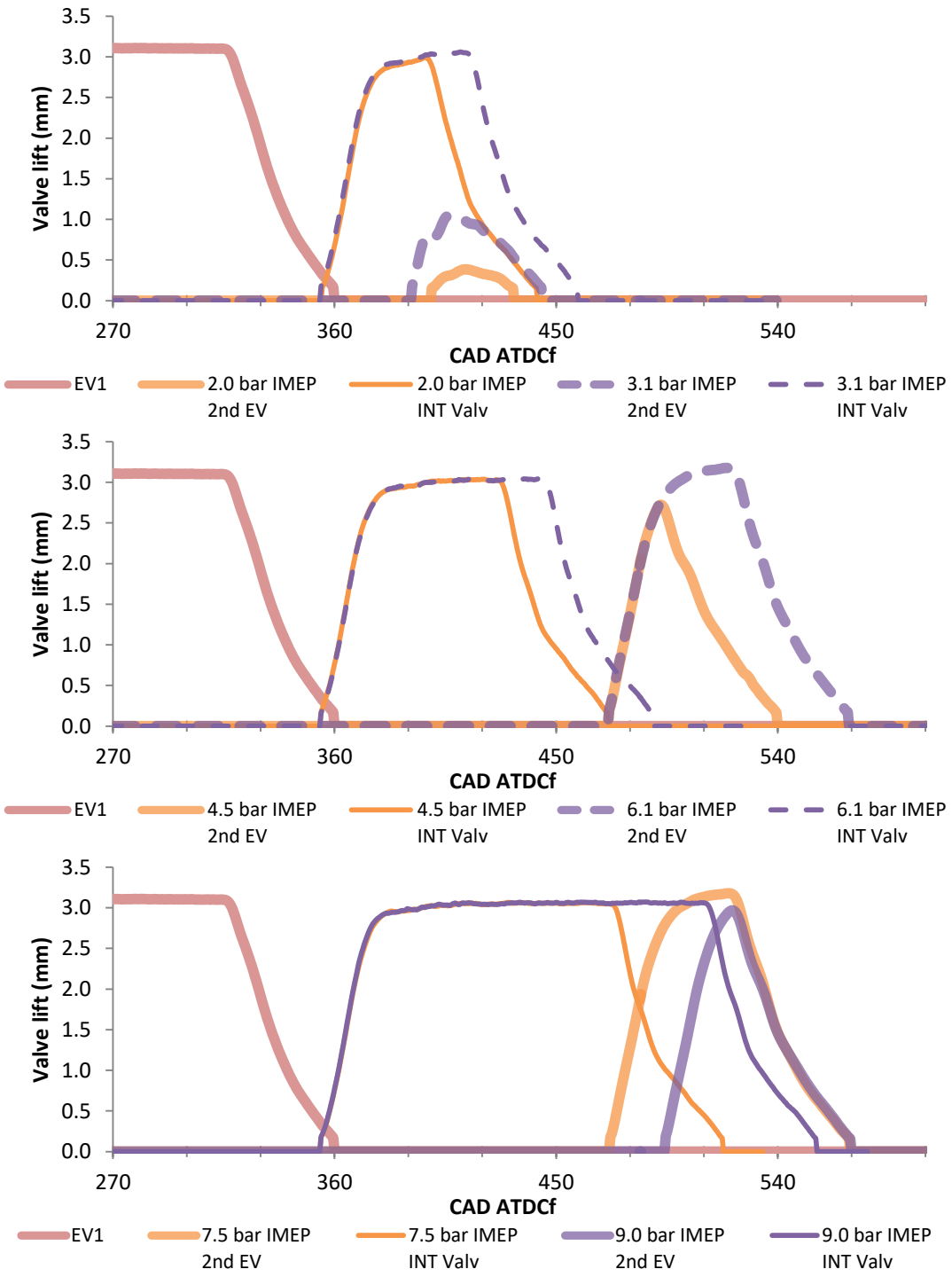

Figure 6.7. Schematics valve lift profiles for optimized exhaust rebreathing operation for several loads and DI E100, 1500 rpm, MBT operation.

A small overlap between 2nd EV and intake valves was required to increase the load for 6.1 bar IMEP. The 2nd EV closure was set to 30 CAD ABDC in order to take advantage of the higher exhaust port pressure to further increase the RGF. SACI combustion was achieved for both PFI and DI methods due to higher combustion temperatures and hotter exhaust gas backflow.

Further IVC delay was required to increase the load to 7.5 bar IMEP, while the 2nd EV event was kept constant. The fresh air flow rate was limited by the advance of the 2nd EV opening due to increased hot exhaust gas backflow. Therefore, after this load, the 2nd EV opening point had to be delayed to increase the load. The high combustion temperatures and hot exhaust gas dilution resulted in SACI combustion for PFI operation while. Conventional spark ignition combustion was dominant for DI operation although SACI could be reached by advancing spark timing with no efficiency gains. For 9.0 bar IMEP load, 2nd EV event closure was kept fixed and the opening had to be delayed to reduce hot RGF. The increase in fresh air trapping to promote the desired load was achieved by further EIVC delay.

Table 6.2. Second exhaust valve and IVC variation according to load for exhaust rebreathing valve strategy with DI and PFI methods at several loads with E100, 1500 rpm, MBT operation..

		2nd exhaust valve			Intake valves
	Load (bar)	max valve lift (mm)	EVO (CAD $ATDC_{intake}$)	EVC (CAD $ATDC_{intake}$)	IVC (CAD $ATDC_{intake}$)
DI	2.1	0.4	39	73	82
	3.2	1.0	31	85	99
	4.5	2.7	111	180	112
	6.1	3.2	111	209	129
	7.6	3.2	111	210	158
	9.1	3.0	132	210	196
PFI	2.1	0.4	38	74	85
	3.1	1.0	31	85	104
	4.6	2.7	111	181	117
	6.1	3.2	111	210	136
	7.7	3.1	119	205	161
	9.1	2.4	140	206	195

So, for ER operation, load control could be attained by both EIVC and 2ndEV positioning and event timings (EVO and EVC). Table 6.2 presents the valve timing parameters that were chosen for ER operation with DI and PFI operation. The first exhaust valve opening was fixed at -190 $ATDC_{intake}$ and the closure point was fixed at TDC_{intake}. Intake valve opening point was fixed at -7 CAD $ATDC_{intake}$.

6.1.4. **Exhaust rebreathing operation: effect of DI timing**

Direct injection timing was tested for the optimized ER 2nd EV even at 28 and 90 CAD $ATDC_{intake}$. Figure 6.8 presents spark timing, combustion duration, combustion efficiency, indicated efficiency, and engine-out emissions data for different direct injection timings and several loads. For the 2.0 and 3.1 bar loads, direct injection during the intake event (28 CAD $ATDC_{intake}$) decreased charge temperature and increased pressure difference between cylinder and exhaust ports. This resulted in slightly higher RGF and required more advanced spark timing when compared to the injection after the intake valves were closed (90 CAD $ATDC_{intake}$). For the other loads, more spark advance was required for later injection timings due to higher in-cylinder cooling effect. Combustion duration was similar for both injection timings at each load except for 2.0 bar IMEP. The higher RGF content of the more advanced injection timing case increased the combustion duration in almost 25%. For the other loads, the combustion duration difference could be related to small combustion phasing differences.

The emission data show a reduction of CO and THC for the more advanced injection timing (28 CAD $ATDC_{intake}$) due to better charge mixing process. The lower CO and THC emissions of the earlier injection cases produced higher combustion efficiencies. In general, NOx emissions were slightly smaller for the later injection due to the in-cylinder cooling effect and less charge homogeneity.

Gas exchange efficiency was very similar for different injection timings as consequence of similar pumping. Thus, the small variations on indicated efficiency between different injection timings could be related to combustion efficiency.

In this scenario, the chosen injection timing for DI operation with exhaust rebreathing strategy was 28 CAD $ATDC_{intake}$ due to the better combustion efficiency achieved.

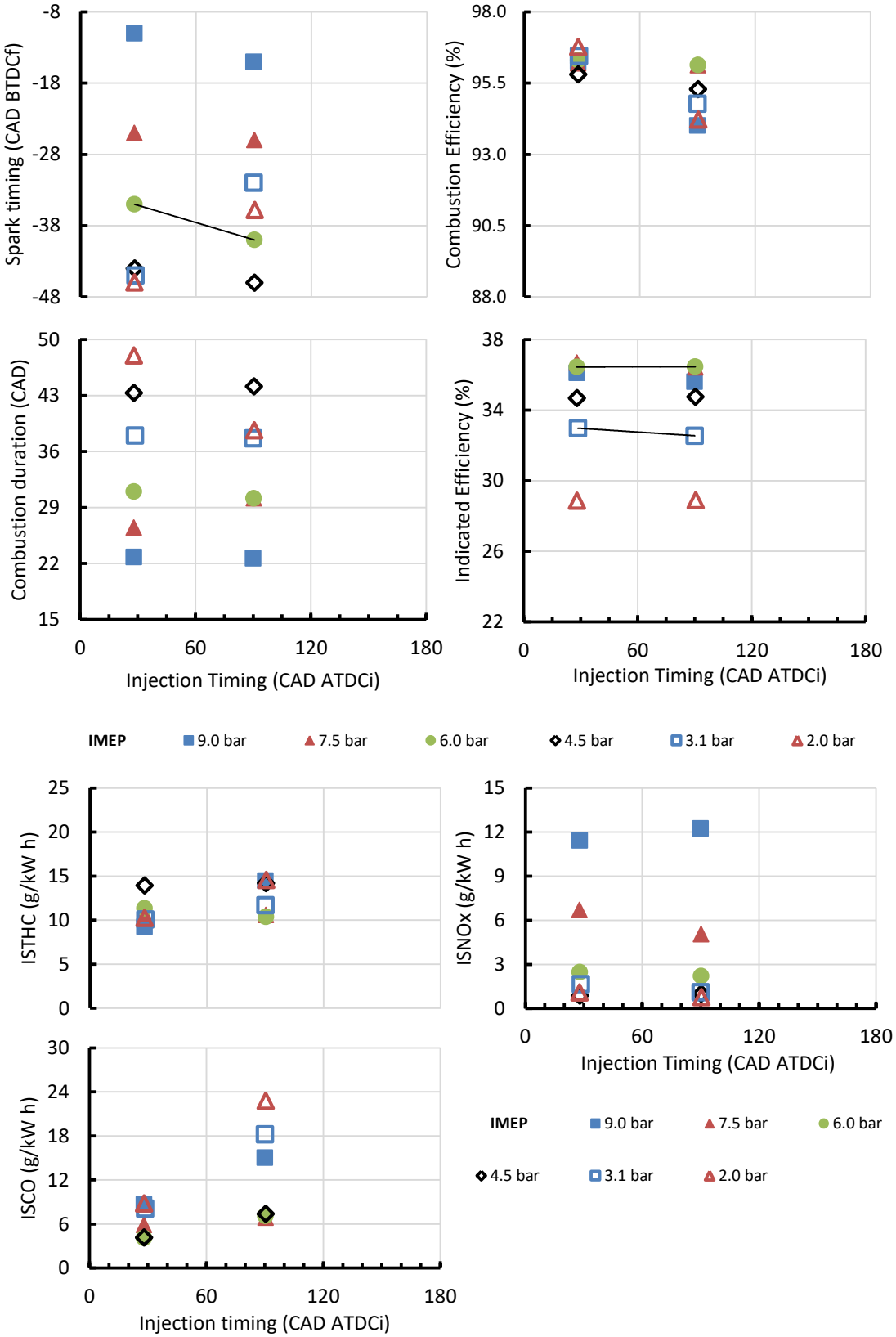

Figure 6.8. Effect of DI timing on spark timing, combustion duration, combustion efficiency, indicated efficiency, and emission data for ER operation at several loads. E100, 1500 rpm, MBT operation.

6.1.5. Exhaust rebreathing operation: effect of spark timing on SACI combustion process of E100 PFI

As shown in other works [118], the main benefit from SACI combustion compared to pure CAI combustion is the combustion phasing controllability. Pure CAI was not reached for any of the tested cases, even when using more aggressive approaches to trap higher hot residual gas fractions (not optimized points). This could be attributed to the high latent heat of vaporization of ethanol, which considerably reduced charge temperature prior to start of compression and end of compression phase temperature. In addition, E100 high auto-ignition resistance decreases ethanol CAI operation capability at the tested compression of 11.7:1.

For loads between 4.6 and 7.6 bar IMEP during the PFI operation, SACI could be reached. SACI combustion could be identified through the analysis of the heat release rate. The abrupt gradient change in the heat release rate denoted the point when the auto-ignition combustion started to contribute for the rate of pressure change, as shown in Figure 6.9. For the 4.6 bar and 6.0 bar IMEP loads, SACI occurred for at all tested spark timings.

For 7.6 bar IMEP cases, the SI to SACI transition was clearly controlled by the spark timing advance. Starting from a retarded spark timing (-15 CAD $ATDC_{firing}$), the SI combustion was initially phased towards TDC with the advance of the spark timing. For the spark timing of -21 CAD $ATDC_{firing}$ there was a visible increase on the HRR peak with an abrupt gradient change just before it. For more advanced spark timing, the auto-ignition process started earlier and the HRR peak increased. Thus, the advance of the spark timing tended to accelerate the combustion process, increase the HRR peak and start the end gas auto-ignition process sooner.

Figure 6.10 presents flame development angle (FDA), combustion duration, combustion phasing (CA50%), maximum pressure and maximum pressure rise rate, and COV_{imep} for different spark timings and different loads. The spark advance tended to increase FDA as a consequence of spark occurrence at lower in-cylinder pressure and temperature. As the spark ignition combustion was advanced, it resulted in faster combustion and earlier auto-ignition occurrence. Combustion phasing was advanced towards TDC at a faster rate as spark timing was advanced.

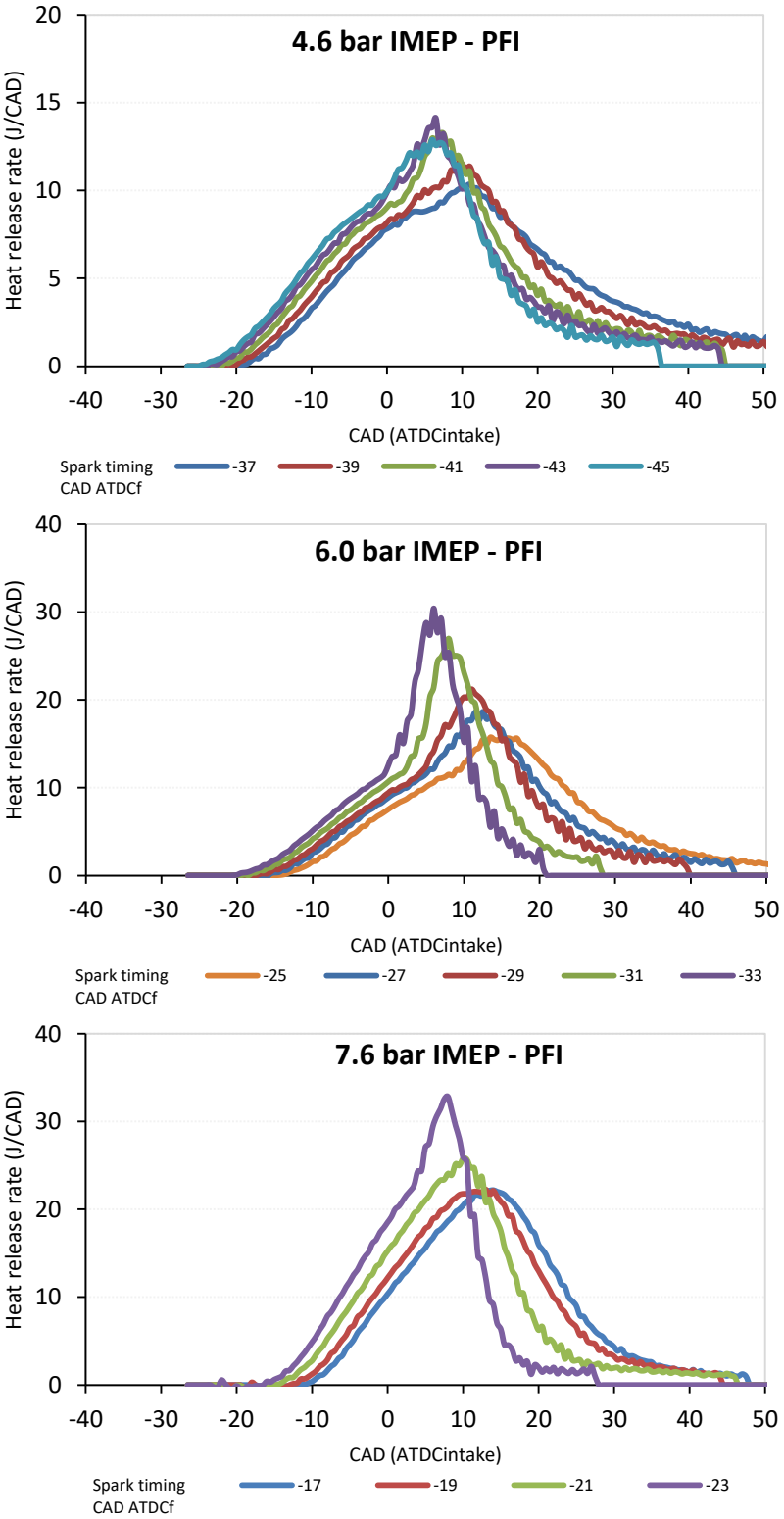

Figure 6.9. Effect of spark timing on heat release rate of E100PFI exhaust rebreathing strategy at different loads, 1500 rpm, MBT operation.

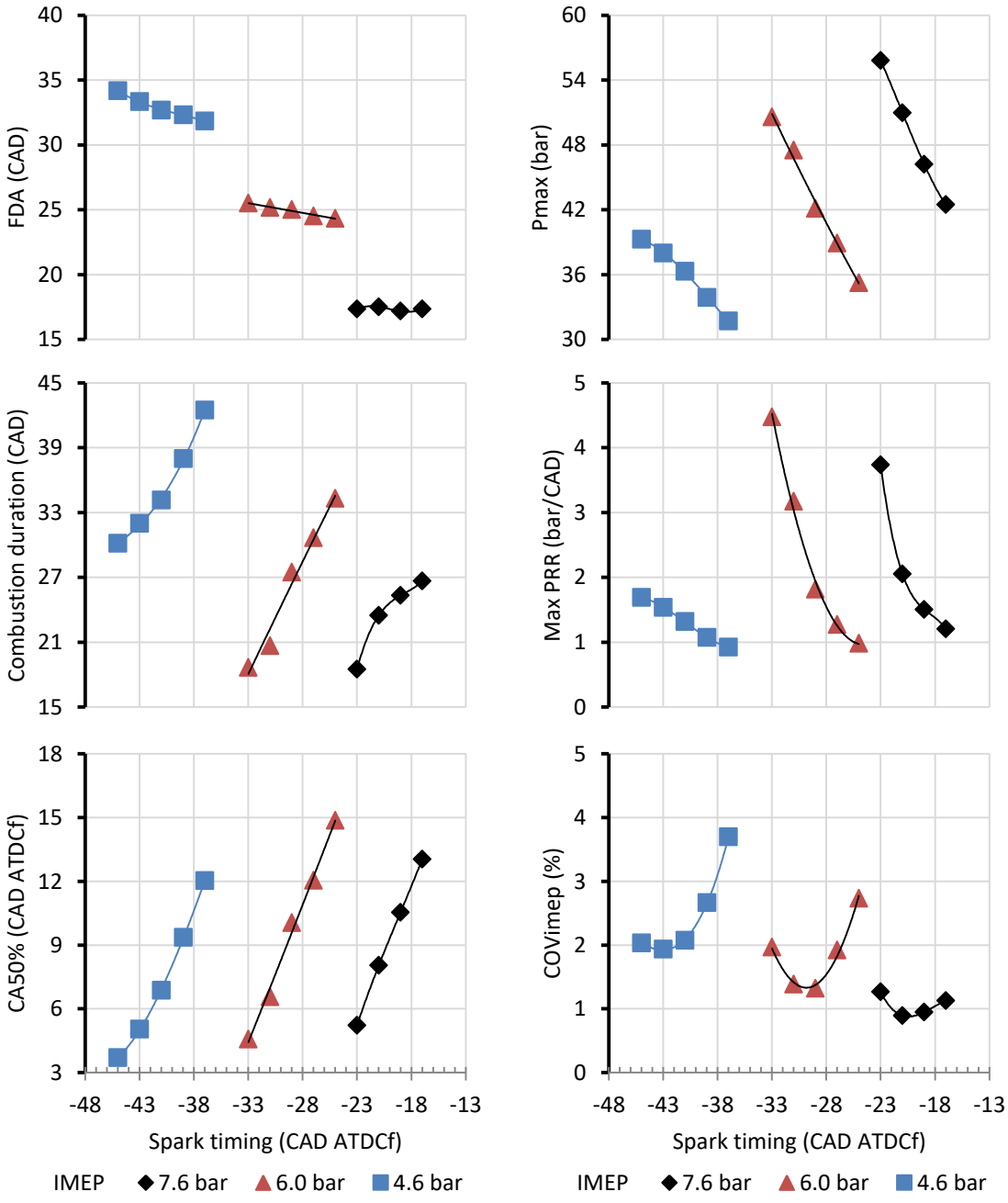

Figure 6.10. Effect of spark timing on combustion related parameters o E100f PFI exhaust rebreathing strategy at different loads, 1500 rpm, MBT operation.

Figure 6.11 presents the engine out emissions and relevant efficiency related parameters. Two distinct behaviours were observed for CO and THC depending on the loads. For 4.6 bar IMEP load, the combustion temperature was expected to be low, affecting the CO and THC conversion mechanisms. Thus, the spark timing advance with the resultant temperature increase was effective to increase CO and THC conversion, thus, reducing both emissions. For the other loads, THC could be

considered constant while CO tended to increase with the increase on spark timing as result of smaller reaction time for CO oxidation.

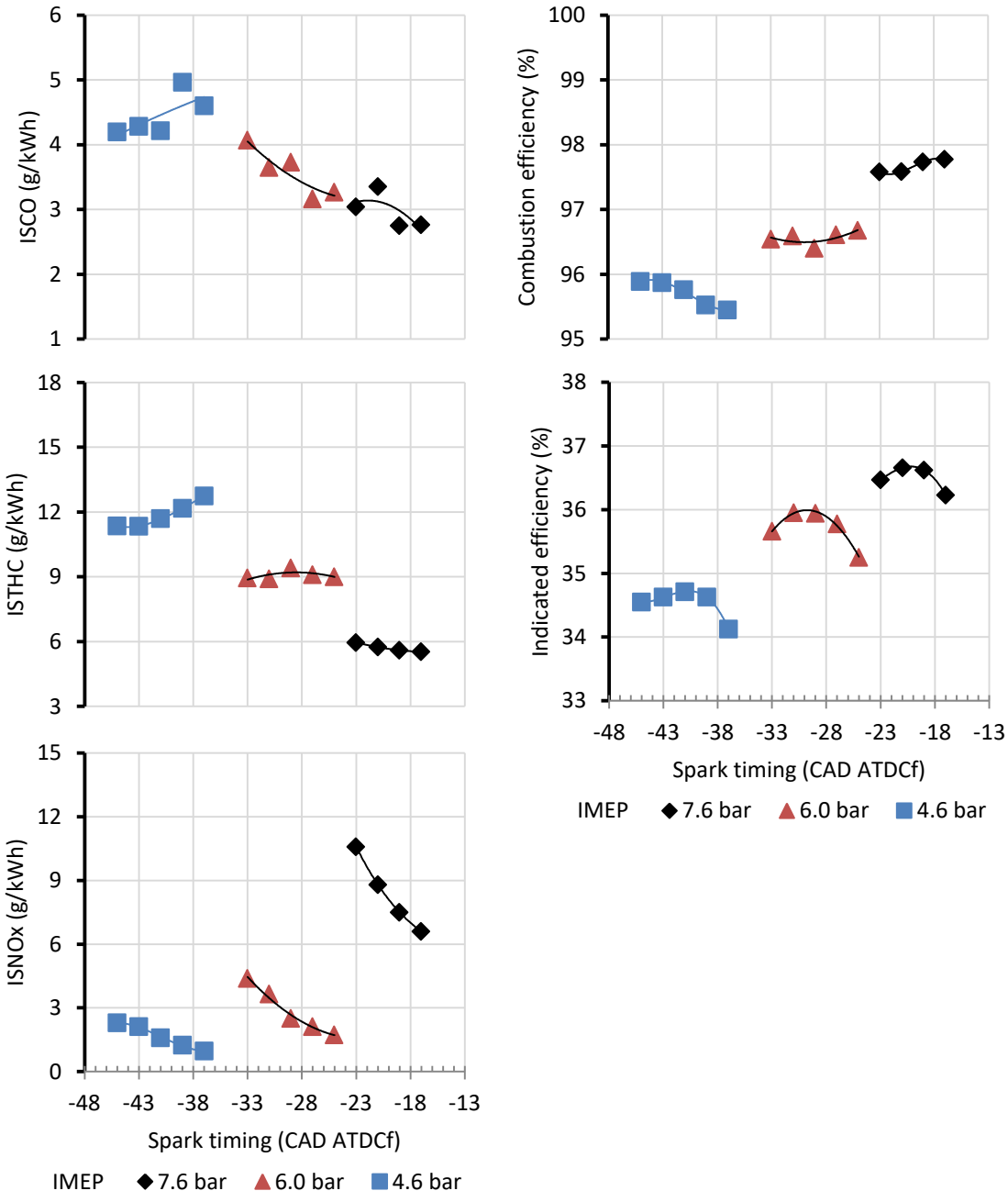

Figure 6.11. Effect of spark timing on engine out emissions and efficiency related parameters of E100PFI exhaust rebreathing strategy at different loads, 1500 rpm, MBT operation.

The increasing trend of the NOx with the spark advance was found for all loads due to the higher combustion temperatures. Even though the more advanced spark timing of the 7.6 bar IMEP load was characterised with the SACI combustion, the temperature dependence was shown to be more important than the combustion mode.

The variation in the combustion efficiency was around 0.5% in all cases. The indicated efficiency results showed that CA50% was between 6 CAD and 10 CAD $ATDC_{firing}$ when MBT spark timing was reached.

6.2. Negative valve overlap with DI and PFI E100 SI operation

Different negative valve overlap durations were evaluated in order to find an optimized trade-off between exhaust emissions and engine efficiency. The exhaust valve closure and intake valve opening points were moved away from the TDC_{intake}. EVC was set several degrees before TDC in order to retain different fractions of hot residuals, which were recompressed until TDC. IVO was positioned to reduce the pumping losses after the expansion period following the recompression phase. EVO was maintained constant at -190 CAD $ATDC_{intake}$. IVC timing was used as load control method with WOT.

The tests were performed at 1500 rpm with the stoichiometric air/fuel ratio for the loads of 2.0, 3.1, 4.5, 6.1, 7.5 and 9.0 bar IMEP (±5.0% IMEP). Spark timing was varied in order to achieve MBT operation and PFI timing was set to TDC_{firing}.

6.2.1. Negative valve overlap period optimization

Different NVO periods were tested for each target load point with PFI strategy. Figure 6.12 presents an example of the valve timing variation for different NVO periods at 4.5 bar IMEP and Table 6.3 provides the valve timing parameters that varied according to the NVO period tested at each load. The EVO timing was kept fixed at -190 CAD $ATDC_{intake}$ and PFI timing at TDC_{firing}.

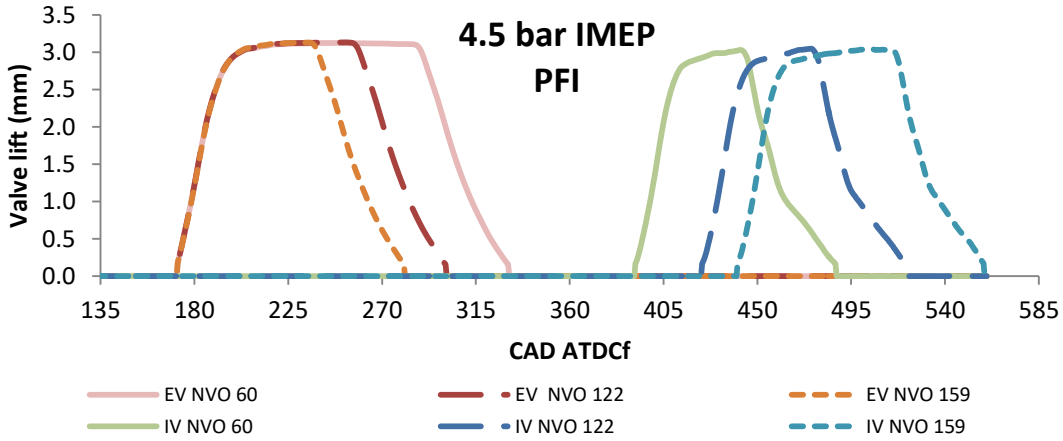

Figure 6.12. Intake and exhaust valve profiles for distinct NVO periods for 4.5 bar IMEO E100 PFI, 1500 rpm, MBT operation.

Table 6.3. Valve timings of NVO period optimization study with PFI injection and several loads.

Load IMEP (bar)	NVO Period (CAD)	EVC (CAD ATDCi)	Max EV lift (mm)	IVO (CAD ATDCi)	IVC (CAD ATDCi)	Max IV lift (mm)
2.0	33	-14	3.1	19	86	2.7
	53	-24	3.1	29	94	2.7
	72	-34	3.1	38	103	2.8
3.1	33	-14	3.1	19	101	2.9
	62	-29	3.1	33	110	2.9
	82	-39	3.1	43	120	2.9
	102	-49	3.1	53	131	2.9
	121	-59	3.1	63	143	2.9
4.6	60	-29	3.1	31	128	3.0
	87	-39	3.1	48	138	3.1
	122	-59	3.1	63	163	3.0
	142	-70	3.1	73	177	3.0
	159	-79	3.1	80	199	3.0
6.1	60	-30	3.1	31	147	3.0
	80	-40	3.1	41	159	3.1
	98	-50	3.1	49	173	3.1
	127	-64	3.1	64	205	3.1
7.6	71	-35	3.1	37	175	3.1
	94	-45	3.1	49	201	3.1
9.1	44	-19	3.1	25	195	3.1

Figure 6.13 presents the impact of the NVO duration on spark timing for MBT operation, CA50, combustion duration and COV_{imep} for several loads and PFI. At 2.0 bar IMEP even a small NVO period was enough to highly dilute the charge and decrease combustion stability. Only for the smaller NVO period tested the spark timing advance was effective to produce stable combustion. For this reason, only one tested NVO duration at 2.0 bar IMEP reached stable operation condition.

When operating at 3.1 bar IMEP the NVO period could be considerably increased, being limited by RGF content which resulted in unstable combustion after NVO duration of 120 CAD (COV_{imep} higher than 3.0%). For all other loads the NVO period was limited by the interaction between RGF and fresh charge. At 4.5 bar, for example, for the NVO period of 159 CAD, the IVC was already occurring after the BDC. Thus, further NVO period increments would result in low fresh charge trapping to maintain the load.

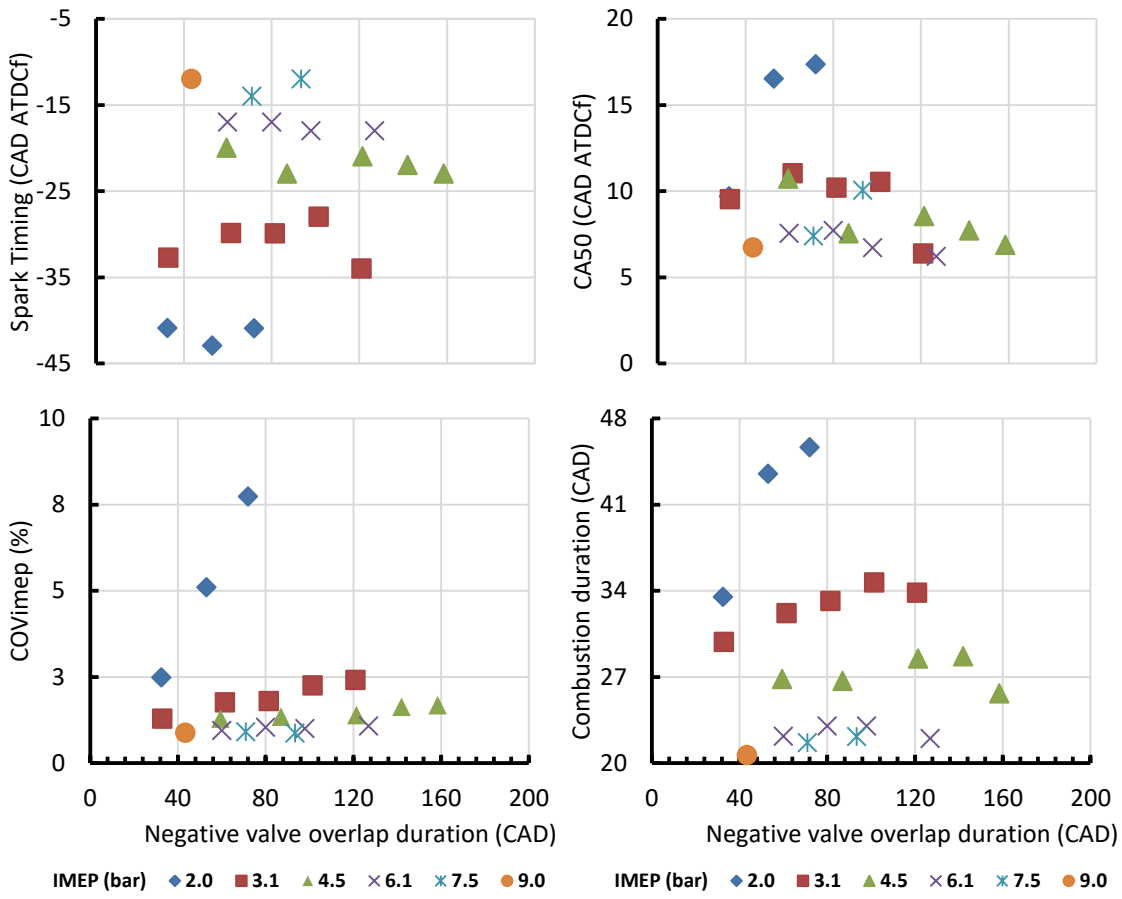

Figure 6.13. Effect of NVO duration on required spark timing for MBT, CA50, COV_{imep} and combustion duration for several loads and E100 PFI, 1500 rpm, MBT operation.

In addition, the charge thermal state increased as the load increased. Thus, more retarded spark timing was required for MBT operation. Another parameter that influenced the spark timing was the IVC. For the same load, as the NVO period increased the IVC was also delayed, so that the higher effective compression ratios were achieved. Thus, the dilution effect of the increased residual gases was compensated by the increase of temperature (due to higher effective compression ratio) and the spark timing could be kept constant for different NVO periods. Figure 6.14 presents the effective compression ratio and pumping mean effective pressure variation as a function of the NVO period. The variation of both parameters was a direct consequence of the variation of the IVC.

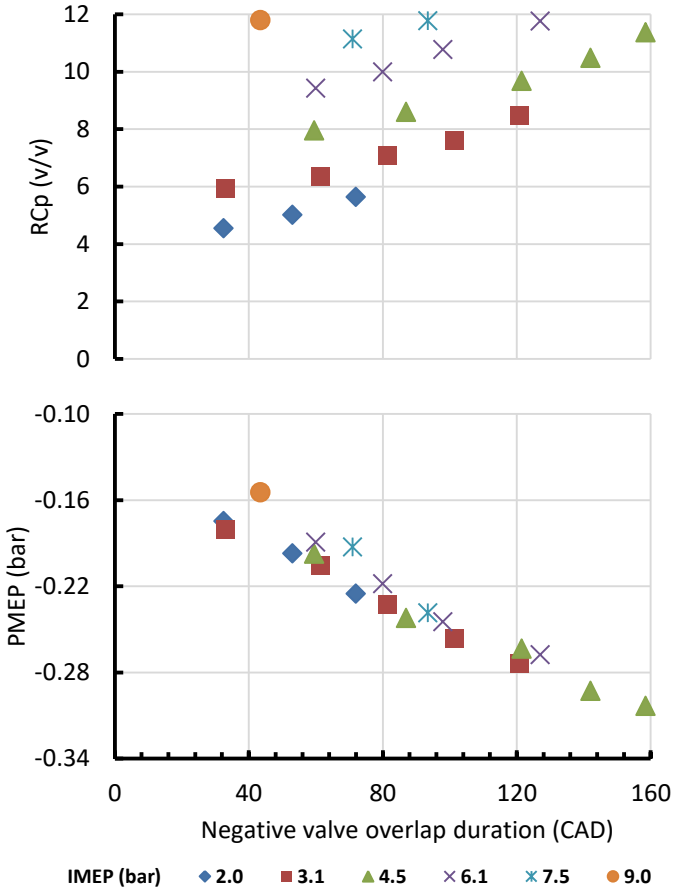

Figure 6.14. Effect of NVO duration on effective compression ratio and pumping mean effective pressure for several loads and E100 PFI, 1500 rpm, MBT operation.

The combustion duration tended to increase with the increase in the NVO period due to slower combustion reactions at lower combustion temperatures. The faster combustion at higher loads occurred due to higher combustion temperatures and lower RGF.

As shown in the PMEP plot, the increase on the NVO period increased the PMEP losses (higher absolute value). There was a small variation in PMEP for the same NVO period and different loads. This fact could be attributed to the flow losses during the IVC event. At lower loads the intake valve closing period was relatively larger (IVC closing period to intake event period ratio was higher at lower loads) than at high loads. Thus, the flow was relatively more restricted and there were higher pumping losses. This directly affected the gas exchange efficiency, which will be discussed later.

Figure 6.15 presents the engine out emissions data. At 2.0 bar IMEP there was a direct relationship between the decrease in CO emissions due to the increase in THC. For the other loads, the CO emissions variation was maintained fairly constant for the same load as the air fuel mixture homogeneity was not expected to vary due to the PFI operation. The small deviations from the mean value (for different NVO periods) could be attributed to small deviations on lambda value.

THC emissions increased with the increase in the NVO period due to lower combustion temperatures. For 7.5 bar IMEP load, the higher RGF dilution effect was not enough to reduce combustion temperatures, thus, THC emissions were fairly the same. On the other hand, the reduction on combustion temperature significantly reduced NOx emissions.

The combustion efficiency was reduced with the increase in the NVO period as a direct consequence of the increase in THC emissions.

The gas exchange efficiency followed the reverse trend of PMEP, being reduced as NVO period was increased. The increase on gas exchange efficiency with the increase in load occurred due of higher pumping losses at lower loads.

Thermodynamic efficiency tended to increase with the increase of the NVO period and load. The increase on thermodynamic efficiency with NVO period could be attributed to lower combustion temperatures which reduced the in-cylinder heat transfer. The increase on thermodynamic efficiency with the load could be related to the faster combustion process, up to the point where the heat release was too high and increased heat transfer.

Thus, the relatively constant indicated efficiency with the increase on NVO period was a consequence of the opposite trends of thermodynamic efficiency to the combustion and gas exchange efficiencies.

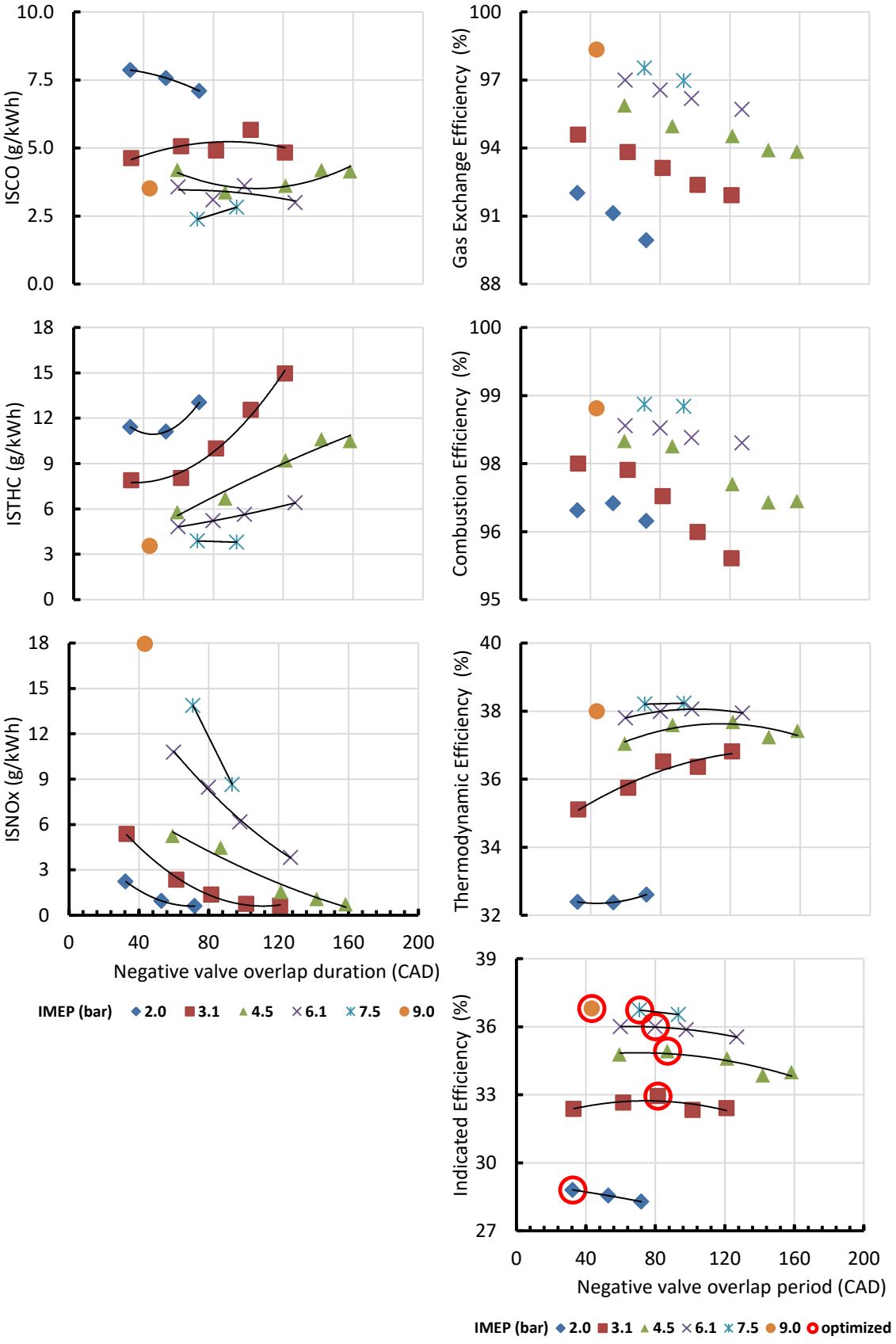

Figure 6.15. Effect of NVO duration on engine out specific emissions and efficiency related parameters for several loads and E100 PFI, 1500 rpm, MBT operation – detail for the optimized operating points.

6.2.2. **Effect of DI timing on ethanol NVO operation**

In order to understand the effects of DI timing on the NVO operation, tests were conducted at the target loads shown by the circled point in Figure 6.15. To reduce the number of experiments, all loads except 2.0 and 9.0 bar IMEP were chosen with an NVO duration around 80 CAD.

The valve timing for DI NVO operation was set according to the findings of section 6.2.1. The direct injection timing was tested during the NVO recompression phase and during the intake phase. In order to guarantee that no fuel was being lost to the exhaust during the exhaust process, the DI start of injection was set to the end of the exhaust valve closure phase so that the charge mixing period was maximized. Table 6.4 presents the optimized valve timing parameters and the injection timing during the recompression period.

Table 6.4. Optimized valve timing parameters for NVO ethanol operation with DI injection timing during the recompression period.

	Load IMEP (bar)	NVO Period (CAD)	EVC (CAD ATDCi)	DI Timing (CAD ATDCi)	IVO (CAD ATDCi)	IVC (CAD ATDCi)	Int event dur (CAD)	Max IV lift (mm)
DI inj during NVO	2.0	41	-19	-30	22	89	67	2.8
	3.1	81	-39	-50	42	115	74	2.9
	4.5	81	-39	-50	42	131	90	3.0
	6.1	81	-39	-50	42	151	109	3.1
	7.5	81	-39	-50	42	173	131	3.1
	9.0	69	-36	-45	33	206	173	3.1

The main effect of the ethanol injection during the NVO recompression period on the pumping loop phase is the reduction on the trapped residual gas temperature. This resulted in lower recompression pressure and slightly smaller pumping losses (Figure 6.16) not enough to affect engine indicated efficiency. Figure 6.17 presents the spark timing, combustion duration, PMEP and COV_{imep} data for the different tested DI timings.

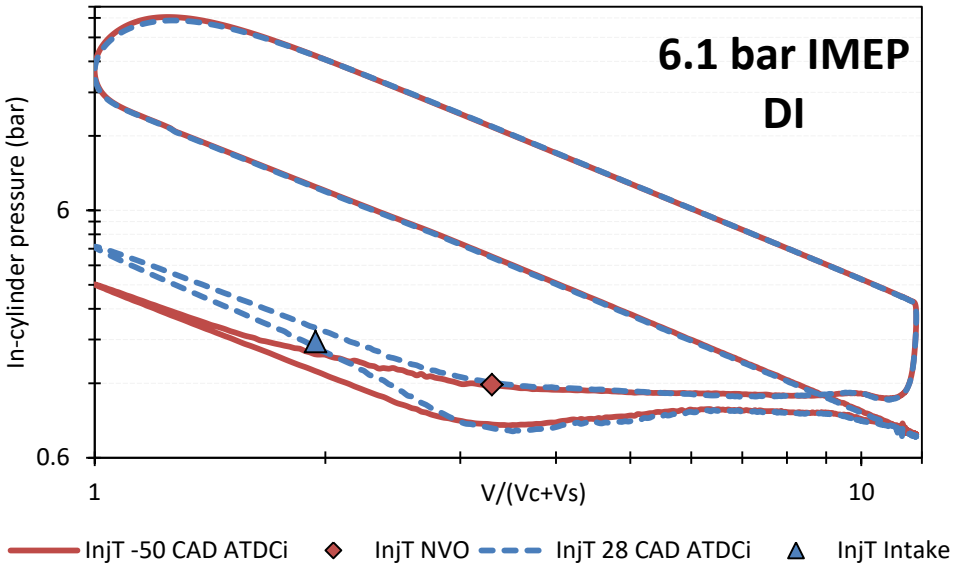

Figure 6.16. Effect of DI timing: comparison between direct E100 injection during NVO recompression period and during the intake phase.1500 rpm, MBT operation.

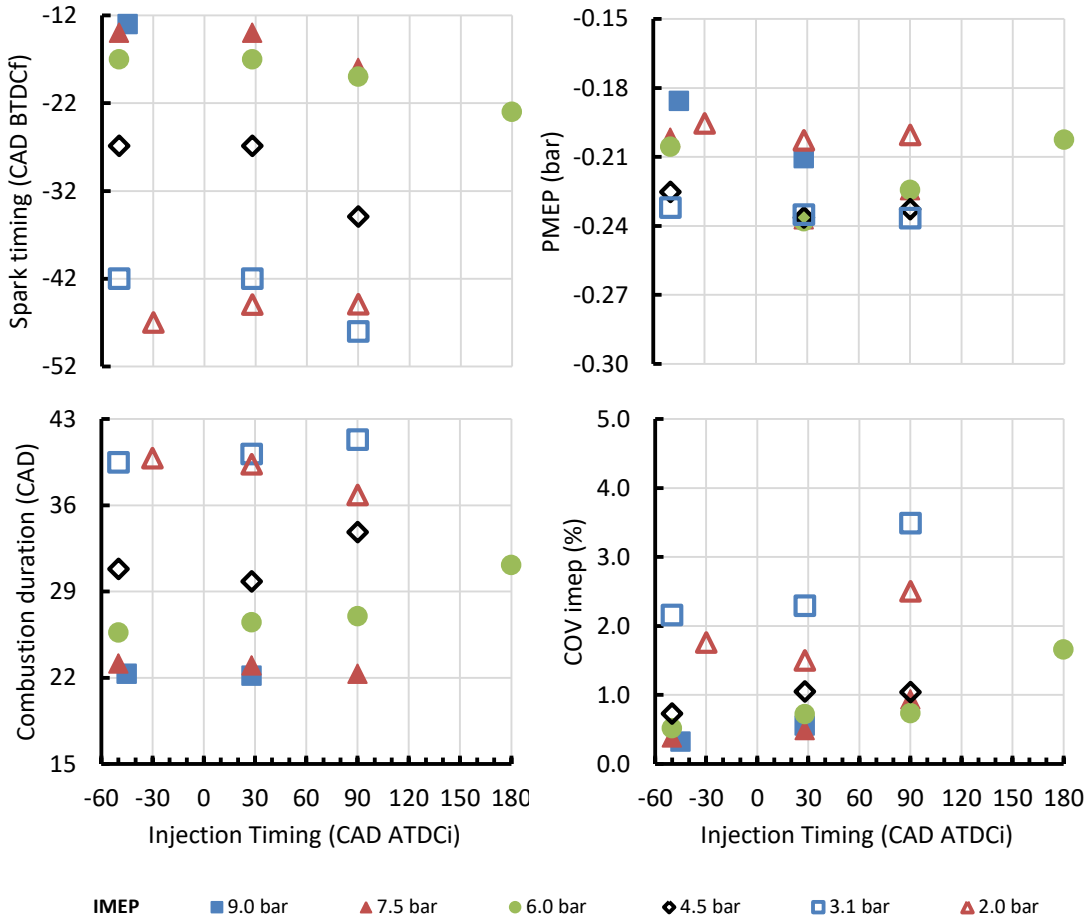

Figure 6.17. Effect of DI timing on spark timing, combustion duration, PMEP and COV_{imep} for several loads with NVO operation. E100, 1500 rpm, MBT operation.

For all loads except 2 bar IMEP, injection timing after 28 CAD $ATDC_{intake}$ required more advanced spark timing to counter the more pronounced DI charge cooling effect. But the combustion duration and COV_{imep} tended to increase with the retarded DI timing.

Figure 6.18 presents engine out emissions and efficiency related parameters. The injection timing during the NVO period resulted in better charge homogeneity. Thus,

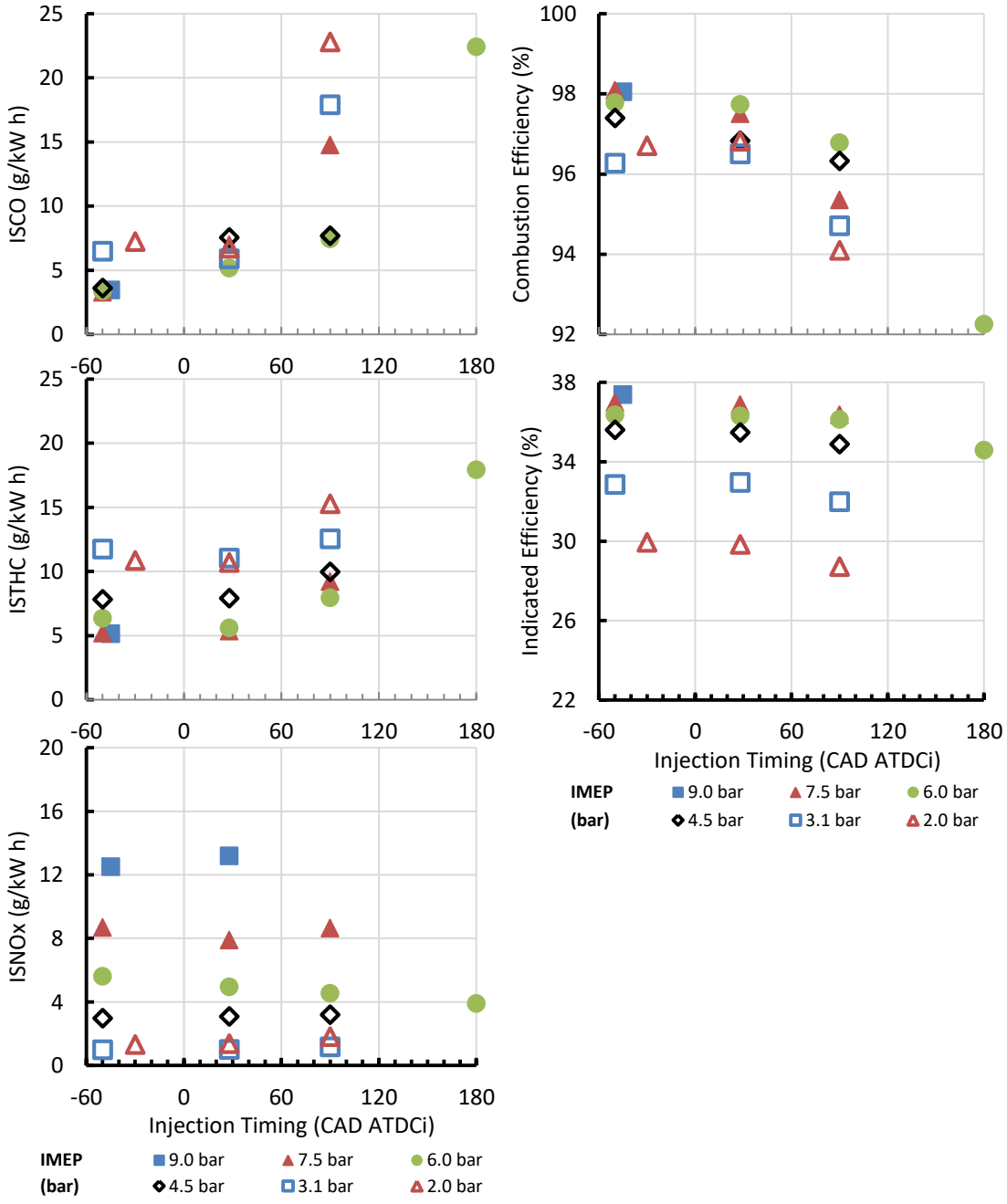

Figure 6.18. Effect of DI timing on engine out emissions and efficiency related parameters for several loads with NVO operation. E100, 1500 rpm, MBT operation.

CO emissions tended to increase with delay on injection timing. THC emissions varied little during the NVO and early intake (28 CAD $ATDC_{intake}$) injection. The later injection produced higher THC, expected to be a result of the poor fuel vaporization process. NOx emissions did not show a clear trend. The later injection charge cooling effect was counter balanced by longer combustion duration and less homogenous charge (prompt NOx formation mechanism). Thus, similar NOx values occurred for injection timing up to 90 CAD $ATDC_{intake}$. The fuel injection during the BDC was more effective in reducing in-cylinder temperature in the end of compression and lowered NOx emissions.

The combustion efficiency decreased with the delay of the injection timing, due to the increase in CO emissions. Only at 2.0 and 3.1 bar IMEP, there was a slight increase in combustion efficiency for the 28 CAD $ATDC_{intake}$ due to a slight increase on THC.

The indicated overall efficiency remained constant for NVO injection and early intake phase injection. The later injection timings tended to reduce the indicated efficiency, as a consequence of the lower combustion efficiency.

Because of their higher overall efficiency and lower CO emission, the NVO injection was chosen for the comparative analysis in the next section.

6.3. Comparative analysis between NVO and ER E100 operation with DI and PFI strategies

6.3.1. Gas exchange process

Figure 6.19 presents the intake plenum pressure and pumping mean effective pressure (PMEP) for the three valve timing strategies and different loads. The unthrottled operation with IVC load control enabled near atmospheric plenum pressure for ER and NVO strategies. The IVC occurred at a certain crank angle when enough air was trapped in the cylinder to achieve the stoichiometric combustion at a desired load. In the throttled control load case, the plenum pressure was reduced to decrease the charge in the cylinder.

The fuel injection in the intake ports displaced intake air requiring higher intake pressure for the same operating load than the DI operation. On the other hand, the DI

injection promoted in-cylinder cooling effect which resulted in a lower in-cylinder pressure prior to the start of compression.

The lower tSI plenum pressure increased the pumping work, the main cause for low partial load SI efficiency. In the NVO case the recompressed exhaust gases (as consequence of early EVC) were expanded until near atmospheric pressure, when IVO occurred. The in-cylinder pressure was maintained until the IVC occurred when an over expansion phase took place. The consumed work of the over expansion phase was partially recovered during the subsequent expansion in the same way that happened in the EIVC strategy presented on the previous chapter.

In the ER strategy different rebreathing periods resulted in distinct PMEP behaviour. For 2 and 3.1 bar IMEP loads, the exhaust rebreathing period was very small and its best positioning occurred while overlapping the intake valve opening period. So, after the IVC, an over expansion took place (as in the NVO). For 4.5 bar IMEP until 9 bar IMEP, a separate rebreathing period with the second valve EVO near the IVC resulted in the best indicated efficiency. For the 4.5 bar IMEP, the best efficiency occurred when closing the exhaust valve at the BDC. For higher loads, the EVC occurred slightly after BDC. Increased exhaust pumping work occurred at higher loads due to only one valve actuation during the exhaust period. This fact increased the PMEP (more negative values) when comparing ER to the NVO strategy.

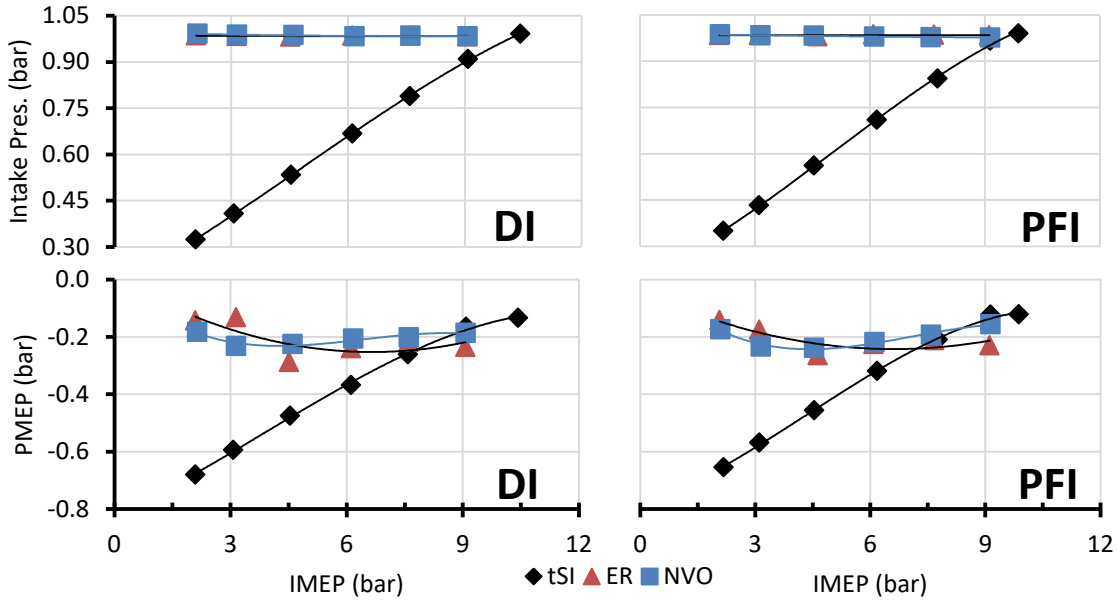

Figure 6.19. Intake pressure and PMEP for different valve strategies and various loads. DI and PFI E100, 1500 rpm, MBT operation.

6.3.2. **Combustion analysis**

Figure 6.20 presents the spark timing and CA50 for MBT, combustion duration and COV_{imep}. Regarding the combustion process, the increase in hot iEGR fraction required much more advanced spark timing to correctly phase the combustion process. Additionally, as the EIVC load control strategy was used, the expected reduction in large scale in-cylinder motion, and consequently lower turbulence levels prior to spark resulted in very long flame development angles. It was not possible to correctly phase the combustion process for some of the low load cases even with the more advanced spark timing. At such points, the increase in spark advanced resulted in misfires. The

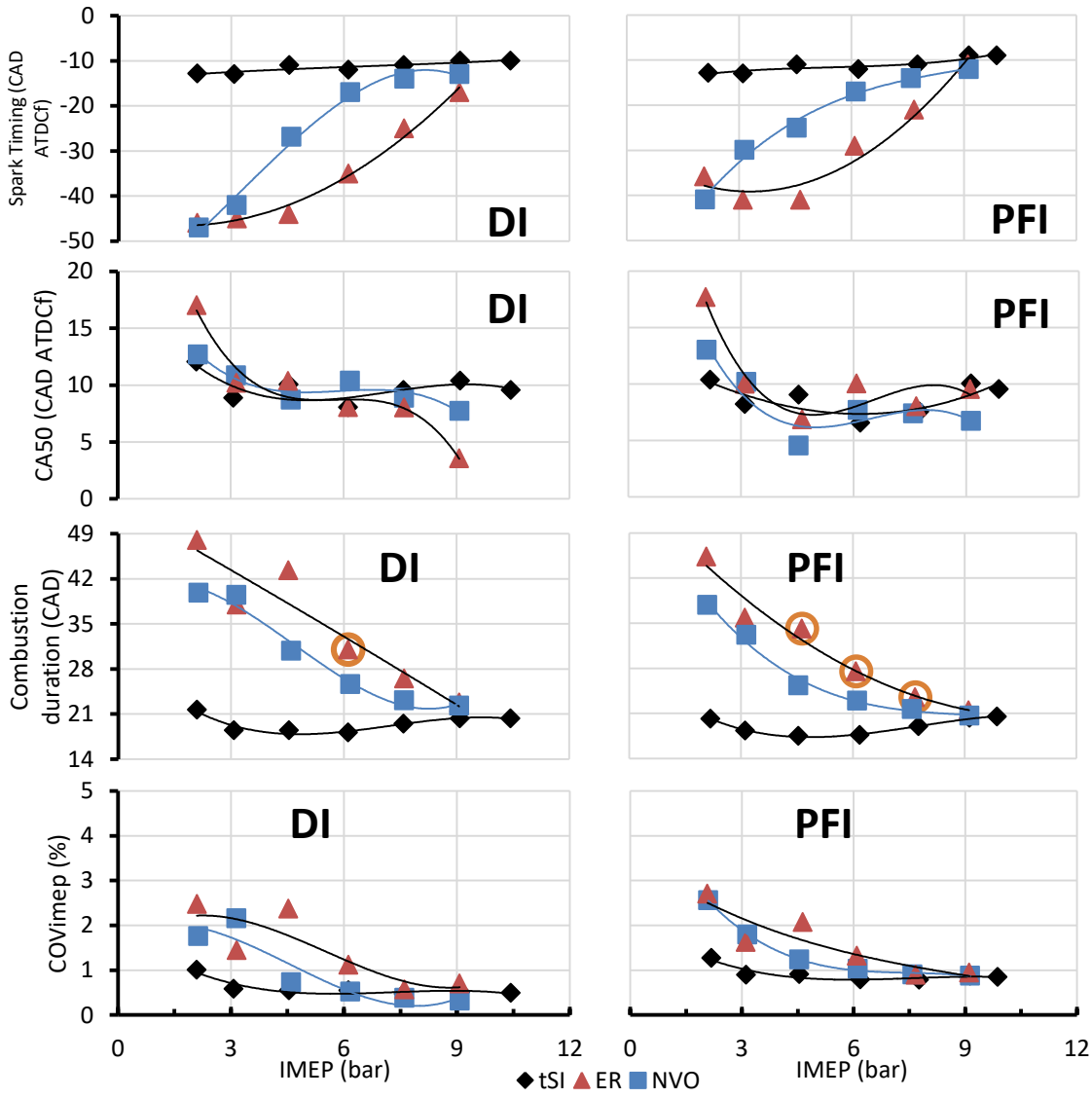

Figure 6.20. Combustion related parameters for different valve strategies and various loads (highlight on operating conditions with SACI combustion). DI and PFI E100, 1500 rpm, MBT operation.

more advanced spark timing in the ER cases was necessary because of higher iEGR fractions. As the valve timings were slightly different for the DI and PFI strategies, there was a small difference in the spark timings. Generally, the lower compression temperature prior to spark in the DI cases required more advanced spark timing as a consequence of the DI cooling effect. This was also reflected in the combustion duration (10-90% mass fraction burned), which tended to be faster in the PFI cases due to higher combustion temperature.

The higher iEGR fraction of the ER strategy resulted in the longest combustion durations, followed by the NVO strategy. In the tSI cases the combustion was purely dominated by flame propagation and there was no knock occurrence. For the NVO strategy the optimized points also resulted in conventional SI combustion. Even then, much longer combustion duration was result of the higher iEGR amount, smaller compression effective compression ratio and expected lower in-cylinder turbulence levels. For some of the tested NVO periods (during NVO period optimization) spark assisted compression ignition (SACI) was achieved when using port fuel injection and very advanced spark timing (after MBT). This resulted in no efficiency benefit.

For the ER strategy and PFI injection the heat release rate showed SACI combustion for several loads. For ER DI, SACI occurred only at 6.1 bar IMEP. The points that presented SACI combustion are circulated in the combustion duration plot in Figure 6.20. The longer combustion duration tended to increase the combustion cyclic variability. In the ER cases, the more complex gas exchange period also contributed for the higher $COV_{imep.}$

Figure 6.21 presents the heat release rate of the different valve strategies. For the same valve strategy, as load increased, the heat release amplitude was increased while the duration was reduced. PFI presented a higher heat release peak with slightly shorter duration than the DI operation at the same load. This indicates that there would be lower in-cylinder temperatures during combustion and lower in-cylinder heat transfer with the DI method due to the ethanol charge cooling effect. Attention should be given to the HRR of the ER cases with PFI which were characterised by SACI combustion. For DI operation, only ER operation at 6.1 bar IMEP exhibited clear SACI combustion. For the ER 7.5 bar IMEP case, the start of the end gas auto ignition occurred near the peak, and for this reason the SACI phenomena was less apparent on the heat release of the average pressure cycle.

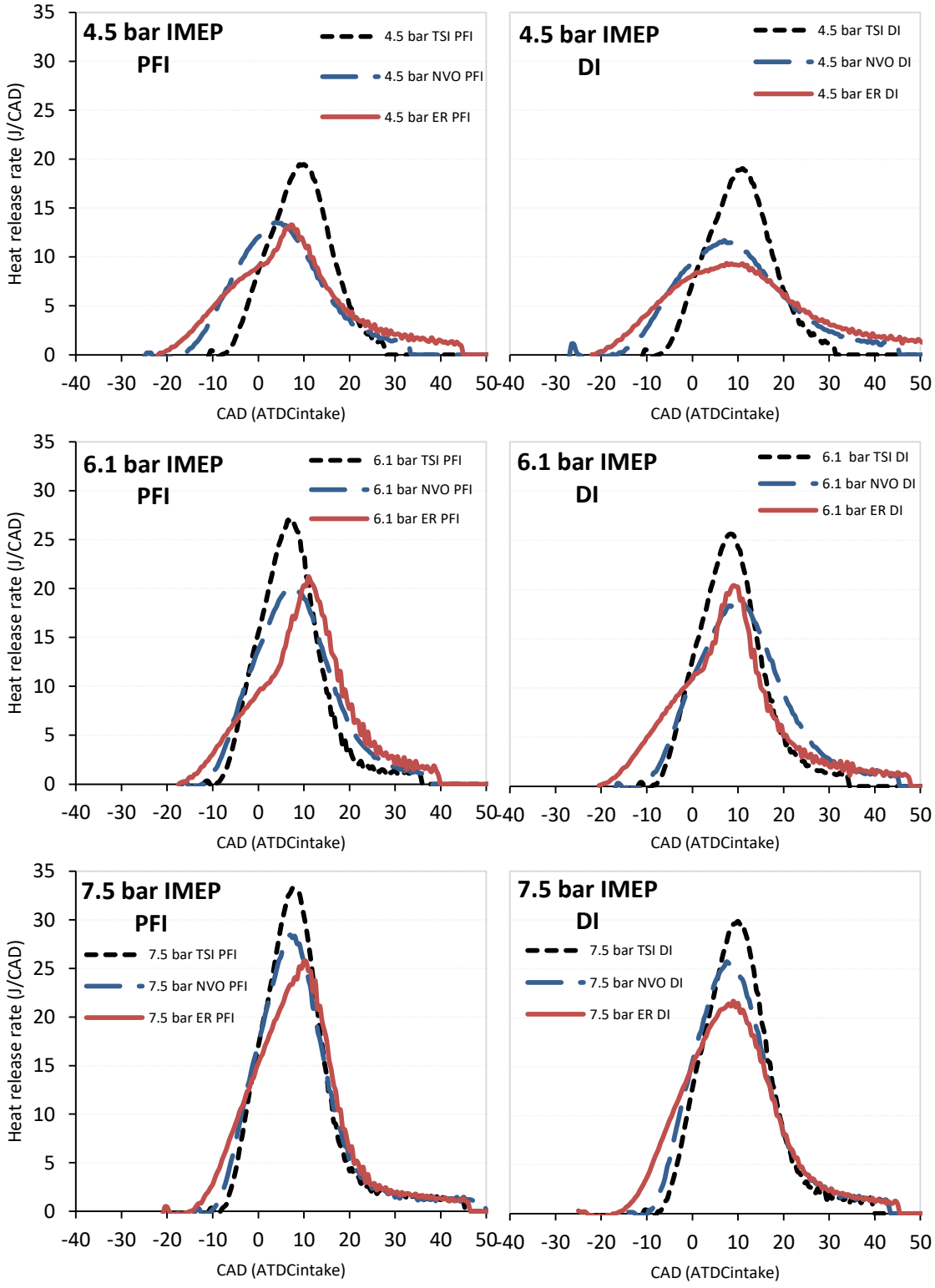

Figure 6.21. Heat release rate of the different valve strategies and injection methods for 4.5 bar, 6.1 bar and 7.5 bar IMEP. DI and PFI E100, 1500 rpm, MBT operation.

Figure 6.22 presents the instantaneous in-cylinder pressure of some operating conditions for the different valve strategies. As a general trend, PFI peak pressure was

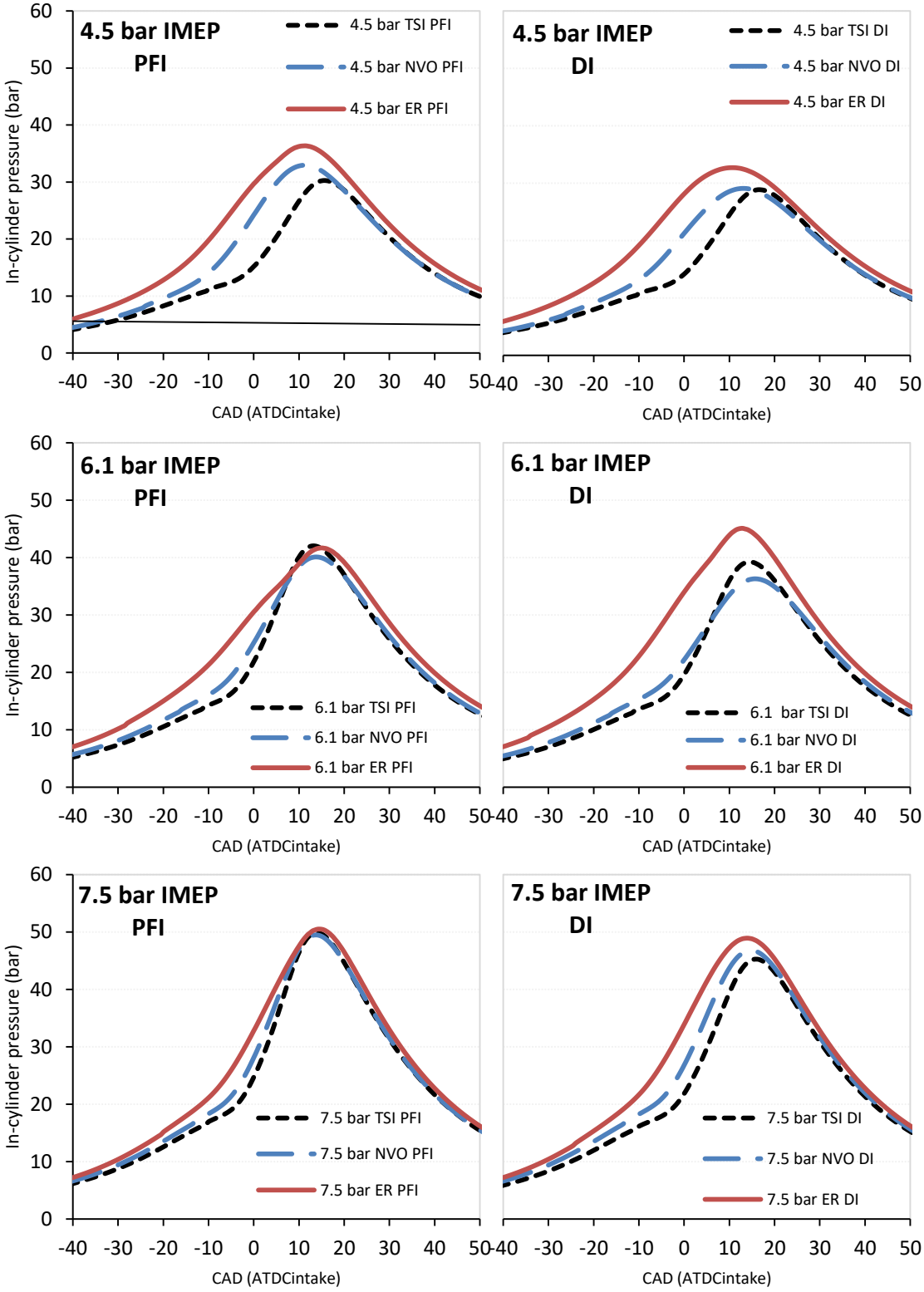

Figure 6.22. In-cylinder pressure of the different valve strategies and injection methods for 4.5 bar, 6.1 bar and 7.5 bar IMEP. DI and PFI E100, 1500 rpm, MBT operation.

higher than DI for the same valve strategy due to higher heat release peak. The increased in-cylinder mass content due to the iEGR addition was the responsible for

the pressure increase of ER and NVO cases. Absolute peak pressure values are presented in Figure 6.23. The pressure rise rate was kept at acceptable levels with a maximum of 3.7 bar/CAD at 9 bar IMEP in the ER DI case.

The exhaust temperatures (Figure 6.23) shown different trends for each valve timing and injection strategies and they remained sufficiently higher for the effective operation of the 3-way catalyst.

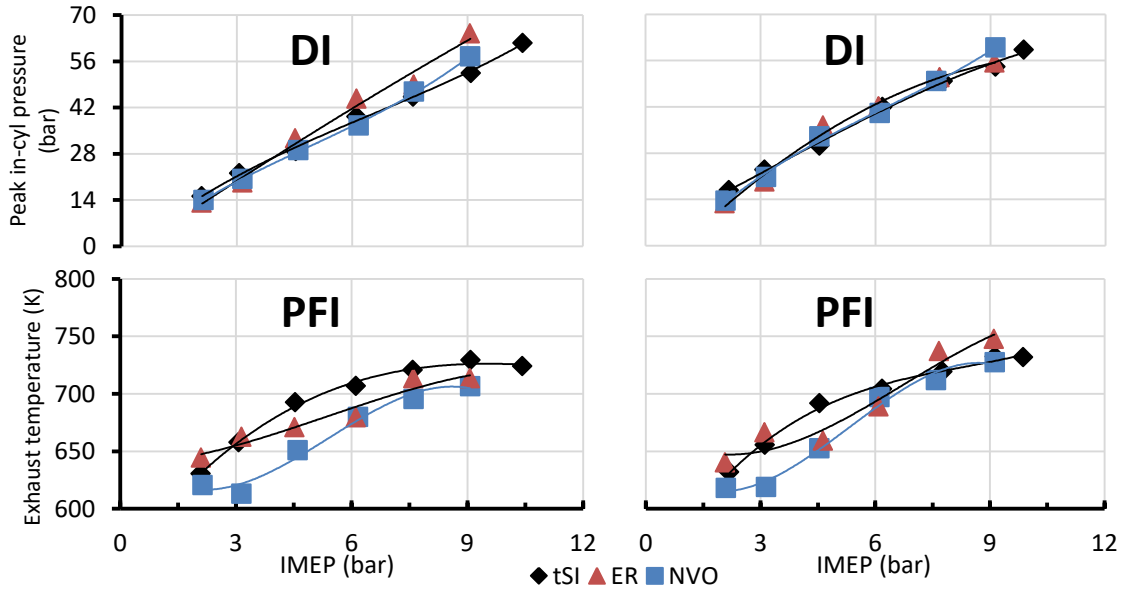

Figure 6.23. Peak in-cylinder pressure and exhaust temperature for different valve strategies and various loads. DI and PFI E100, 1500 rpm, MBT operation.

6.3.3. **Specific emissions**

The indicated specific CO, THC and NOx emissions are presented in Figure 6.24. The lowest CO formation occurred for the NVO valve timing strategy, followed by ER and tSI. NVO with early injection during the recompression provided the longest period for charge mixing process between the DI cases. As CO formation was directly linked to charge mixture homogeneity, this strategy provided the lowest CO formation. On the other hand, the tSI DI injection during the initial phase of the intake process showed a decrease in in-cylinder homogeneity with the increase in load due to more fuel being injected at once. For the ER case, there was a direct relationship of decrease in CO and increase in THC. This occurred due to the low combustion temperature which was not enough to partially oxidize the fuel molecules. In this case, in-cylinder homogeneity played a minor role. In the PFI cases, CO emissions were lower than in the DI cases due to the long mixture formation period in the intake plenum.

The THC trend of each strategy was similar for the DI and PFI strategies. PFI produced less THC but higher NOx emissions than DI operation due to higher combustion temperatures.

When comparing the different valve timing strategies, the lower NOx emissions at mid loads ER were related to the higher iEGR amount which led to the lowest combustion temperatures. Due to the early DI injection during the recompression phase, the vaporization process of the fuel reduced the iEGR temperature. This resulted in lower compression temperature prior to spark and consequent lower combustion temperatures. Thus, NVO DI operation produced less NOx emissions than the NVO PFI case.

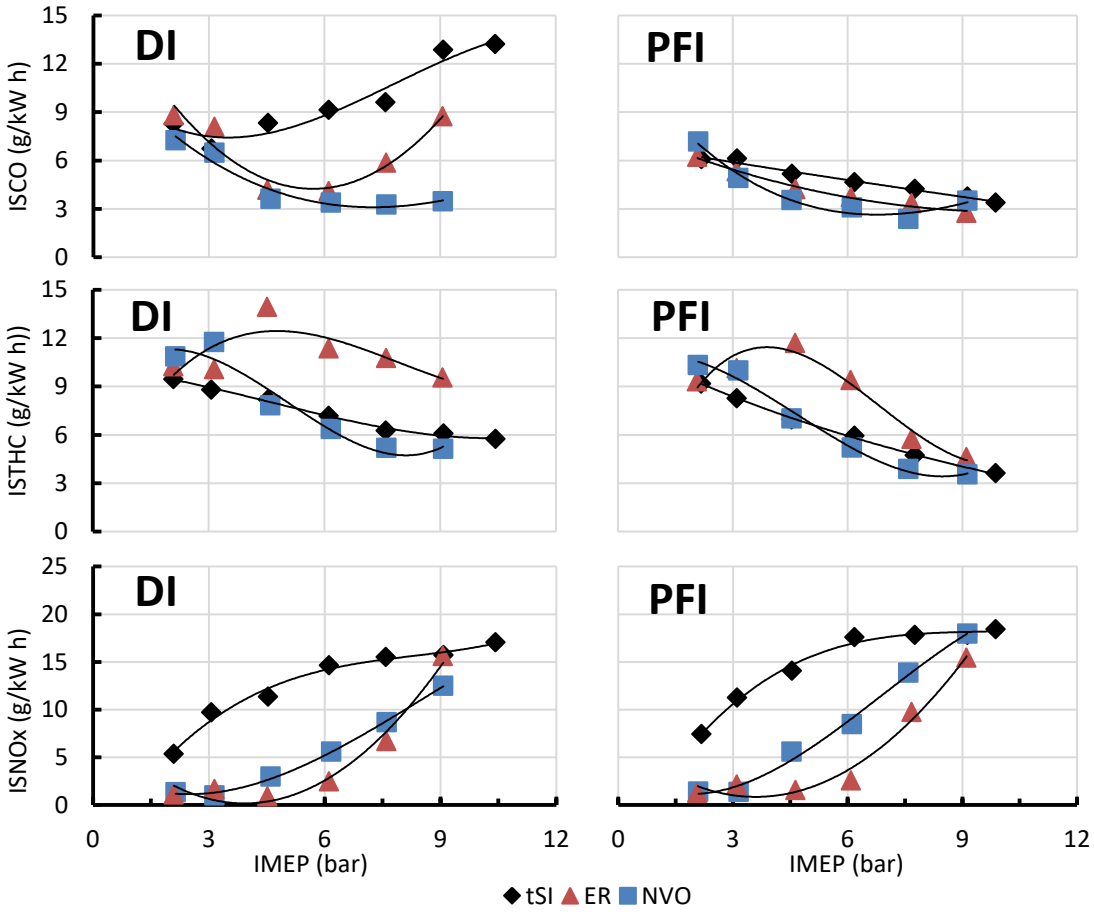

Figure 6.24. Engine-out emissions for different valve strategies and various loads. DI and PFI E100, 1500 rpm, MBT operation.

6.3.4. **Efficiencies**

The tSI throttling load control strategy had the lowest gas exchange efficiency. NVO and ER showed similar gas exchange efficiencies. At loads higher than 4 bar IMEP

loads, the restricted exhaust process caused by only one valve actuation reduced the ER gas exchange efficiency compared to NVO.

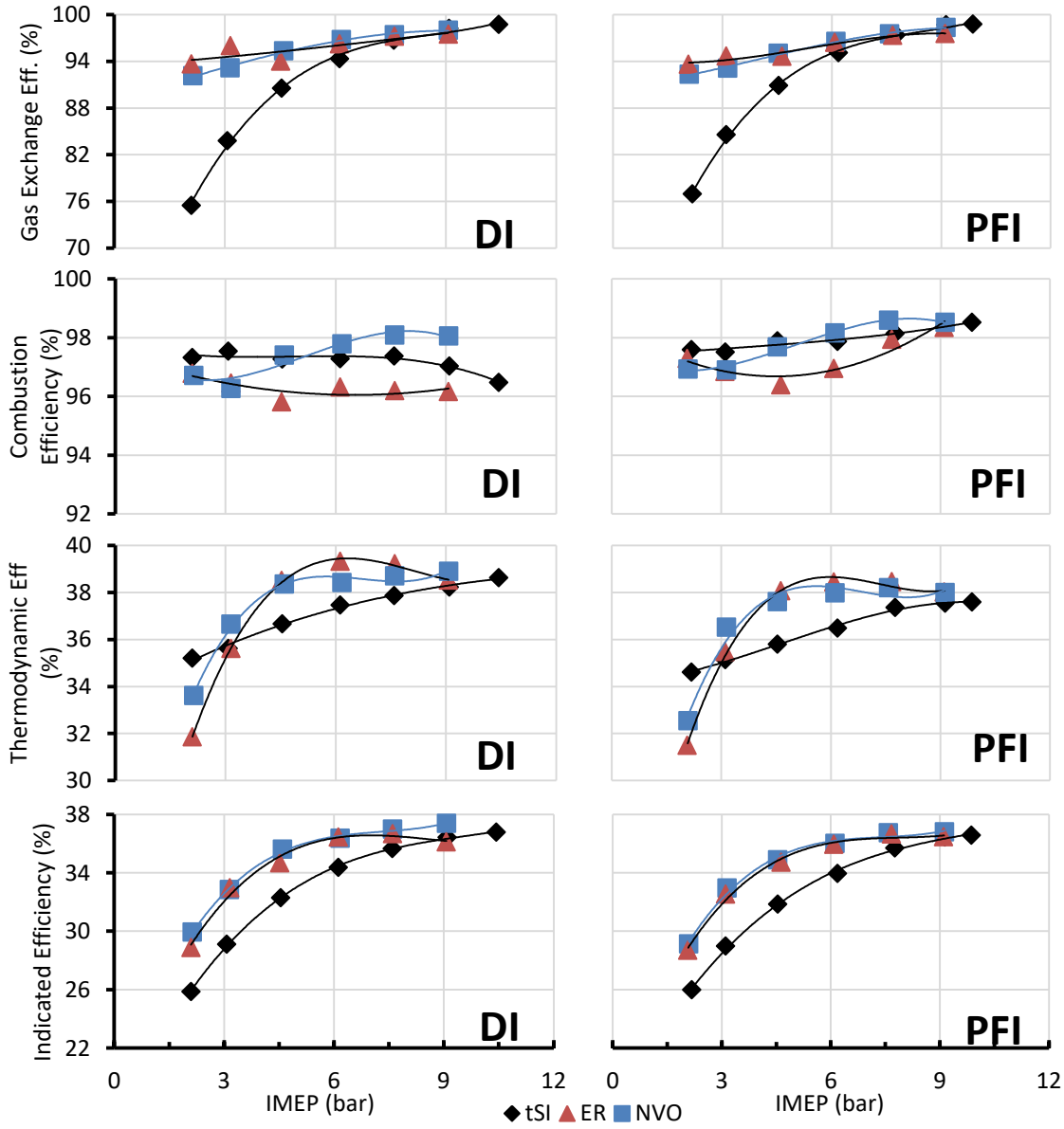

Figure 6.25. Efficiency related parameters for different valve strategies and various loads. DI and PFI E100, 1500 rpm, MBT operation.

The lower THC and CO emissions from the PFI strategy resulted in higher combustion efficiency than DI. Lower combustion efficiency occurred in the ER cases due to higher THC emissions. The lower THC emission led to higher combustion efficiency of the NVO operation than the tSI. At higher load, the increased CO emission was the main cause to the decreased combustion efficiency in tSI DI operation.

The ER strategy with SACI combustion process produced the best fuel conversion into work (thermodynamic efficiency) at part load. It could be explained by the lower in-cylinder heat transfer caused by lower combustion temperatures. As the load increased, the heat losses were also increased. Comparing DI and PFI, the DI cooling effect reduced in-cylinder temperatures, also reducing the in-cylinder heat losses.

Because the indicated efficiency is determined by the gas exchange efficiency, combustion efficiency and the thermodynamic efficiency, the low indicated efficiency of part load tSI operation can be explained by the low gas exchange efficiency and low thermodynamic efficiency. Even though their thermodynamic efficiency was not always the highest, the NVO operation exhibited higher efficiency for all the operating points because of the better trade-off amongst the three efficiencies. Finally, the DI operation produced higher indicated efficiency than PFI as a consequence of their higher thermodynamic efficiency.

6.4. Summary

The results presented in the chapter have shown that

(1) When using the NVO strategy, the injection during the recompression period provided a good charge mixing. For this reason, similar high combustion efficiency to the PFI injection cases was achieved;

(2) Better combustion process occurred when using NVO and ER strategies;

(3) The enhanced combustion process with SACI resulted in higher thermodynamic efficiency.

(4) The reduction in pumping work through inlet valve closing load control is of major importance to increase SI engine part load efficiency.

Therefore, NVO and ER valve strategies showed similar potential to considerably increase the engine efficiency of a naturally aspirated spark ignition engine operating at the stoichiometric air/fuel ratio. The main challenge to apply such valve timing strategies would be cost related due to the necessity of more complex valve train systems.

Chapter 7.

Gasoline, anhydrous and wet ethanol spark ignition operation with different valve strategies

7.1. Introduction

This chapter presents the comparative analyses of engine operations fuelled with gasoline (GRON95), anhydrous ethanol (E100) and wet ethanol (E85W15) using three different valve strategies. The valve strategies used in this chapter were based on the studies presented in the previous chapters, which were optimized for E100 operation. The conventional throttled SI valve strategy (tSI) was used as baseline comparison between the three fuels. The variable positive valve overlap with the intake valve phasing approach (PVOvar) was tested as it is commonly applied in production engines. The last valve strategy used for comparison was NVO due to its high potential to increasing combustion efficiency with low pumping losses. This may help to overcome the expected high THC emissions of wet ethanol operations, a problem found in the previous studies [164], [172], [177], [180], [182], [186], [189], [213], [214]. All tests were performed at 1500 rpm. DI and PFI methods were investigated for all three valve control strategies.

7.2. Throttled spark ignition (tSI) operation with different fuels and DI and PFI strategies

Throttle spark ignition (tSI) valve profile was characterized by fixed valve timing with almost zero valve overlap, EVO at -190 CAD $ATDC_{intake}$ and IVC at 200 CAD $ATDC_{intake}$. Load control was achieved by use of the throttle.

7.2.1. Effect of DI timing on tSI operation with E85W15

Different direct injection timings were tested for the 3.1 bar and 6.1 bar IMEP loads with E85W15. The first injection timing point was set at 28 CAD $ATDC_{intake}$. More advanced points were not tested in order not to wash the lubricant from the liner due to increased

water-in-ethanol content. The delay on injection timing resulted in the increase of combustion duration and more advanced spark timings were necessary. The combustion stability became worst due to increased charge cooling effect.

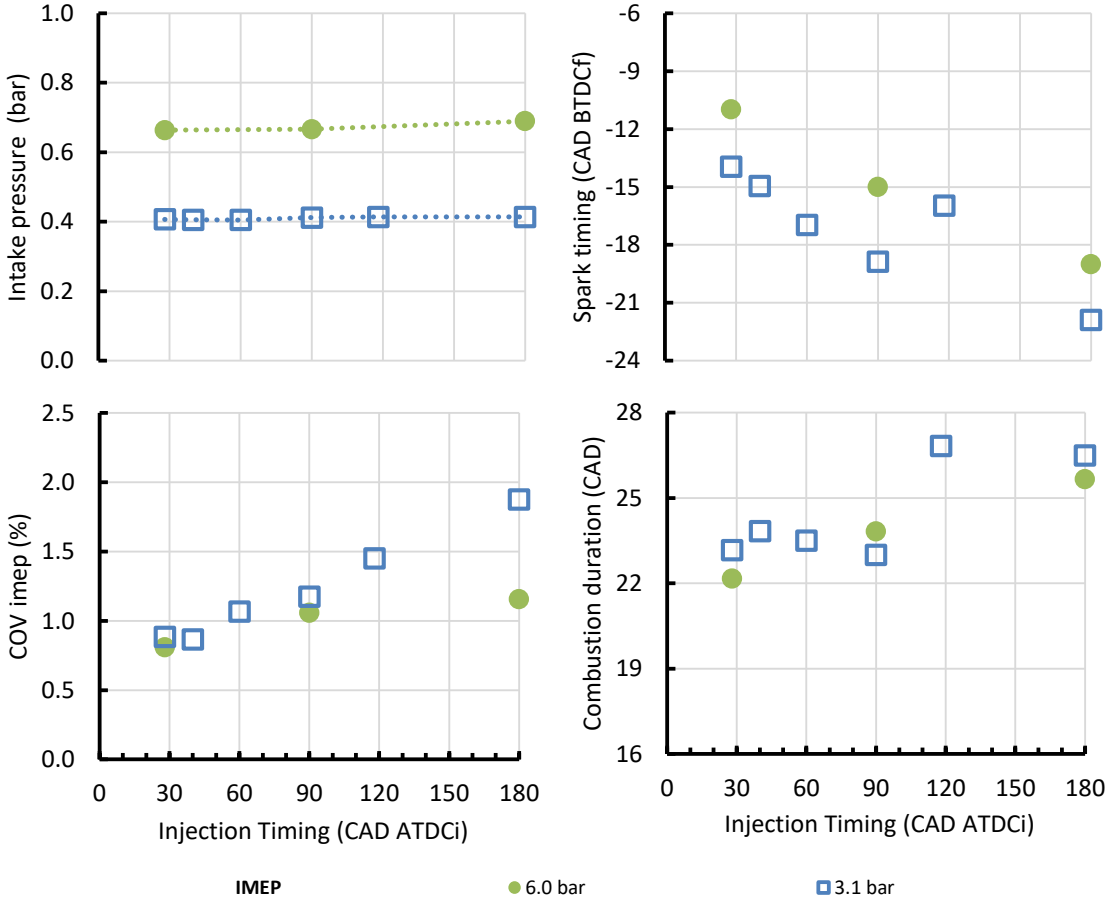

Figure 7.1. Effect of direct injection timing on intake pressure, spark timing, combustion duration and COV_{imep} of tSI operation E85W15, 1500 rpm, MBT operation.

In addition to the increased cyclic variability, which reduces indicated efficinecy, later injection highly increased CO and THC emissions. CO emissions shown no specific trend, and were dependent on in-cylinder flow to fuel spray interaction. For this reason,at later injection timing (120 CAD $ATDC_{intake}$) the CO emissions were lower than earlier injection timing. But even then, much higher than the initial injection timing at 28 CAD $ATDC_{intake.}$

There was an increase in THC emissions with the delayed injection timing for both loads. The higher the load, the more fuel was to be injected and vaporised, increasing the THC emissions.

NOx emissions initially decreased for more delayed injection timings as a consequence of higher charge cooling effect. For the more retarded injection timing the more advanced spark timing increased combustion temperatures. In addition, the poor charge homogeneity also contributed to increase NOx emissions.

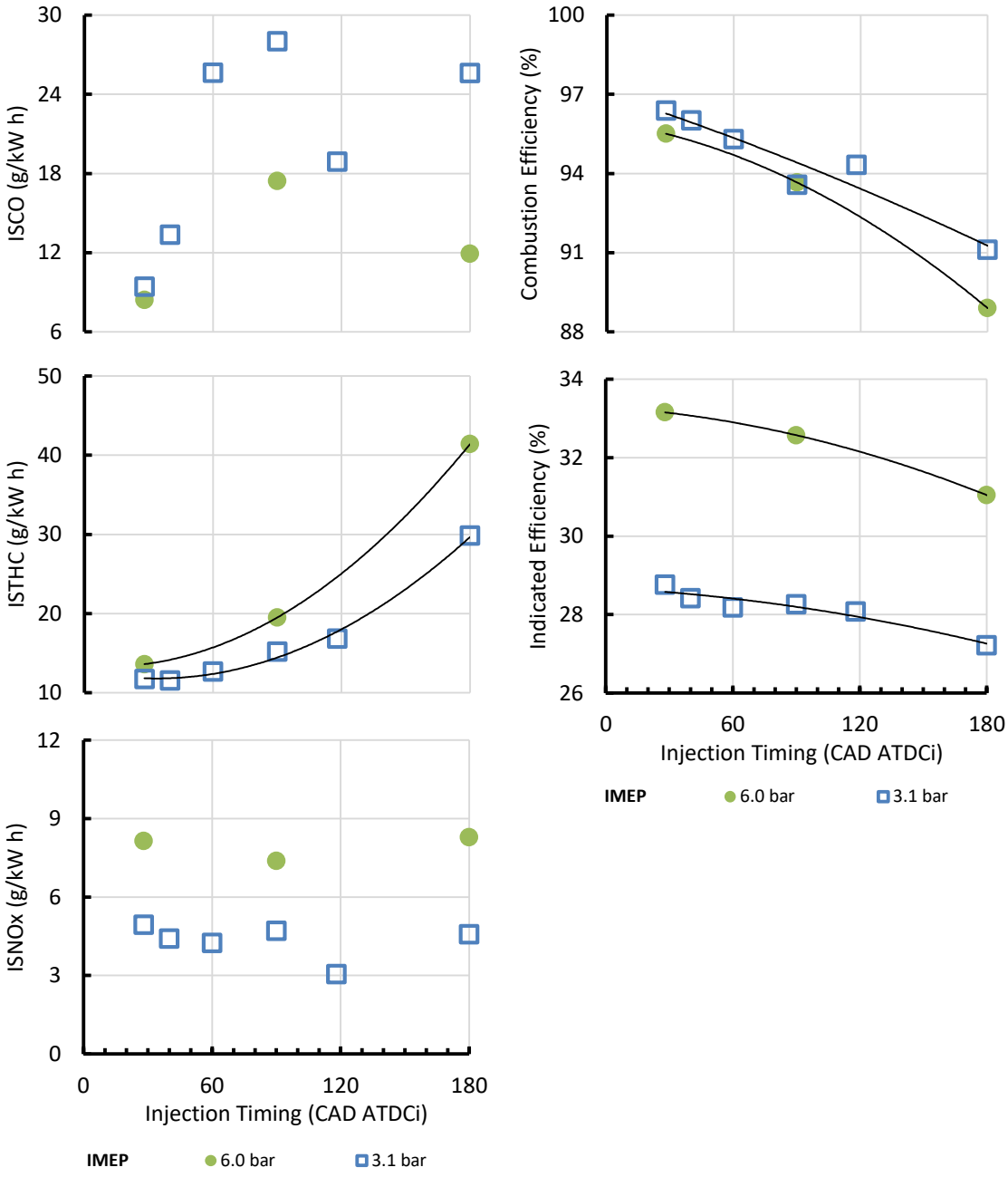

Figure 7.2. Effect of direct injection timing on engine out emissions and efficiency related parameters with E85W15, 1500 rpm, MBT operation.

Combustion efficiency rapidly decreased due to the poor charge mixing process. In order to maintain load constant, more fuel had to be injected. Thus, higher intake pressure was required for stoichiometric combustion. The net indicated efficiency was considerably reduced with the delayed injection timing mainly due to the reduced combustion efficiency.

The results showed that the injection timing at 28 CAD $ATDC_{intake}$ provided the best results in both engine out emissions and indicated efficiency, as it was found for E100. Thus, this DI timing was chosen for the subsequent PVOvar valve operations.

7.2.2. DI and PFI gasoline, E100 and E85W15 tSI operation comparison

7.2.2.1. Gas exchange related parameters

Intake pressure, pump mean effective pressure and gas exchange efficiencies of the three tested fuels and tSI valve strategy is presented in Figure 7.3. Two main effects were dominant for each injection strategy: intake port air displacement by fuel and in-cylinder cooling effect. Due to air displacement, the PFI operation tended to require slightly higher intake pressure compared to DI in order attain the same load. E85W15 PFI method displaced the larger air mass (due to higher fuel flow rate) requiring slightly higher intake pressure. On the other hand, the DI intake pressure presented null variation.

In general, E100 required the lower air flow rate for the same load as a consequence of higher indicated efficiency. Pumping work (PMEP) of E85W15 was the smallest for all loads with both injection methods. For the DI cases this could be attributed to higher in-cylinder mass, while for PFI cases it was also a consequence of higher intake pressure. As a result, E85W15 operation resulted in the highest gas exchange efficiency, more noticeable in the PFI low load cases.

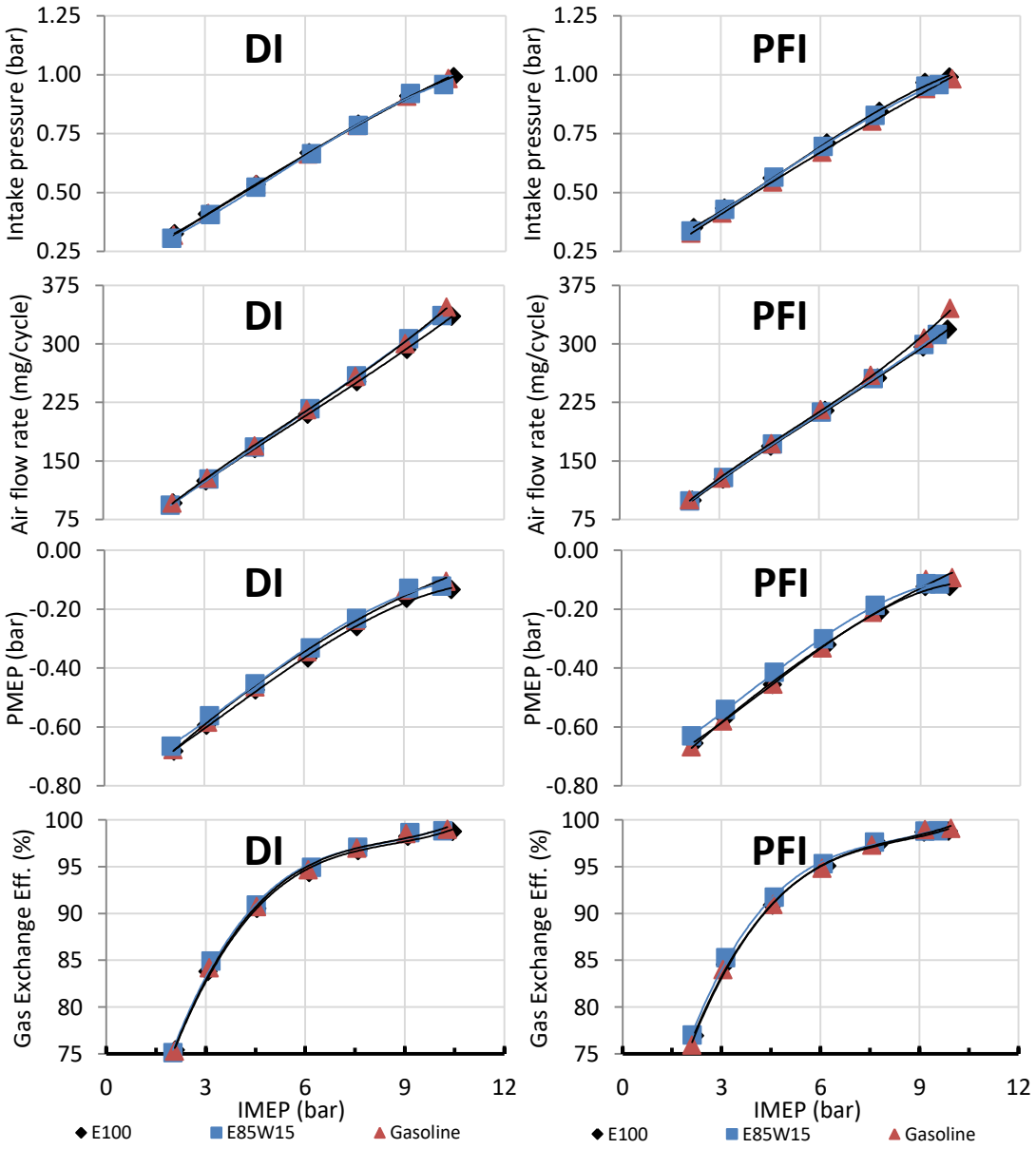

Figure 7.3. Gas exchange related parameters of tSI valve strategy and different fuels – DI and PFI operation. 1500 rpm, MBT operation.

7.2.2.2. Combustion related parameters

Figure 7.4 presents the main parameters related to combustion. MBT spark timing showed the same trend of less spark timing advance with load for all fuels and injection methods. E85W15 required the more advanced spark timing, especially for the DI cases, where the in-cylinder cooling effect was expected to decrease charge temperature prior to ignition. MBT could be attained for all tested points with E100 and E85W15. The centre of combustion (CA50) remained in the range 9 CAD ATDC ± 2 CAD. Gasoline WOT operation resulted in knock occurrence and required very retarded spark timing in order to not damage the engine and keep the pressure rise

rates at acceptable level. Heat release rate profiles at several interesting points are presented in Figure 7.5, and pressure related parameters and exhaust temperature are presented in Figure 7.6.

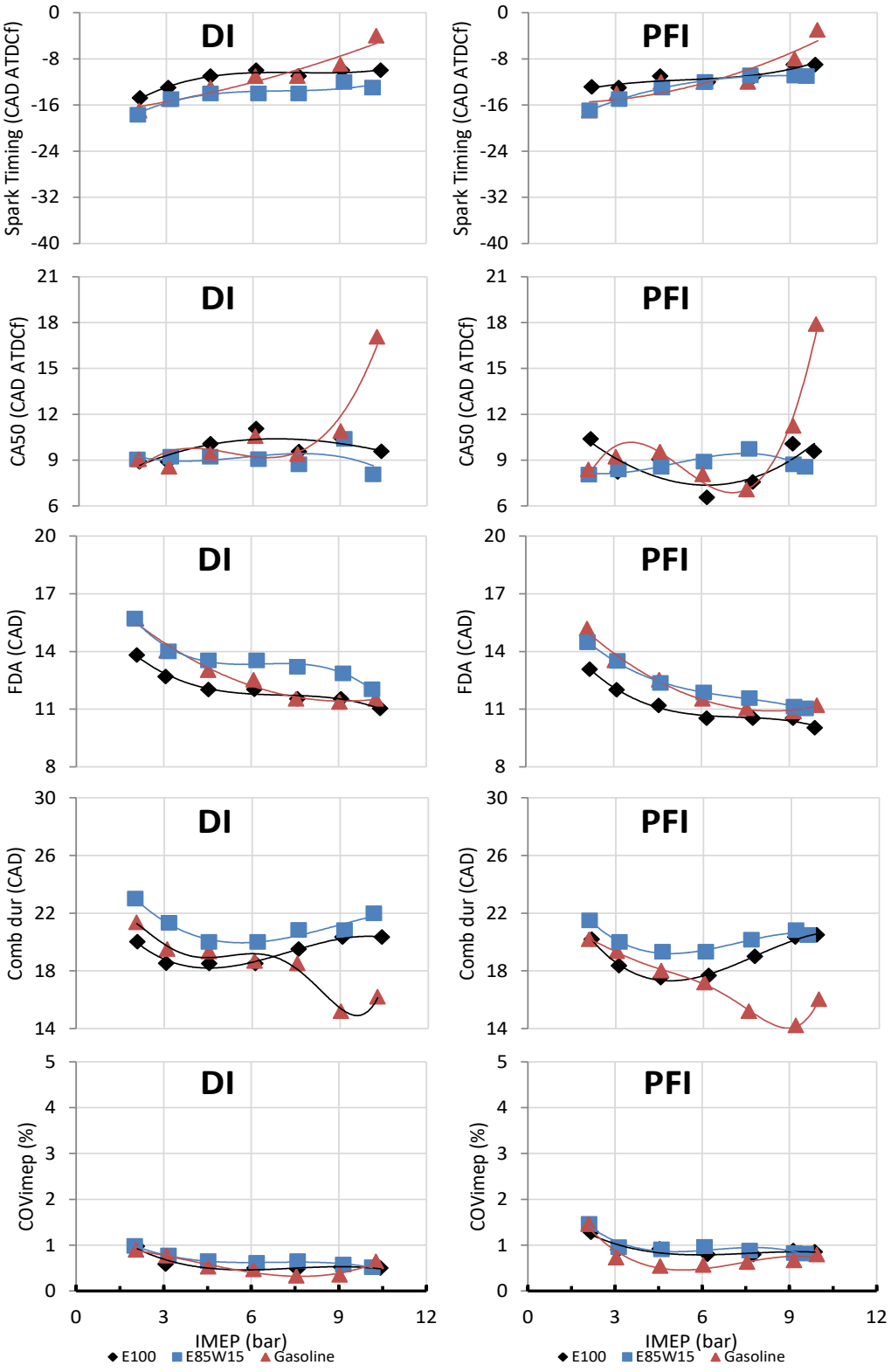

Figure 7.4. Combustion related parameters of tSI valve strategy and different fuels – DI and PFI operation. 1500 rpm, MBT operation.

The flame development angle (FAD) exhibited the same decreasing trend with the increased load for all fuels. At low load, ethanol had the smallest FDA. E85W15 had the longest FDA due to the higher charge heat capacity which decreased the combustion temperature. At high load operations, ethanol and gasoline had similar FDAs. Due to the DI in-cylinder cooling effect, FDA of DI cases tended to be higher.

The change in the main combustion duration with load for gasoline was different from alcohol based fuels. Gasoline combustion tended to become faster with the load, while alcohol fuels combustion initially decreased with load and then increased by 2 CAD to 3 CAD. As shown in the heat release rate profile plots, the heat release peak occurred around 10 CAD $ATDC_{fire}$ and the longer the combustion duration, the lower the heat release peak.

The heat release rate trace shown an increasing gradient after the maximum value for the case of gasoline operation at 7.5 bar IMEP load and PFI strategy, At this point, the dP/dCAD was about 2.5 bar/CAD but further spark timing advance resulted in audible knock and rapid rise in dP/dCAD. This effect was absent during the DI injection operation due to the charge cooling effect. Although at 9.0 bar IMEP load it was still possible to achieve CA50 combustion in the MBT range, light knock was already occurring and further spark advance would not be possible. The high heat release peak in the PFI case was accompanied by high combustion temperature and increased in-cylinder heat transfer, which would decrease engine fuel conversion to work (thermodynamic) efficiency.

For WOT operation it was impossible to achieve MBT spark timing due to heavy knock. Due to the retarded spark timing, peak cylinder pressure was reduced and its position was shifted away from the TDC decreasing the expansion work and overall engine efficiency. Nevertheless, stable operation could be achieved and very low combustion cyclic variability occurred.

E100 and E85W15 exhaust temperatures could be considered the same (considering experimental setup variability). Although E85W15 combustion temperatures were expected to be lower (almost the same peak in-cylinder pressure with higher in-cylinder trapped mass), the longer combustion duration reduced the burned gas expansion potential. Gasoline produced the highest exhaust gas temperature due to higher combustion temperature.

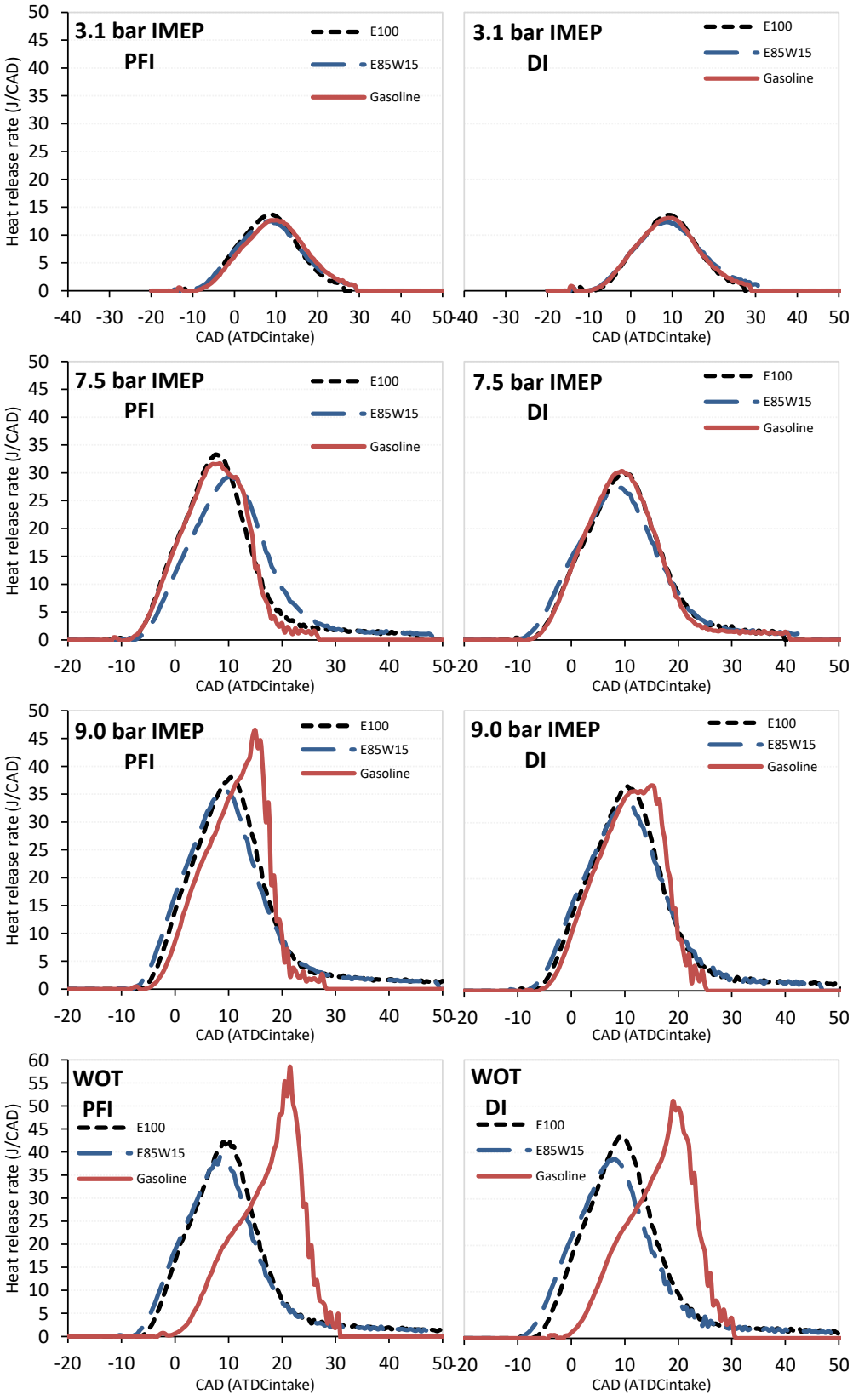

Figure 7.5. Heat release rates of tSI valve strategy and different fuels – DI and PFI operation. 1500 rpm, MBT operation.

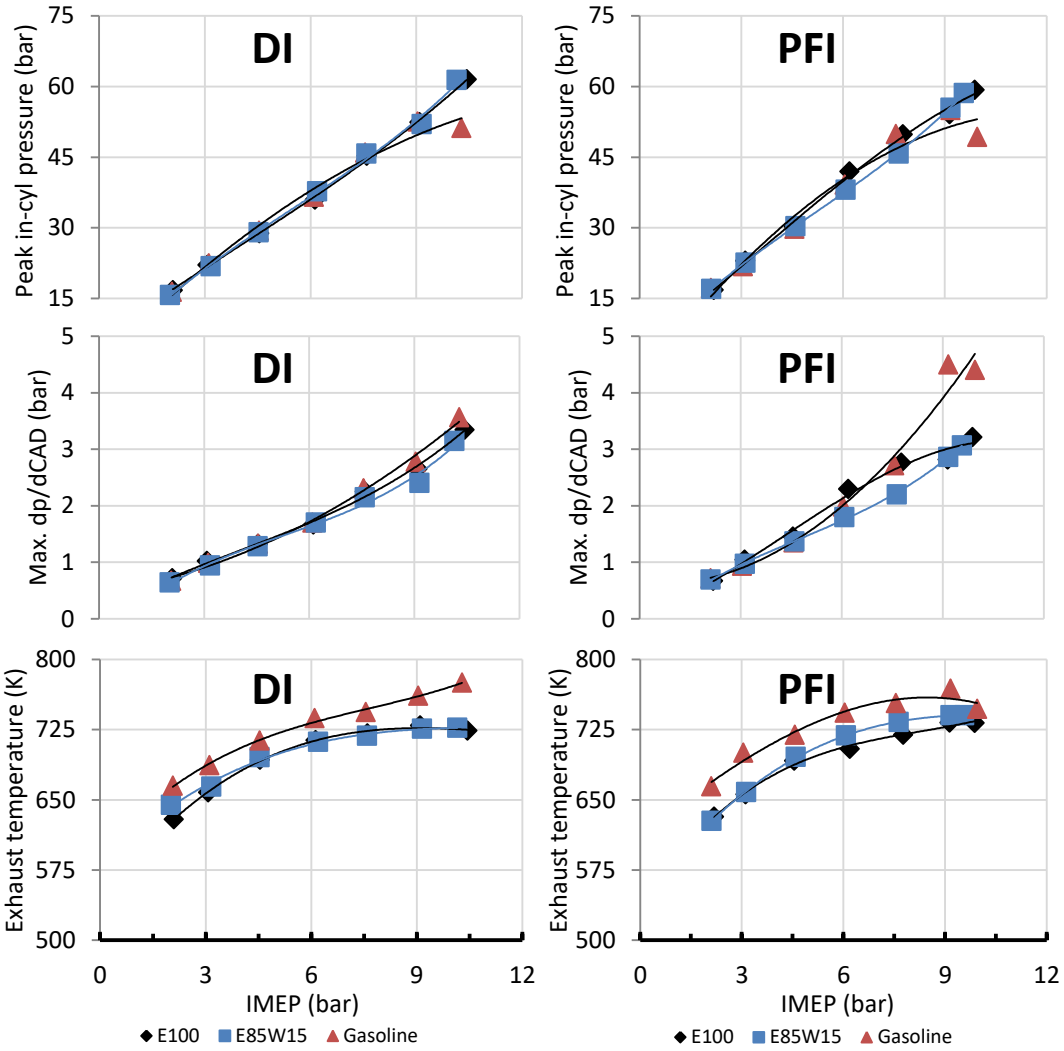

Figure 7.6. Peak in-cylinder pressure, maximum pressure rise rate and exhaust temperature of tSI valve strategy and different fuels – DI and PFI, 1500 rpm, MBT operation.

7.2.2.3. Gaseous emissions

Figure 7.7 presents the influence of properties of fuels and their injections on engine out emissions. In general, CO emissions with the DI method tended to be higher than PFI emissions. While similar CO emissions levels were achieved with E100 and E85W15, different emission trends were found for DI and PFI methods. CO tended to increase with the load for the DI method as consequence of worst in-cylinder homogeneity and charge cooling effect. On the other hand, CO emissions of the PFI cases tended to decrease with the load due to higher combustion temperature. Gasoline CO emissions were at the same level for both injection methods and decreased with the load

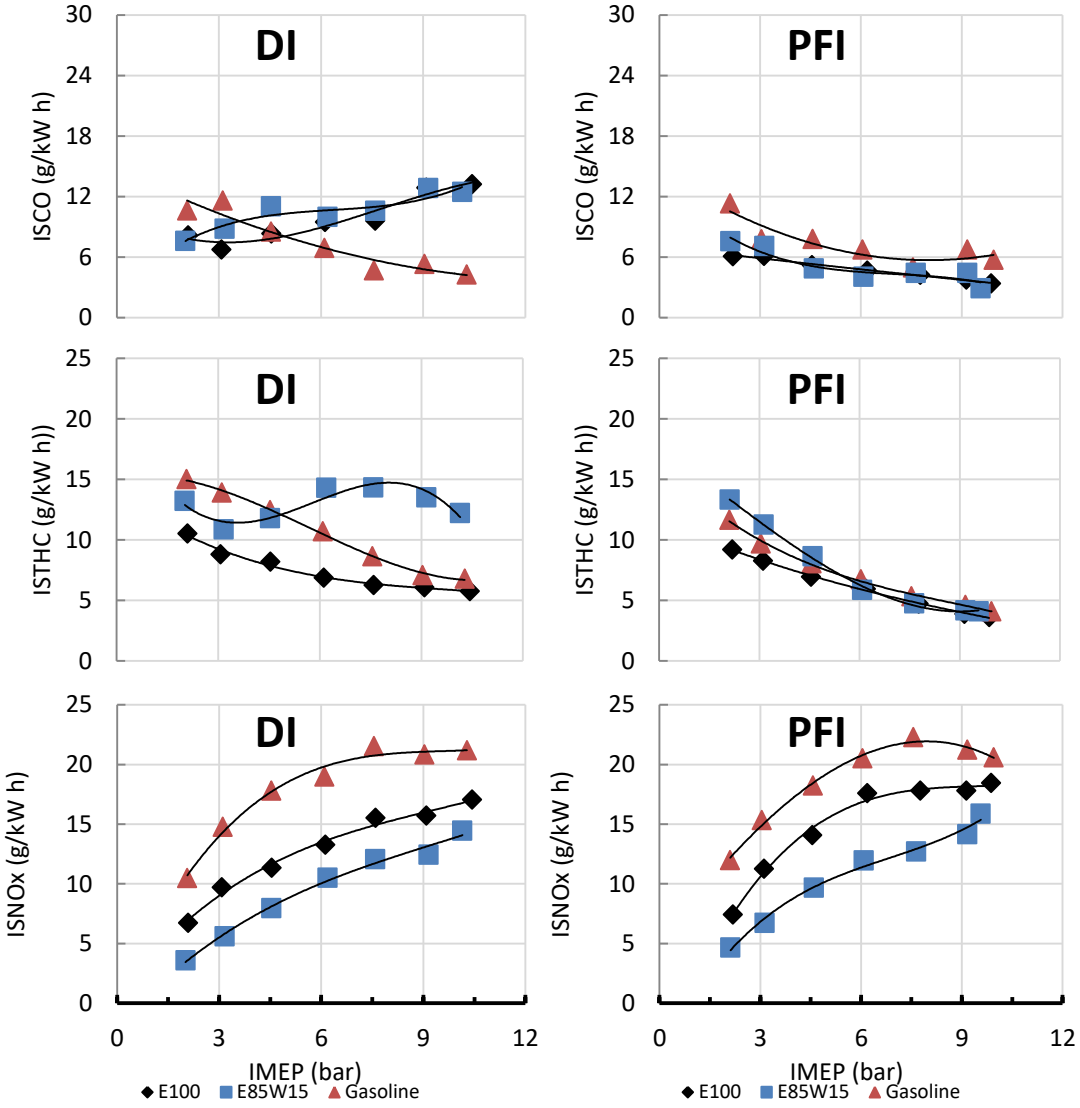

Figure 7.7. Engine out emissions of tSI valve strategy and different fuels – DI and PFI operation, 1500 rpm, MBT operation.

Regarding THC emissions, with the exception of E85W15 DI case, all other cases showed a reduction trend of THC emission with the increase in load. This occurred due to the influence of higher combustion temperature. The increased THC of the E85W15 DI case at higher loads could be a consequence of higher spray penetration and difficult fuel vaporization which resulted in fuel impingement. In general, THC levels of the PFI cases were lower than the DI due to higher combustion temperatures.

NOx emission levels were a direct indicative of the reduction in combustion temperature for the alcohol fuels. The higher heat of vaporization of the ethanol (840 kJ/kg) compared to gasoline (350 kJ/kg) considerably decreased charge temperature

prior to spark. The additional water content (with a latent heat of vaporization of 2250 kJ/kg) further decreased combustion temperatures resulting in NOx reduction around 50% when comparing gasoline to E85W15 at low loads and around 30% at high loads. DI cooling effect was responsible for lower DI NOx emissions than PFI.

7.2.3. **Efficiencies**

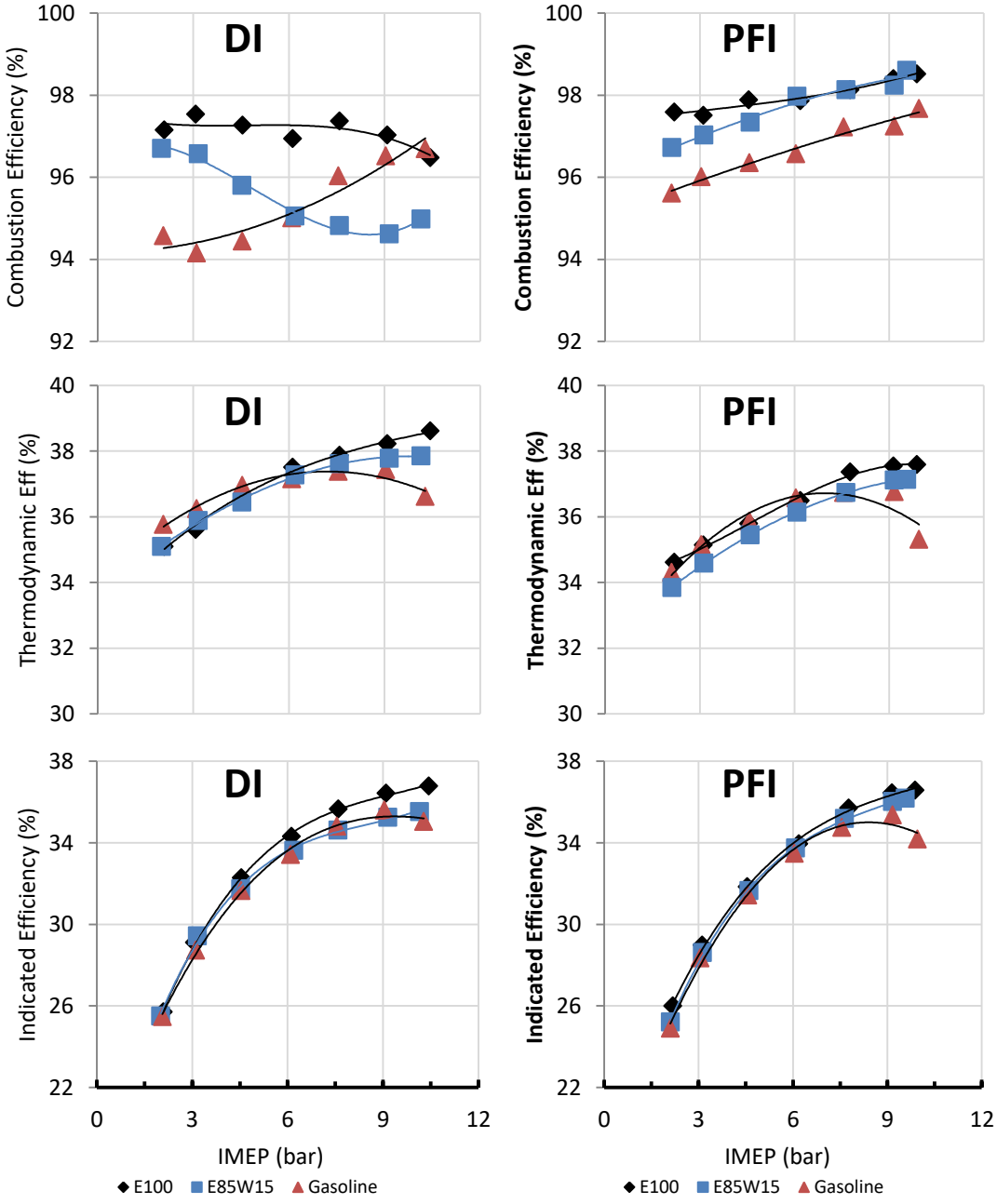

Figure 7.8. Efficiency related parameters of tSI valve strategy and different fuels – DI and PFI operation, 1500 rpm, MBT operation.

Combustion efficiency was a direct consequence of the THC and CO emissions. The lower PFI emission levels of THC and CO resulted in the highest combustion efficiency. E100 showed the best overall combustion efficiency of all tested fuels, while gasoline was the worst.

The higher combustion temperature would lead to higher heat loss to the coolant and hence the lower thermodynamic efficiency, which may explain the higher thermodynamic efficiency of DI than the PFI cases. Because of their retarded spark timings to avoid knocking combustion, the gasoline operations had noticeable lower thermodynamic and overall engine efficiency.

As a general trend for both fuel injection methods and different tested fuels, the increase on engine indicated efficiency with the load for tSI valve strategy was a direct result of lower pumping losses caused by throttle load control method. The slight differences between each fuel were a consequence of the thermodynamic and combustion efficiencies in a higher level than gas exchange efficiency. E100 presented the highest indicated efficiencies for all loads due to the higher thermodynamic and combustion efficiencies. Gasoline and E85W15 presented the same efficiency levels at part load. At 9.0 bar IMEP and WOT, gasoline indicated efficiency was limited by knock which directly affected combustion phasing and decreased thermodynamic efficiency.

7.3. Variable positive valve overlap (PVOv) operation with different fuels and DI and PFI strategies

Positive valve overlap strategy using the intake phasing approach was tested in order to access the effects of wet ethanol in production engines with variable valve timing (VVT) devices. Direct injection timing was set to 28 CAD $ATDC_{intake}$ and port fuel injection timing was set to the TDC_f. Stoichiometric air to fuel ratio was used.

7.3.1. Gas exchange related parameters

E100 results are the same presented on 4.2.2. The intake valve phasing used for both E85W15 was based on these optimized points, with slight modifications when necessary. Exhaust valve opening and closure angles were kept constant (EVO at -

191±2 CAD $ATDC_{intake}$ and EVC at 20±2 CAD $ATDC_{intake}$). Intake duration was kept constant at 230±2 CAD, and the whole valve profile was phased towards the $BDC_{exhaust}$ in order to promote burned gas backflow to the intake ports. As previously explained, the optimal IVO was found to be dependent on load, as the consequent RGF directly impair the combustion stability. Appendix 3 presents the valve timing parameters used in each test point.

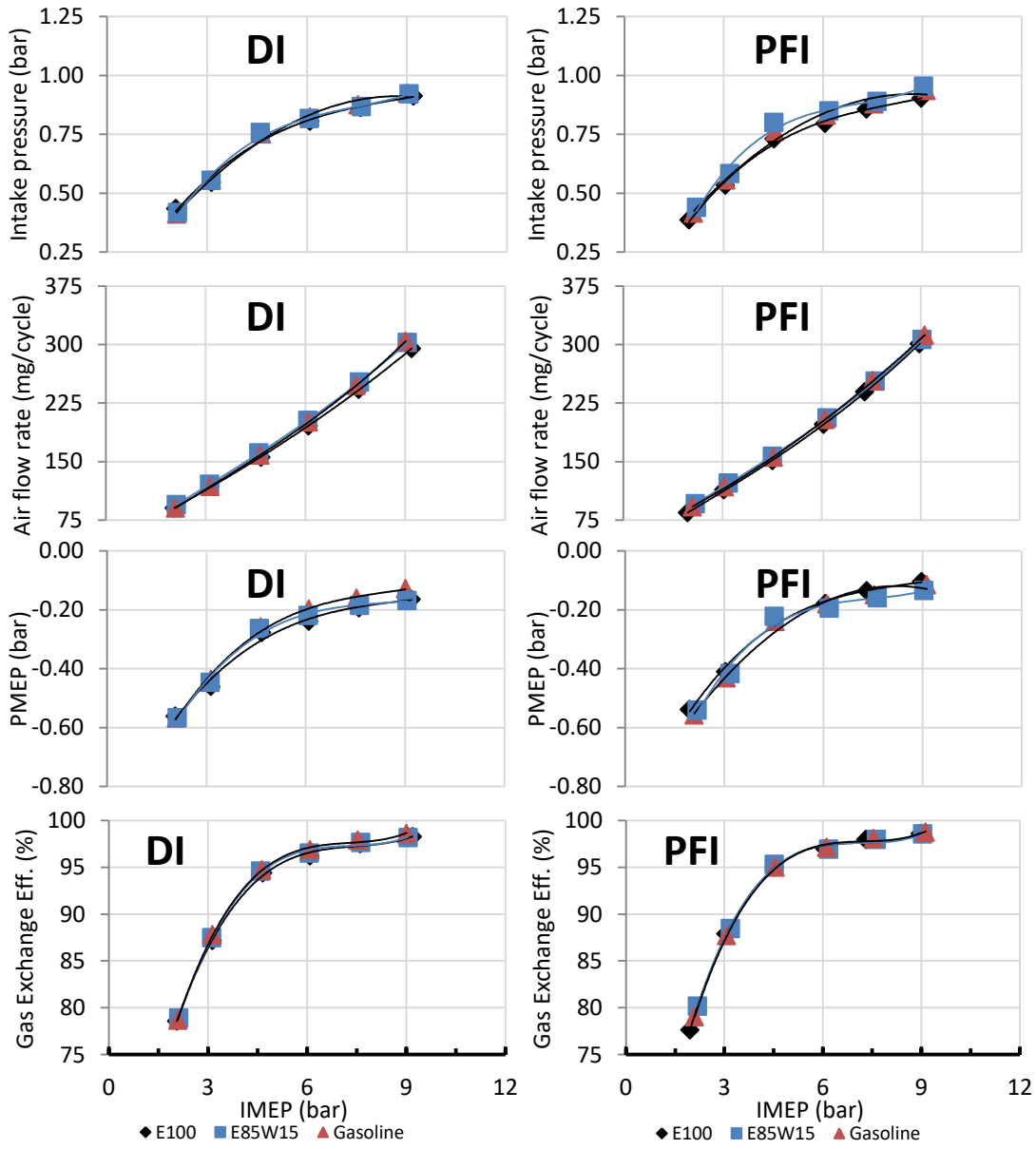

Figure 7.9. Gas exchange parameters of PVOvar valve strategy and different fuels – DI and PFI operation, 1500 rpm, MBT operation.

Compared to the E100 DI baseline, two different valve timings were used for E85W15. For the 9.0 bar IMEP with E85W15 PFI operation, the higher intake pressure increased

the in-cylinder scavenging when using IVO at -45 CAD $ATDC_{intake}$. This resulted in some charge short circuiting which increased the THC emissions. In order to get rid of this problem, IVO was delayed to -10 CAD $ATDC_{intake}$. For the other load cases, the IVO was delayed by 5 CAD in order to reduce burned gas backflow to the intake ports. This reduced RGF and improved combustion stability. As shown in the section “4.2.2. Optimized intake profile phasing for high efficiency E100 SI throttled operation”, PVO durations between 50 and 80 CAD, with IVO around -40 and -60 CAD $ATDC_{intake}$ provided almost the same indicated efficiency potential for medium and high part load engine operation.

Figure 7.9 presents the gas exchange related parameters of the tested points. As occurred in the previous tSI tests, E85W15 required the highest intake pressure for both DI and PFI strategies due to the higher in-cylinder mass trapped. The variation in the air flow rate for the DI cases was more evident than in the PFI cases due to larger efficiency. In general, PMEP variations and hence the change in gas exchange efficiencies were very small.

7.3.1. **Combustion related parameters**

Figure 7.10 presents the spark timing, centre of combustion, flame development and combustion duration, and COV_{imep} data of the tested points. The MBT spark timings were more advanced for the E85W15 DI than E100 and gasoline due to the higher charge cooling effect of the ethanol-water mixture.

Centre of combustion (CA50%) for MBT operation was kept in the range of 9±2 CAD $ATDC_f$. For gasoline low load cases, slightly more advanced combustion phasing was necessary in order to promote more stable combustion.

In general, E100 presented the faster flame development process. At 2.0 bar IMEP the FDA was increased in the DI case because of the increased residual gas fraction due to the larger PVO. Considering that the latent heat of vaporization of E100 is more than twice of the gasoline, the similar FDA represents that ethanol flame development process was faster. This is further evidenced by the FDA plot for PFI operations, where E100 FDA was much faster than gasoline when the charge cooling effect was absent. The effect of elevated water-in-ethanol content combined to the residual gases contributed to reduce fuel reactivity and increase both FDA duration and main combustion phase (10-90% mass fraction burn) duration of E85W15 operations.

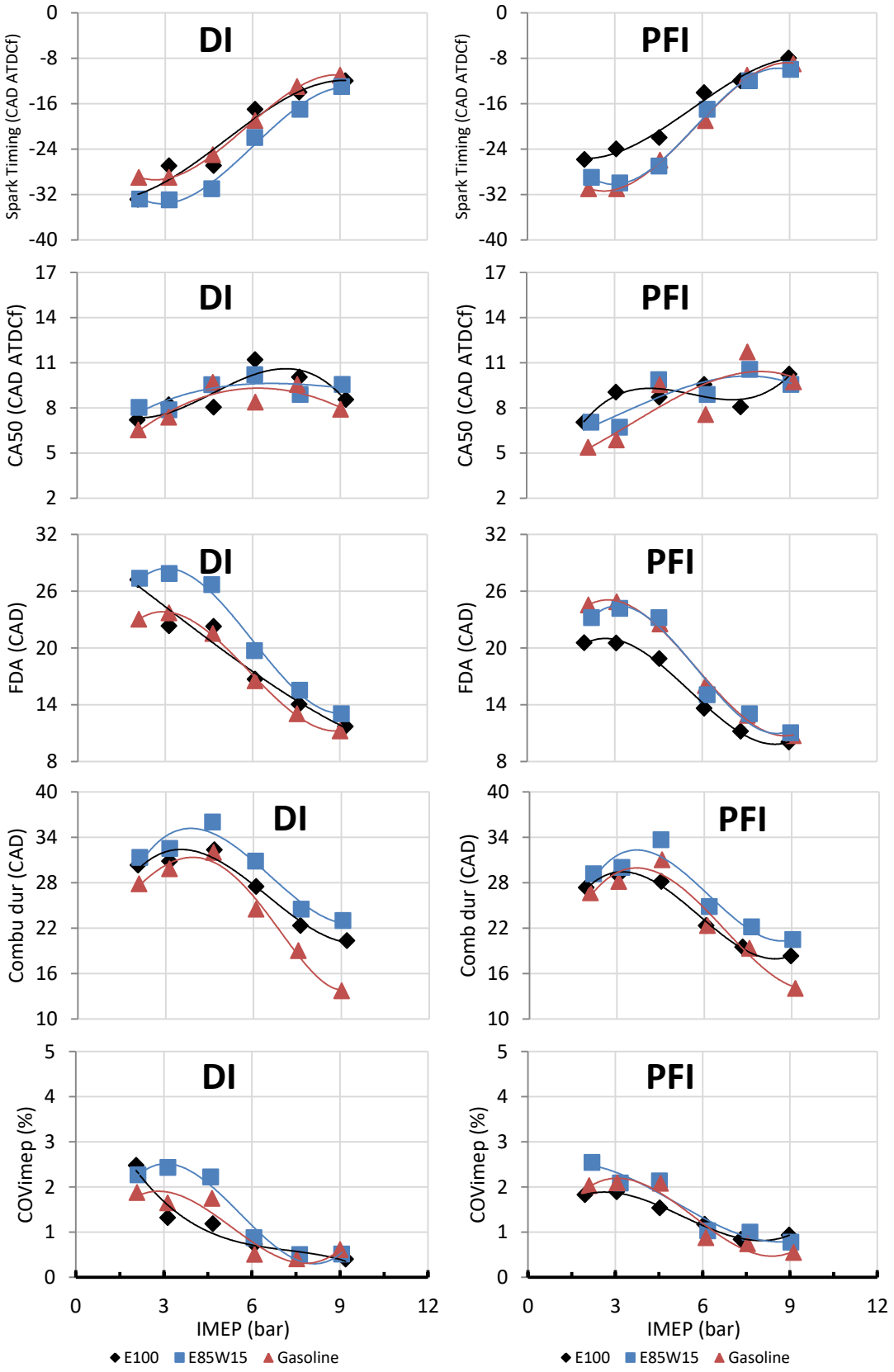

Figure 7.10. Combustion related parameters of PVOvar valve strategy and different fuels – DI and PFI operation, 1500 rpm, MBT operation.

The fast decrease in gasoline combustion duration for both PFI and DI strategies could be attributed to end gas auto-ignition occurrence in the form of SACI combustion. For both PFI and DI, the 9.0 bar gasoline operation was on the borderline knock, which means that any further spark advance would result in knock occurrence and maximum rates of pressure rise (MRPR) above 5 bar/CAD. Figure 7.10 shows the effect of spark timing on gasoline combustion mode transition at 3 loads. presents in-cylinder pressure related parameters and exhaust temperature for the different fuels and injection methods.

A strong dependence between the spark timing and the end gas auto-ignition could be noticed in Figure 7.10 for the gasoline operation. Due to the lower octane number of gasoline compared to ethanol, gasoline was more prone to auto-ignition. The end gas auto-ignition resulted in a more pronounced change in the in-cylinder pressure trace as shown by the start of the second peak on the heat release rate in Figure 7.11. The fast burning of the end gas during promoted an abrupt increase on the heat release which contributed to decrease combustion duration. Also, the end of combustion (post oxidation reactions in the end of the heat release process) was highly reduced after end gas auto-ignition took place. The impact of DI cooling effect on the control of the end gas auto-ignition process is illustrated on the 6.1 bar plots in Figure 7.11. For the same spark timing, DI HRR shown lower peak and longer combustion process than PFI. PFI end-gas auto ignition started for the -19 CAD $ATDC_f$ spark timing, while for DI operation this occurred only for the more advanced spark timing. The same behaviour was observed for all other higher loads. DI cooling effect at 9 bar IMEP load (where maximum spark advance was limited by knock in the PFI operation) enabled 2 CAD spark timing advance.

On the other hand, ethanol fuels didn’t present SACI combustion at MBT at any load. The effect of different fuels on HRR is presented in Figure 7.13. For this reason, MRPR was well below the maximum admissible value of 5 bar/CAD. Ethanol fuels presented lower HRR when compared to gasoline. Comparing wet ethanol and anhydrous ethanol, for each injection strategy, one of the fuels presented a higher HRR peak trend. In the DI cases the higher cooling effect of wet ethanol decreased the combustion rates and increased the combustion duration, reducing the HRR peak. On the other hand, the more spark advance of the PFI E85W15 cases led to higher HRR than E100. In general, gasoline HRR peak value was always higher than that of ethanol fuels for both injection strategies.

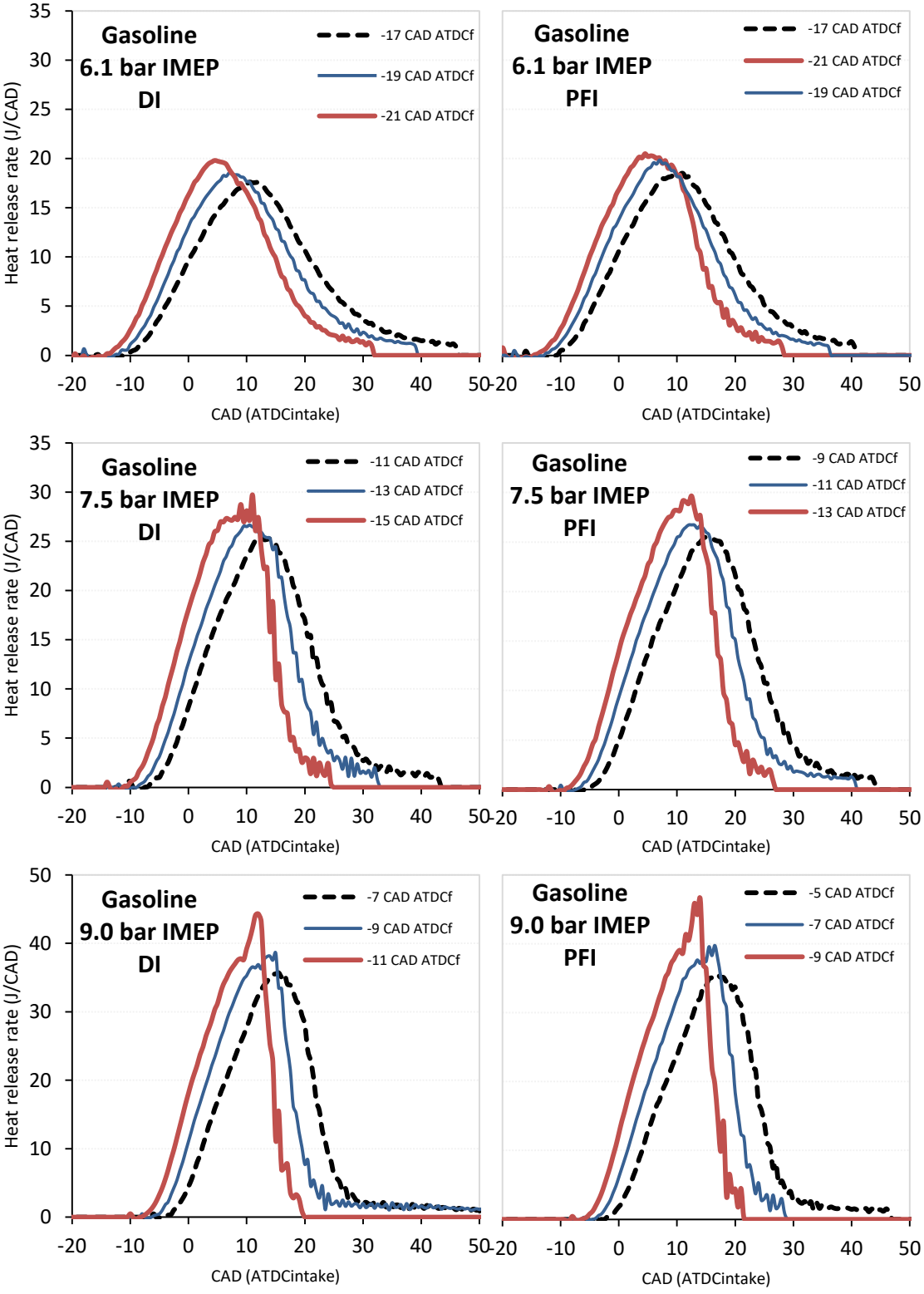

Figure 7.11. Effect of spark timing on combustion mode transition from SI to SACI for different loads and injection methods with gasoline and PVOvar valve strategy, 1500 rpm, MBT operation.

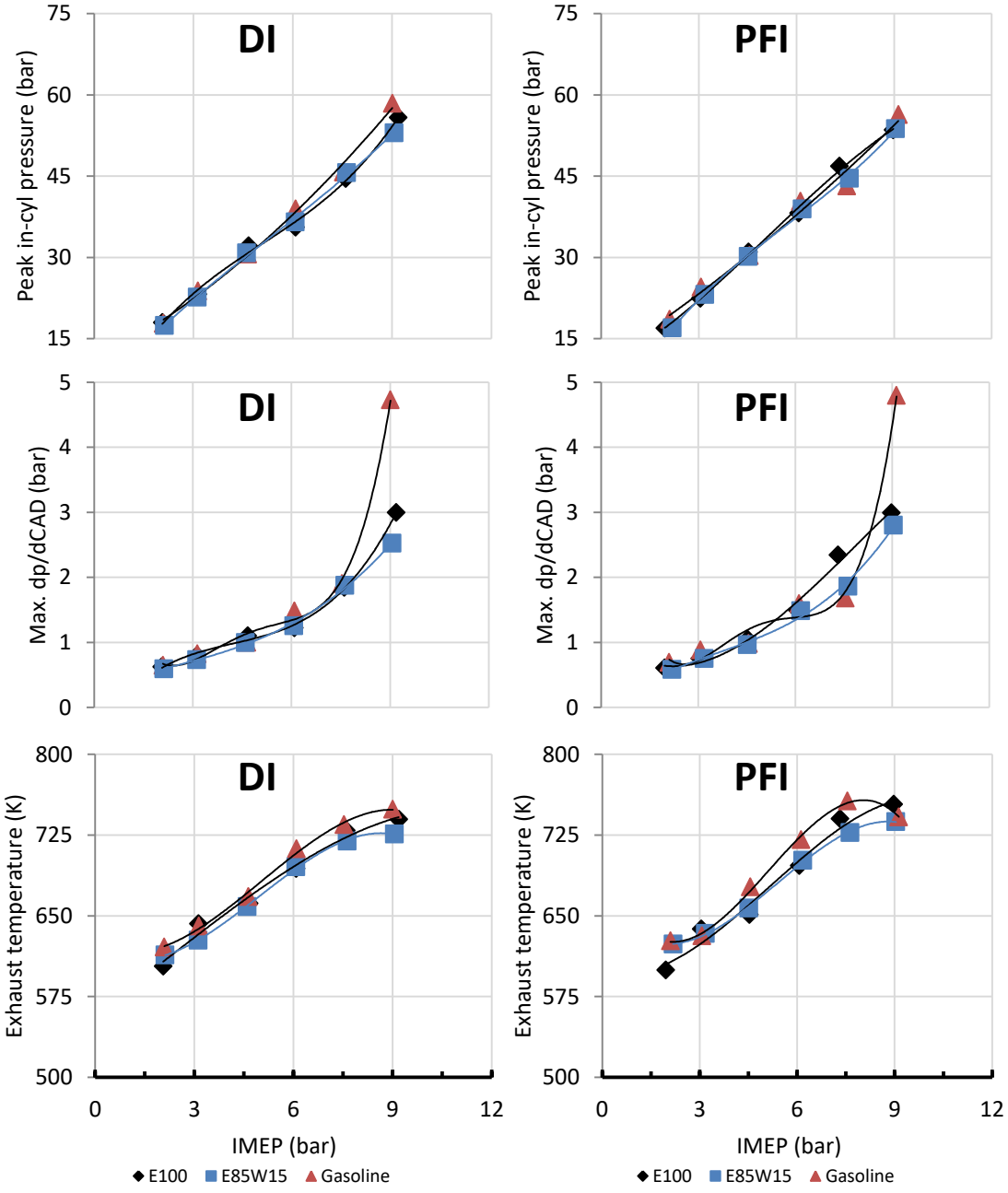

Figure 7.12. In-cylinder pressure and maximum rate of pressure rise, and exhaust gas temperature of PVOvar valve strategy and different fuels – DI and PFI operation, 1500 rpm, MBT operation.

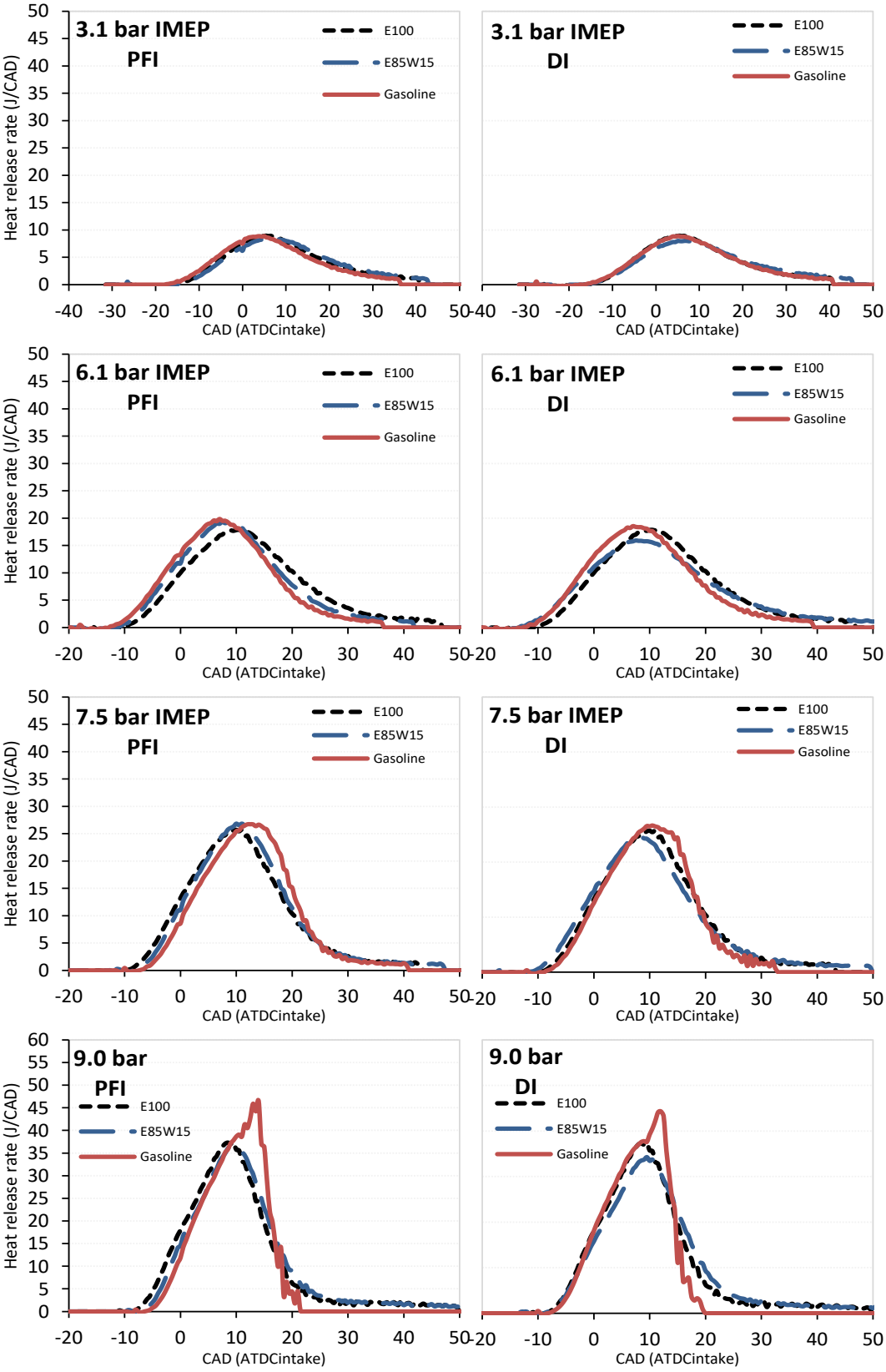

Figure 7.13. Effect of fuel on HRR at different loads for DI and PFI methods with PVOvar valve timing strategy, 1500 rpm, MBT operation.

Regarding the exhaust temperature, ethanol fuels presented very similar values for all load ranges, except for the lowest load case, where valve timing was slightly different. Because of the water content dilution effect in wet ethanol, the combustion duration was extended and combustion temperature lowered, with exhaust temperature little affected by the water content. Gasoline exhaust gas temperatures were in general higher due to higher temperature combustion process.

The valve timings and hence the RGF was found to have similar effect for all the cases. The small variation in the peak cylinder pressure was more affected by the spark timing than the fuel.

7.3.2. **Exhaust emissions**

Engine out exhaust emissions for the PVOvar valve strategy are provided in Figure 7.14. Carbon monoxide emissions exhibited different trends for each fuel and injection methods. With gasoline, CO emissions were higher in DI than in the PFI case, due to mixture inhomogeneity created by the direct injection. In comparison, CO emissions were reduced by the direct injection of anhydrous and wet ethanol than the premixed port fuel injection. In the case of ethanol fuels the charge cooling effect was much more pronounced both due to higher injected mass per cycle as well the higher latent heat of vaporization. For this reason, combustion of ethanol produced higher THC emissions than that of gasoline. As the combustion temperature was increased with load, the THC decreased until about 7.5 bar IMEP, above which THC started to rise as the injection duration was significantly extended producing more local rich mixture zones.

The relationship between DI injection cooling effect and combustion temperature was directly translated to the NOx emissions. Because of the residual gas backflow process during the early intake opening period, the charge cooling effect of ethanol PFI had much less effect on the charge temperature and hence the NOx emissions. For this reason, at higher loads, PFI gasoline and E100 resulted in very similar NOx emissions. On the other hand, the more diluted charge caused by the water addition of the E85W15 case resulted in the lowest NOx emissions in all cases. Direct injection of E100 provided considerable NOx emissions reduction compared to the PFI case.

For loads up to 4.5 bar IMEP, DI injection of E85W15 and E100 produced NOx emissions lower than 0.5 g/kWh. DI gasoline NOx emissions were at least 4 times higher than those of E85W15 for loads up to 6.1 bar IMEP. For PFI operation, gasoline

NOx emissions were at least three times higher than those of wet ethanol for loads up to 4.5 bar IMEP.

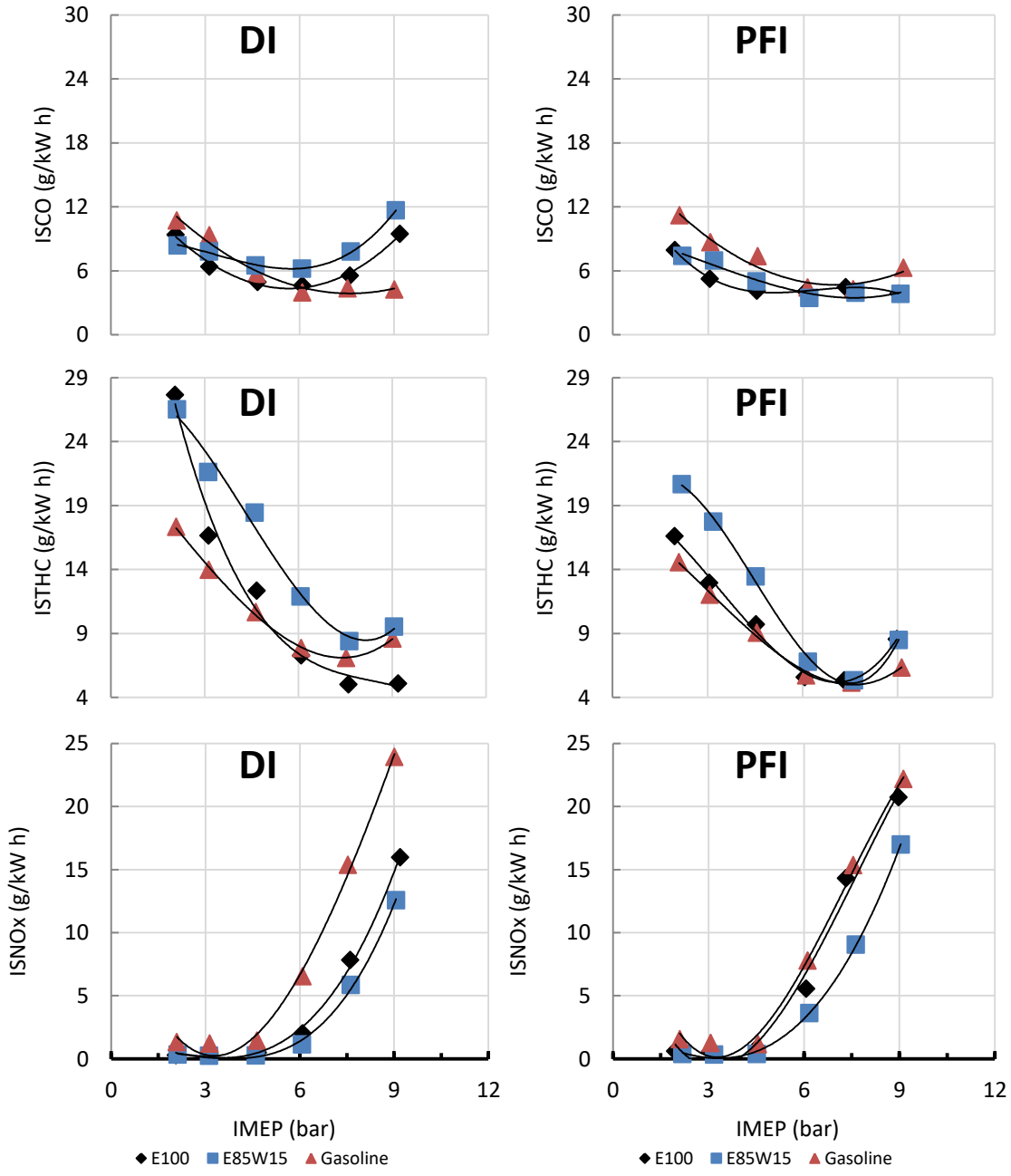

Figure 7.14. Engine out emissions of PVOvar valve strategy and different fuels – DI and PFI operation, 1500 rpm, MBT operation.

7.3.3. **Efficiencies**

The analyses of efficiency related parameters are shown in Figure 7.15. E100 produced the highest combustion efficiency of all tested fuels for the great majority of scenarios although the E100 THC emissions and CO emissions were not the lowest. The comparison between combustion efficiency of alcohol fuels and gasoline is not straight forward from the emissions data as different LHV of each fuel determine the unburned hydrocarbons share on the combustion efficiency. Thus, as gasoline LHV is around 40% higher than ethanol's, gasoline THC emissions affected more its combustion efficiency. In general, the reduction in CO and THC emissions with load was responsible for the increase in combustion efficiency until 7.5bar IMEP, above which the combustion efficiency became lower due to extended fuel injection durations.

Wet ethanol had lower combustion efficiency than E100 due to the more diluted charge with higher water content and the lowest combustion temperature. For the PFI operation and higher loads, E85W15 presented very similar levels to E100 because of the lower influence of its latent heat of vaporization for charge cooling due to the charge preparation process of the PVOvar with burned gas backflow to the intake ports. Comparing wet ethanol to gasoline, similar levels were found for DI operation and low load PFI. At higher loads and PFI operation E85W15 presented better combustion efficiency.

Thermodynamic efficiency is related to the combustion process and the subsequent conversion of heat into mechanical work. The faster combustion at lower combustion temperature of E100 DI produced the highest overall thermodynamic efficiency In the case of wet ethanol, the lower thermodynamic efficiency was linked to the longer combustion duration. Whilst the lower thermodynamic efficiency of gasoline could be explained by the increased heat losses of higher combustion temperature at part-load and the more retarded spark timing at higher load.

Regarding the initial rise and then fall in the thermodynamic efficiency, this can be attributed to several factors, especially the amount of RGF. At the lowest loads, the very long combustion duration was not very efficient at converting fuel energy into work. But as the combustion duration decreased, the engine became more efficient. For gasoline and E100, the best trade-off between the combustion duration and heat transfer occurred at 4.5 bar IMEP due to a very diluted charge (RGF). For wet ethanol, this occurred at 6.1 bar IMEP as the combustion temperature was not enough to achieve complete combustion at 4.5 bar IMEP. For all fuels, after such point, the increased combustion temperature tended to increase in-cylinder heat losses which

decreased the thermodynamic efficiency. Due to the more pronounced DI cooling effect of E100 and E85W15, the combustion temperature reduction resulted in lower heat losses. On the other hand, the high gasoline combustion temperature at high loads considerable decreased thermodynamic efficiency. Comparing DI and PFI operation, combustion temperature was the main factor to reduce PFI thermodynamic efficiency compared to DI. The lack charge cooling effect highly increased the heat losses at higher loads.

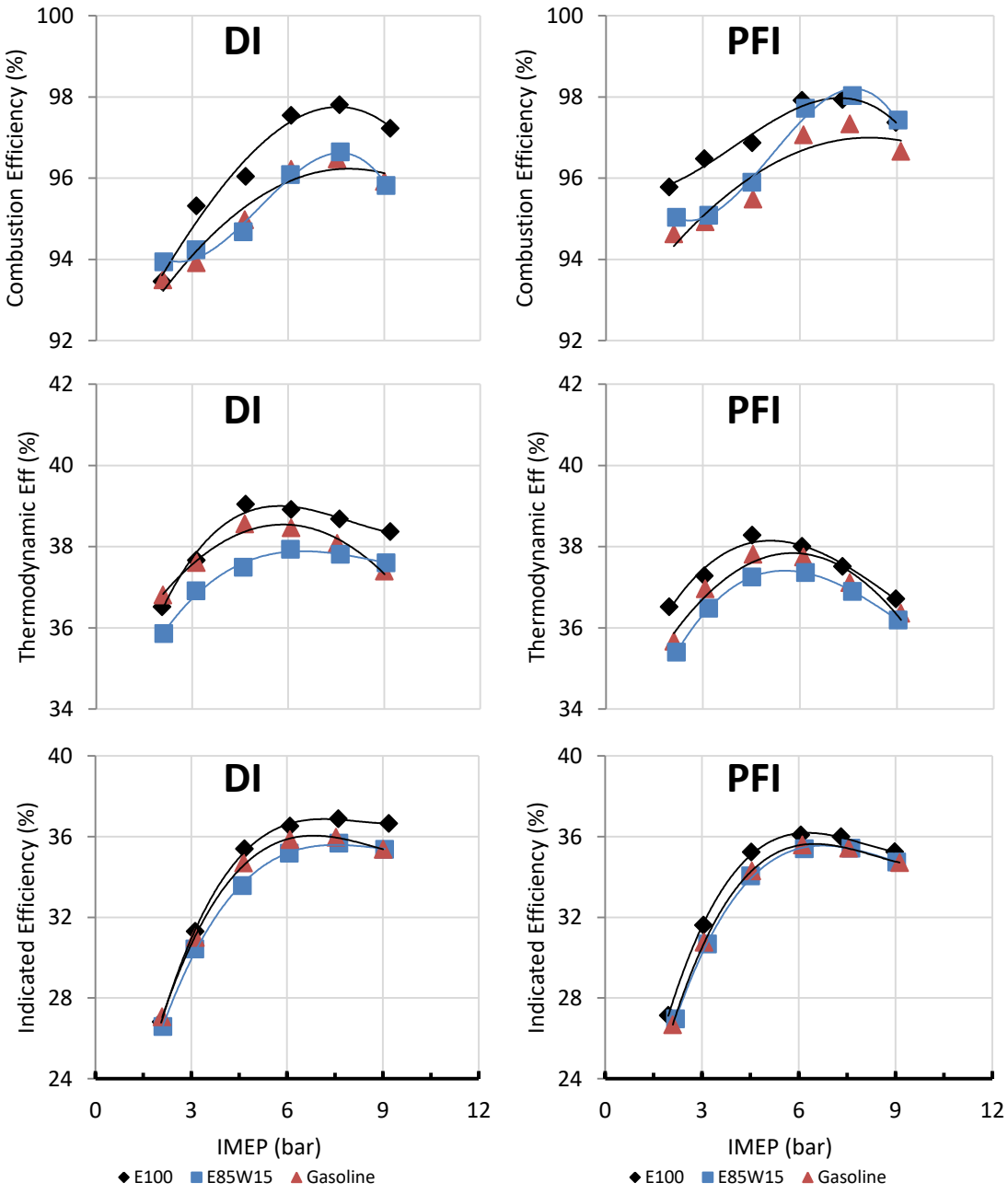

Figure 7.15. Efficiency related parameters of PVOvar valve strategy and different fuels – DI and PFI operation, 1500 rpm, MBT operation.

As gas exchange efficiency variation between all fuels was virtually zero, only combustion efficiency and thermodynamic efficiency had considerable effect on indicated efficiency. E100 DI operation resulted in the highest overall indicated efficiency due to better combustion and thermodynamic efficiencies. Comparatively, E85W15 showed a lower indicated efficiency than gasoline for DI operation at lower loads due to the impaired thermodynamic efficiency. On the other hand, due to the lack of charge cooling effect which contributed to better combustion efficiency, E85W15 PFI operation and gasoline provided virtually the same indicated efficiency.

As previously found in the tSI study, PFI provided better overall efficiency than DI when using wet ethanol. This could be attributed to the better combustion process with better charge preparation and fuel conversion efficiency. It is expected that E85W15 DI operation would be better suited for boosted operation at PFI knock limited conditions.

7.4. Unthrottled negative valve overlap (NVO) operation with different fuels

The use of NVO in order to increase RGF trapping with load control through early intake valve closure (EIVC) has been described in a previous chapter for E100. In this sub-chapter a comparison between different fuels is demonstrated. The main reason for the use of NVO instead of ER strategy is the higher combustion efficiency achieved for both DI and PFI operations.

7.4.1. Gas exchange related parameters

Gasoline and E85W15 operation with NVO and EIVC strategy provided better combustion stability when using partial throttling instead of WOT. Compared to E100, DI case, there was a slight difference in the valve profile, but this could be attributed to the higher tolerance of E100 to RGF. The use of partial throttle increased the compression due to later IVC and promoted higher temperature at spark timing. Comparing PFI and DI cases, due to the DI cooling effect, partial throttling was required up to 3.1 bar IMEP, while for the PFI operation this was necessary only for 2.0 bar IMEP load. Due to the increased E85W15 cooling effect, lower intake pressure was used in order to further delay the IVC compared to gasoline cases. Appendix 4 provides the valve timings and injection timings used in these tests.

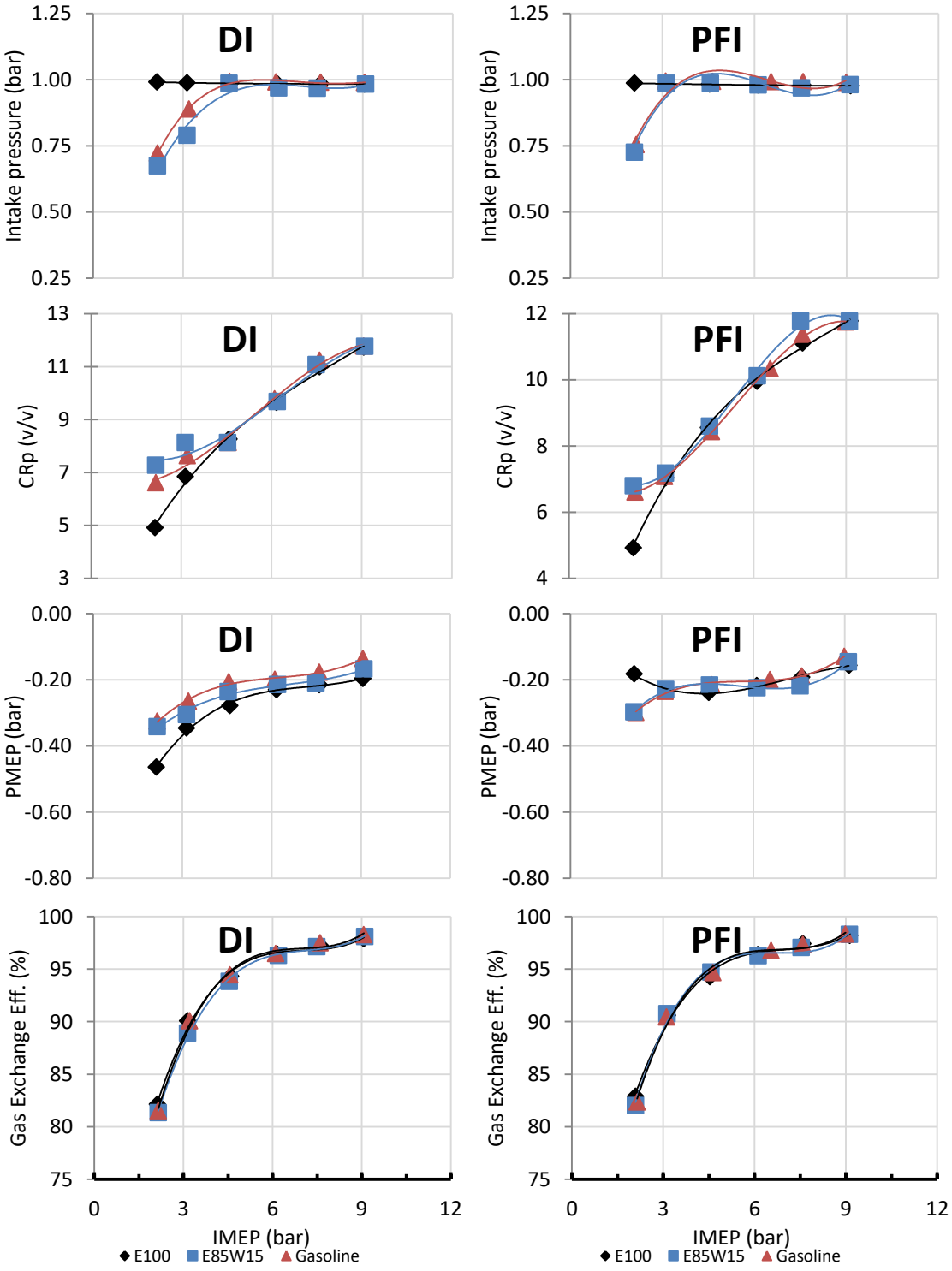

Figure 7.16. Intake pressure, PMEP, gas exchange efficiency and effective compression ratio of NVO valve strategy and different fuels – DI and PFI operation, 1500 rpm, MBT operation.

As a consequence of the lower intake pressure, higher pumping losses occurred when partial throttling was used. For this reason, slightly lower gas exchange efficiency was occurred for the gasoline and E85W15 cases. Gas exchange efficiency was virtually

the same for the different fuels for the operating conditions were WOT operation was possible.

7.4.2. **Combustion related parameters**

Figure 7.17 presents spark timing and CA50 required for MBT operation. Almost all operating conditions produced COV_{imep} below 3.0% as shown in Figure 7.18, with the exception of E85W15 DI 2.0 bar IMEP at which it was not possible to achieve more stable combustion even with the highly advanced spark timing. The high COV_{impe} of the lower load DI cases could be attributed to the high FDA, which is known to influence more on the COV_{imep} than the main combustion phase. And this was a result of cooler RGF due to injection during the initial phase of NVO. The delayed CA50 of gasoline 9.0 bar IMEP load for both DI and PFI injection methods was necessary due to knock limited operation.

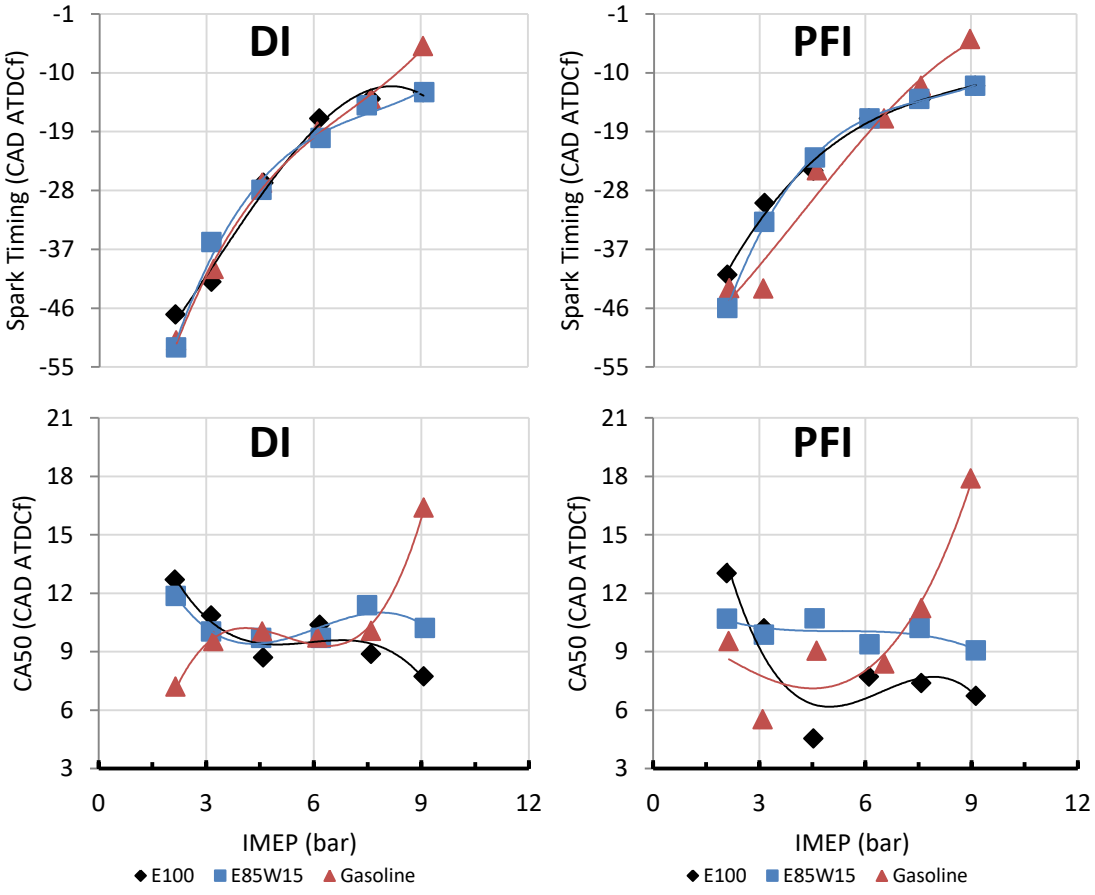

Figure 7.17. Spark timing and CA50 of NVO valve strategy and different fuels – DI and PFI operation, 1500 rpm, MBT operation.

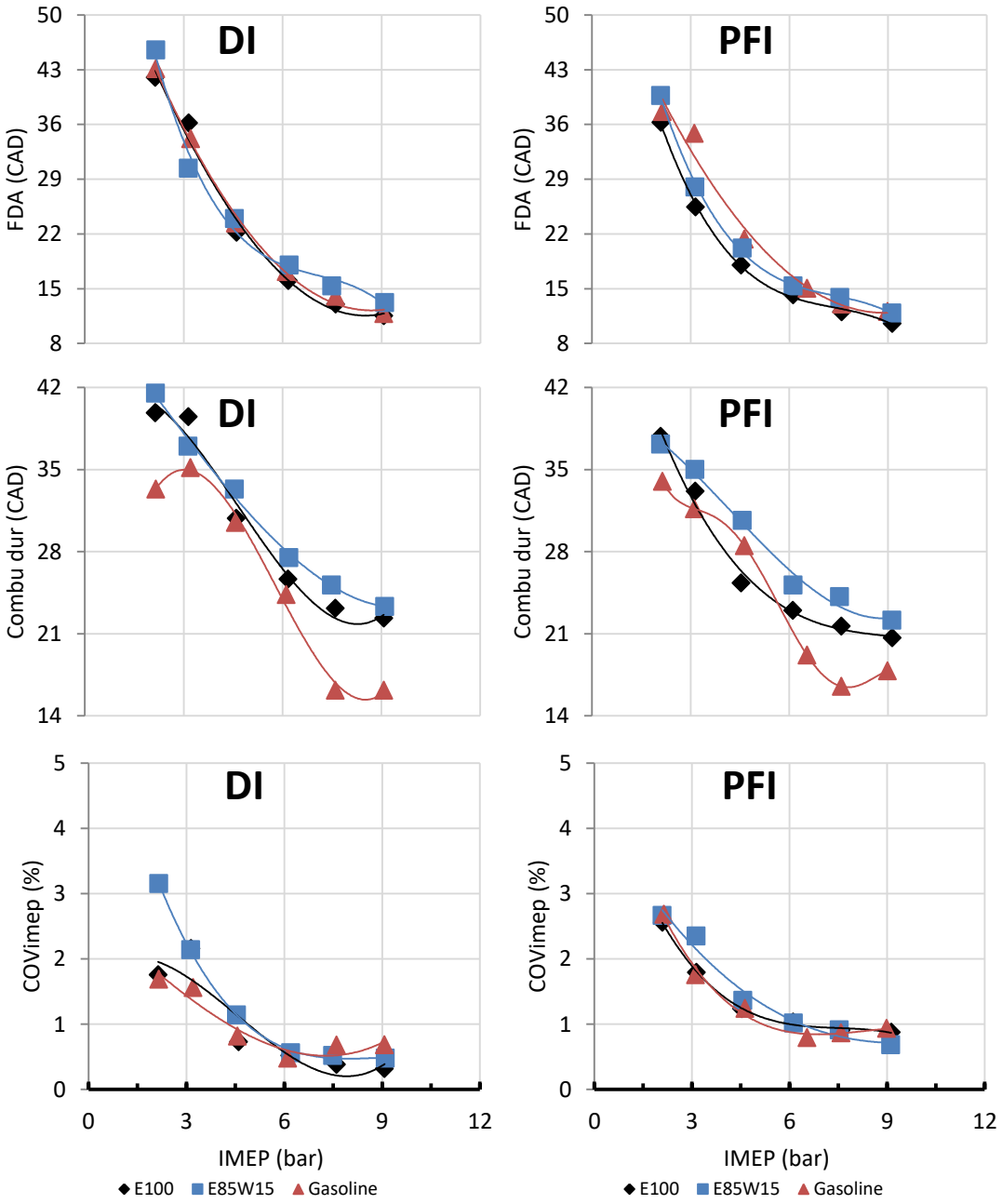

Figure 7.18. Flame development angle, combustion duration and COV_{imep} of NVO valve strategy and different fuels – DI and PFI operation, 1500 rpm, MBT operation.

Anhydrous ethanol higher reactivity compared to other fuels had the lowest FDA in the majority of the cases. The faster FDA of E85W15 at 3.1 bar IMEP could be attributed to higher temperature at the end of the compression stroke by the partial throttling and later IVC. On the other hand, the higher cooling effect of DI ethanol resulted in slower burning rates and increased main phase combustion duration than gasoline. The faster

gasoline combustion after 6.1 bar IMEP could be attributed to SACI combustion, as occurred in the PVOvar valve strategy for some of the tested points.

Another two factors expected to accelerate the combustion were the increase of the effective compression ratio with the load and the better large flow motion structure maintenance with the later IVC. The higher CR_p resulted in higher temperatures in the end of the compression which improved ignition delay and increased flame speed. In addition, as explained in the previous chapter about EIVC operation, the EIVC event may cause the breakup of the large tumble flow motion structure prematurely during the compression stroke. This result in decrease in the turbulence intensity when piston approaches TDC due to dissipation of the smaller eddies as shear stress.

Figure 7.19 presents the heat release rates of the different fuels at four loads and both injection methods. Due to faster combustion, gasoline always presented the highest heat release peak, followed by E100 and E85W15. Ethanol fuels presented conventional flame deflagration combustion due to ethanol's higher resistance to auto-ignition. Even with the use of higher spark advance it was impossible to reach SACI combustion.

Gasoline presented end gas auto-ignition for loads higher than 6.1 bar IMEP load. For DI 6.1 bar IMEP, SACI could be achieved with further spark timing advance than the MBT at the expense of reduced efficiency. In the PFI case, the higher combustion temperature (no DI cooling effect) promoted SACI even for delayed spark timings. At 7.5 bar IMEP, both injection methods presented SACI combustion with operation near the knock boarder, as shown by the high max PRR near the value of 5 bar/CAD. As explained before, at the load of 9.0 bar IMEP, spark timing had be delayed due to the fast burn of the end gas which caused abrupt increase in the HRR and PRR levels above 5 bar/CAD. Audible knock could be heard at this condition.

Gasoline presented overall highest exhaust gas temperatures than ethanol fuels. E85W15 longer combustion duration was the major reason for its highest combustion temperature than E100. Similar exhaust temperatures were found for DI and PFI methods due to opposing trends of higher DI combustion duration and higher PFI combustion temperatures.

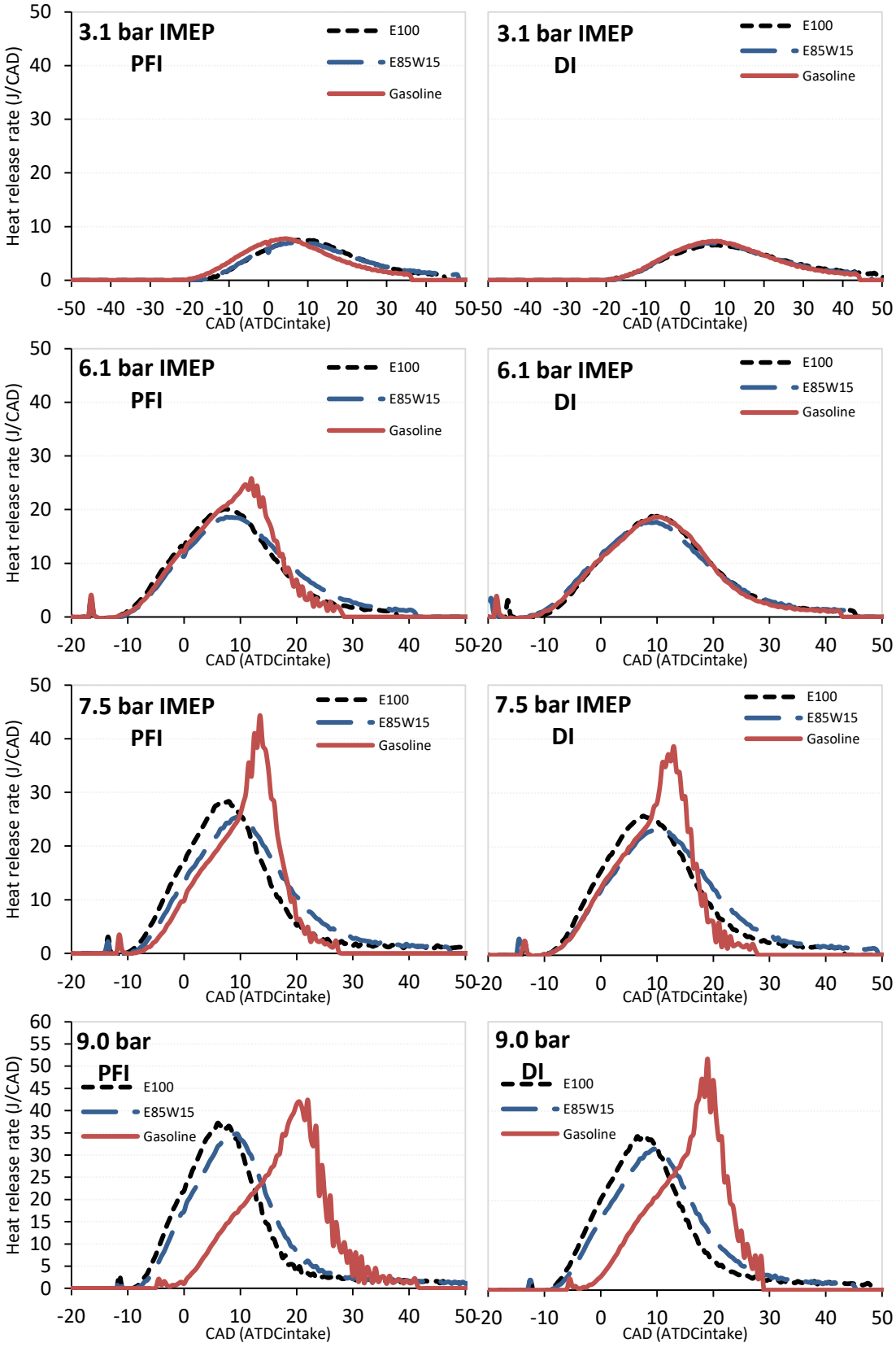

Figure 7.19. Heat release rates of NVO valve strategy and different fuels – DI and PFI operation, 1500 rpm, MBT operation.

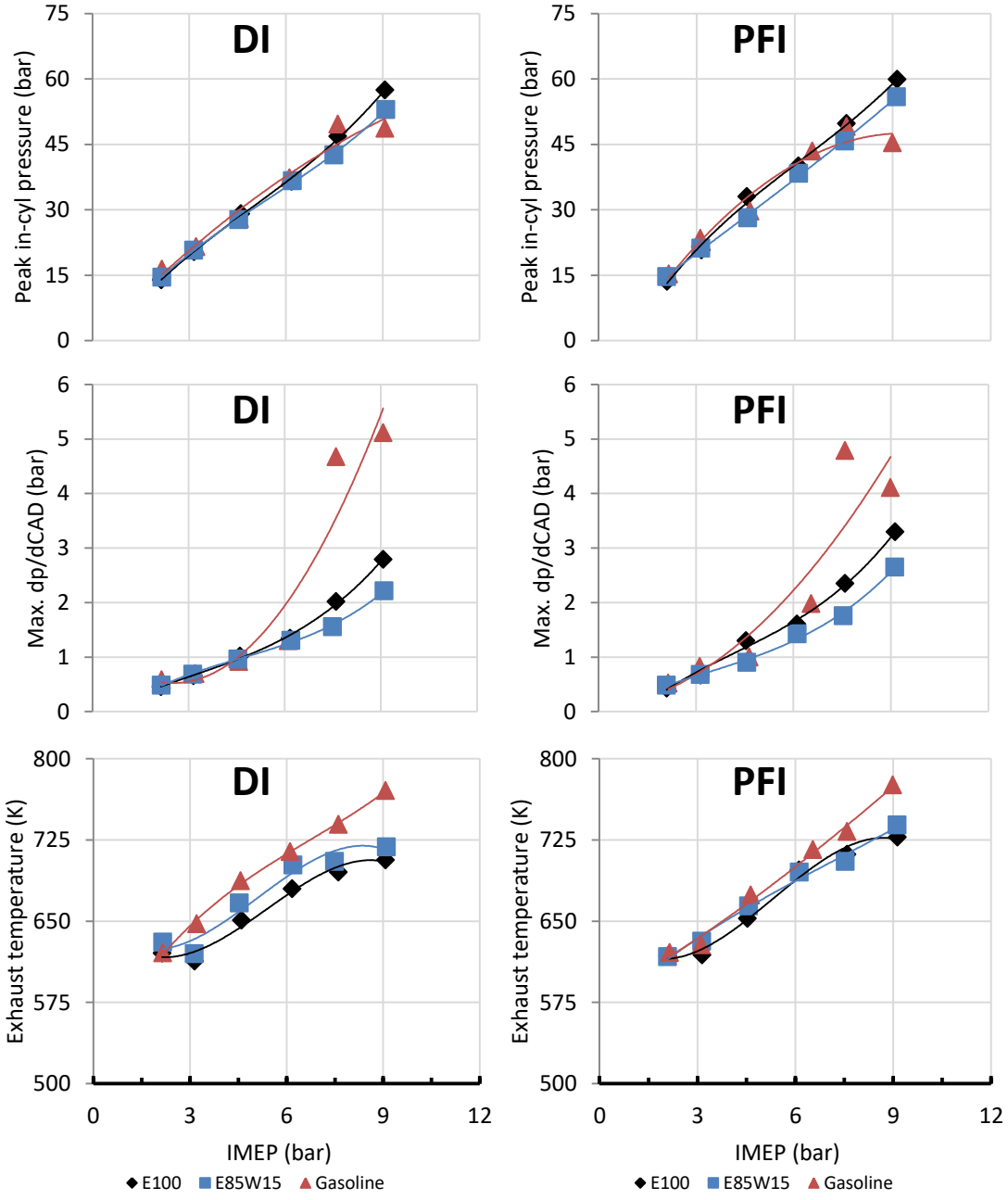

Figure 7.20. Maximum in-cylinder pressure, maximum pressure rise rate and exhaust gas temperature of NVO valve strategy and different fuels – DI and PFI operation, 1500 rpm, MBT operation.

7.4.3. **Engine out emissions**

NVO strategy engine out emissions for the different tested fuels and injection methods are presented in Figure 7.21. The major advantage of the NVO strategy over all other valve strategy methods is the best mixing process. Due to the long mixing period promoted by the DI injection during the early phase of the NVO phase, better in-

cylinder homogeneity could be achieved for all fuels. For this reason, DI and PFI CO emission levels were very similar for all fuels and different loads.

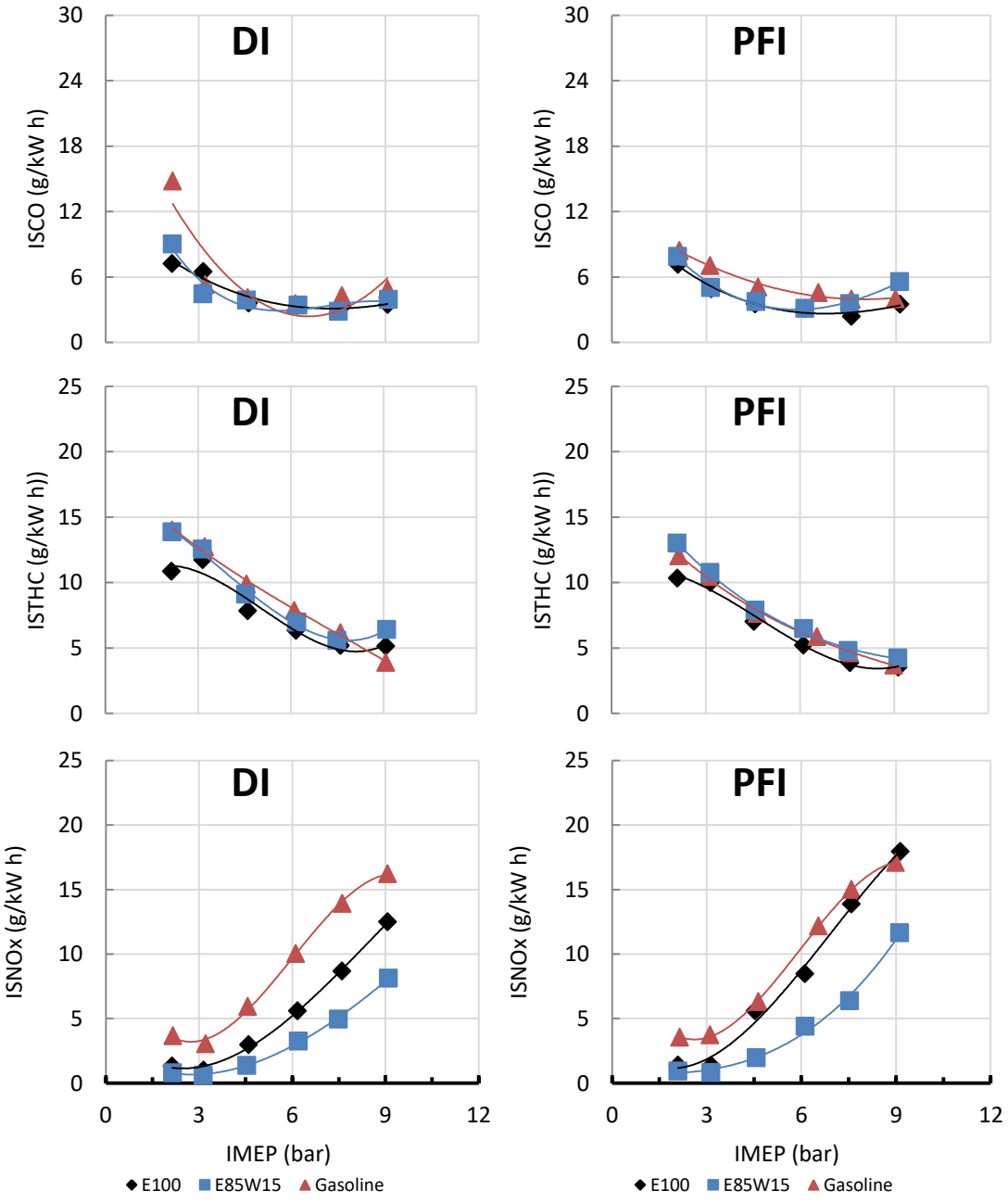

Figure 7.21. Engine out emissions of NVO valve strategy and different fuels – DI and PFI operation, 1500 rpm, MBT operation.

Regarding THC emissions, the hot RGF enhanced fuel vaporization for the DI injection strategy. This was especially important for the wet ethanol, which had more fuel mass injected and higher heat capacity. Thus, very similar THC emissions levels were found

for most loads of E100 and E85W15. Due to the charge cooling effect of DI method, lower in-cylinder temperatures resulted in higher THC emissions compared to PFI method.

The increased water content of E85W15 which resulted in higher charge heat capacity was the responsible for the lowest overall NOx emissions of this fuel, for both DI and PFI injection methods. Gasoline and E100 NOx emissions at load higher than 4.5 bar IMEP were more similar than in the DI case due to the absence of DI charge cooling effect. Even though the E100 injected mass with PFI results in intake charge temperature drop there was plenty of time for heat transfer (intake ports to charge) due to the long period (from $TDC_{fire)}$ until midle of the intake stroke). This reduced the effect of the E100 latent heat of vaporization on combustion temperature. On the other hand, the water content of E85W15 seemed to play an important role in NOx emissions reduction even with PFI.

7.4.4. **Efficiency related parameters**

Combustion efficiencies of E85W15 and E100 were very similar due to the excellent vaporization process provided by the direct injection during the NVO period, which resulted in similar emissions levels for E100 and E85W15 (Figure 7.22).). For the PFI method, the combustion efficiency difference between these fuels was slightly higher. PFI combustion efficiency tended to be slightly higher than that of DI cases. The use of NVO valve strategy was very effective in increasing E85W15 combustion efficiency for loads higher than 3.1 bar IMEP, especially for the DI method (as shown in Figure 7.23). Gasoline had the lowest overall combustion efficiency due to its higher LHV although the CO and THC emission levels were similar to those found for ethanol fuels.

E100 thermodynamic efficiency was the highest due to relative short combustion duration, low exhaust gas temperature and MBT combustion phasing. As DI provided lower temperature combustion, less heat transfer was expected which resulted in higher combustion temperature. For the 2.0 bar IMEP DI case, E100 very low effective compression ratio directly impaired the combustion process, thus, thermodynamic efficiency. The reasons for the lower E85W15 are similar to those of the PVOvar valve strategy: longer combustion duration and increased exhaust enthalpy due to the higher calorific value of the charge. Thus, higher energy fraction was wasted in the exhaust gases than occurred for E100. For the gasoline cases, the higher combustion

temperatures were expected to increase heat transfer. Additionally, at higher loads, knock limited combustion decreased thermodynamic efficiency.

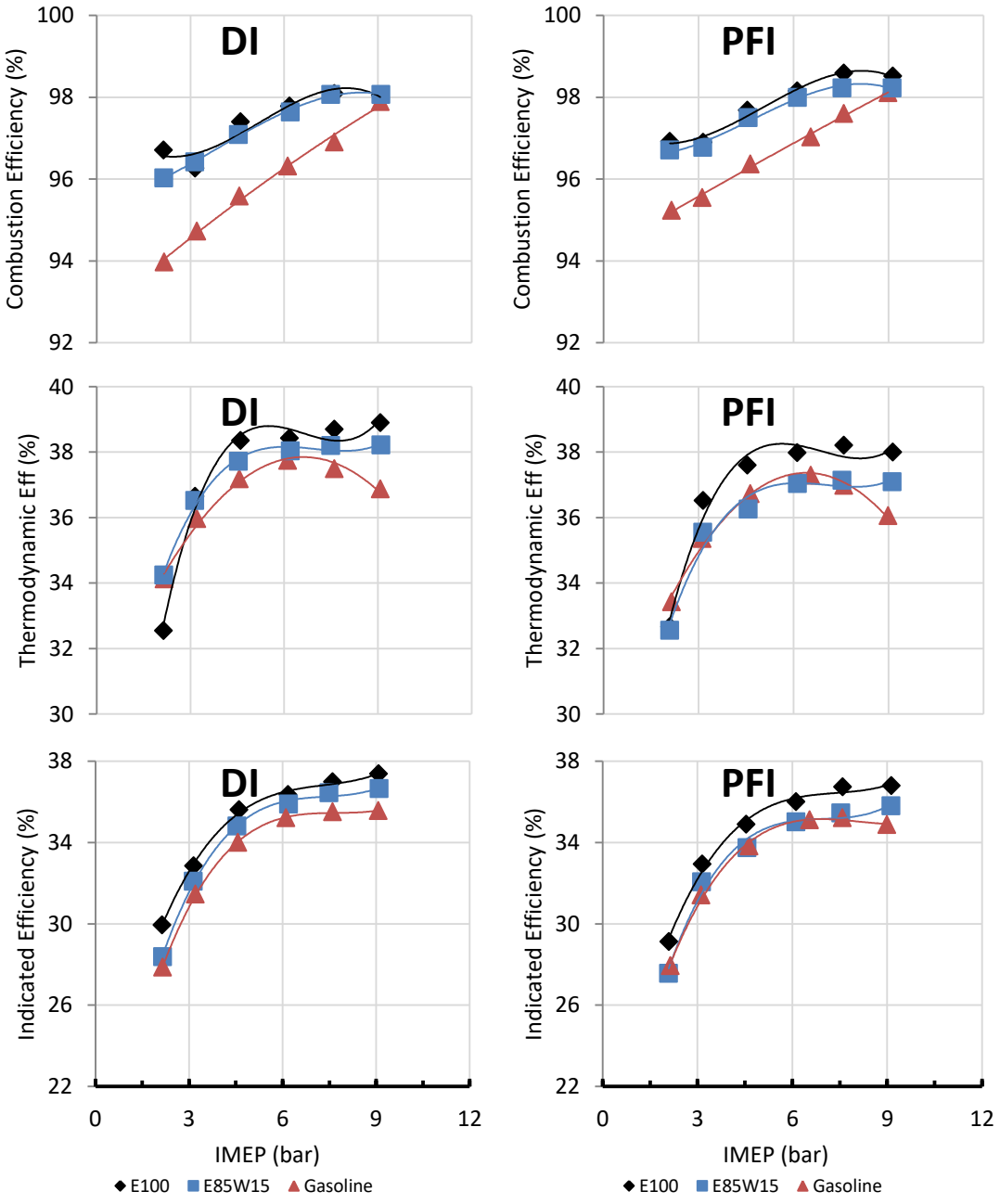

Figure 7.22. Efficiency related parameters of NVO valve strategy and different fuels – DI and PFI operation, 1500 rpm, MBT operation.

As shown in Figure 7.16, with the exception of 2.0 bar IMEP gasoline and E85W15, and E85W15 3.1 bar IMEP load with DI, similar gas exchange efficiency would not be expected to impair the indicated efficiency. Thus, the difference in indicated efficiency

between E100 and E85W15 could be directly attributed to the slower combustion process and higher energy loss as exhaust gas enthalpy, once combustion efficiency was virtually at the same levels. Higher DI indicated efficiency was mainly caused by the thermodynamic efficiency difference between DI and PFI.

7.5. Investigation of the best strategy for E85W15

As previously discussed, one of the main reasons for the lower E85W15 indicated efficiency when compared to E100 was the increased THC and CO emissions, which directly affected the combustion efficiency. Figure 7.23 presents the combustion efficiency comparison between the different injection strategies for each valve timing strategy and different loads

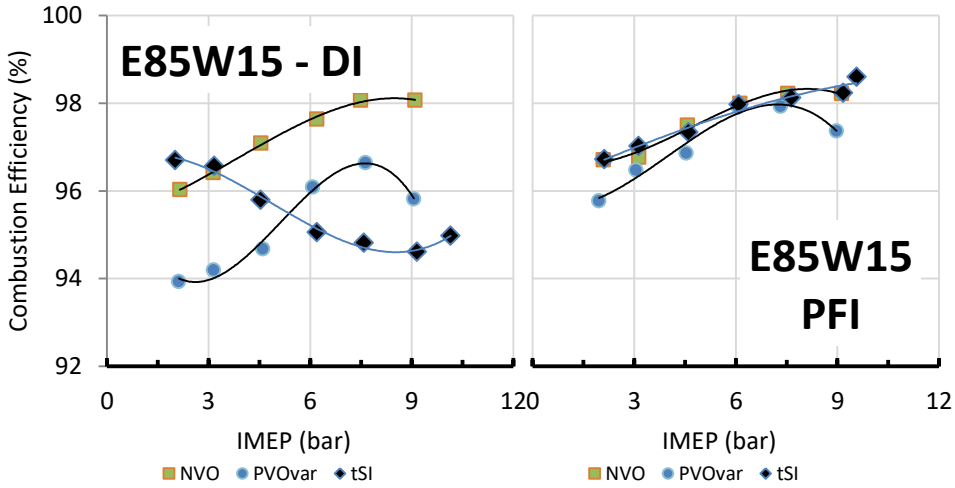

Figure 7.23. Effect of valve strategy and fuel injection method on combustion efficiency of E85W15 for different loads, 1500 rpm, MBT operation.

Starting from the baseline case tSI, the decrease in combustion efficiency was related to the poor mixing process and fuel vaporization. As more fuel was injected to increase the load the spray penetration was expected to increase, and the water content decreased the combustion temperature which decreased ethanol oxidation process. The use of PVOvar increased fresh charge thermal state which contributed to spray vaporization process at higher loads. Adversely, the increased RGF content at low loads highly decreased combustion temperatures, which highly reduced NOx emission compared to other strategies. In the NVO case, the fuel injection with the highest RGF

temperature promoted the best DI vaporization and mixing process overall. This highly increased the combustion efficiency compared to other valve strategies and DI operation.

On the other hand, better mixing process by PFI promoted more similar combustion efficiency levels, where PVOvar shown the lowest combustion efficiency due to the expected higher RGF content. Thus, depending on the valve timing strategy to be used, PFI operation seemed to be more advantageous than DI. In order to illustrate this, relative indicated efficiency gain (RIEG) between DI and PFI was calculated as:

$$RIEG = \frac{\eta_{I,DI}}{\eta_{I,PFI}} - 1 \tag{31}$$

As the test load slightly varied and this would have an impact in the absolute numbers division of RIEF, 3rd, 4th and 5th order polynomial fits were used in order to predict the indicated efficiency at desired loads. The polynomial order was chosen in order to use R^2 values higher than 0.9990. Figure 7.24 shows the RIEG between DI and PFI for each tested valve strategy.

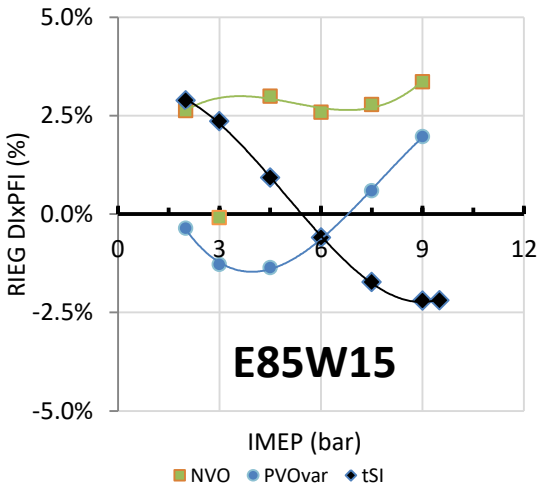

Figure 7.24. Relative indicated efficiency gain between DI and PFI E85W15 operation for the different valve strategies, 1500 rpm, MBT operation.

Thus, different injection strategies would need to be selected for a specific operating condition depending on the valve strategy used. For example, DI would produce better indicated efficiency than PFI at low part load. Adversely, PVO strategy would result in better efficiency with PFI strategy for most loads with exception of 7.5 and 9.0 bar IMEP loads. These facts could be directly attributed to the previously discussed effects of the combustion efficiency. Finally, NVO operation consistently produced better results for DI operation. At 3.0 bar IMEP, the required partial throttling of DI operation reduced the possible gain in the range of 2.5%.

Figure 7.25 presents the absolute values of indicated efficiency for all tested scenarios with E85W15 (Appendix 5 presents the comparison of indicated efficiency between different tested valve strategies for DI method and different fuels). NVO DI was the more suitable strategy for E85W15 for some reasons: thermodynamic efficiency gains compared to PFI scenarios; better combustion efficiency than other fuels with DI; better gas exchange efficiency at low loads than other valve strategies (Figure 7.26).

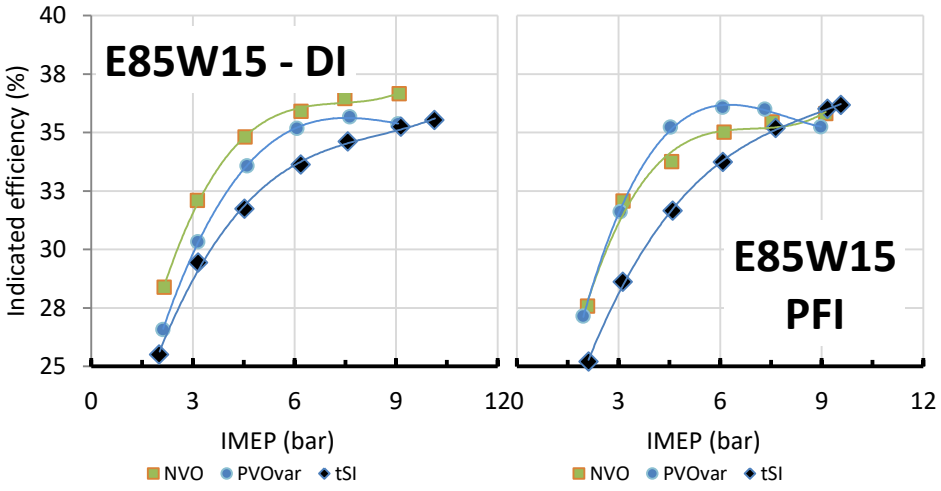

Figure 7.25. Indicated efficiencies for different valve strategies and E85W15 injection methods, 1500 rpm, MBT operation.

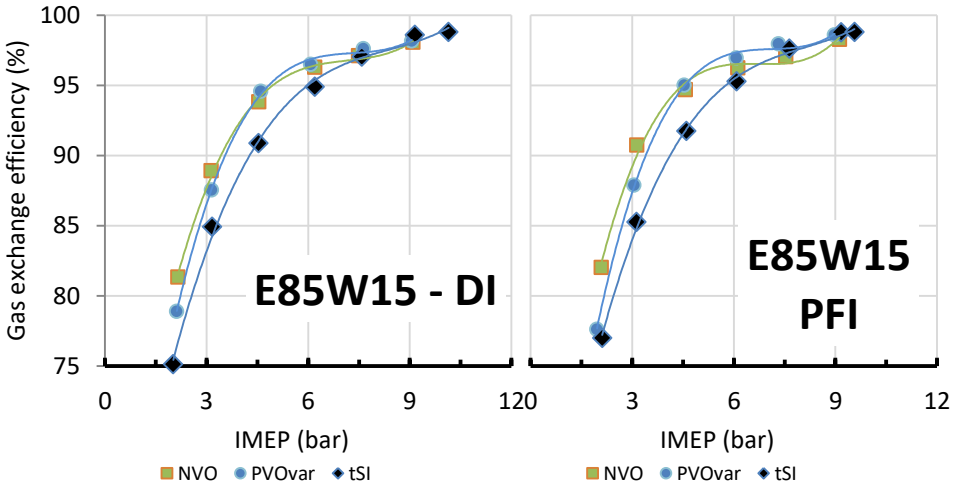

Figure 7.26. Gas exchange efficiency for different valve strategies and E85W15 injection methods, 1500 rpm, MBT operation.

A comparison in terms of achievable efficiency gains between the simplest valve strategy to be implemented (tSI and PFI) and the more complex scenario (NVO with DI) can be evaluated by the analysis of RIEG, as shown in Table 7.1. The major gains would occur especially at lower loads, with an average RIEG between 2.0 and 4.5 bar IMEP of 11.6%.

Table 7.1. Indicated efficiency gains of wet ethanol with NVO

IMEP (bar)	Indicated efficiency (%)			
	tSI PFI	NVO DI	RIEG (%)	
2.0	25.2	28.4	12.6	
3.0	28.6	32.1	12.2	11.6
4.5	31.7	34.8	10.0	
6.0	33.7	35.9	6.4	
7.5	35.2	36.4	3.6	3.9
9.0	36.0	36.7	1.8	

Chapter 8.
Conclusions

8.1. Summary of the thesis

Experimental thermodynamic tests were carried out on a single cylinder camless engine to evaluate the potential of different valve strategies, in order to improve the SI engine part load efficiency when using alcohol fuels. Direct injection and port fuel injection methods were compared. Anhydrous and wet ethanol, and gasoline fuels were compared.

Primarily, through literature review, it was possible to understand the flame deflagration based combustion process and the SI engine operation weaknesses which degrade part load engine efficiency. To tackle pumping losses by the use of FVVA system and by increasing thermodynamic efficiency using residual gas dilution were the two main points found to have potentials to increase part load stoichiometric spark ignition engine efficiency.

A brief review regarding the impacts of using ethanol to diversify the liquid fuels energy matrix was also presented in the literature review. The ethanol production process was presented and the hypothesis of reducing ethanol production cost by stopping the distillation process before the azeotrope water-ethanol point was investigated. An energy cost/benefit analysis of several first generation ethanol production paths (different crops) was done based on the available ethanol production literature data. The results found in this literature review agreed with the literature showing that the best energy gains in ethanol production occur when ethanol-in-water fractions vary in the range of 85% to 90% (v/v).

Literature regarding the application of wet ethanol in SI engines showed that the main problem to be tackled when increasing the water-in-ethanol content was the combustion efficiency degradation due to increased unburned fuel. Thus, several valve timing studies using anhydrous ethanol were proposed to find the best strategies that would enable high efficiency wet ethanol operation.

In this way, other research objectives were reached when several throttled PVO valve strategies were tested to study the effect of PVO on SI operation. In addition, unthrottled SI operation was studied using the EIVC and LIVC concepts and compared to a baseline case. Diluted SI stoichiometric operation was studied using NVO and ER

valve concepts, using the best valve event based load control method found in the EIVC and LIVC study. From these E100 studies, it was decided to run comparative analysis tests for E85W15 and gasoline with the baseline tSI valve strategy, the optimized PVO valve strategy and NVO valve strategy. All tests were evaluated for both DI and PFI methods.

8.2. Conclusions

The main conclusions regarding the different tested valve timing strategies with E100 were:

a) The most important effect of the increase in the positive valve overlap period on SI E100 operation was on pumping work. The initial increase on the PVO period results in increased RGF. This required partial dethrottling which increased intake system pressure. This decreased the pumping work which directly increased the indicated efficiency. On the other hand, the increased RGF increased CO and THC emissions, decreasing combustion efficiency and degrading the combustion process. If the temperature was high enough to support higher RGF contents, the intake backflow process would have been impaired by the high intake temperature and then the RGF would start to decrease. Thus, for each load condition there would be a specific RGF content which would decrease the pumping work while keeping the engine operation stability at acceptable levels. DI method had always shown better potential in increased part load efficiency due to its cooling effect which increased engine thermodynamic efficiency.

b) It was possible to operate the engine with WOT and stoichiometric operation without residual gas dilution using EIVC at all tested loads. On the other hand, LIVC operation at very low loads was impaired due to IVC and spark events proximity. EIVC showed best potential to increase naturally aspirated SI engine part load efficiency due to lower pumping losses caused by the reduced intake gas exchange period. On the other hand, LIVC showed better combustion stability due to the large flow motion structures maintenance during the compression stroke which decreased combustion duration compared to EIVC. Even then, EIVC was chosen as the best strategy to be used in part load SI engine operation. The effects of the maximum valve lift were accessed and the main conclusion was found: the highest intake valve lift possible should be used

for unthrottled SI engine operation with EIVC in order to reduce valve restriction flow losses.

c) The study on E100 operation with residual gas dilution using NVO and ER strategies showed that SACI combustion mode may improve indicated efficiency due to increased thermodynamic efficiency. This would only occur as long as the CA50% can be kept around the MBT point. EIVC load control strategy could be used effectively with both residual gas trapping methods. NVO and ER indicated efficiency showed similar potential to increase indicated efficiency. NVO tended to increase indicated efficiency mainly due to improved combustion efficiency. On the other hand, ER improved indicated efficiency due to better thermodynamic efficiency. Gas exchange efficiency of the ER case was impaired due to only one valve opening during the exhaust stroke. ER valve control strategy was shown to be more complicated than the NVO valve control strategy.

From these studies it was possible to choose three valve strategies in order to evaluate wet ethanol operation potentials:

1st) baseline tSI: in order to evaluate the performance of E85W15 compared to E100 and gasoline using SI like valve strategy. E85W15 operation showed better indicated efficiency than PFI at low loads due to DI higher thermodynamic efficiency. At higher than 4.5 bar IMEP loads, the DI increased THC emissions which degraded combustion efficiency and impaired indicated efficiency. Due to intake port air to fuel displacement, maximum achieved load was reduced from 10.2 bar IMEP to 9.6 bar IMEP.

2nd) Variable PVO: in order to evaluate the potentials of using a modern CVVL system with such fuels; E85W15 showed better indicated efficiency for the PFI operation up to 9.0 bar IMEP, mainly due to considerably higher combustion efficiency.

3rd) NVO: in order to take advantage of the increased combustion efficiency characteristic. DI increased combustion efficiency due to injection timing during the NVO period enabled a 2% average indicated efficiency gain compared to PFI. This strategy also provided the highest overall efficiency for all tested fuels due to a combination of higher thermodynamic efficiency, combustion efficiency and good gas exchange efficiency.

The use of tSI and PVOvar valve strategies is already a common practice in the automotive industry. On the other hand, the implementation of EIVC and LIVC valve strategies will become more popular with larger implementation of CVVL technology, such as described in the literature review. The main advantage of EIVC and LIVC strategies compared to the tSI was the huge reduction in pumping losses. Additionally, the use NVO and ER strategies would require even more complex CVVL technologies than the already provided in the market, making its implementation in real world applications more restrict to high end vehicles. The calibration process complexity would increase with the increase in the complexity in the CVVL, but considerable gains in spark ignition engine efficiency would be possible for stoichiometric operation.

The use of wet ethanol for automotive purposes is still a challenge. During the whole period of this work, three fuel pumps designed for anhydrous ethanol operation failed due to higher than 5% v/v water content. Investigations of the broken parts showed early failure of the bearings.

Even though in a well-to-wheel analysis there would be considerable energy savings when using wet ethanol with higher water content than that present in conventional hydrous ethanol (E95W05), such fuels would be more suitable for dedicated engines. Flex fuel cars would suffer from water separation in the fuel tank if gasoline and wet ethanol were mixed without other additives. More expensive materials would be required in the fuel line systems to stand the more corrosive fuel. Conversely, higher knock resistance could be expected due to lower temperature combustion and heavy downsizing would be enabled. Thus, more research is still required to implement such fuels in automotive sector.

8.3. Suggestions for future works

Based on the performed studies, some future work possibilities are suggested to expand knowledge on the use of anhydrous and hydrous ethanol fuels. These suggested studies do not require engine hardware modifications:

1st) Extend the operating load range using the already installed super-charger capability;

2nd) Study the impacts of the water addition on particulate emissions and develop exhaust gases speciation;

3rd) Study DI and PFI concomitant injection in order to find the best compromise between both at each load;

4th) Evaluate the effect of different valve strategies on turbulence levels prior to spark using 3D CFD simulations;

5th) Design 1D gas exchange models for residual gas fraction and temperature estimations;

6th) Extend operation range of unconventional valve strategies and evaluate lean operation.

Other actions aiming to enhance the engine hardware to achieve higher engine efficiency are: to increase the geometric compression ratio using a different piston dome shape in order to take advantage of the higher knock resistance of alcohol fuels; to remove the intake valve masking in order to decrease in-cylinder heat transfer and enhance intake flow; to change the injector side positioning to central positioning; to increase intake valves diameter by decreasing the exhaust valves diameter.

References

[1] M. M. Ojapah, “Experimental studies of performance and emissions in a 2/4-stroke engine with gasoline and ethanol,” PhD Thesis: Brunel University London, 2014.

[2] Y. Zhang, “Experimental investigation of CAI combustion in a two-stroke poppet valve DI engine,” PhD Thesis: Brunel University London, 2014.

[3] R. K. Pachauri and L. Meyer, “Climate change 2014-Synthesis Report,” Geneva, Switzerland, 2014.

[4] United Nations, “Adoption of the Paris Agreement,” in *Framework Convention on Climate Change*, 2015, no. FCCC/CP/2015/L.9/Rev.1, p. 32.

[5] European Commission, “EU Transport in Figures,” 2014.

[6] US EPA, “DRAFT Inventory of U . S . Greenhouse Gas Emissions and Sinks : 1990 – 1998,” 2016.

[7] U. S. E. I. Administration, “International Energy Outlook 2016,” 2016.

[8] OECD/ITF, *ITF Transport Outlook 2017*. Paris: OECD Publishing, 2017.

[9] International Council on Clean Transportation (ICCT), “EU CO2 standards for passenger cars and light-commercial vehicles,” 2014.

[10] J. A. Caton, “A Cycle Simulation Including the Second Law of Thermodynamics for a Spark-Ignition Engine : Implications of the Use of Multiple-Zones for Combustion,” *Sae Tech. Pap. Ser.*, no. 2002-01–0007, 2002.

[11] J. A. Caton, “Implications of fuel selection for an SI engine: Results from the first and second laws of thermodynamics,” *Fuel*, vol. 89, no. 11, pp. 3157–3166, 2010.

[12] I. Sezer and A. Bilgin, “Effects of charge properties on exergy balance in spark ignition engines,” *Fuel*, vol. 112, pp. 523–530, 2013.

[13] J. A. Caton, “Combustion phasing for maximum efficiency for conventional and high efficiency engines,” *Energy Convers. Manag.*, vol. 77, pp. 564–576, Jan. 2014.

[14] N. Ozdor, M. Dulger, and E. Sher, “Cyclic Variability in Spark Ignition Engines A Literature Survey,” *SAE Tech. Pap.*, no. 940987, 1994.

[15] D. L. Lord, R. W. Anderson, D. D. Brehob, and Y. Kim, “The Effects of Charge Motion on Early Flame Kernel Development,” *SAE Tech. Pap.*, no. 930463, Mar. 1993.

[16] P. Aleiferis, A. Taylor, K. Ishii, and Y. Urata, “The nature of early flame development in a lean-burn stratified-charge spark-ignition engine,” *Combust. Flame*, vol. 136, no. 3, pp. 283–302, Feb. 2004.

[17] G. T. Kalghatgi, “Early flame development in a spark-ignition engine,” *Combust. Flame*, vol. 60, no. 3, pp. 299–308, 1985.

[18] B. Khalighi, “Intake-Generated Swirl and Tumble Motions in a 4-Valve Engine with Various Intake Configurations-Flow Visualization and Particle Tracking Velocimetry,” *SAE Tech. Pap.*, no. 900059, Feb. 1990.

[19] S. F. Benjamin, “A phenomenological model for ‘barrel’ swirl in reciprocating engines,” *Arch. Proc. Inst. Mech. Eng. Part D J. Automob. Eng. 1989-1996 (vols 203-210)*, vol. 206, no. 14, pp. 63–71, 1992.

[20] K. Y. Kang and J. H. Baek, “Tumble Flow and Turbulence Characteristics in a Small Four-Valve Engine,” *SAE Tech. Pap.*, no. 960265, Feb. 1996.

[21] P. G. Hill and D. Zhang, “The effects of swirl and tumble on combustion in spark-ignition engines,” *Prog. Energy Combust. Sci.*, vol. 20, no. 5, pp. 373–429, Jan. 1994.

[22] A. Floch, J. Van Frank, and A. Ahmed, “Comparison of the Effects of Intake-Generated Swirl and Tumble on Turbulence Characteristics in a 4-Valve Engine,” *SAE Tech. Pap.*, no. 952457, 1995.

[23] T. Urushihara, T. Murayama, K.-H. Lee, and Y. Takagi, “Turbulence and Cycle Variation of Mean Velocity Generated by Swirl and Tumble Flow, and Their Effects on Combustion,” *SAE Tech. Pap.*, no. 950813, 1995.

[24] S. Pischinger and J. B. Heywood, “How Heat Losses to the Spark Plug Electrodes Affect Flame Kernel Development in an SI-Engine,” *SAE Pap.*, no. 900021, 1990.

[25] J.-F. Le Coz, S. Henriot, and P. Pinchon, “An experimental and computational analysis of the flow field in a four-valve spark ignition engine - Focus on cycle-resolved turbulence,” *SAE Tech. Pap.*, no. 900056, 1990.

[26] K. Lee, C. Bae, and K. Kang, “The effects of tumble and swirl flows on flame propagation in a four-valve S.I. engine,” *Appl. Therm. Eng.*, vol. 27, no. 11–12, pp. 2122–2130, 2007.

[27] G. Kalghatgi, I. Algunaibet, and K. Morganti, “On Knock Intensity and Superknock in SI Engines,” *SAE Int. J. Engines*, vol. 10, no. 3, pp. 2017-01–0689, Mar. 2017.

[28] S. Pischinger, M. Günther, and O. Budak, “Abnormal combustion phenomena with different fuels in a spark ignition engine with direct fuel injection,” *Combust. Flame*, vol. 175, pp. 123–137, 2016.

[29] O. A. Kuti *et al.*, “A fundamental investigation into the relationship between lubricant composition and fuel ignition quality,” *Fuel*, vol. 160, pp. 605–613, Nov. 2015.

[30] M. C. Kocsis, T. Briggs, and G. Anderson, “The Impact of Lubricant Volatility, Viscosity and Detergent Chemistry on Low Speed Pre-Ignition Behavior,” *SAE Int. J. Engines*, vol. 10, no. 3, pp. 2017-01–0685, Mar. 2017.

[31] H. Vafamehr, A. Cairns, O. Sampson, and M. M. Koupaie, “The competing chemical and physical effects of transient fuel enrichment on heavy knock in an optical spark ignition engine,” *Appl. Energy*, vol. 179, pp. 687–697, 2016.

[32] G. T. Kalghatgi, “The outlook for fuels for internal combustion engines,” *Int. J. Engine Res.*, vol. 15, no. 4, pp. 383–398, 2014.

[33] D. Splitter, B. Kaul, J. Szybist, and G. Jatana, “Engine Operating Conditions and Fuel Properties on Pre-Spark Heat Release and SPI Promotion in SI Engines,” *SAE Int. J. Engines*, vol. 10, no. 3, 2017.

[34] Z. Wang *et al.*, “Investigation on Pre-ignition and Super-Knock in Highly Boosted Gasoline Direct Injection Engines,” *SAE Tech. Pap.*, no. 2014-01–1212, 2014.

[35] M. Khosravi, H. Ruhland, T. Lorenz, and C. Weber, “Investigation into Occurrence of Megaknock and Auto-Ignition in GTDI Engines,” no. 2017-01–0690, 2017.

[36] K. Hatano, K. Lida, H. Higashi, and S. Murata, “Development of a New Multi-Mode Variable Valve Timing Engine,” *SAE Tech. Pap.*, no. 930878, 1993.

[37] P. H. Dugdale, R. J. Rademacher, B. R. Price, J. W. Subhedar, and R. L. Duguay, “Ecotec 2 . 4L VVT : A Variant of GM ’ s Global 4-Cylinder Engine,” *SAE Tech. Pap.*, no. 2005-01–1941, 2005.

[38] I. Gentile, M. Pirelli, and G. Mastrangelo, “The New FIRE 1 , 4 8v and 16v VVT Engine Family : an The New FIRE 1 , 4 8v and 16v VVT Engine Family : a n Unique Approach to Reduce Fuel Consumption,” *SAE Tech. Pap.*, no. 2005-24–076, 2005.

[39] M. Hakariya, T. Toda, and M. Sakai, “The New Toyota Inline 4-cylinder 2.5L Gasoline Engine,” *SAE Tech. Pap.*, no. 2017-01–1021, 2017.

[40] C. Brüstle and D. Schwarzenthal, “VarioCam Plus - A Highlight of the Porsche 911 Turbo Engine,” *SAE Tech. Pap. 2001-01-0245*, vol. 2001, no. 724, 2001.

[41] G. Vent, C. Enderle, N. Merdes, F. Kreitmann, and R. Weller, “The New 2 .0l Turbo Engine from the Mercedes- Benz 4-Cylinder Engine Family,” in *2nd Aachen Colloquium China*, 2012, pp. 1–23.

[42] M. Shibata *et al.*, “New 1.0L I3 Turbocharged Gasoline Direct Injection Engine,” *SAE Tech. Pap.*, no. 2017-01–1029, Mar. 2017.

[43] R. Flierl and M. Kluting, “The Third Generation of Valvetrains – New Fully Variable Valvetrains for Throttle-Free Load Control,” *SAE Tech. Pap.*, no. 2000-01–1227, 2000.

[44] C. Luttermann, E. Schueenemann, and N. Klauer, “Enhanced VALVETRONIC technology for meeting SULEV emission requirements.,” *Soc. Automot. Eng. [Special Publ. SP*, vol. SP-2025, no. Advanced Catalysts and Substrates 2006, pp. 7–11, 2006.

[45] W. Gottschalk, U. Lezius, and L. Mathusall, “Investigations on the Potential of a Variable Miller Cycle for SI Knock Control,” Apr. 2013.

[46] I. Trevas, C. Pimenta, H. Fernandes, M. Carvalho, and R. Montemor, “Combustion Analysis on a Variable Valve Actuation Spark Ignition Engine Operating With E22 and E100,” *SAE Tech. Pap.*, no. 2017-01–1069, 2017.

[47] S. Takemura *et al.*, “A Study of a Continuous Variable Valve Event and Lift (VEL) System,” *SAE Tech. Pap.*, no. 2001-01–0243, 2001.

[48] T. Sugiyama, R. Hiyoshi, S. Takemura, and S. Aoyama, “Technology for Improving Engine Performance using Variable Mechanisms,” *SAE Tech. Pap.*, no. 2007-01–1290, 2007.

[49] T. Fujita, K. Onogawa, S. Kiga, Y. Mae, Y. Akasaka, and K. Tomogane, “Development of Innovative Variable Valve Event and Lift (VVEL) System,” *SAE Tech. Pap.*, no. 2008-01–1349, 2008.

[50] A. Titolo, “The Variable Valve Timincl - System - Application on a V8 Engine,” *SAE Tech. Pap.*, no. 910009, 2015.

[51] M. Haase and T. Piecyk, “Get ready for the combustion strategies of tomorrow: Variable Valvetrain,” *Schaeffler Symp. 2014*, pp. 188–201, 2014.

[52] L. A. Gould, W. E. Richeson, and F. L. Erickson, “Performance Evaluation of a Camless Engine Using Valve Actuators with Programmable Timing,” *SAE Tech. Pap.*, no. 910450, Feb. 1991.

[53] M. Pischinger, W. Salber, F. Staay, H. Baumgarten, and H. Kemper, “Benefits of the Electromechanical Valve Train in Vehicle Operation,” *SAE Tech. Pap.*, no. 2000-01–1223, 2000.

[54] J. Allen and D. Law, “Production Electro-Hydraulic Variable Valve-Train for a New Generation of I . C . Engines,” *SAE Tech. Pap.*, no. 2002-01–1109, 2002.

[55] J. W. G. Turner, M. D. Bassett, R. J. Pearson, G. Pitcher, and K. J. Douglas, “New Operating Strategies Afforded by Fully Variable Valve Trains,” *SAE Tech. Pap.*, no. 2004-01–1386, 2004.

[56] N. Milovanovic, D. Blundell, S. Gedge, and J. Turner, “Cam Profile Switching (CPS) and phasing strategy vs Fully Variable Valve Train (FVVT) strategy for transitions between spark ignition and controlled auto ignition modes,” *SAE Tech. Pap.*, no. 2005-01–0766, 2005.

[57] RICARDO, “Case Study: Stroke of genius for gasoline downsizing,” *Q3, 2008 Ricardo Q. Rev.*, pp. 8–14, 2008.

[58] D. Shao, X. Sichuan, and A. Du, “Research on a New Electromagnetic Valve

Actuator Based on Voice Coil Motor for Automobile Engines A New Design of Voice Coil Electromagnetic Valve," *SAE Tech. Pap.*, no. 2017-01–1070, 2017.

[59] Freevalve, "Freevalve Technology," 2017. [Online]. Available: http://www.freevalve.com/. [Accessed: 18-Apr-2017].

[60] Y. Zhang and H. Zhao, "Investigation of combustion, performance and emission characteristics of 2-stroke and 4-stroke spark ignition and CAI/HCCI operations in a DI gasoline," *Appl. Energy*, vol. 130, pp. 244–255, Oct. 2014.

[61] G. A. Lavoie, E. Ortiz-Soto, A. Babajimopoulos, J. B. Martz, and D. N. Assanis, "Thermodynamic sweet spot for high-efficiency, dilute, boosted gasoline engines," *Int. J. Engine Res.*, vol. 14, no. 3, pp. 260–278, 2013.

[62] L. Mikulic, J. Schommers, B. Geringer, K. Wolf, and C. Enderle, "Variable Gas Exchange Systems for S.I. Engines - Layout and Experimental Data," *SAE Tech. Pap.*, no. 920296, 1992.

[63] P. Kreuter, P. Heuser, and M. Schebitz, "Strategies to improve SI-engine performance by means of variable intake lift , timing and duration," *SAE Tech. Pap.*, p. 920449, 1992.

[64] Y. Urata, H. Umiyama, K. Shimizu, Y. Fujiyoshi, H. Sono, and K. Fukuo, "A Study of Vehicle Equipped with Non-Throttling S.I. Engine with Early Intake Valve Closing Mechanism," *SAE Tech. Pap.*, no. 930820, 1993.

[65] S. Nagumo and S. Hara, "Study of fuel economy improvement through control of intake valve closing timing: cause of combustion deterioration and improvement," *JSAE Rev.*, vol. 16, no. 1, pp. 13–19, 1995.

[66] M. Battistoni and F. Mariani, "Fluid Dynamic Study of Unthrottled Part Load SI Engine Operations with Asymmetric Valve Lifts," *SAE Tech. Pap.*, no. 2009-24–17, 2009.

[67] I. Bücker, D.-C. Karhoff, M. Klaas, and W. Schröder, "Engine In-Cylinder Flow Control via Variable Intake Valve Timing," *SAE Tech. Pap.*, no. 2013-24–0055, 2013.

[68] F. Soderberg and B. Johansson, "Fluid flow, combustion and efficiency with early and late inlet valve closing," *SAE Tech. Pap.*, no. 972937, 1997.

[69] P. Stansfield *et al.*, “Unthrottled engine operation using variable valve activation: the impact on the flow field, mixing and combustion.,” *SAE Tech. Pap.*, no. 2007011414, 2007.

[70] R. Patel *et al.*, “Un-throttling a direct injection gasoline homogeneous mixture engine with variable valve actuation,” *Int. J. Engine Res.*, vol. 11, no. 6, pp. 391–411, 2010.

[71] D. Cleary and G. Silvas, “Unthrottled engine operation with variable intake valve lift , duration , and timing,” *SAE Tech. Pap.*, vol. 2007, no. 724, pp. 2007-01–1282, 2007.

[72] S. Shiga, H. Nakamura, T. Karasawa, S. Yagi, M. Morita, and T. Matsumoto, “Effect of early-closing of intake-valve on the engine performance in a spark-ignition engine,” *SAE Tech. Pap.*, no. 960585, 1996.

[73] M. M. Ojapah, H. Zhao, and Y. Zhang, “Effects of Ethanol on Performance and Exhaust Emissions from a DI Spark Ignition Engine with Throttled and Unthrottled Operations Experimental Set-Up,” *SAE Tech. Pap.*, no. 2014-01–1393, 2015.

[74] M. M. Ojapah, H. Zhao, and Y. Zhang, “Effects of ethanol on combustion and emissions of a gasoline engine operating with different combustion modes,” *Int. J. Engine Res.*, vol. 17, no. 9, pp. 998–1011, Mar. 2016.

[75] Y. Wan and A. Du, “Reducing part load pumping loss and improving thermal efficiency through high compression ratio over-expanded cycle,” *SAE Tech. Pap.*, no. 2013-01–1744, 2013.

[76] K. C. Tsao, C. L. Wang, and E. M. Miller, “Performance of Gasoline-Water Fuel in a Modified SI Engine,” *SAE Tech. Pap.*, no. 841399.

[77] Y. Li, H. Zhao, P. Stansfield, and P. Freeland, “Synergy between Boost and Valve Timings in a Highly Boosted Direct Injection Gasoline Engine Operating with Miller Cycle Experimental Set-Up,” *SAE Tech. Pap.*, no. 2015-01–1262, 2015.

[78] G. B. Parvate-Patil, H. Hong, and B. Gordon, “An assessment of intake and exhaust philosophies for variable valve timing,” *SAE Tech. Pap.*, no. 2003-32–0078, 2003.

[79] S. C. Blakey, R. J. Saunders, T. H. Ma, and A. Chopra, “A Design and Experimental Study of an Otto Atkinson Cycle Engine Using Late Intake Valve Closing,” *SAE Tech. Pap.*, no. 910451, 1991.

[80] M. Sellnau and E. Rask, “Two-step variable valve actuation for fuel economy, emissions, and performance,” *SAE Tech. Pap.*, no. 2003-01–0029, 2003.

[81] S. M. Rabia and M. Abd-El-Halim, “Effect of Valve Timing and Exhaust Back Pressure on the Performance of,” *J. Eng. Sci. Assiut Univ.*, vol. 38, no. 3, pp. 685–696, 2010.

[82] J. Taylor, N. Fraser, R. Dingelstadt, and H. Hoffmann, “Benefits of late inlet valve timing strategies afforded through the use of intake Cam-In-Cam applied to a gasoline turbocharged downsized engine,” *SAE Tech. Pap.*, no. 2011-01–0360, 2011.

[83] C. Wang, R. Daniel, and X. Ma, “Comparison of Gasoline (ULG), 2 , 5-Dimethylfuran (DMF) and Bio-Ethanol in a DISI Miller Cycle with Late Inlet Valve Closing Time,” *SAE Tech. Pap.*, no. 2012-01–1147, 2012.

[84] D. J. Haugen, P. L. Blackshear, and M. J. Pipho, “Modifications of a Quad 4 Engine to Permit Late Intake Valve Closure,” *SAE Tech. Pap.*, no. 921663, 1992.

[85] M. E. S. Martins and T. D. M. Lanzanova, “Full-load Miller cycle with ethanol and EGR: Potential benefits and challenges,” *Appl. Therm. Eng.*, vol. 90, pp. 274–285, 2015.

[86] M. Scheidt, J. Kuhl, M. Elicker, and D. Wolf, “Potential of combustion control by valvetrain variability (in German),” in *Engine Combustion Processes - Current Problems and Modern Techniques (XIIIth Congress)*, 2017, pp. 409–425.

[87] J. Corberan, A. Perez, and R. Royo, “Study about burned gas fraction and its relationship with engine performance at low loads,” *SAE Tech. Pap.*, no. 940215, 1994.

[88] H. Sandquist, J. Wallesten, K. Enwald, and S. Stromberg, “Influence of Valve Overlap Strategies on Residual Gas Fraction and Combustion in a Spark-ignition Engine at Idle,” *SAE Tech. Pap.*, no. 972936, 1997.

[89] H. A. Cikanek, M. Haghgooie, C. E. Newnan, G. C. Davis, and F. M. Co, “The Effect of Valve Overlap on Idle Operation : Comparison of Model and

Experiment," *SAE Tech. Pap.*, no. 932751, 1993.

[90] A. Ghauri, S. H. Richardson, and C. J. E. Nightingale, "Variation of Both Symmetric and Asymmetric Valve Events on a 4-Valve SI Engine and the Effects on Emissions and Fuel Economy," *SAE Tech. Pap.*, no. 2000-01–1222, 2000.

[91] C. Yang, H. Zhao, and T. Megaritis, "Investigation of CAI Combustion with Positive Valve Overlap and Enlargement of CAI Operating Range," *SAE Tech. Pap.*, no. 2009-01–1104, 2009.

[92] H. Yun, N. Wermuth, and P. Najt, "High Load HCCI Operation Using Different Valving Strategies in a Naturally-Aspirated Gasoline HCCI Engine," *SAE Tech. Pap.*, no. 2011-01–0899, 2011.

[93] L. Li, H. Xie, T. Chen, W. Yu, and H. Zhao, "Experimental Study on Spark Assisted Compression Ignition (SACI) Combustion with Positive Valve Overlap in a HCCI Gasoline Engine," *SAE Tech. Pap.*, no. 2012-01–1126, 2012.

[94] H. Xie, L. Li, T. Chen, W. Yu, X. Wang, and H. Zhao, "Study on spark assisted compression ignition (SACI) combustion with positive valve overlap at medium-high load," *Appl. Energy*, vol. 101, pp. 622–633, 2013.

[95] J. B. Heywood, *Internal Combustion Engine Fundamentals*, 1st ed., vol. 21. McGraw-Hil, 1988.

[96] A. Wolany, C. Glahn, H.-J. Berner, and M. Bargende, "Investigation of the Gas Exchange (Scavenging) on a Single-Scroll Turbocharged Four Cylinder GDI Engine," *SAE Tech. Pap.*, no. 2016-01–1024, Apr. 2016.

[97] D. Law, D. Kemp, J. Allen, G. Kirkpatrick, and T. Copland, "Controlled Combustion in an IC-Engine with a Fully Variable Valve Train," *SAE Tech. Pap.*, no. 2001-01–0251, 2001.

[98] L. Koopmans and I. Denbratt, "A four-stroke camless engine, operated in homogeneous charge compression ignition mode with commercial gasoline," *SAE Tech. Pap.*, no. 2001-01–3610, 2001.

[99] H. Zhao, J. Li, T. Ma, and N. Ladommatos, "Performance and analysis of a 4-stroke multi-cylinder gasoline engine with CAI combustion," no. 2002-01–0420, 2002.

[100] Y. Zhang, B.-Q. He, H. Xie, and H. Zhao, “The Combustion and Emission Characteristics of Ethanol on a Port Fuel Injection HCCI Engine,” *SAE Tech. Pap.*, no. 2006-01–0631, 2006.

[101] T. Urushihara, K. Hiraya, A. Kakuhou, and T. Itoh, “Expansion of HCCI operating region by the combination of direct fuel injection, negative valve overlap and internal fuel reformation,” *SAE Tech. Pap.*, no. 10.4271/2003-01-0749, 2003.

[102] G. Gnanam, M. Johnson, A. Sobiesiak, and G. Reader, “HCCI Combustion With Internal Fuel Reforming , Varied Levels of EGR and Charge Preheat - A Computational Study,” *SAE Tech. Pap.*, no. 2005-01–0140, 2005.

[103] M. Tongroon and H. Zhao, “Analysis of the effect of direct injection of alcohol fuel on minor heat release reactions and controlled autoignition combustion,” *Proc. Inst. Mech. Eng. Part D J. Automob. Eng.*, vol. 226, no. 12, pp. 1678–1688, May 2012.

[104] H. Zhao, *HCCI and CAI engines for the automotive industry*. Woodhead Pub., 2007.

[105] V. Knop, L. de Francqueville, F. Duffour, and F. Vangraefschèpe, “Influence of the Valve-lift Strategy in a CAI^{TM} Engine using Exhaust Gas Re-Breathing - Part 2: Optical Diagnostics and 3D CFD Results,” *SAE Int. J. Engines*, vol. 2, no. 1, pp. 2009-01–0495, Apr. 2009.

[106] A. Fuerhapter, W. F. Piock, and G. K. Fraidl, “CSI - Controlled Auto Ignition - the Best Solution for the Fuel Consumption - Versus Emission Trade-Off?,” *SAE Tech. Pap.*, no. 2003-01–0754, 2003.

[107] a Fuerhapter, E. Unger, W. F. Piock, and G. K. Fraidl, “The new AVL CSI Engine – HCCI Operation on a Multi Cylinder Gasoline Engine,” *SAE Tech. Pap.*, no. 2004-01–0551, 2004.

[108] F. Duffour, F. Vangraefschèpe, V. Knop, and L. De Francqueville, “Influence of the Valve-lift Strategy in a CAI^{TM} Engine using Exhaust Gas Re-Breathing – Part 1: Experimental Results and 0D Analysis,” *SAE Tech. Pap.*, no. 2009-01–0299, 2009.

[109] D. Tomazic, H. Kleeberg, S. Bowyer, J. Dohmen, K. Wittek, and B. Hakke, “Two-Stage Variable Compression Ratio (VCR) System to Increase Efficiency in Gasoline Powertrains,” *Directions in Engine-Efficiency and Emissions Research*

(DEER), 2012. [Online]. Available: https://energy.gov/sites/prod/files/2014/03/f8/deer12_tomazic.pdf. [Accessed: 20-Jan-2017].

[110] S. Wolfgang, H. Sorger, S. Loesch, W. Unzeitig, T. Huettner, and A. Fuerhapter, “The 2-Step VCR Conrod System - Modular System for High Efficiency and Reduced CO2,” *SAE Tech. Pap.*, no. 2017-01–0634, 2017.

[111] M. H. Shelby, T. G. Leone, K. D. Byrd, and F. K. Wong, “Fuel Economy Potential of Variable Compression Ratio for Light Duty Vehicles,” *SAE Int. J. Engines*, vol. 10, no. 3, pp. 2017-01–0639, 2017.

[112] P. Borgqvist, P. Tunestål, and B. Johansson, “Investigation and Comparison of Residual Gas Enhanced HCCI using Trapping (NVO HCCI) or Rebreathing of Residual Gases,” *SAE Pap.*, no. 2011-01–1772, pp. 925–942, 2011.

[113] M. Sjöberg, E. Lars-Olof, T. Eliassen, L. Magnusson, and H. E. Ãngstrom, “GDI HCCI: Effects of Injection Timing and Air Swirl on Fuel Stratification, Combustion and Emission Formation,” *SAE Tech. Pap.*, no. 2002-01–01, 2002.

[114] S. M. Aceves, D. Flowers, J. R. Smith, and R. Dibble, “HCCI Engine Control by Thermal Management,” *SAE Tech. Pap.*, no. 200-01–2869, 2000.

[115] Nikkei, “Mazda’s new engine boosts fuel efficiency by 30%,” 2017. [Online]. Available: http://asia.nikkei.com/Business/Companies/Mazda-s-new-engine-boosts-fuel-efficiency-by-30. [Accessed: 20-Jan-2017].

[116] H. Persson, J. Sit, E. Kristensson, and B. Johansson, “Study of Fuel Stratification on SparkAssisted Compression Ignition (SACI) Combustion with Ethanol Using High Speed Fuel PLIF Study of Fuel Stratification on Spark Assisted Compression Ignition (SACI) Combustion with Ethanol Using High Speed Fuel PLIF,” no. 724, pp. 776–790, 2008.

[117] L. Manofsky, J. Vavra, D. Assanis, and A. Babajimopoulos, “Bridging the Gap between HCCI and SI: Spark-Assisted Compression Ignition,” *SAE Tech. Pap.*, no. 2011-01–1179, 2011.

[118] L. M. Olesky, J. B. Martz, G. a. Lavoie, J. Vavra, D. N. Assanis, and A. Babajimopoulos, “The effects of spark timing, unburned gas temperature, and negative valve overlap on the rates of stoichiometric spark assisted compression ignition combustion,” *Appl. Energy*, vol. 105, pp. 407–417, May 2013.

[119] D. Lorenz and D. Morris, *How much energy does it take to make a gallon of ethanol?*, no. August. Institute for Local Self-Reliance, 1995.

[120] H. Shapouri, J. Duffield, and M. Wang, “The energy balance of corn ethanol revisited.,” *Trans. Soc. Agric. Eng.*, vol. 46, no. 4, pp. 959–968, 2003.

[121] J. Hill, “Environmental costs and benefits of transportation biofuel production from food- and lignocellulose-based energy crops . A review To cite this version : Environmental costs and benefits of transportation biofuel production from food- and lignocellulose-ba,” 2007.

[122] M. O. S. Dias, M. P. Cunha, C. D. F. Jesus, and I. G. Mirna, “Simulation of ethanol production from sugarcane in Brazil : economic study of an autonomous distillery,” 2010.

[123] M. O. S. Dias, M. Modesto, A. V. Ensinas, S. a. Nebra, R. M. Filho, and C. E. V. Rossell, “Improving bioethanol production from sugarcane: evaluation of distillation, thermal integration and cogeneration systems,” *Energy*, vol. 36, no. 6, pp. 3691–3703, Jun. 2011.

[124] F. A. Pazuch, C. E. C. Nogueira, S. N. M. Souza, V. C. Micuanski, L. Friedrich, and A. M. Lenz, “Economic evaluation of the replacement of sugar cane bagasse by vinasse, as a source of energy in a power plant in the state of Paraná, Brazil,” *Renew. Sustain. Energy Rev.*, vol. 76, no. March, pp. 34–42, 2017.

[125] D. Dai, Z. Hu, G. Pu, H. Li, and C. Wang, “Energy efficiency and potentials of cassava fuel ethanol in Guangxi region of China,” *Energy Convers. Manag.*, vol. 47, no. 13–14, pp. 1686–1699, Aug. 2006.

[126] T. L. T. Nguyen, S. H. Gheewala, and S. Garivait, “Energy balance and GHG-abatement cost of cassava utilization for fuel ethanol in Thailand,” *Energy Policy*, vol. 35, no. 9, pp. 4585–4596, Sep. 2007.

[127] R. Prakash, A. Henham, and I. Krishnan Bhat, “Net energy and gross pollution from bioethanol production in India,” *Fuel*, vol. 77, no. 14, pp. 1629–1633, Nov. 1998.

[128] E. R. E. C. (EREC), *Renewable Energy in Europe: Markets, Trends, and Technologies*, Second Ed. London: Earthscan Ltd, 2010.

[129] A. Walter *et al.*, “Sustainability assessment of bio-ethanol production in Brazil considering land use change, GHG emissions and socio-economic aspects,” *Energy Policy*, vol. 39, no. 10, pp. 5703–5716, Oct. 2011.

[130] M. R. Maroun and E. L. La Rovere, “Ethanol and food production by family smallholdings in rural Brazil: Economic and socio-environmental analysis of micro distilleries in the State of Rio Grande do Sul,” *Biomass and Bioenergy*, vol. 63, pp. 140–155, Apr. 2014.

[131] M. Bruins and J. Sanders, “Small-scale processing of biomass for biorefinery,” *Biofuels, Bioprod. Biorefining*, pp. 135–145, 2012.

[132] F. D. Mayer, L. A. Feris, N. R. Marcilio, and R. Hoffmann, “Why small-scale fuel ethanol production in Brazil does not take off?,” *Renew. Sustain. Energy Rev.*, vol. 43, pp. 687–701, Mar. 2015.

[133] F. Rosillo-Calle and L. A. B. Cortez, “Towards ProAlcool II—a review of the Brazilian bioethanol programme,” *Biomass and Bioenergy*, vol. 14, no. 2, pp. 115–124, Mar. 1998.

[134] C. R. Soccol *et al.*, “Brazilian biofuel program: An overview,” *J. Sci. Ind. Res. (India).*, vol. 64, no. 11, pp. 897–904, 2005.

[135] D. Bentivoglio, A. Finco, and M. Bacchi, “Interdependencies between Biofuel, Fuel and Food Prices: The Case of the Brazilian Ethanol Market,” *Energies*, vol. 9, no. 6, p. 464, Jun. 2016.

[136] G. B. Machado, T. C. C. de Melo, and L. A. de Mendonça Soares, “Flex Fuel Engine - Influence of Fuel Composition on the CA50 at Maximum Brake Torque Condition,” *SAE Tech. Pap.*, no. 2015360215, Sep. 2015.

[137] J. A. DUFFIELD, I. M. XIARCHOS, and S. A. HALBROOK, “ETHANOL POLICY. PAST, PRESENT, AND FUTURE,” *SdL Rev*, vol. 53, p. 425, 2008.

[138] J. D. Stephen, W. E. Mabee, and J. N. Saddler, “Will second-generation ethanol be able to compete with first-generation ethanol? Opportunities for cost reduction,” *Biofuels, Bioprod. Biorefining*, vol. 6, no. 2, pp. 159–176, Mar. 2012.

[139] M. Henderson, N. Koehler, J. Seurer, and B. Dinneen, “2017 ETHANOL INDUSTRY OUTLOOK,” 2017.

[140] European Parliament, “Directive 2009/28/EC of the European Parliament and of the Council of 23 April 2009,” *Off. J. Eur. Union*, vol. 140, no. 16, pp. 16–62, 2009.

[141] European Union, “Directive 2009/30/EC of the European Parliament and of the Council,” *Off. J. Eur. Union*, no. April, p. L140/88-L140/113, 2009.

[142] Biofuelsdigest.com, “Biofuels mandates around the world: 2016.” [Online]. Available: http://www.biofuelsdigest.com/bdigest/2016/01/03/biofuels-mandates-around-the-world-2016/. [Accessed: 11-Apr-2017].

[143] U.S. Department of Energy, “Alternative Fuels Data Center,” *Global Ethanol Production*, 2016. [Online]. Available: http://www.afdc.energy.gov/data/?q=ethanol. [Accessed: 11-Apr-2017].

[144] RFA, “Industry Statistics - World Fuel Ethanol Production,” 2017. [Online]. Available: http://www.ethanolrfa.org/. [Accessed: 11-Apr-2017].

[145] J. Hill, E. Nelson, D. Tilman, S. Polasky, and D. Tiffany, “Environmental, economic, and energetic costs and benefits of biodiesel and ethanol biofuels.,” *Proc. Natl. Acad. Sci. U. S. A.*, vol. 103, no. 30, pp. 11206–10, Jul. 2006.

[146] C. Manzatto and E. Assad, “Zoneamento agroecológico da cana-de-açúcar: expandir a produção, preservar a vida, garantir o futuro. [In Portuguese],” Rio de Janeiro - Brasil, 2009.

[147] S. Bringezu, H. Schütz, M. O´Brien, L. Kauppi, R. W. Howarth, and J. McNeely, *Towards sustainable production and use of resources: assessing biofuels*. UNEP (United Nations Environment Programme), 2009.

[148] A. Elbehri, A. Segerstedt, and P. Liu, *Biofuels and the sustainability challenge: A global assessment of sustainability issues, trends and policies for biofuels and related feedstocks*. Rome: Food And Agriculture Organization of the United Nations (FAO), 2013.

[149] DG MOVE - Expert group on future transport fuels, *State of the Art on Alternative Fuels Transport Systems in the European Union*. 2015.

[150] D. Özçimen and B. Inan, “An Overview of Bioethanol Production From Algae,” in *Biofuels - Status and Perspective*, InTechOpen, 2015.

[151] U.S. Department of Energy, “Scientists Accidentally Turned CO2 Into Ethanol,” 2016. [Online]. Available: energy.gov/articles/scientists-accidentally-turned-co2-ethanol. [Accessed: 12-Apr-2017].

[152] R. A. Stein, J. E. Anderson, and T. J. Wallington, “An Overview of the Effects of Ethanol-Gasoline Blends on SI Engine Performance, Fuel Efficiency, and Emissions,” *SAE Int. J. Engines*, vol. 6, no. 1, pp. 2013-01–1635, Apr. 2013.

[153] T. G. Leone, E. D. Olin, J. E. Anderson, H. H. Jung, M. H. Shelby, and R. A. Stein, “Effects of Fuel Octane Rating and Ethanol Content on Knock, Fuel Economy, and CO2 for a Turbocharged DI Engine,” *SAE Int. J. Fuels Lubr.*, vol. 7, no. 1, pp. 9–28, 2014.

[154] P. Yuen, W. Villaire, and J. Beckett, “Automotive Materials Engineering Challenges and Solutions for the Use of Ethanol and Methanol Blended Fuels,” *SAE Tech. Pap.*, no. 2010-01–0729, 2010.

[155] X. Lou and P. M. Singh, “Role of water, acetic acid and chloride on corrosion and pitting behaviour of carbon steel in fuel-grade ethanol,” *Corros. Sci.*, vol. 52, no. 7, pp. 2303–2315, 2010.

[156] T. C. C. De Melo *et al.*, “Different Hydrous Ethanol-Gasoline Blends - FTIR Emissions of a Flex-Fuel Engine and Chemical Properties of the Fuels,” *SAE Tech. Pap.*, no. 2011-36–0080.

[157] B. M. Masum, H. H. Masjuki, M. a. Kalam, I. M. Rizwanul Fattah, S. M. Palash, and M. J. Abedin, “Effect of ethanol–gasoline blend on NOx emission in SI engine,” *Renew. Sustain. Energy Rev.*, vol. 24, pp. 209–222, Aug. 2013.

[158] M. Thewes, M. Müther, A. Brassat, S. Pischinger, and A. Sehr, “Analysis of the Effect of Bio-Fuels on the Combustion in a Downsized DI SI Engine,” *SAE Int. J. Fuels Lubr.*, vol. 5, no. 1, pp. 274–288, 2012.

[159] J. A. Quintero, M. I. Montoya, O. J. Sánchez, O. H. Giraldo, and C. A. Cardona, “Fuel ethanol production from sugarcane and corn: Comparative analysis for a Colombian case,” *Energy*, vol. 33, no. 3, pp. 385–399, Mar. 2008.

[160] M. R. Ladisch and K. Dyck, “Dehydration of ethanol: new approach gives positive energy balance.,” *Science*, vol. 205, no. 4409, pp. 898–900, Aug. 1979.

[161] H. J. Huang, S. Ramaswamy, U. W. Tschirner, and B. V. Ramarao, “A review of

separation technologies in current and future biorefineries," *Sep. Purif. Technol.*, vol. 62, no. 1, pp. 1–21, 2008.

[162] W.-C. Chen *et al.*, "Optimizing the efficiency of anhydrous ethanol purification via regenerable molecular sieve," *Appl. Energy*, vol. 135, pp. 483–489, Dec. 2014.

[163] D. L. Flowers, S. M. Aceves, and J. M. Frias, "Improving Ethanol Life Cycle Energy Efficiency by Direct Utilization of Wet Ethanol in HCCI Engines," in *SAE Technical Paper*, 2007, no. 2007-01–1867, pp. 1070–1078.

[164] J. H. Mack, S. M. Aceves, and R. W. Dibble, "Demonstrating direct use of wet ethanol in a homogeneous charge compression ignition (HCCI) engine," *Energy*, vol. 34, no. 6, pp. 782–787, Jun. 2009.

[165] E. L. López-Plaza *et al.*, "Experimental and Theoretical Study of the Energy Savings from Wet Ethanol Production and Utilization," *Energy Technol.*, vol. 2, no. 5, pp. 440–445, May 2014.

[166] J. L. S. Fagundez, M. E. S. Martins, and N. P. G. Salau, "Study of Wet Ethanol Energy Balance: From Production to Fuel," *SAE Tech. Pap.*, no. 2015360485, Sep. 2015.

[167] J. L. S. Fagundez, R. L. Sari, F. D. Mayer, M. E. S. Martins, and N. P. G. Salau, "Determination of optimal wet ethanol composition as a fuel in spark ignition engine," *Appl. Therm. Eng.*, vol. 112, pp. 317–325, Feb. 2017.

[168] D. A. Salla, F. de P. B. Furlaneto, C. Cabello, and R. A. D. Kanthack, "Estudo energético da produção de biocombustível a partir do milho Energetic study of ethanol production from the corn crops," *Ciência Rural*, vol. 40, no. 9, pp. 2017–2022, 2010.

[169] D. A. Salla, F. de P. B. Furlaneto, C. Cabello, and R. A. D. Kanthack, "Avaliação energética da produção de etanol utilizando como matéria-prima a cana-de-açúcar," *Ciência Rural*, vol. 39, no. 8, pp. 2516–2520, 2009.

[170] D. A. Salla, "Análise energética de sistemas de produção de etanol de mandioca, cana-de-açúcar e milho," UNIVERSIDADE ESTADUAL PAULISTA Faculdade De Ciências Agronômicas Campus De Botucatu, 2008.

[171] H. Shapouri, J. A. Duffield, and M. Wang, "The Energy Balance of Corn Ethanol: An Update," 2002.

[172] T. D. M. Lanzanova, M. Dalla Nora, and H. Zhao, “Performance and economic analysis of a direct injection spark ignition engine fueled with wet ethanol,” *Appl. Energy*, vol. 169, pp. 230–239, May 2016.

[173] H. a Saffy, W. F. Northrop, D. B. Kittelson, and A. M. Boies, “Energy , carbon dioxide and water use implications of hydrous ethanol production,” *Energy Convers. Manag.*, vol. 105, pp. 900–907, 2015.

[174] R. Wiebe and J. C. Porter, *Alcohol-water injection for spark-ignition engines*. Peoria, Illinois, 1949.

[175] A. Rotz, M. Cruz, R. Wilkinson, and B. Stout, *Utilization of alcohol in spark ignition and diesel engines - Extension Bulletin E01426*. Michigan: Michigan State University, 1980.

[176] J. L. Taraba, M. Turner, and R. Razor, *The Use of Ethanol as an Unmixed Fuel for Internal Combustion Engines by*. Lexington, Kentucky: Department of Agricultural Engineering, 1981.

[177] J. Olberding, D. C. S. Beyerlein, J. Steciak, and M. Cherry, “Dynamometer Testing of an Ethanol-Water Fueled Transit Van,” in *SAE Technical Paper*, 2005, no. 2005-01–3706.

[178] S. Beyerlein, D. McIlroy, D. Blackkketter, J. Steciak, E. Clarke, and A. Morton, “Homogeneous Charge Combustion of Aqueous Ethanol,” *Final Report, Res. Spec. Programs Adm. - U.S. Dep. Transp.*, 2001.

[179] D. Cordon, E. Clarke, S. Beyerlein, J. Steciak, and M. Cherry, “Catalytic Igniter to Support Combustion of Ethanol-Water/Air Mixtures in Internal Combustion Engines,” *SAE Tech. Pap.*, no. 2002-01–2863, 2002.

[180] S. Brewster, D. Railton, M. Maisey, and R. Frew, “The effect of E100 water content on high load performance of a spray guide direct injection boosted engine,” *SAE Tech. Pap.*, no. 2007-01–2648, 2007.

[181] A. Dal Bem, “Análise de desempenho de um motor ciclo Otto alimentado com álcool de 75 INPM,” Thesis of: Universidade de São Paulo [in Portuguese], 2008.

[182] A. Megaritis, D. Yap, and M. L. Wyszynski, “Effect of water blending on bioethanol HCCI combustion with forced induction and residual gas trapping,”

Energy, vol. 32, no. 12, pp. 2396–2400, Dec. 2007.

[183] A. Megaritis, D. Yap, and M. L. Wyszynski, “Effect of inlet valve timing and water blending on bioethanol HCCI combustion using forced induction and residual gas trapping,” *Fuel*, vol. 87, no. 6, pp. 732–739, May 2008.

[184] S. Saxena, S. Schneider, S. Aceves, and R. Dibble, “Wet ethanol in HCCI engines with exhaust heat recovery to improve the energy balance of ethanol fuels,” *Appl. Energy*, vol. 98, pp. 448–457, Oct. 2012.

[185] R. Munsin, Y. Laoonual, S. Bavornsethanan, and S. Jugjai, “An Experimental Study on Aldehyde Emissions of a Hydrous Ethanol Fuelled Small SI Engine Generator Set,” in *The First TSME International Conference on Mechanical Engineering*, 2010, p. 8.

[186] R. Munsin, Y. Laoonual, S. Jugjai, and Y. Imai, “An experimental study on performance and emissions of a small SI engine generator set fuelled by hydrous ethanol with high water contents up to 40%,” *Fuel*, vol. 106, pp. 586–592, Apr. 2013.

[187] G. Li *et al.*, “A novel strategy for hydrous-ethanol utilization: Demonstration of a spark-ignition engine fueled with hydrogen-rich fuel from an onboard ethanol/steam reformer,” *Int. J. Hydrogen Energy*, vol. 38, no. 14, pp. 5936–5948, May 2013.

[188] T. D. M. Lanzanova *et al.*, “Performance Analysis of a Spark Ignited Engine Running on Different Water-in-Ethanol Mixtures,” *SAE Tech. Pap.*, no. 2013-36–0202, Oct. 2013.

[189] M. Martins, T. Lanzanova, and R. Sari, “Low Cost Wet Ethanol for Spark-Ignited Engines: Further Investigations,” *SAE Int. J. Fuels Lubr.*, vol. 8, no. 2015-01–0954, pp. 367–373, 2015.

[190] W. M. Ambrós *et al.*, “Experimental analysis and modeling of internal combustion engine operating with wet ethanol,” *Fuel*, vol. 158, pp. 270–278, 2015.

[191] A. Augoye and P. Aleiferis, “Characterization of Flame Development with Hydrous and Anhydrous Ethanol Fuels in a Spark-Ignition Engine with Direct Injection and Port Injection Systems,” *SAE Tech. Pap.*, no. 2015-9–2, Oct. 2014.

[192] M. Dalla Nora, “Experimental and numerical study of a two-stroke poppet valve

engine fuelled with gasoline and ethanol," PhD Thesis: Brunel University London, 2015.

[193] ANVISA, "Alcoometria," in *Farmacopeia Brasileira - Volume 1*, 5th ed., Brasilia, 2010, p. 852.

[194] W. K. Cheng, T. Summers, and N. Collings, "THE FAST-RESPONSE FLAME IONIZATION DETECTOR," vol. 1285, pp. 89–124, 1998.

[195] A. L. Randolph, "Methods of Processing Cylinder-Pressure Transducer Signals to Maximize Data Accuracy," *SAE Tech. Pap.*, no. 900170, 1990.

[196] M. F. J. Brunt and C. R. Pond, "Evaluation of Techniques for Absolute Cylinder Pressure Correction," *SAE Tech. Pap.*, no. 970036, 1997.

[197] N. Ladommatos and H. Zhao, *Engine Combustion Instrumentation and Diagnostics*. SAE International, 2001.

[198] Economic Commission for Europe of the United Nations, "Regulation No 49 of the Economic Commission for Europe of the United Nations (UN/ECE)," *Off. J. Eur. Union*, no. 171, pp. 1–390, 2013.

[199] T. de Melo, M. de Brito, G. Machado, and C. Paiva, "Procedure for Uncertainty of Measurement Determination of Spark Ignition Engine Emission Tests," *SAE Tech. Pap.*, no. 2012-36–0488, 2012.

[200] K. Kar and W. K. Cheng, "Speciated Engine-Out Organic Gas Emissions from a PFI-SI Engine Operating on Ethanol/Gasoline Mixtures," vol. 2, no. 2, pp. 91–101, Nov. 2009.

[201] K. Kar, R. Tharp, M. Radovanovic, I. Dimou, and W. K. Cheng, "Organic gas emissions from a stoichiometric direct injection spark ignition engine operating on ethanol/gasoline blends," *Int. J. Engine Res.*, vol. 11, no. 6, pp. 499–513, Dec. 2010.

[202] T. Wallner, "Correlation Between Speciated Hydrocarbon Emissions and Flame Ionization Detector Response for Gasoline/Alcohol Blends," *J. Eng. Gas Turbines Power*, vol. 133, no. 8, p. 82801, 2011.

[203] W. Attard, N. Fraser, P. Parsons, and E. Toulson, "A Turbulent Jet Ignition Pre-Chamber Combustion System for Large Fuel Economy Improvements in a

Modern Vehicle Powertrain," *SAE Tech. Pap.*, no. 2010-01–1457, 2010.

[204] W. P. Attard and P. Parsons, "Flame Kernel Development for a Spark Initiated Pre-Chamber Combustion System Capable of High Load , High Efficiency and Near Zero NOx Emissions," *SAE Tech. Pap.*, no. 2010-01–2260, 2012.

[205] P. Chinnathambi, M. Bunce, and L. Cruff, "RANS Based Multidimensional Modeling of an Ultra-Lean Burn Pre-Chamber Combustion System with Auxiliary Liquid Gasoline Injection," *SAE Tech. Pap.*, no. 2012-01–0823, 2015.

[206] M. C. Sellnau, J. Sinnamon, K. Hoyer, J. Kim, M. Cavotta, and H. Husted, "Part-Load Operation of Gasoline Direct-Injection Compression Ignition (GDCI) Engine," *SAE Tech. Pap.*, no. 2013-01–0272, 2013.

[207] M. Sellnau, M. Foster, W. Moore, J. Sinnamon, K. Hoyer, and W. Klemm, "Second Generation GDCI Multi-Cylinder Engine for High Fuel Efficiency and US Tier 3 Emissions," *SAE Tech. Pap.*, no. 2016-01–0760, 2016.

[208] T. Alger and S. Wooldridge, "Measurement and Analysis of the Residual Gas Fraction in an SI Engine with Variable Cam Timing," *SAE Tech. Pap.*, no. 2004-01–1356, 2004.

[209] S. Diana, B. Iorio, V. Giglio, and G. Police, "The Effect of Valve Lift Shape and Timing on Air Motion and Mixture Formation of DISI Engines Adopting Different VVA Actuators," *SAE Tech. Pap.*, no. 2001013553, 2001.

[210] O. Hadded and I. Denbratt, "Turbulence Characteristics of Tumbling Air Motion in Four-Valve S.I. Engines and their Correlation with Combustion Parameters," *SAE Tech. Pap.*, no. 910478, 1991.

[211] Y. Li, H. Zhao, Z. Peng, and N. Ladommatos, "Analysis of tumble and swirl motions in a four-valve SI engine.," *SAE Tech. Pap.*, no. 2001013555, 2001.

[212] T. Wang, D. Liu, B. Tan, G. Wang, and Z. Peng, "An investigation into in-cylinder tumble flow characteristics with variable valve lift in a gasoline engine," *Flow, Turbul. Combust.*, vol. 94, no. 2, pp. 285–304, 2015.

[213] A. Villela and G. Machado, "Multifuel Engine Performance, Emissions and Combustion Using Anhydrous and Hydrous Ethanol," *SAE Tech. Pap.*, no. 2012-36–0475, 2012.

[214] S. Saxena, D. Vuilleumier, D. Kozarac, M. Krieck, R. Dibble, and S. Aceves, “Optimal operating conditions for wet ethanol in a HCCI engine using exhaust gas heat recovery,” *Appl. Energy*, vol. 116, pp. 269–277, Mar. 2014.

Appendix 1. Ethanol production data to support ethanol WTT analysis

Tabel A. 1. Ethanol production energy expense from sugarcane and corn (Brazilian scenario).

Salla 2009 [42]		
Sugarcane Ethanol		
Sugar Cane Crop Production Phase	**Energy Expense (MJ L^-1)**	**% Energy expense**
Area preparation	0.1	0.47%
Plantation	0.1	0.47%
Agricultural inputs	0.9	4.21%
Crop maintenance	0.3	1.40%
Harvesting	0.3	1.40%
Transport to industry	0.2	0.93%
Energy deprectiation	0.1	0.47%
Sub Total	**2**	**9.35%**
Milling	0.7	3.27%
Hydrolisis / sacharification / broth treatment	13.8	64.49%
Fermentation	0.1	0.47%
Distillation	4.7	21.96%
Machine Maintenance	0.1	0.47%
Sub Total	**19.4**	**90.65%**
Total	**21.4**	**100.00%**
ETOH ENRGY / PROD. ENERGY	**0.99**	

Salla 2010 [168]		
Corn Ethanol		
Corn Crop Production Phase	**Energy Expense**	**% Energy expense**
Area preparation	0.4	1.87%
Plantation	0.2	0.93%
Agricultural inputs	6.1	28.50%
Crop maintenance	0.7	3.27%
Harvesting	0.3	1.40%
Transport to industry	0.1	0.47%
Energy deprectiation	0.1	0.47%
Sub Total	**7.9**	**36.92%**
Milling	0.7	3.27%
Hydrolisis / sacharification / broth treatment	5.9	27.57%
Fermentation	0.1	0.47%
Distillation	5.1	23.83%
Machine Maintenance	0	0.00%
Sub Total	**11.8**	**55.14%**
Total	**19.7**	**100.00%**
ETOH ENRGY / PROD. ENERGY	**1.08**	

Tabel A. 2. Ethanol production energy expense for cassava (Brazilian scenario).

Salla 2008 [170]		
Cassava Ethanol Brazil		
Cassava Plantation		
Cassava Crop Production Phase	**Energy Expense (MJ L^-1)**	**% Energy expense**
Area preparation	0.27	1.26%
Plantation	0.08	0.37%
Agricultural inputs	0.55	2.57%
Crop maintenance	0.14	0.65%
Harvesting	0.33	1.54%
Transport to industry	0.11	0.51%
Energy deprectiation	0.07	0.33%
Sub Total	**1.55**	**7.24%**
Ethanol Production phase		
Milling	0.22	1.03%
Hydrolisis / sacharification / broth treatment	6.67	31.17%
Fermentation	0.02	0.09%
Distillation	4.85	22.66%
Machine Maintenance	0	0.00%
Sub Total	**11.76**	**54.95%**
Total	**13.31**	**100.00%**
ETHANOL ENERGY / PROD. ENERGY	**1.59**	

Tabel A. 3. Ethanol production energy expense for cassava (Chinese scenario).

Dai 2005 [125]			
Cassava Ethanol China			
		Energy Expense (MJ L^-1)	**% Energy expense**
Plantation		4.336	25.91%
N fertilizer	0.937		
P fertilizer	0.282		
K fertilizer	0.255		
Herbicide	1.728		
Diesel fuel	0.310		
Electricity	0.003		
Stem cuttings	0.002		
Labor	0.82		
Conversion		11.90	71.11%
Coal	11.93		
Electricity output	- 0.029		
Denaturing		0.042	0.25%
Transport		0.452	2.70%
Distribution		0.005	0.03%
Total		16.73	

Tabel A. 4. Ethanol production energy expense for corn (USA scenario A).

Flowers 2007 [163] **- Corn Ethanol**		
Corn Production		
Corn Production Phase	**Energy Expense (MJ L^-1)**	**% Energy expense**
Corn Production	6.03	22%
Transport to industry	0.63	2%
Sub Total	**6.66**	**24%**
Ethanol production phase		
Mashing and cooking	4.36	16%
Distillation	6.27	23%
Dehydration	3.82	14%
Ethanol Distribution	0.44	2%
Sub total	**14.89**	**55%**
Net energy gain in coproducts	4.06	15%
Net energy gain in ethanol	1.62	6%
Total	**21.55**	**100%**
ETHANOL ENERGY / PRODUCTION ENERGY	**1.34**	

Tabel A. 5. Ethanol production energy expense for corn (USA scenario B and C).

Shapouri 2002 [171] **- Corn Ethanol**				
Corn Production Phase	**Dry-Milling**		**Wet-Milling**	
	Energy Expense (MJ L^-1)	**% Energy expense**	**Energy Expense (MJ L^-1)**	**% Energy expense**
Corn Production Phase	6.08	29%	5.98	27%
Corn Transport	0.64	3%	0.63	3%
Ethanol Conversion	13.61	66%	15.13	68%
Ethanol Distribution	0.44	2%	0.44	2%
Total	**20.77**		**22.18**	
ETHANOL ENERGY / PRODUCTION ENERGY	**1.02**		**0.96**	

Tabel A. 6. Energy requirement for ethanol production from different crops.

Energy Requirement (MJ/L)							
Production phase	**Sugarcane (Salla 2009)**	**Cassava (Salla 2008)**	**Cassava (Dai 2005)**	**Corn (Salla 2010)**	**Corn +**	**Corn ++**	**Corn +++**
Feedstock Production	2.00	1.55	4.34	7.90	6.66	6.72	6.61
Ethanol conversion	19.40	11.76	12.36	11.80	14.89	14.05	15.58
Total	21.40	13.31	16.69	19.70	21.55	20.77	22.18
Distillation %	22.0%	22.7%	29.0%	23.8%	23.0%	37.0%	37.0%
Dehydration %					14.0%		
+Flower et al 2007, ++ Shapouri 2002 dry-milling, +++ Shapouri 2002 wet-milling.							

Tabel A. 7. Ethanol energy expense during industrial phase for different crops according to the water-in-ethanol content.

ETHANOL CONVERSION COST								
		Sugar Cane° [42]	**Corn °°** [168]	**Cassava^** [170]	**Cassava^^** [125]	**Corn*** [163]	**Corn**** [171]	**Corn***** [171]
E100 Energy production cost		19.4	11.8	11.8	16.7	14.9	13.6	15.1
Distillation and Dehydration cost		4.7	5.1	4.9	4.9	10.1	9.2	10.2
E96W04	Energy Reduction	1.8	1.9	1.8	1.9	3.8	3.5	3.9
	Production Cost	17.6	9.9	9.9	14.9	11.1	10.1	11.3
	Production Cost Reduction	9.2%	16.4%	15.6%	11.1%	25.6%	25.6%	25.6%
E90W10	Energy Reduction	3.3	3.6	3.4	3.5	7.1	6.3	7.3
	Production Cost	16.1	8.2	8.3	13.3	7.7	7.3	7.8
	Production Cost Reduction	17.2%	30.6%	29.2%	20.8%	48.0%	46.1%	48.3%
E85W15	Energy Reduction	3.5	3.8	3.6	3.7	7.6	6.7	7.7
	Production Cost	15.9	8.0	8.1	13.1	7.3	6.9	7.4
	Production Cost Reduction	18.2%	32.4%	30.9%	22.0%	50.8%	49.2%	51.1%
E80W10	Energy Reduction	3.6	3.9	3.7	3.8	7.7	6.9	7.9
	Production Cost	15.8	7.9	8.0	13.0	7.2	6.7	7.2
	Production Cost Reduction	18.6%	33.2%	31.6%	22.5%	52.0%	50.5%	52.2%
E70W10	Energy Reduction	3.8	4.1	3.9	3.9	8.1	7.2	8.2
	Production Cost	15.6	7.7	7.9	12.8	6.8	6.4	6.9
	Production Cost Reduction	19.4%	34.6%	33.1%	23.5%	54.3%	53.0%	54.5%
E60W40	Energy Reduction	3.9	4.3	4.1	4.1	8.4	7.6	8.6
	Production Cost	15.5	7.5	7.7	12.6	6.5	6.0	6.5
	Production Cost Reduction	20.2%	36.1%	34.5%	24.5%	56.6%	55.6%	56.8%

Brasil	° Salla 2009
	°° Salla 2010
	^ Salla 2008
Asia	^^ Dai 2005: Considering the distillation energy fraction equal to Salla 2008.
USA	* Flowers 2007: considering that 68% of the energy for ethanol conversion is spent in distillation and dehydration
	, * Shappouri 2002: considering that 68% of the energy for ethanol conversion is spent in distillation and dehydration, and 62.2% of this amount is spent in distillation only.

Tabel A. 8. Ethanol production energy expense during considering industrial and farming activities for different crops according to the water-in-ethanol content.

INDUSTRIAL AND PLANTATION PRODUCTION COST								
		Sugar Cane°	**Corn °°**	**Cassava^**	**Cassava^^**	**Corn***	**Corn****	**Corn*****
Agricultural Production Cost (MJ/L)		2.0	7.9	1.6	4.3	6.7	6.7	6.6
E100 Energy production cost (MJ/L)		19.4	11.8	11.8	16.7	14.9	13.6	15.1
Total Energy Expense used in anhydrous ethanol production (MJ/L)		21.4	19.7	13.3	21.1	21.5	20.3	21.7
E96W04	Production cost not considering dehydration (MJ/L)	19.6	17.8	11.5	19.2	17.7	16.8	17.9
	Energy expense reduction	8.3%	9.8%	13.8%	8.8%	17.7%	17.2%	17.8%
E90W10	Distillation until 90% E/W (MJ/L)	17.7	15.6	9.5	17.2	13.5	13.2	13.6
	Energy expense reduction	17.5%	20.6%	29.0%	18.5%	37.2%	35.2%	37.6%
E85W15	Distillation until 85% E/W (MJ/L)	17.5	15.5	9.3	17.0	13.2	12.9	13.3
	Energy expense reduction	18.1%	21.4%	30.1%	19.2%	38.6%	36.7%	39.0%
E80W20	Distillation until 80% E/W (MJ/L)	17.5	15.4	9.2	17.0	13.1	12.8	13.1
	Energy expense reduction	18.4%	21.7%	30.5%	19.5%	39.2%	37.3%	39.6%
E70W30	Distillation until 70% E/W (MJ/L)	17.4	15.3	9.1	16.8	12.9	12.5	12.9
	Energy expense reduction	18.9%	22.3%	31.4%	20.1%	40.3%	38.5%	40.7%
E60W40	Distillation until 60% E/W (MJ/L)	17.2	15.2	9.0	16.7	12.6	12.3	12.6
	Energy expense reduction	19.4%	22.9%	32.3%	20.6%	41.4%	39.6%	41.8%

Tabel A. 9. Fuel LHV/Production Energy cost for different water-in-ethanol contents and ethanol from different crops.

FINAL FUEL LHV / PRODUCTION ENERGY COST (considering E100 LHV = 21.2 MJ/l)							
Ethanol Concentration (v/v)	**Sugar Cane°** [42]	**Corn °°** [168]	**Cassava^** [43	**Cassava^^** [125]	**Corn*** [163]	**Corn**** [171]	**Corn***** [171]
100	99%	108%	159%	101%	98%	104%	98%
96	104%	115%	177%	106%	115%	121%	114%
90	106%	119%	193%	108%	132%	136%	132%
85	101%	114%	186%	104%	129%	132%	129%
80	95%	107%	177%	98%	123%	126%	123%
70	84%	95%	157%	87%	110%	113%	110%
60	73%	82%	137%	75%	97%	100%	97%

Brasil	° Salla 2009
	°° Salla 2010
	^ Salla 2008
Asia	^^ Dai 2005: Considering the distillation energy fraction equal to Salla 2008.
USA	* Flowers 2007: considering that 68% of the energy for ethanol conversion is spent in distillation and dehydration
	, * Shappouri 2002: considering that 68% of the energy for ethanol conversion is spent in distillation and dehydration, and 62.2% of this amount is spent in distillation only.

Appendix 2. Residual gas fraction estimation

Tabel A. 10. Estimated residual gas fraction based on the work of Alger and Wooldridge [208] used for in-cylinder temperature calculation. Table values are RGF values given by the relationship betwen intake manifold pressure and valve overlap.

Considered valve overlap (CAD)	Intake manifold pressure (bar)					
	0.50	**0.53**	**0.56**	**0.60**	**0.63**	**0.70**
0	0.09	0.09	0.08	0.08	**0.08**	0.07
25	0.15	0.14	**0.13**	0.12	0.12	0.10
30	0.16	0.15	0.14	0.13	0.12	0.11
43.5	0.25	**0.23**	0.21	0.18	0.17	0.14
60	0.37	0.33	0.30	0.25	0.23	0.17

XXXX	Value taken from Alger and Wooldridge [208]
XXXX	Interpolated value
XXXX	Used for calculation procedure

Appendix 3. Valve timing data for PVOvar and different injection strategies

Tabel A. 11. Valve timing data for PVOvar with PFI strategies.

Port fuel injection PVOvar

	IMEP (bar)	IVC (CAD $ATDC_{int}$)	IVO (CAD $ATDC_{int}$)	EVC (CAD $ATDC_{int}$)	EVO (CAD $ATDC_{int}$)	PVO (CAD)
E100	2.0	216	-15	22	-193	36
	3.1	206	-25	22	-193	46
	4.5	186	-45	22	-193	67
	6.1	187	-45	22	-193	67
	7.3	177	-55	22	-193	77
	9.0	186	-45	22	-193	67
		IVC	IVO	EVC	EVO	PVO
E85W15	2.2	216	-15	22	-190	36
	3.2	206	-25	21	-190	45
	4.5	176	-55	22	-190	77
	6.2	177	-55	22	-190	77
	7.6	186	-45	22	-190	67
	9.0	221	-10	22	-190	32
		IVC	IVO	EVC	EVO	PVO
Gasoline	2.1	215	-15	22	-193	36
	3.1	205	-25	22	-193	47
	4.6	185	-45	21	-193	66
	6.1	185	-45	22	-193	67
	7.6	185	-45	22	-193	67
	9.1	185	-45	22	-193	67

Appendix 3. Continuation

Tabel A. 12. Valve timing data for PVOvar with DI strategies.

Direct fuel injection PVOvar

	IMEP (bar)	IVC (CAD $ATDC_{int}$)	IVO (CAD $ATDC_{int}$)	EVC (CAD $ATDC_{int}$)	EVO (CAD $ATDC_{int}$)	PVO (CAD)
E100	2.1	209	-20	22	-190	41
	3.1	204	-25	22	-190	46
	4.7	184	-45	23	-190	68
	6.1	184	-45	21	-190	66
	7.6	184	-45	22	-190	67
	9.2	184	-45	22	-190	66
	Load	IVC	IVO	EVC	EVO	PVO
E85W15	2.1	214	-15	22	-190	36
	3.1	204	-24	21	-190	45
	4.6	185	-45	22	-190	66
	6.1	184	-45	22	-190	66
	7.6	184	-45	22	-190	67
	9.1	184	-44	22	-190	66
	Load	IVC	IVO	EVC	EVO	PVO
Gasoline	2.1	215	-15	22	-193	36
	3.1	206	-25	22	-193	47
	4.6	185	-45	22	-193	67
	6.1	185	-45	22	-193	67
	7.5	185	-45	22	-193	67
	9.0	185	-45	22	-193	67

Appendix 4. Valve timing data of NVO strategies and different injection strategies

Tabel A. 13. Valve timing data of NVO with PFI strategies.

Port fuel injection @ TDC_{firing}– Variable NVO

	IMEP (bar)	IVC (CAD $ATDC_{int}$)	IVO (CAD $ATDC_{int}$)	EVC (CAD $ATDC_{int}$)	EVO (CAD $ATDC_{int}$)	NVO Period (CAD)
E100	2.1	93	19	-19	-190	37
	3.1	120	43	-39	-189	81
	4.5	138	48	-39	-189	87
	6.1	159	41	-39	-189	80
	7.6	175	37	-34	-189	70
	9.1	196	25	-18	-189	43
	Load	IVC	IVO	EVC	EVO	NVO
E85W15	2.1	111	28	-24	-190	51
	3.1	120	43	-38	-190	81
	4.6	138	43	-38	-190	81
	6.1	159	43	-39	-190	81
	7.5	188	43	-40	-190	83
	9.1	206	26	-19	-190	44
	Load	IVC	IVO	EVC	EVO	NVO
Gasoline	2.1	111	33	-25	-193	57
	3.1	120	38	-39	-193	77
	4.6	137	38	-39	-193	77
	6.5	163	38	-39	-193	77
	7.6	184	38	-39	-193	77
	9.0	206	23	-24	-193	47

Appendix 4. Continuation

Tabel A. 14. Valve timing data of NVO with PFI strategies.

Direct fuel injection – Variable NVO

	IMEP (bar)	IVC (CAD $ATDC_{int}$)	IVO (CAD $ATDC_{int}$)	EVC (CAD $ATDC_{int}$)	EVO (CAD $ATDC_{int}$)	NVO Period (CAD)	INJ timing (CAD $ATDC_{int}$)
E100	2.1	89	22	-19	-191	41	-30
	3.1	115	42	-39	-190	81	-50
	4.6	131	42	-39	-190	81	-50
	6.2	151	42	-39	-191	80	-50
	7.6	173	42	-39	-190	81	-50
	9.1	206	33	-36	-190	69	-45
	Load	IVC	IVO	EVC	EVO	PVO	
E85W15	2.2	112	28	-24	-190	52	-34
	3.1	126	43	-38	-190	81	-49
	4.5	127	43	-39	-190	81	-49
	6.2	148	43	-39	-190	81	-49
	7.5	167	43	-39	-190	81	-49
	9.1	206	33	-36	-189	69	-49
	Load	IVC	IVO	EVC	EVO	PVO	
Gasoline	2.2	111	33	-24	-193	56	-29
	3.2	122	38	-39	-193	77	-50
	4.6	131	38	-39	-193	77	-50
	6.1	152	38	-39	-193	77	-50
	7.6	176	38	-39	-193	76	-50
	9.1	206	23	-30	-193	53	-35

Appendix 5. Fuel indicated efficiency comparison for different valve strategies and direct injection operation

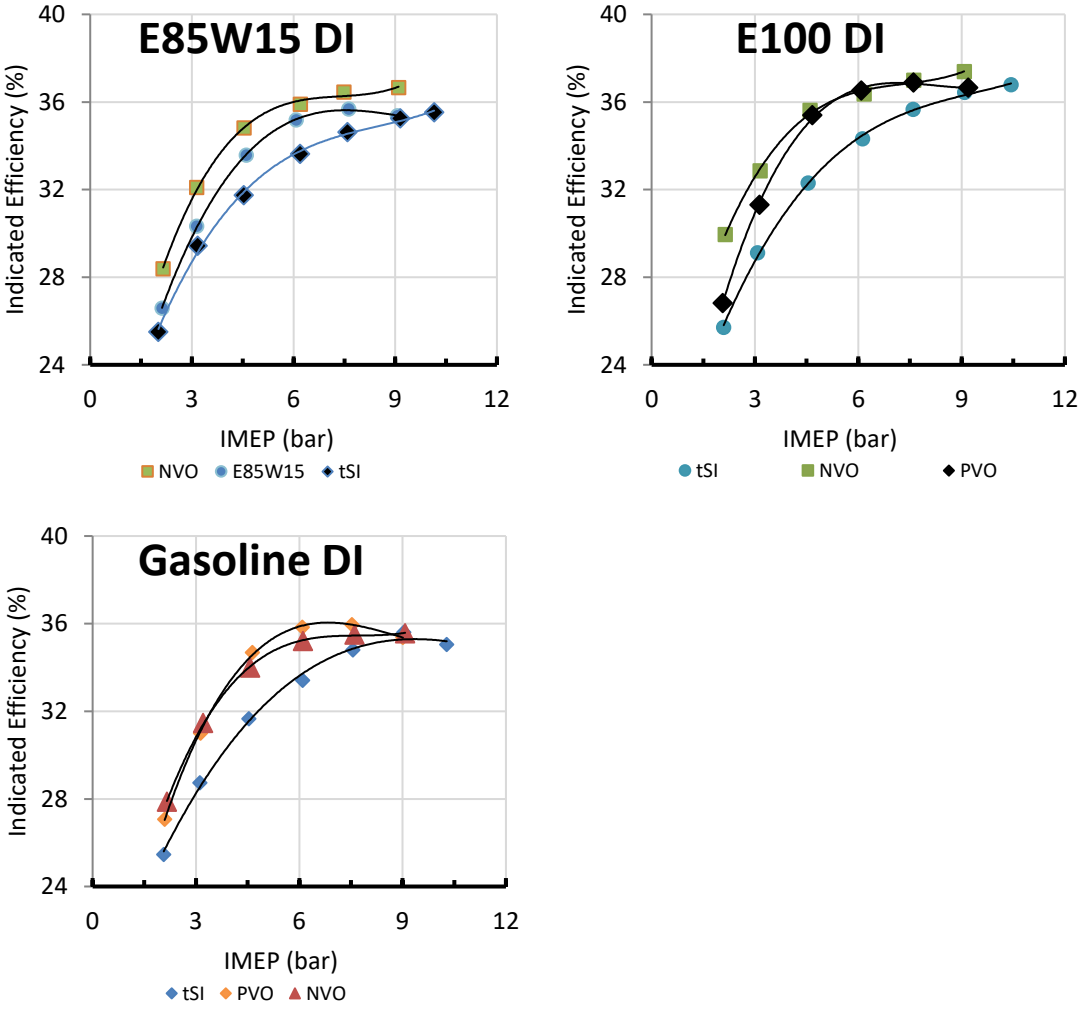

Figure A. 1. Indicated efficiency comparison for different valve strategies and direct injection operation of different fuels.

Appendix 6. Publications to date

Publications related to the research topic:

[1] T. Lanzanova, M. D. Nora, and H. Zhao, “Investigation of Early and Late Intake Valve Closure Strategies for Load Control in a Spark Ignition Ethanol Engine,” SAE Int. J. Engines, vol. 10, no. 2017-01–0643, 2017.

[2] T. Lanzanova, H. Zhao, and M. Dalla Nora, “Advanced valve timing strategies for high efficiency SI operation with ethanol,” in Engine Combustion Processes - Current Problems and Modern Techniques (XIIIth Congress), 2017, pp. 427–437.

[3] M. Dalla Nora, T. D. M. Lanzanova, and H. Zhao, “Effects of valve timing, valve lift and exhaust backpressure on performance and gas exchanging of a two-stroke GDI engine with overhead valves,” Energy Convers. Manag., vol. 123, pp. 71–83, 2016.

[4] M. Dalla Nora, T. Lanzanova, Y. Zhang, and H. Zhao, “Engine Downsizing through Two-Stroke Operation in a Four-Valve GDI Engine,” SAE Tech. Pap., 2016.

[5] M. Dalla Nora, T. D. M. Lanzanova, Y. Zhang, and H. Zhao, “Extreme engine downsizing by doubling the firing frequency in a boosted direct injection gasoline engine_Rev,” in Internal Combustion Engines Conference - Institution of Mechanical Engineers (IMechE), 2015.

[6] M. Martins, T. Lanzanova, and R. Sari, “Low Cost Wet Ethanol for Spark-Ignited Engines: Further Investigations,” SAE Int. J. Fuels Lubr., 2015.

[7] M. E. S. Martins and T. D. M. Lanzanova, “Full-load Miller cycle with ethanol and EGR: Potential benefits and challenges,” Appl. Therm. Eng., vol. 90, pp. 274–285, 2015.

[8] W. M. Ambrós, T. D. M. Lanzanova, J. L. S. Fagundez, R. L. Sari, D. K. Pinheiro, M. E. S. Martins, and N. P. G. Salau, “Experimental analysis and modeling of internal combustion engine operating with wet ethanol,” Fuel, 2015.

[9] T. D. M. Lanzanova, H. A. Vielmo, R. L. Sari, H. M. Dornelles, G. A. Tatsch, M. E. S. Martins, and L. Michels, “Performance Analysis of a Spark Ignited Engine Running on Different Water-in-Ethanol Mixtures,” SAE Tech. Pap., no. 2013-36–0202, Oct. 2013.

[10] T. D. M. Lanzanova, M. E. S. Martins, H. A. Vielmo, P. R. M. Machado, and R. L. Sari, “Numerical Simulation of the Performance Parameters of an Otto Engine Running on Ethanol At Different Percentages of Hydration,” in Proceedings of Encit 2012, 2012.

[11] M. E. S. Martins, T. D. M. Lanzanova, R. Sari, P. R. M. Machado, and H. A. Vielmo, “Low Cost Wet Ethanol Fuel : Benefits and Challenges,” in 21st Aachen Colloquium Automobile and Engine Technology 2012, 2012.